Final Report

Durability of Cementitious Systems Incorporating Calcined Low-Grade Kaolin Clays

FDOT Contract Number BDV25-977-59

Date: February 2022

Submitted To: Dr. Harvey DeFord, Ph.D.

Structural Materials Research Specialist

Florida Department of Transportation

Materials Research Office

5007 NE 39th Avenue

Gainesville, FL 32609

Phone: 352-955-6671

Email: Harvey.deford@dot.state.fl.us

Submitted By: Dr. Abla Zayed, Ph.D.

Department of Civil and Environmental Engineering

University of South Florida

4202 E Fowler Avenue

Tampa, FL 33620

Phone: 813-974-5823

zayed@usf.edu

Disclaimer

The opinions, findings, and conclusions expressed in this publication are those of the authors and not necessarily those of the State of Florida Department of Transportation (FDOT) or the U.S. Department of Transportation (USDOT) or the Federal Highway Administration (FHWA).

Approximate Conversions to SI Units (from FHWA)				
Symbol	**When You Know**	**Multiply By**	**To Find**	**Symbol**
Length				
in	inches	25.4	millimeters	mm
ft	feet	0.305	meters	m
yd	yards	0.914	meters	m
mi	miles	1.61	kilometers	km
Area				
in^2	square inches	645.2	square millimeters	mm^2
ft^2	square feet	0.093	square meters	m^2
yd^2	square yard	0.836	square meters	m^2
mi^2	square miles	2.59	square kilometers	km^2
Volume				
fl oz	fluid ounces	29.57	milliliters	mL
gal	gallons	3.785	liters	L
ft^3	cubic feet	0.028	cubic meters	m^3
yd^3	cubic yards	0.765	cubic meters	m^3
NOTE: volumes greater than 1000 L shall be shown in m^3				
Mass				
oz	ounces	28.35	grams	g
lb	pounds	0.454	kilograms	kg
Temperature (exact degrees)				
°F	Fahrenheit	5 (F-32)/9 or (F-32)/1.8	Celsius	°C
Illumination				
fc	foot-candles	10.76	lux	lx
fl	foot-Lamberts	3.426	candela/m^2	cd/m^2
Force and Pressure or Stress				
lbf	pound-force	4.45	newtons	N
lbf/in^2	pound-force per square inch	6.89	kilopascals	kPa

Technical Report Documentation Page

1. Report No.	2. Government Accession No.	3. Recipient's Catalog No.
4. Title and Subtitle Durability of Cementitious Systems Incorporating Calcined Low-Grade Kaolin Clays		5. Report Date February 2022 6. Performing Organization Code
7. Author(s) Abla Zayed, Kyle Riding, Dhanushika Mapa, Hai Zhu, Nicholas Fowler, Farzaneh Nosouhian, Yuri Stetsko		8. Performing Organization Report No.
9. Performing Organization Name and Address Department of Civil and Environmental Engineering University of South Florida 4202 E Fowler Avenue; ENB 118 Tampa, FL 33620-5350		10. Work Unit No. (TRAIS) 11. Contract or Grant No. BDV25-977-59
12. Sponsoring Agency Name and Address Florida Department of Transportation 605 Suwannee St, MS 30 Tallahassee, FL 32399		13. Type of Report and Period Covered Final Report August 8, 2018-February 28, 2022 14. Sponsoring Agency Code
15. Supplementary Notes		

16. Abstract

One ordinary portland cement (OPC), five portland limestone cements (IL), and five calcined clays were used to assess the strength development, external sulfate durability, chloride penetration, and carbonation resistance in calcined clay blended cementitious systems. The as-received materials were tested for their physical, chemical, and mineralogical composition using Blaine fineness, laser particle size distribution, specific gravity, X-ray fluorescence (XRF), and X-ray diffraction (XRD) coupled with Rietveld refinement. The cements varied in their tricalcium aluminate, tricalcium silicate, calcite contents, and fineness. The clays varied in their kaolin content, gibbsite content, and fineness. Two of the clays were commercial calcined clays from the same source, but with different fineness. The remaining clays were calcined at 850℃ for 1 hour using a laboratory furnace. While strength development of mortar cubes was assessed at two cement replacement levels (10% and 20%), external sulfate durability was assessed using ASTM C1012 at a constant water-to-cementitious materials (w/cm) ratio and 20% cement replacement. Selected calcined clay blended mixtures were optimized for sulfate content based on heat of hydration measurements according to ASTM C563 and adding hemihydrate as a partial replacement of clay. The latter were subsequently assessed for sulfate durability. Chloride durability of the calcined clay blended cementitious mixtures were assessed by conducting chloride ion penetration studies using ASTM C1556 and chloride binding experiments. Carbonation resistance of the mixtures were assessed under natural exposure conditions. Phase assemblage studies were performed on pastes, mortars, and concrete using quantitative X-ray diffraction and thermodynamic modeling. The findings indicated the significance of kaolin and gibbsite contents and of fineness on enhancing strengths and sulfate resistance. Sulfate optimization of clay blended cementitious systems using isothermal calorimetry was found to improve sulfate resistance of the blended systems. Calcined clay incorporation improved the resistance against chloride ion penetration even in clays with low kaolin contents. Carbonation studies indicated that for the low-kaolin-clay blended systems, carbonation resistance was similar but lower than the control mixtures.

17. Key Word	18. Distribution Statement		
Low grade calcined clay chemical, mineralogical, and physical properties, kaolin and gibbsite content, sulfate optimization, sulfate durability, chloride penetration, carbonation			
19. Security Classif. (of this report) None	20. Security Classif. (of this page) None	21. No. of Pages 186	22. Price

Form DOT F 1700.7 (8-72) Reproduction of completed page authorized

Acknowledgement

This work has been sponsored by the Florida Department of Transportation (FDOT) and the Federal Highway Administration (FHWA). The Principal Investigator appreciates the valuable discussions with the Project Manager, Dr. Harvey DeFord.

Executive Summary

E.1 Background

Supplementary cementitious materials (SCMs) are widely used in concrete to improve its strength and durability performance and offer longer concrete structure service life. The most common currently used SCM in the state of Florida is Class F fly ash. However, the current demand for fly ash indicates that there will be a scarcity of fly ash resources to adequately meet the demand. Therefore, it is imperative to identify new materials which could demonstrate similar performance in concrete. Recent research studies have identified low-grade calcined clay as a new SCM with promising results in improving concrete durability performance. Currently metakaolin (MK), a high-purity kaolin clay, is being effectively used in concrete; however, its cost is substantially higher than fly ash (ten-fold). The availability of low-grade clay in abundance in many parts of the world and its lower processing costs make it a viable option for use in concrete as an SCM. However, the clay characteristics may demonstrate variable effects on concrete performance, including strength evolution, sulfate ion penetration, chloride ion ingress, and carbonation. As a consequence, this investigation highlights the desirable materials characteristics of the blended system necessary for durable performance of low-grade calcined clay blended concrete mixtures.

E.2 Research Objectives

The objectives of this investigation were:

1. Investigate the effects of the chemical and physical characteristics and of the replacement levels of calcined low-grade kaolin clays on strength evolution in cementitious systems.
2. Establish the impact of calcined low-grade kaolin clays characteristics and substitution levels on the durability of cementitious systems exposed to aggressive exposure conditions common in Florida during service life.

Satisfying these objectives would provide the Florida Department of Transportation (FDOT) with the scientific knowledge necessary to modify specifications pertaining to metakaolin to include low-grade kaolin containing pozzolans in structural concrete mixtures while ensuring a sustainable and durable infrastructure in the state of Florida.

In order to achieve these objectives, a series of laboratory experiments were conducted to assess strength development, sulfate resistance, sulfate balance, chloride durability, and carbonation resistance of calcined clay blended cementitious systems. The cements utilized in this study included Type I/II (MH) and Type IL cements to show the variable effects of tricalcium silicate (C_3S), tricalcium aluminate (C_3A), limestone contents, and fineness. The selected clays varied in their kaolin content, gibbsite content, and fineness. Two clays were commercial clays from the same source but with different fineness. The other clays were calcined at 850ºC for 1 hour at a laboratory furnace. The as-received cementitious materials were characterized using X-ray fluorescence (XRF), quantitative X-ray diffraction (QXRD), Blaine fineness, laser particle size analyzer, and specific gravity.

The strength development of plain cement and calcined clay blended mixtures were assessed by incorporating two cement replacement levels of 10% and 20% and two exposure solutions (saturated lime and 5 w/o sulfate). The effect of the physical and chemical characteristics of clays on sulfate durability, chloride ion ingress, and carbonation was also investigated at a cement replacement level of 20%. Sulfate durability was assessed on both control and clay blended mixtures following ASTM C1012. Chloride penetration resistance was assessed for the control and blended concrete mixtures following ASTM C1556 as well as chloride binding isotherms experiments conducted on control and blended pastes. Carbonation resistance was assessed on control and blended concrete mixtures exposed to natural environment. Phase assemblage studies were conducted using thermodynamic modeling and QXRD.

E.3 Main Findings

The findings indicated that calcined clay substitution generally results in compressive strengths similar or higher than plain cement mixtures. However, the calcined clay blended mixtures prepared with coarser grind commercial calcined clay showed lower strengths, especially at 20% replacement level. Among all mixtures, compressive strengths were considerably higher when clays were blended with IL cements attributed to increased clay reactivity in presence of limestone.

In terms of external sulfate durability, Type I/II(MH) and Type IL cements demonstrated moderate or high sulfate resistance due to the moderate C_3A levels in both cement types and lower clinker factor in Type IL cements. However, calcined clay incorporation showed variable effects on mortar expansion and strength development in sulfate environment, due to variation in kaolin

content and fineness of the calcined clays as well as the sulfate balance of the blended system. Calcined clay-blended mortars with high kaolin contents and/or gibbsite content and higher fineness showed consistently higher strengths and excellent sulfate resistance. In terms of the two commercial calcined clays, the fine grind calcined clay blended mixtures demonstrated better sulfate resistance compared to the coarse grind. Moreover, sulfate optimization of the low-grade kaolin clays, determined using isothermal calorimetry, enhanced the sulfate resistance of the blended system. However, this requires further investigation and testing.

With regard to chloride ion ingress, calcined clay incorporation resulted in lower apparent diffusion coefficients compared to plain cement mixtures likely due to refined pore structure as well as chloride binding effect. On the other hand, carbonation of calcined clay blended mixtures was slightly higher compared to the plain cement mixtures; however, it did not appear to substantially affect service life at the calcined clay replacement levels studied.

E.4 Recommendations

Based on the findings of this study, the following recommendations can be made:

- Require optimization of clay sulfate levels based on the cementitious system constituents.
- Perform heat of hydration measurements using isothermal calorimetry to optimize clay sulfate levels.
- Require testing for external sulfate durability according to ASTM C1012, for a period of 18 months, as part of the approval process for calcined clay-blended mixtures.
- Initiate a demonstration project on calcined clay use in construction. The demonstration project should involve the use of concrete containing low-grade calcined clay, preferably in a pavement or other non-structural member. Use of concrete containing calcined clay on an actual construction project would demonstrate the ability of calcined clay to be produced, batched, placed, and provide acceptable mechanical properties for use in transportation infrastructure. This would reduce the risk for contractors of using concrete containing calcined clay and reduce costs to use it in future projects.

E.5 Recommendations for Future Study

Based on the findings of this study, the following are recommended:

- Initiate a study to assess the sulfate optimization of calcined low-grade kaolin clay blended cementitious systems and their effects on sulfate durability, using calcined clays of varying kaolin contents and cements currently available in Florida.
- Initiate a study to investigate the effect of calcined clay characteristics on concrete temperature rise.
- Initiate a study to assess the effect of calcined low-grade clay characteristics such as kaolin content, gibbsite content, and fineness on cracking resilience of calcined clay-blended cementitious mixtures.

Table of Contents

Contents page

Disclaimer ii

Approximate Conversions to SI Units (from FHWA) iii

Technical Report Documentation Page iv

Acknowledgement v

Executive Summary vi

E.1 Background vi

E.2 Research Objectives vi

E.3 Main Findings vii

E.4 Recommendations viii

E.5 Recommendations for Future Study viii

List of Figures xv

List of Tables xix

Chapter 1 Literature Review 1

1.1 Introduction 1

1.1.1 Limestone – Calcined Clay Blends 1

1.1.2 Potential Use of Clays in Florida 2

1.2 Sulfate Optimization 2

1.2.1 Determination of Optimum SO_3 Content 3

1.2.2 Effect of SO_3 Content on Cement Hydration 5

1.2.3 Effect of SO_3 Content on Paste Properties 7

1.2.3.1 Porosity 8

1.2.3.2 Strength 8

1.2.3.3 Shrinkage and Expansion 8
1.2.4 Factors Affecting Optimum SO_3 Content 9
1.2.4.1 Availability of SO_3 9
1.2.4.2 Alkalis 10
1.2.4.3 Fineness 11
1.2.4.4 Age 12
1.2.4.5 Temperature 13
1.2.4.6 SCMs Effects 13
1.3 Concrete Temperature Rise 15
1.3.1 SCMs Effects 16
1.3.2 Heat Evolution in LC^3 Systems 17
1.4 Sulfate Durability 18
1.4.1 Mechanism of External Sulfate Attack 18
1.4.1.1 Physical Sulfate Attack 19
1.4.1.2 Chemical Sulfate Attack 20
1.4.2 Influence Factors 22
1.4.2.1 Curing 22
1.4.2.2 Impact of the Type of Cation and Anion Combinations 22
1.4.2.3 Effect of Cement Composition 23
1.4.2.4 Effect of SCMs 23
1.4.2.5 Limestone and Limestone-Clay Combinations 25
1.4.2.6 Impact of pH of Concrete Pore Solution 27
1.5 Chloride Ingress 28
1.5.1 Mechanism and Effects on Cementitious Systems 28

1.5.2 Effects of Calcined Clays and Limestone on Chloride Ingress 28
1.6 Carbonation Corrosion 31
1.6.1 Mechanism and Effects on Cementitious Systems 31
1.6.2 Effects of Calcined Clays and Limestone on Carbonation 32
1.7 Conclusion 33
1.8 References 34
Chapter 2 Material Characterization 48
2.1 Introduction 48
2.2 Elemental Oxide Composition 48
2.2.1 XRF Analysis of Cements 48
2.2.2 XRF Analysis of Clays 51
2.3 Mineralogical Analysis 52
2.3.1 X-Ray Diffraction 52
2.3.1.1 X-ray analysis of cements and inorganic processing additions 54
2.3.1.2 X-Ray Analysis of Clays 56
2.3.2 Thermogravimetric Analysis 58
2.4 Physical Characteristics 61
2.4.1 Cement Physical Characteristics 61
2.4.2 Physical Characteristics of Calcined Clays 64
2.5 Conclusions 67
2.6 References 68
Chapter 3 Effect of Calcined Low-Grade Kaolin Clay on Strength Evolution of Cementitious Mixtures 71
3.1 Introduction 71

3.2 Experimental methods 72
3.3 Results and Discussion 76
3.3.1 Compressive Strength Evolution of Cements in Lime Solution and 5% Sodium Sulfate Solution 76
3.3.2 Effect of Cement and Clay Characteristics and Clay Substitution Levels on Strength Evolution 78
3.3.2.1 Compressive Strength Development in Saturated Lime Solution 78
3.3.2.2 Compressive Strength Development in 5% Sodium Sulfate Solution 86
3.3.3 Thermodynamic Modeling 93
3.4 Conclusions 105
3.5 References 106
Chapter 4 Effect of Low-Grade Calcined Clay on Sulfate Durability, Carbonation, and Chloride Ingress in Cementitious Systems 110
4.1 Introduction 110
4.2 Materials and Methods 112
4.2.1 Materials 112
4.2.2 Expansion Measurements for External Sulfate Attack 115
4.2.2.1 Isothermal Calorimetry Measurements for Sulfate Optimization 115
4.2.3 Testing for Chloride Ion Ingress 116
4.2.4 Testing for Bound Chloride Content 118
4.2.5 Carbonation Testing 119
4.2.6 X-Ray Diffraction Analysis 122
4.3 Results and Discussion 123
4.3.1 Length Change Measurements in Sodium Sulfate Solution according to ASTM C1012 123

4.3.1.1 As-Received Cement Systems 123
4.3.1.2 As-Received Clay-Blended Systems 124
4.3.1.3 Sulfate-Added Clay Blended Systems 128
4.3.1.4 X-Ray Diffraction Analysis of Mortar Bars after Sulfate Exposure 132
4.3.2 Chloride Durability 136
4.3.2.1 Chloride Diffusivity 136
4.3.2.2 XRD Analysis of Concrete Samples after Chloride Exposure 145
4.3.2.3 Chloride Binding 148
4.3.2.4 XRD Analysis of Paste Samples before and after Chloride Exposure 149
4.3.3 Carbonation Resistance 151
4.3.3.1 Carbonation Depth and Carbonation Coefficient 151
4.3.3.2 XRD Analysis of Concrete Samples after Natural Carbonation 156
4.4 Conclusions 156
4.5 References 158
Chapter 5 Summary, Conclusions and Recommendations 164
5.1 Summary and Conclusions 164
5.2 Recommendations 165
5.3 Suggestions for Future Work 166

List of Figures

Figure 1-1: Determination of optimum based on Gaussian fit and 2nd order polynomial fit (adapted from [24]) 4
Figure 1-2: Heat flow definition for optimum SO_3 content 5
Figure 1-3: Heat of hydration curve 7
Figure 1-4: Solubility of different calcium sulfate forms (adapted from [39]) 10
Figure 1-5: Optimum sulfate content as a function of curing time (adapted from [46]) 12
Figure 1-6: Phase diagram for sodium sulfate (adapted from [65]) 19
Figure 2-1: TGA and DTG of as-received clays 59
Figure 2-2: Example of tangent method for GAB4 60
Figure 2-3: Incremental particle size distribution for as-received cements 63
Figure 2-4: Cumulative particle size distribution for as-received cements 64
Figure 2-5: Incremental particle size distribution for calcined clays 66
Figure 2-6: Cumulative particle size distribution for calcined clays 67
Figure 3-1: Compressive strength development of control mortars in lime solution 77
Figure 3-2: Compressive strength development of control mortars in 5% sodium sulfate solution 78
Figure 3-3: Compressive strength development of cement HA+10% clay mortars in lime solution 80
Figure 3-4: Compressive strength development of cement GILOP+10% clay mortars in lime solution 81
Figure 3-5: Compressive strength development of cement THIL+10% clay mortars in lime solution 82
Figure 3-6: Compressive strength development of HA+20% clay mortars in lime solution 83
Figure 3-7: Compressive strength development of cement GILOP+20% clay mortars in lime solution 84
Figure 3-8: Compressive strength development of cement THIL+20% clay mortars in lime solution 85
Figure 3-9: Compressive strength evolution of HA+10% clay mortars in 5% sodium sulfate solution 87

Figure 3-10: Compressive strength evolution of GILOP+10% clay mortars in 5% sodium sulfate solution 88
Figure 3-11: Compressive strength evolution of THIL+10% clay mortars in 5% sodium sulfate solution 89
Figure 3-12: Compressive strength evolution of HA+20% clay mortars in 5% sodium sulfate solution 91
Figure 3-13: Compressive strength evolution of GILOP+20% clay mortars in 5% sodium sulfate solution 92
Figure 3-14: Compressive strength evolution of THIL+20% clay mortars in sulfate solution 93
Figure 3-15: Predicted phase assemblage for control mixtures 94
Figure 3-16: Predicted phase assemblage for clay mixtures (a) at 10% (b) at 20% substitution levels 95
Figure 3-17: Predicted phase assemblage for (a) Control HA (b) Control GILOP (c) Control THIL mixtures immersed in 5% Na_2SO_4 solution 98
Figure 3-18: Predicted phase assemblage for (a) HA+10CCF (b) HA+10GAB4 mixtures immersed in 5% Na_2SO_4 solution 99
Figure 3-19: Predicted phase assemblage for (a) GILOP+10CCF (b) GILOP+10GAB4 mixtures immersed in 5% Na_2SO_4 solution 100
Figure 3-20: Predicted phase assemblage for (a) THIL+10CCF (b) THIL+10GAB4 mixtures immersed in 5% Na_2SO_4 solution 101
Figure 3-21: Predicted phase assemblage for (a) HA+20CCF (b) HA+20GAB4 mixtures immersed in 5% Na_2SO_4 solution 102
Figure 3-22: Predicted phase assemblage for (a) GILOP+20CCF (b) GILOP+20GAB4 mixtures immersed in 5% Na_2SO_4 solution 103
Figure 3-23: Predicted phase assemblage for (a) THIL+20CCF (b) THIL+20GAB4 mixtures immersed in 5% Na_2SO_4 solution 104
Figure 4-1: CO_2 concentration in the atmosphere 120
Figure 4-2: Temperature of the environment 121
Figure 4-3: Relative humidity of the environment 121
Figure 4-4: Length change of as-received cements mortar bars in 5% sodium sulfate solution 124
Figure 4-5: Length change of clay EMD1 mortar bars in 5% sodium sulfate solution 125

Figure 4-6: Length change of clay CCC mortar bars in 5% sodium sulfate solution 125
Figure 4-7: Length change of clay CCF mortar bars in 5% sodium sulfate solution 126
Figure 4-8: Length change of clay GAB1 mortar bars in 5% sodium sulfate solution 126
Figure 4-9: Length change of clay GAB4 mortar bars in 5% sodium sulfate solution 127
Figure 4-10: Total heat vs. sulfate levels in HA+20CCF mixture 129
Figure 4-11: Total heat vs. sulfate levels in THIL+20CCF mixture 129
Figure 4-12: Length change of sulfate added HA+20CCF mortar bars in 5% sodium sulfate solution, *Note:* Parenthesis of mix ID (total SO_3 content) 131
Figure 4-13: Length change of sulfate added THIL+20CCF mortar bars in 5% sodium sulfate solution, *Note:* Parenthesis of mix ID (total SO_3 content) 131
Figure 4-14: Total chloride concentration profiles for control CIL mixture 136
Figure 4-15: Total chloride concentration profiles for CIL+20CCC mixture 137
Figure 4-16: Total chloride concentration profiles for CIL+20EMD1 mixture 137
Figure 4-17: Total chloride concentration profiles for CIL+20GAB1 mixture 138
Figure 4-18: Total chloride concentration profiles for CIL+20GAB4 mixture 138
Figure 4-19: Total chloride concentration profiles for CIL+20CCF mixture 139
Figure 4-20: Total chloride concentration profiles for control GILOP mixture 139
Figure 4-21: Total chloride concentration profiles for GILOP+20CCC mixture 140
Figure 4-22: Total chloride concentration profiles for GILOP+20EMD1 mixture 140
Figure 4-23: Total chloride concentration profiles for GILOP+20GAB1 mixture 141
Figure 4-24: Total chloride concentration profiles for GILOP+20GAB4 mixture 141
Figure 4-25: Total chloride concentration profiles for GILOP+20CCF mixture 142
Figure 4-26: Chloride binding isotherms of CIL mixtures 148
Figure 4-27: Phenolphthalein indicator test results of control CIL (3-day lime curing) (a) immediately after spraying (b) after 24 h 151
Figure 4-28: Phenolphthalein indicator test results of CIL+20CCC (3-day lime curing) (a) immediately after spraying (b) after 24 h 152
Figure 4-29: Phenolphthalein indicator test results of control CIL+20GAB1 (3-day lime curing) (a) immediately after spraying (b) after 24 h 152
Figure 4-30: Carbonation depths of cement CIL mixtures 153
Figure 4-31: Carbonation depths of cement GILOP mixtures 153

Figure 4-32: Carbonation coefficients of cement CIL mixtures 155
Figure 4-33: Carbonation coefficients of cement GILOP mixtures..... 155

List of Tables

Table 2-1: Oxide chemical composition of as-received cements 49
Table 2-2: Oxide chemical composition of processing additions 50
Table 2-3: Oxide chemical composition of clays 52
Table 2-4: Crystalline structures used for weight fraction analysis 54
Table 2-5: Crystalline and amorphous weight percentages in cements 55
Table 2-6: Crystalline and amorphous weight percentages in additions 55
Table 2-7: Limestone content estimated from QXRD analysis 56
Table 2-8: Mineralogical analysis of clays 57
Table 2-9: Kaolin content determined by TGA and XRD 61
Table 2-10: Particle size analysis, Blaine fineness, and density of cements 62
Table 2-11: Sieve analysis results of CCC calcined clay 65
Table 2-12: Particle size analysis, Blaine fineness, and density of calcined clays 66
Table 3-1: Oxide chemical composition of cements 73
Table 3-2: Mineralogical analysis, Blaine fineness, and MPS of cements 73
Table 3-3: Oxide chemical composition of clays 74
Table 3-4: Mineralogical analysis, Blaine fineness, and MPS of clays 74
Table 3-5: Mortar mix proportions (9-cube mix) 75
Table 3-6: Compressive strength at later ages relative to the 28-day strength (in sulfate solution) for cement HA+10% clay mixtures exposed to 5% sodium sulfate solution 88
Table 3-7: Compressive strength at later ages relative to the 28-day strength (in sulfate solution) for cement GILOP+10% clay mixtures exposed to 5% sodium sulfate solution 89
Table 3-8: Compressive strength at later ages relative to the 28-day strength (in sulfate solution) for cement THIL+10% clay mixtures exposed to 5% sodium sulfate solution 89
Table 3-9: Compressive strength at later ages relative to the 28-day strength (in sulfate solution) for cement HA+20% clay mixtures exposed to 5% sodium sulfate solution 91
Table 3-10: Compressive strength at later ages relative to the 28-day strength (in sulfate solution) for cement GILOP+20% clay mixtures exposed to 5% sodium sulfate solution 92
Table 3-11: Compressive strength at later ages relative to the 28-day strength (in sulfate solution) for cement THIL+20% clay mixtures exposed to 5% sodium sulfate solution 93

Table 4-1: Oxide chemical composition of cements 113
Table 4-2: Mineralogical analysis, Blaine fineness, and MPS of cements 113
Table 4-3: Oxide chemical composition of clays 114
Table 4-4: Mineralogical analysis, Blaine fineness, and MPS of clays 114
Table 4-5: Isothermal calorimetry paste mixture design 116
Table 4-6: Concrete mixture design, yd^3 (m^3) 116
Table 4-7: Determined optimum sulfate contents in clay-blended mixtures 130
Table 4-8: Phase quantification of control mortar bars stored in 5% Na_2SO_4 solution 132
Table 4-9: Phase quantification of clay CCC blended mortar bars stored in 5% Na_2SO_4 solution 133
Table 4-10: Phase quantification of clay CCF blended mortar bars stored in 5% Na_2SO_4 solution 134
Table 4-11: Phase quantification of clay EMD1 blended mortar bars stored in 5% Na_2SO_4 solution 134
Table 4-12: Phase quantification of clay GAB1 and GAB4 blended mortar bars stored in 5% Na_2SO_4 solution 135
Table 4-13: Surface chloride concentration and apparent diffusivity of cement CIL mixtures . 144
Table 4-14: Surface chloride concentration and apparent diffusivity of cement GILOP mixtures 144
Table 4-15: Phase quantification of control concrete mixtures after 35 day-exposure to 165 g/L NaCl solution 146
Table 4-16: Phase quantification of cement CIL-clay blended concrete mixtures after 35 day-exposure to 165 g/L NaCl solution 147
Table 4-17: Phase quantification of cement GILOP-clay blended concrete mixtures after 35 day-exposure to 165 g/L NaCl solution 147
Table 4-18: Binding coefficients of Freundlich isotherms and corresponding coefficients of determination (R2) 148
Table 4-19: Phase quantification of cement CIL paste mixtures before and after two months of chloride exposure by XRD 150
Table 4-20: Portlandite content at the core and the surface of 3-day lime cured mixtures as detected by XRD 156

Chapter 1 Literature Review

1.1 Introduction

Supplementary cementitious materials (SCMs) are generally used in structural elements in order to improve the concrete fresh and hardened properties. Class F fly ash is the most commonly used SCM in Florida. However, due to the limited supplies of fly ash, this study was initiated to assess the suitability of an alternative natural pozzolanic resource; namely, low-grade calcined kaolin clays for use as a supplementary cementitious material in the state of Florida. Similar efforts are now being undertaken in several countries across the world [1–13].

1.1.1 Limestone – Calcined Clay Blends

Kaolinite clays become reactive when calcined at temperatures between 600°C and 850°C. It is now being used as a pozzolan in countries such as Brazil, where other common SCMs are in short supply [14]. Substitution of cement content by up to 30% calcined clay has been used. Further reduction of the clinker factor, by up to an additional 15%, has been implemented through the addition of limestone without any adverse effects on the mechanical performance [14, 15]. Incorporation of limestone into the calcined clay-cement blend enhances hardened concrete properties beyond those achieved when using calcined clay alone [10, 16–20]. This is due to the formation of hydration products, such as hemi- and mono-carboaluminate, from the chemical reaction between calcite from limestone, C_3A from the clinker, and amorphous alumina phases from the calcined clay that contribute to concrete strength.

Ternary blends of limestone, calcined clay, and portland cement are referred to in the literature as LC^3 (limestone calcined clay cement). At a clinker factor of 50%, enhanced overall performance was indicated in the reported collaborative research studies involving researchers in Switzerland, India, and Cuba [14, 17]. The use of LC^3 has exhibited several advantages [14, 15]. LC^3 can reduce CO_2 emissions typically associated with cement production by up to 30%. LC^3 research indicates that calcined kaolin clays, with kaolin mineral contents as low as 40 wt.%, are sufficient in enhancing the strength of cementitious systems. This material is considered cost effective because low-grade clays are available in abundance in existing quarries and are often considered overburden or underburden. Moreover, the fuel consumption for clay calcination is less

than that required for clinker production, where temperatures of 1450°C are needed for manufacturing the latter.

1.1.2 Potential Use of Clays in Florida

A recent study identified kaolin clay resources in Florida and assessed their mineralogies and suitability as SCMs [2]. The mineralogy and strength activity indices of all local calcined kaolin clays surpassed the requirements listed for natural pozzolans in ASTM C618 [21], establishing their potential as suitable SCMs. The compressive strengths at 7 and 28 days indicated that calcined Florida kaolinitic clay substitutions can yield similar compressive strengths to those achieved with the same amounts of Class F fly ash. However, the performance of these calcined clays in the presence of limestone has not been addressed but is expected to be enhanced when compared to using calcined clay alone.

Prior to the implementation of calcined low-grade kaolin clays (LKC) as SCMs in concrete mixtures, it is imperative that their influence on the sulfate optimization of the cementitious system be assessed, especially because it is a high-alumina natural pozzolan. Optimizing sulfate content in a cementitious system has significant effect on concrete durability and strength. This review will address the current state of knowledge on the effect of LKC use as an SCM and its impact on strength and durability of the cementitious system.

1.2 Sulfate Optimization

Calcined Clay Portland-Limestone Cement (CCIL) is a binary cementitious system of limestone cement (IL, ASTM C595/C595M [22]) blended with calcined clay (CC), ASTM C618 [21]. While IL is optimized for its sulfate content, once CC is blended with IL, sulfate re-optimization of the binary system must be verified for optimum strength and durability performance. Gypsum ($CaSO_4 \cdot 2H_2O$) or other forms of calcium sulfate are added to clinker during cement production to control early aluminate reaction and prevent flash set of cement with the addition of water. Varying gypsum levels influence the rate of early hydration and the hydration products as explained in later sections. These changes in the microstructure of the hardened cement paste affect its physical properties. Therefore, the addition of SO_3 not only prevents flash set but also enhances the strength and durability of concrete. However, excessive amounts of SO_3 in cement can bring detrimental effects to hardened concrete. Too much SO_3 will result in lower compressive strengths and excessive expansion. The existence of an optimum SO_3 content within

the cement composition was discussed by several researchers [23–28]. This optimum SO_3 content is identified as that which provides the highest compressive strength and hydration heat at early age with the least expansion and drying shrinkage. Nevertheless, the cements optimized for one property may not be necessarily optimized for another [27].

Studies pertaining to SO_3 optimization in LC^3 systems or any other SCM-blended systems are rare in the literature. The following sections discuss the effect of SO_3 content on hydration, paste properties, and the factors affecting the optimum SO_3 levels, while considering the cementitious system as a whole.

1.2.1 Determination of Optimum SO_3 Content

Lerch [29] reported that the optimum SO_3 content with respect to compressive strength of mortar cubes shows a strong correlation with the heat of hydration measured by isothermal calorimetry and also with the length change of mortar bars stored in water. Typically, the sulfate level of a cement is set based on the maximum strength and/or heat at 1 day by cement producers in accordance with ASTM C563. The most recent ASTM C563-18 [30] identifies three methods to approximate the SO_3 which gives maximum performance based on heat and/or strength; namely, visual fit, least square parabolic fit, and asymmetric fit.

Most of the published literature [24, 26, 27, 29, 31] on SO_3 optimization describes the use of compressive strengths and/or heat of hydration to determine the optimum SO_3 content of cement. Niemuth [24] used four methods to determine the optimum sulfate levels for fly-ash-blended systems:

1) Fitting a Gaussian distribution to the SO_3 content-property data

2) Fitting a second order polynomial

3) Qualitative estimate based on visual inspection of the strength versus sulfate trends

4) Position of the sulfate depletion peak relative to the main hydration peak

The first and the second methods (Gaussian distribution and second order polynomial fit) were used assuming a symmetric peak for strength and/or heat versus SO_3 content curve (Figure 1-1). In the third method, the optimum was determined by visual inspection of strength and/or heat versus SO_3 content to locate the corresponding SO_3 level for maximum strength and/or heat. The fourth method identified the optimum as the minimum amount of sulfate needed to have a clear

distinction between the sulfate depletion peak and the main hydration peak, which was the same method proposed by Lerch [29]. Figure 1-2 shows the heat flow curve for under-sulfated, optimum, and over-sulfated systems.

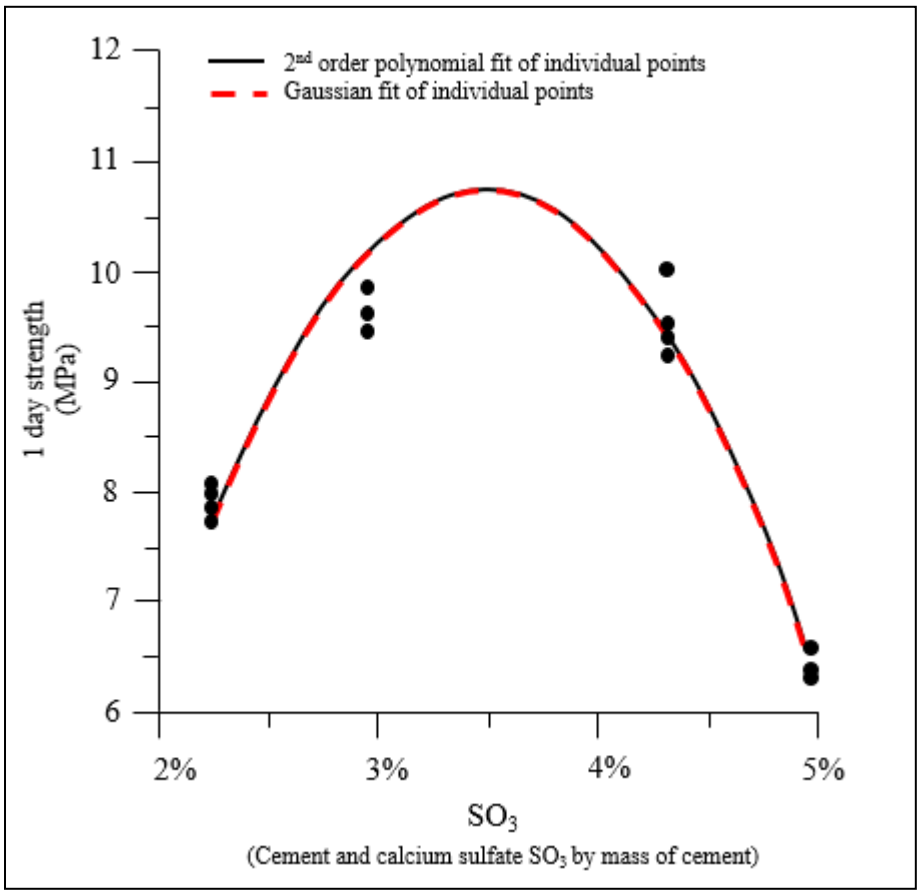

Figure 1-1: Determination of optimum based on Gaussian fit and 2nd order polynomial fit (adapted from [24])

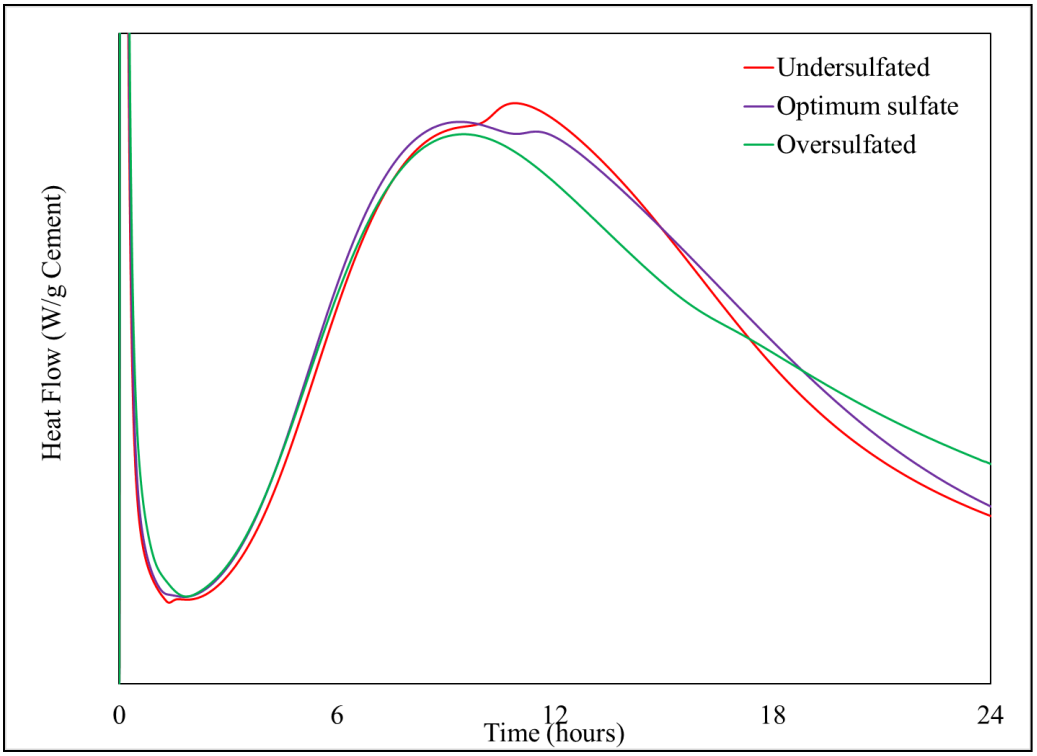

Figure 1-2: Heat flow definition for optimum SO_3 content

Analyzing these four methods, Niemuth suggested that a mathematical fitting method such as Gaussian distribution fit and second order polynomial fit should be used to determine optimum SO_3 levels from strength versus SO_3 level plots as the visual interpretation can lead to significantly different values [24].

1.2.2 Effect of SO_3 Content on Cement Hydration

C_3A reacts with sulfate phases and forms ettringite when there is an ample supply of sulfates available. If the sulfates are consumed before the complete hydration of C_3A, ettringite is transformed to monosulfoaluminates. If the supply of sulfate from gypsum dissolution is inadequate in the system, monosulfoaluminate may form before ettringite [32]. If this monosulfoaluminate is brought into contact with a new source of sulfate ions, ettringite can be reformed resulting in sulfate attack causing expansion and unsoundness in hardened concrete. The hydration of C_4AF in the presence of sulfate forms an iron substituted ettringite which has a lower tendency for expansion [24, 27]. Additionally, it is reported that alite hydration adsorbs a considerable amount of SO_3 that is bound by the C-S-H gel, and this might influence the optimum

SO_3 content [27]. Thus, SO_3 is consumed or removed from solution not only by the aluminate phases formed during hydration, but also by the C-S-H that is formed.

The heat of hydration curve for a typical portland cement is shown in Figure 1-3. The initial peak is an indication of rapid dissolution of ions due to the reaction between cement and water, which is exothermic in nature. During this initial reaction, ettringite is the main hydration product formed [33]. The initial peak is followed by an induction period. A gradual increase in the heat flow is observed when C-S-H formation is initiated, which marks the start of the main hydration peak. Once C-S-H is produced around the calcium silicate grains, it acts as a barrier for ionic diffusion and, as a result, the reaction decelerates. Ettringite continues to form around the aluminate grains until all the sulfates in the system are consumed. A third peak occurs when there is an excess of C_3A and the sulfate in the system is depleted. The time of this peak depends on the C_3A-to-SO_3 ratio, and it relates to the time when ettringite transforms to monosulfoaluminate. Another shoulder peak is often observed just after the main alite peak but before the sulfate depletion point, which corresponds to some solid gypsum consumption and the acceleration of aluminate phase. However, during this time the aluminate hydration product still appears to be ettringite, possibly formed from the previously adsorbed sulfate in the C-S-H phase [33, 34]. Moreover, it was reported that not only the third peak (following sulfate depletion point), but also the shape and intensity of the second peak (main alite peak) are influenced by the SO_3 concentration in the system [27, 35]. It is mentioned that the rate of heat generation initially increases with the SO_3 concentration in the system, reaches a maximum, and then gradually decreases with further additions of SO_3 [35]. Furthermore, increasing the SO_3 content past the maximum decreases the intensity of the third peak and shifts it to longer hydration times.

`

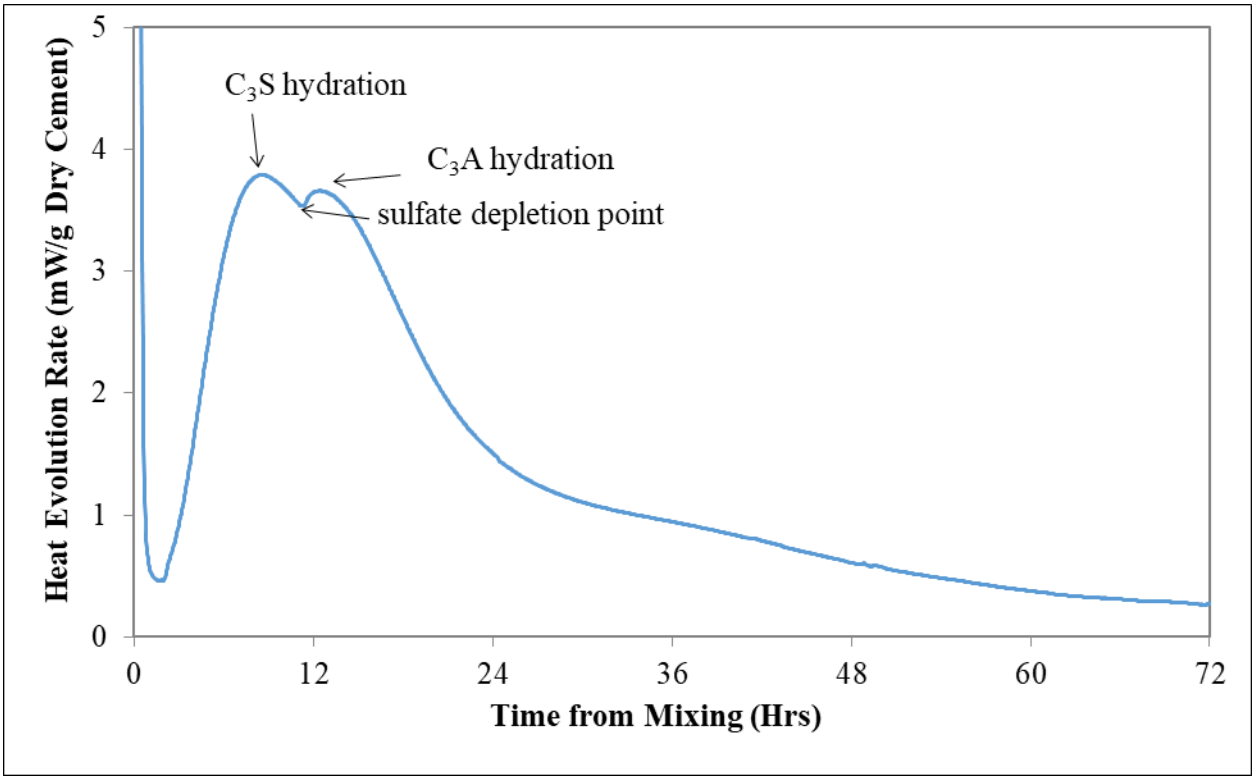

Figure 1-3: Heat of hydration curve

1.2.3 Effect of SO_3 Content on Paste Properties

According to the method proposed by Lerch [29] to determine the optimum SO_3 in portland cement systems, the second stage in hydration following the induction period should depict a separation between the main hydration peak and the sulfate depletion peak in the calorimetry curve, with the former occurring slightly prior to the latter. Therefore, approximately the same optimum is expected for maximum strength and minimum shrinkage [27]. With inadequate levels of SO_3 in the system, the aluminate phase is insufficiently retarded and reacts before the alite, resulting in flash set. However, with too much SO_3 present in the system, aluminate hydration is delayed until alite is hydrated and hardened with the SO_3 combining in the C-S-H gel resulting in a weaker structure. Moreover, the adsorbed sulfate in C-S-H can be desorbed later causing internal sulfate attack. This variability in sulfate levels influences the paste properties such as porosity, strength, expansion, and drying shrinkage.

1.2.3.1 Porosity

As reported in literature, the optimum SO_3 level is likely the one which results in the least porosity with ettringite and silicate formation [27]. The pore size distribution is also affected by gypsum content. The pore size is reported to coarsen with high amounts of gypsum [36]. For low gypsum contents, pores sizes were in the range of 4 nm-50 nm, and when the gypsum content was higher, the pore sizes were in excess of 500 nm.

1.2.3.2 Strength

Lerch [29] reported that the heat of hydration and strengths increased with increasing SO_3 content to a maximum and then begin to decrease with higher SO_3 levels. The decrease in strength on either side of the optimum sulfate content is attributed to the aluminate phase reactions. Formation of ettringite increases with increasing SO_3 content, with subsequent increases in compressive strength. Above the optimum, sulfate content has two opposing effects on the strength; increased volume of ettringite and the decreased density of C-S-H phase (lower space-filling capacity) due to water content [25, 36]. Tsamatsoulis and Nikolakakos [23, 26] correlated the compressive strength of mortar specimens to mass ratios of SO_3 and clinker (CL) and molar ratios of SO_3 and C_3A. For three pure cement systems, they found a common region containing the optimum SO_3/CL mass ratio to be between 3.5 and 3.7 (expressed as percentages) and SO_3/C_3A molar ratio to be between and 1.1 and 1.2.

1.2.3.3 Shrinkage and Expansion

High SO_3 content results in deleterious expansion in cement paste due to the formation of ettringite at later ages [27, 37]. As reported in literature, a very low expansion is observed when SO_3 is increased up to an optimum value determined by the strength curves; however, with further increase in SO_3 content, a corresponding increase in expansion is observed [27]. Therefore, the expansion threshold limit of SO_3 also lies close to the optimum SO_3 level for strength. Conversely, the drying shrinkage of the paste decreases with increasing the SO_3 content [29]. It is reported that the optimum SO_3 level for shrinkage could be equal to or lower than that of compressive strength and expansion [27].

1.2.4 Factors Affecting Optimum SO_3 Content

Several parameters which affect the optimum SO_3 content are identified in the literature [24, 26, 27]. Availability of SO_3 (distribution, source, and solubility), C_3A, C_3S, and alkali contents, cement fineness, and age of the mix are the main factors which influence the optimum SO_3 content for a cementitious system. Additionally, when concrete is considered, additional factors will affect the sulfate optimum; namely, water-to-cementitious ratio, supplementary cementitious materials (SCMs), physical and chemical characteristics, as well as the substitution level, temperature, and chemical admixtures.

1.2.4.1 Availability of SO_3

The distribution and the form of sulfate in cements affects the early aluminate hydration. The regions rich in sulfate form well-defined ettringite needles, whereas in regions with lower sulfate contents, a gel-like material (identified as an AFm type phase[38]) [27] forms. Inter-grinding gypsum with cement provides better physical distribution and thus a higher solubility that better controls early aluminate hydration and improves compressive strength. The fineness and particle size of gypsum also affect its solubility and, therefore, it may influence the optimum SO_3 content. It was reported that higher gypsum fineness lowers the SO_3 requirement [31].

The initial hydration rate of C_3A is significantly influenced by the type of sulfate source due to differences in solubility and dissolution rates [28]. The solubility of different calcium sulfate forms are shown in Figure 1-4 where the solid and dashed curves indicate the stable and metastable phases, respectively [39]. Hemihydrate ($CaSO_4 \cdot xH_2O$ (x=0.5 and 0.6)) (α and β forms) and soluble anhydrite ($CaSO_4$ (III)) are also used as sulfate sources in cements due to their higher solubility than gypsum. However, insoluble anhydrite ($CaSO_4$ (II)) - burnt anhydrite can lead to severe early stiffening and higher water demand [24, 27]. Therefore, the presence of hemihydrate and soluble anhydrite are more desirable in the system. The literature indicates for gypsum-C_3A early reaction, formation of monosulfoaluminate and ettringite can occur while under the same experimental conditions, the presence of hemihydrate prevents precipitation of monosulfoaluminate in the first few hours of the reaction [28]. It can therefore be concluded that the form of sulfates interground with portland cement clinker will affect the phase assemblage of a cementitious system and subsequently rheology and durability of concrete.

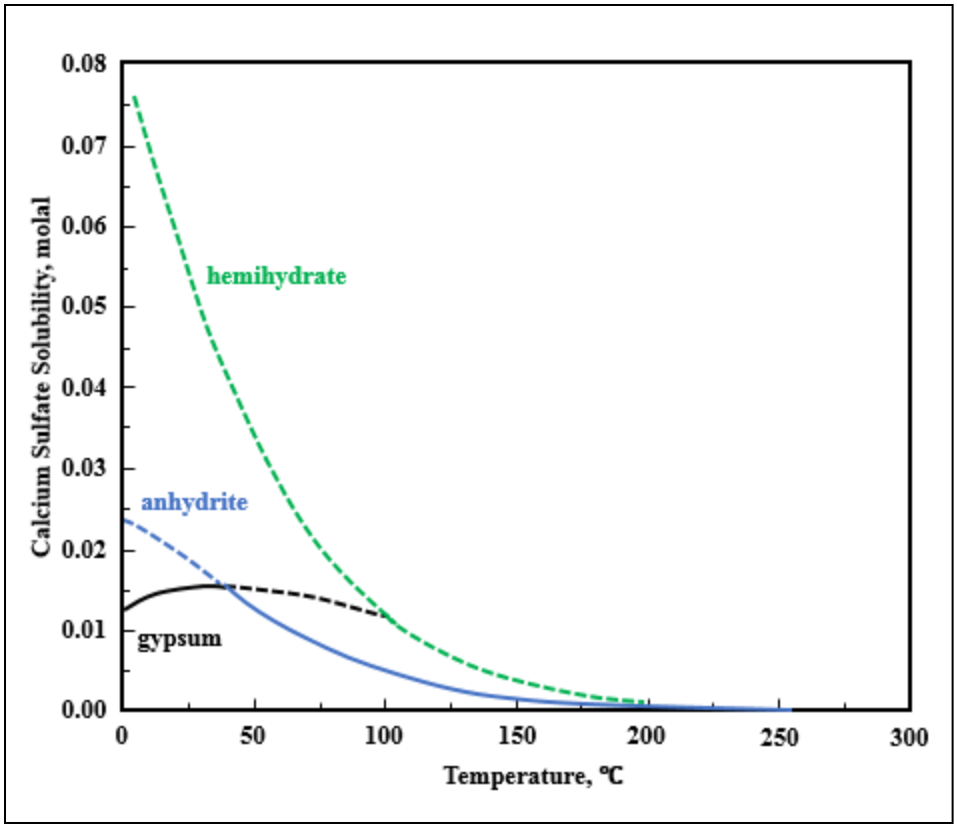

Figure 1-4: Solubility of different calcium sulfate forms (adapted from [39])

1.2.4.2 Alkalis

The presence of alkalis is known to accelerate both alite and aluminate hydration. More detailed studies on alkalis indicate that the role of alkalis depend on the form in which they are present in a cement clinker. If alkalis are present as oxides, they are typically incorporated into the crystal lattice of clinker minerals. However, if present as alkali sulfates, they occur as a distinct mineral with higher solubility [40]. Lerch [29] work showed that the aluminate phases are more reactive when alkalis are present and, therefore, a higher sulfate content is required for proper retardation. This was later confirmed by several other researchers [2, 5, 11, 31].

Whether alkalis are present as oxides or sulfates will reflect on their effect on cement hydration. However, potassium and sodium oxides or sulfates do not necessarily have an equivalent effect on cement hydration kinetics. C_3A hydration is considerably decelerated by the presence of Na_2O and accelerated by K_2O [40]. Furthermore, it was noted that setting times were greatly reduced by K_2SO_4 compared to Na_2SO_4 [40]. This is due to the formation of syngenite

($K_2SO_4 \cdot CaSO_4 \cdot H_2O$) which leads to quick setting and also the consumption of sulfates thus affecting the retardation of C_3A hydration [42].

The presence of alkalis in cement can have a significant effect on delayed ettringite formation (DEF) [43]. For cements high in SO_3 content, high alkali contents increase the expansion while for low SO_3 content cements, alkalis do not have any significant effect on expansion [37]. However, the effect of K_2SO_4 versus KOH on DEF is more pronounced than that of Na_2SO_4 versus Na_2O. However, Kelham [38] indicates that K_2SO_4 and KOH have the same effect on DEF, if additional sulfate is present with KOH such that there is similar K_2O and SO_3 contents in the system. Taylor et al. [37] reported that the ettringite volume increases due to the increase in the rate of hydration in systems with high alkali and SO_3 contents. However, it is also stated that although high sulfate amounts are required for high alkali cements, these cements can resist excessive expansion as high pH conditions are less favorable for ettringite precipitation [44]. On the other hand, during storage in water, alkalis would leach out and the pH of the pore solution would decrease, favoring the release of adsorbed sulfates from C-S-H and, consequently, monosulfate would be replaced by ettringite [37]. Nevertheless, these alkalis are often present in cements as sulfates, and therefore, the initial sulfate content in the cement can be high, and the required additional SO_3 content to retard the aluminate hydration can be less, as a result.

Correlations derived between the optimum SO_3 and C_3A and equivalent Na_2O in cement systems show the influence of alkalis on the optimum at a given fineness (Equation 1-1 and 1-2) [42]. These correlations indicate a high dependence of the optimum sulfate content on cement equivalent alkali content.

$$\text{Opt } (SO_3\%) = 1.841 + 0.0950\ (C_3A\%) + 1.6364\ (\text{Equivalent } Na_2O\%) \qquad \text{Equation 1-1}$$

$$\text{Opt } (SO_3\%) = 0.789 + 0.1149\ (C_3A\%) + 1.872\ (\text{Equivalent } Na_2O\%) \qquad \text{Equation 1-2}$$

1.2.4.3 Fineness

Cements with higher fineness have higher sulfate demand, especially in high C_3A cements, as the increase in surface area accelerates the rate of reaction and, as a result, more SO_3 is required to control the aluminate hydration [29].

1.2.4.4 Age

The SO_3 optimization method described in ASTM C563 [30] uses 1-, 3-, and 7-day compressive strengths for mortar cubes and heat of hydration obtained from isothermal calorimetry. As reported in the literature, the optimum SO_3 content with respect to strength increases with age to accommodate the higher C-S-H volume as more ettringite is required to minimize porosity [24]. It is found that the increase in optimum SO_3 at an early age is significant compared to that at a later age; increase in optimum SO_3 level from 1 day to 3 days is higher than that from 3 days to 7 days (Figure 1-5). Therefore, it is reported that at least two optimum SO_3 levels for strength are required, one for early age and one for 28 days [31]. However, Hawkins [45, 46] suggested that SO_3 should be determined based on the 3-day compressive strength instead of 1-day strength as the 3-day strength optimization not only improved the strength but also the sulfate resistance by reducing porosity and drying shrinkage. The need to adopt a similar approach in SO_3 optimization in systems with SCMs such as slag (SCMs with high alumina contents) was also highlighted in the same study. The variation of optimum sulfate content as a function of time is shown in Figure 1-5, [46].

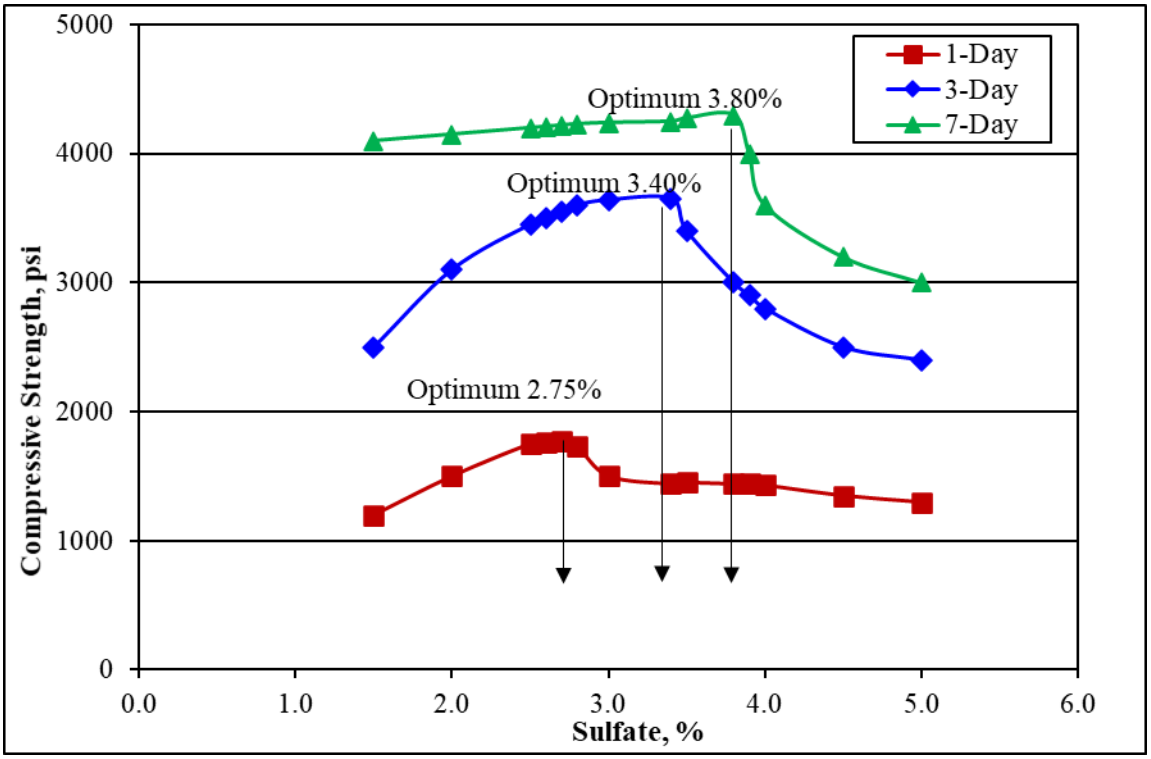

Figure 1-5: Optimum sulfate content as a function of curing time (adapted from [46])

1.2.4.5 Temperature

Curing temperature influences the optimum sulfate content. It was reported that higher temperatures increase the optimum sulfate level in portland cement and this value may exceed the maximum SO_3 limit at room temperature [24, 47]. Under steam-cured conditions (at 65°C), Zhang et al. reported increased sulfate levels of 4-5% [47]. This is likely due to the increase in the amount of sulfate adsorption by C-S-H with increasing curing temperatures. Desorption of these sulfates at later ages can lead to destructive expansion caused by DEF. This effect could be worse at higher sulfate levels [24].

1.2.4.6 SCMs Effects

When SCMs such as fly ash, slag, and calcined clay are added, the SO_3 requirement for the blended system is affected. This is mainly due to additional amorphous alumina added to the system from the SCMs [24, 25]. Moreover, the fineness, alkali content, calcite content, and SO_3 content in the SCMs also influence the optimum sulfate level in the blended system [24, 48, 49]. Hence, a re-optimization of the SO_3 content is needed. While several studies discussing SO_3 optimization in pure cement systems can be found in the literature, studies that investigate sulfate optimization in blended cementitious systems, including systems that incorporate chemical admixtures, are rare. Several studies conducted on SO_3 optimization in blended cementitious systems are briefly discussed in the following paragraphs [3, 6, 7, 17, 25, 48, 50] .

Tsamatsoulis and Nikolakakos [23, 26] used cements blended with fly ash and determined the optimum SO_3/clinker (CL) ratio at 7 days and 28 days. They also determined the optimum SO_3/CL ratio for three different cement systems. The optimum SO_3/CL ratios for the cement systems were approximately the same; however, the optimum SO_3/CL of the fly-ash-blended system was higher. Niemuth [24] also reported that the majority of SO_3 in fly ash is inert, but some can still contribute to SO_3 optimization, based on a multiple-correlation analysis of the optimum sulfate level for 1-day strength. This could be due to the unavailability of fly ash SO_3 in soluble forms at early age, because about 60% of the sulfate in fly ash used in this study was in $CaSO_4$ anhydrite form. However, cementitious blends with some fly ashes can have a higher demand for sulfates due to the presence of alkalis and C_3A in fly ash. Niemuth [24] used compressive strength and isothermal calorimetry to determine sulfate balance, focusing more on the high-calcium Class C fly ash. It was found that incorporating fly ash can increase the optimum sulfate level at 1 day,

and this effect was predominant in Class C fly ash, while low-lime Class F fly ash had little to no effect. He also reported that additions of K_2SO_4, $Ca(OH)_2$, and CaO increased the required optimum sulfate in the system.

Adu-Amankwah et al. [25] performed a study on the effect of SO_3 additions on hydration, microstructure, and strength of a portland clinker-slag-limestone cement system. Three systems with variable sulfate content (undersulfated, optimized, and oversulfated) were considered in this study through the addition of anhydrite. The findings indicated that increasing the sulfate level in the portland clinker-slag-limestone system resulted in an increase in ettringite content compared to AFm phases, coarser porosity, and a lower water content in the C-S-H phase. Ternary limestone cements (limestone added to the binary system of cement and slag) reduced the clinker factor while maximizing the efficiency of SCMs. The calcite from limestone in these cements reacts with aluminates to form hemi- and monocarboaluminate phases instead of monosulfate phases, which results in ettringite stabilization leading to a decrease in porosity and an increase in strength. However, this increase in ettringite volume is controlled by the adsorption of sulfates by C-S-H. Therefore, there appears to be two opposing effects occurring in the system with increasing sulfate additions: first, increasing sulfate content increases ettringite content which enhances the paste strength through reducing the microstructure total porosity and second, increasing sulfate content can decrease the C-S-H space filling capacity due to lower water content, which lowers the paste strength. Additionally, higher molar MgO-to-Al_2O_3 ratio (M/A) is an indication of the resistance to sulfate attack in this ternary system at the optimum sulfate content; Mg can help resist sulfate attack by binding Al to form hydrotalcite instead of monosulfoaluminate [51].

The influence of limestone additions on the optimum SO_3 content in portland cement was studied by Campiteli and Florindo [48] using Brazilian portland cement clinker, natural gypsum, and limestone. The limestone additions varied from 0 to 15% by weight and the Blaine fineness of the samples were 300, 400, and 500 m^2/kg. It was found that the optimum SO_3 decreased exponentially with increasing limestone content. This exponential decrease in optimum SO_3 content was explained as a combined effect of two occurrences: reduction of the clinker fraction in the system due to the limestone addition and, therefore, a lower C_3A content, and reaction between limestone and the clinker ($CaCO_3$ in limestone reacts with C_3A in the clinker to form carboaluminate phases). It is noteworthy that for the materials used in this study, the addition of limestone ground together with the clinker lowered the strengths compared to that of the system

with 0% limestone addition (only portland clinker and gypsum), even at optimum SO_3, and at all addition levels and fineness. This strength decrease was attributed to the increase in the water-to-clinker ratio due to the reduced clinker fraction.

The properties of metakaolin-blended pastes (30% by weight) and mortars were investigated by Moulin et al. [50] considering several potential activators for metakaolin. These blends were prepared by intergrinding. They studied the rheological behavior, initial setting time, and compressive strength development by varying the total sulfate content, type of the added $CaSO_4$, and the free lime content. Three levels of total SO_3 contents were considered: 3%, 3.5% and 4% by weight of clinker. For each sulfate content, three types of sulfates were considered: 100% gypsum, 100% hemihydrate, and a blend of 50% gypsum + 50% hemihydrate. It was observed that the type of calcium sulfate does not affect the 3-day compressive strength while the rheological properties appear to be influenced.

Antonio et al. [17] investigated the coupled substitution of metakaolin and limestone in portland cement. Isothermal calorimetry results showed the effect of metakaolin on the sulfate depletion point, which was that higher metakaolin content resulted in stronger and earlier peak occurrence. The system with higher levels of metakaolin appeared to be undersulfated as the sulfate depletion point and the main hydration peak were not clearly distinguishable. Increasing gypsum content showed distinguishable peaks and the compressive strength at 1 day was improved. Therefore, the impact of the addition of extra gypsum when using calcined clay to maintain proper sulfate balance is important, as it affects the early-age strength by controlling the aluminate reaction.

In a study performed to evaluate the pozzolanic activity of calcined clay in LC^3 systems of varying kaolinite content, Avet et al. [7] optimized the sulfate-to-calcined-clay mass ratio using heat flow curves and the rapid, relevant, and reliable pozzolanic activity test, R^3. The optimized ratio was identified as that which corresponds to the highest total heat, which favors the formation of ettringite at about 1 day of hydration. Increasing the sulfate/calcined clay ratio above this value decreased the total heat, indicating a slower pozzolanic reaction.

1.3 Concrete Temperature Rise

Cement hydration is accompanied by heat evolution, which results in a temperature rise in concrete. The heat evolution of mass concrete such as dams, footings, and bridge piles is particularly important as restrained volume change during or after a high temperature rise can

cause cracking in these structures. Temperature gradients are generated within a mass concrete element when the heat being produced is dissipated to the surrounding environment resulting in a lower temperature at the surface of concrete compared to that of the interior. This temperature differential causes contraction of the concrete element. Moreover, tensile stresses can be induced due to an external restraint on the deformation of the concrete element. Cracking occurs when the tensile stresses are larger than the early-age tensile strength of concrete. Thermal cracking can occur not only in mass concrete, but also in other concrete structures such as concrete pavements, walls, etc. [52]. In addition to the cementitious system heat of hydration, concrete temperature rise is affected by the size of the concrete element and the specific heat capacity, thermal diffusivity, and emissivity of the concrete [53].

1.3.1 SCMs Effects

The use of SCMs as a partial replacement of cement in concrete mixtures is considered a viable solution to minimize the potential of thermal cracking in massive elements. As stated previously, temperature rise in mass concrete is critical, because it is the primary factor which governs thermal cracking at early-ages. Several studies reported in the literature [20, 54, 55], indicate that partial replacement of cement by SCMs such as fly ash (FA) or ground granulated blast furnace slag (GGBS) can reduce the heat of hydration and thereby reduce concrete temperature rise. The pozzolanic reaction generates less heat than OPC and is equivalent to C_2S reaction [32, 55]. However, not all SCMs can reduce the heat of hydration. SCMs such as silica fume (SF) and metakaolin (MK) generate higher hydration heats (per unit mass of material reacted) than OPC; therefore, such SCMs can adversely affect the temperature rise in concrete [56, 57]. In 1957, Khanna and Puri [58] reported on the use of calcined shale as a pozzolan in concrete used in constructing the Bhakra Dam in India. After performing extensive testing, they advocated the use of calcined shale as a partial replacement of cement in concrete for dam construction as it reduced the heat generation [58]. In general, the amount of heat generated by a specific SCM will depend on the material chemical composition, physical properties, reactivity, dosage, and temperature. In this regard, LC^3 is a relatively new cementitious system and, therefore, studies on the LC^3 system and their effect on concrete temperature rise are rare. Although this system has shown promising performance with respect to strength, its use in mass concrete, in which the temperature rise is a major concern, is still questionable.

1.3.2 Heat Evolution in LC^3 Systems

Few studies [17, 19, 49, 59, 60] discuss the heat evolution of limestone-calcined clay-cement systems. Incorporation of MK is known to accelerate hydration due to its higher fineness, which provides extra surfaces for heterogenous nucleation [49, 57]. This results in a higher heat release, causing a higher temperature rise in concrete [57]. Nevertheless, addition of limestone to these systems may reduce the heat release to a moderate extent according to isothermal calorimetry results [17].

Mishra et al. [60] studied the effect of a limestone-calcined clay (LC^2) blend on cement hydration with 10%, 20%, and 30% replacements of OPC with LC^2 (CC:L = 2:1) using isothermal calorimetry. Higher total heats were observed in the LC^2 blends. The rate of heat release curves of these blends showed a shift in the main hydration peak indicating an acceleration of hydration. As stated in the literature [49], [17], the use of calcined clays with high surface area significantly affects the reactivity of the aluminate phases. The aluminate peak corresponding to sulfate depletion in these systems occurs earlier and stronger with higher calcined clay contents and, therefore, the system appears undersulfated, as the sulfate depletion peak occurs prior to the main silicate hydration peak. This illustrates the importance of adding extra sulfate to achieve a properly sulfated system, as discussed in Section 1.2.

Avet [59] investigated the effect of calcined kaolinite content on the kinetics of LC^3 hydration. LC^3-50 blends incorporating 50% clinker and calcined clays with kaolinitic contents of 50.3% and 95% were studied. Quartz was used as an inert material to assess the filler effect. Due to the filler effect of calcined clay, the C_3S hydration in LC^3 blends was enhanced as observed by a higher slope of the main hydration peak. Moreover, the intensity of the peak increased with increasing calcined kaolinite content, indicating the onset of the reaction between the metakaolin and portlandite. Similar trends were observed in the cumulative heat release curves. Although the system with the highest kaolinite content showed the highest heat release initially, after 3 days, the rate of heat release was notably lower, and after 5 days the total heat of this system was lower than that of the blend with 50.3% kaolinite content. This was likely due to limited available space for hydration to proceed. However, this effect was not observed in the strength results up to 7 days, as the strength was linearly correlated with the calcined kaolinite content.

1.4 Sulfate Durability

Sulfates are widely distributed in soil and seawater. Many concrete structures are exposed to sulfate-bearing environments, such as piers in soil or sea water, coastal dams, and pavement slabs. Most soils contain sulfates in the form of gypsum ($CaSO_4 \cdot 2H_2O$), but the solubility of gypsum in water at ambient temperatures is low. Higher concentrations of sulfates in groundwater and soil are caused by the presence of magnesium, sodium, and potassium sulfates [61]. When sulfate ions penetrate hardened concrete, they can interact with the cement hydration products both physically and chemically. Depending on the metallic ion, the mechanism of attack can be different. Calcium sulfate will react with calcium aluminate hydrates to produce expansive ettringite ($3CaO \cdot Al_2O_3 \cdot 3CaSO_4 \cdot 32H_2O$). Reaction of magnesium sulfate and calcium hydroxide will form brucite ($Mg(OH)_2$) and gypsum with formation of ettringite and deterioration of the C-S-H binder. Sodium sulfate (Na_2SO_4) will also react with calcium hydroxide, to form gypsum and expansive ettringite [62].

Generally, pozzolan-blended cements increase the resistance of concrete to sulfate attack. However, a combination of cement and pozzolan may reduce the resistance if reactive alumina compounds are present in the pozzolan [62]. The incorporation of calcined kaolinitic clays can be beneficial for the durability of concrete, mainly due to pore size refinement and lime consumption by the pozzolanic reaction [63]. However, due to additional alumina introduced to the cementitious system by the clay, there is an increase in the calcium aluminate hydrate content in the system that subsequently could enhance the formation of expansive ettringite when exposed to external sulfates. In addition, the use of calcined clays with high surface area significantly improves the reactivity of aluminate phases, which will change the hydration process and of the corresponding hydration products if not properly sulfated [17]. There has been a concern that limestone-calcined clay cement, which contains both additional aluminates and carbonates, will have a higher potential to experience external sulfate attack. Some recent research studies have been done on this topic, and the overall effect of this ternary system on sulfate durability depends on many factors that require further research.

1.4.1 Mechanism of External Sulfate Attack

Degradation of concrete can happen as a result of physical and chemical reactions between hydrated portland cement and sulfate ions; the reaction products are less dense than the reactants,

leading to a total volume increase that can manifest in the form of expansion and cracking of the concrete. After cracking, sulfates can penetrate the concrete easier and accelerate the process of deterioration. Sulfate attack can cause strength decrease and loss of mass due to reduced cohesiveness of the cement hydration products [61].

1.4.1.1 Physical Sulfate Attack

Physical sulfate attack is related to the diffusion and precipitation of dissolved sulfate salts in concrete pores. The sulfates will crystallize in the pores, especially due to drying and evaporation, which tends to concentrate the sulfate ions near the surface where evaporation occurs. The volume increase of the crystallized sulfate salts exerts internal pressure in the concrete that can cause cracking and spalling of the surface [64].

The most common type of pernicious sulfate is sodium sulfate. Two crystalline forms of sodium sulfate exist: thenardite ($NaSO_4$) and mirabilite ($NaSO_4 \cdot 10H_2O$) depending on temperature and RH as shown in Figure 1-6. Precipitation of mirabilite generates crystallization pressure resulting in tensile stresses and cracking of concrete [65].

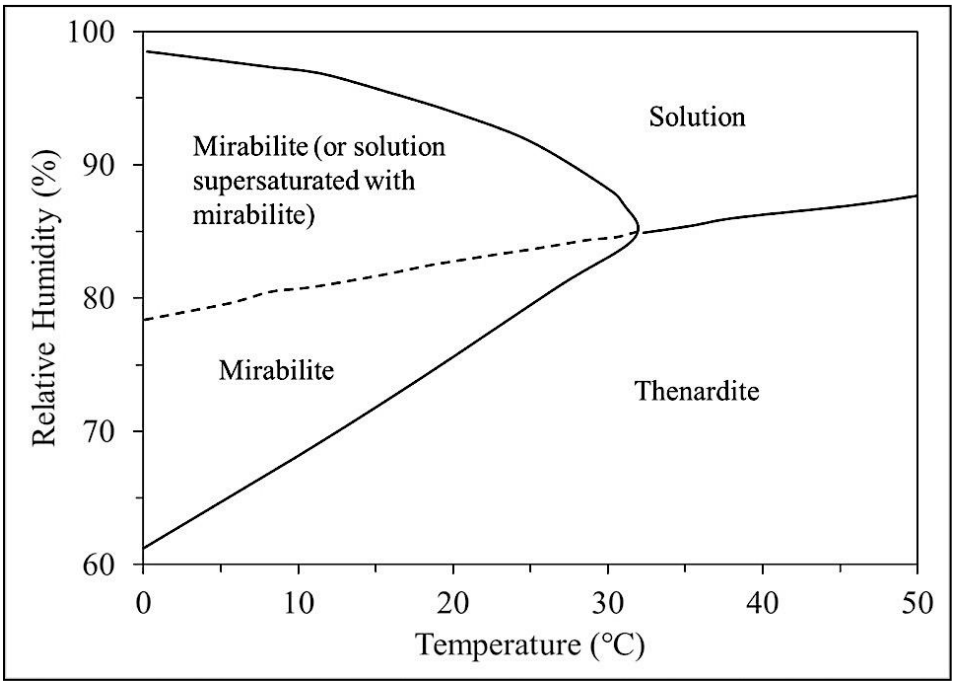

Figure 1-6: Phase diagram for sodium sulfate (adapted from [65])

Damage in physical salt attack will be favored if cyclic wetting and drying exists [66]. The high supersaturation due to dissolution of thenardite leads to precipitation of mirabilite and subsequently crystallization pressure. This is why the damage occurs during the rewetting step [65].

1.4.1.2 Chemical Sulfate Attack

When concrete is exposed to an external source of sulfate, the most common chemical reaction sequence related to AFm/AFt phases [67] can be expressed by the following equations:

$$CH + SO_4^{2-} \rightarrow C\bar{S}H_2 + 2OH^- \qquad \text{Equation 1-3}$$

$$C_4A\bar{S}H_{12}\ (AFm) + 2C\bar{S}H_2 + 16H \rightarrow C_6A\bar{S}_3H_{32}\ (AFt) \qquad \text{Equation 1-4}$$

There is general agreement that sulfate-induced ettringite precipitation is accompanied by an expansion in solid volume of about 120% [32]. During the past decades, several theories have been proposed for possible explanation of the expansion caused by formation of ettringite, such as swelling pressure [68], topochemical growth [69], and crystallization pressure [70]. Recently, crystallization pressure theory has been supported by several observations, which indicates that crystal growth under supersaturation of the pore solution is the most likely mechanism for expansion [71]. During the sulfate ingress process, sulfate ions first react with aluminate hydrates in larger pores to form ettringite without expansion. Once these aluminate hydrates are consumed, the concentration of sulfate ions in the pore solution increases, leading to supersaturation of the pore solution and precipitation of ettringite crystals within small confined pores (less than 0.1 μm) in the C-S-H, thus leading to expansion of the cement matrix [71]. Mullauer indicated a stress of up to 8 MPa can occur due to formation of ettringite in small pores (10-50 nm), which exceeds the tensile strength of the binder matrix. Comparing to the situation in small pores, the expansion of ettringite precipitation in larger pores is negligible as a result of insufficient pressure generated [72].

In addition to ettringite-induced expansion, deterioration can also be caused by the degradation of the calcium silicate hydrate (C–S–H) gel through decalcification in the presence of magnesium sulfate. This process leads to loss of C–S–H gel cohesiveness and stiffness, thus leading to overall deterioration of the cement paste matrix [73].

In the presence of carbonates and particularly at lower temperatures, another type of sulfate attack may also occur as a result of formation of thaumasite ($CaSiO_3 \cdot CaCO_3 \cdot CaSO_4 \cdot 15H_2O$). This type is commonly known as thaumasite sulfate attack (TSA), which is different from conventional sulfate attack in that it involves calcium silicate hydrate and carbonate ions rather than aluminate hydrates and portlandite. These reactions may result in expansion and softening of the hardened cement pastes, finally leading to cracking and loss of strength [74].

The mechanism of thaumasite formation has been widely discussed and two different mechanisms are proposed by Bensted, including direct reaction between calcium, carbonates, sulfates, and silicates (from C-S-H), or indirectly between ettringite, silicates, and carbonates [75]. Crammond proposed that the formation could be from ettringite by substituting silica and sulfate ions for alumina and carbonates ions, respectively [76]. The two possible routes of reaction are given below:

$$3Ca^{2+} + SiO_3^{2-} + CO_3^{2-} + SO_4^{2-} + 15H_2O \rightarrow 3CaO \cdot SiO_2 \cdot CO_2 \cdot SO_3 \cdot 15H_2O \qquad \text{Equation 1-5}$$

$$C_3S_2H_3 + C_6A\overline{S}_3H_{32} + 2C\overline{C} + 4H \rightarrow 2C_3S \cdot \overline{C}\overline{S}H_{15} + C\overline{S}H_2 + AH_3 + 4CH \qquad \text{Equation 1-6}$$

The product is a white, mushy, non-cohesive substance without binding capacity. In general, it is preferentially formed at low temperatures (< 15℃) in the presence of calcium silicate, sulfate and carbonate ions, and sufficient moisture, but small quantities also formed at room temperature [77, 78]. Formation of thaumasite at room temperature is thermodynamically very slow, but it remains stable up to 30℃ once it is formed [79]. Bellmann and Stark stated that thaumasite can be formed from C-S-H and portlandite at very low sulfate levels, but higher sulfate level is required if without portlandite [80, 81].

The crystal structure of thaumasite is similar to ettringite where alumina is substituted by six-fold-coordinated silicate ions, and it is also a member of the AFt phases [82]. In fact, the presence of ettringite is considered as a precursor for thaumasite formation and ettringite controls the rate of thaumasite formation [83]. Research shows that thaumasite starts to form only after all alumina has reacted to form secondary ettringite and it precipitates very slowly due to its slow reaction kinetics [84]. Presence of concrete cracks is a prerequisite for the formation of thaumasite [85].

1.4.2 Influence Factors

1.4.2.1 Curing

External sulfate attack is driven by the ingress of sulfate ions, mainly through diffusion. Therefore, the sulfate durability significantly depends on the pore structure and the use of a lower water-cementitious ratio (w/cm) will improve concrete sulfate resistance. The higher w/cm is accompanied by higher porosity and permeability which favors sulfate ingress and lowers durability.

Proper curing, which is beneficial to concrete pore structure refinement, will influence the sulfate resistance. Additional moisture curing will lead to higher degree of hydration and finer pore structure. However, some research shows that the resistance to sulfate ingress of concrete under air-curing is higher than for water-curing. This is attributed to the formation of a carbonation layer that improves impermeability [86].

1.4.2.2 Impact of the Type of Cation and Anion Combinations

The accompanying cation introduced with sulfates affects the mode of sulfate deterioration. Comparatively, calcium sulfate is the least aggressive sulfate salt due to its low solubility. Sodium sulfate is the most common type, and it is abundant, especially in seawater and coastal areas. Another kind of alkali sulfate is potassium sulfate, which is also seen in field exposures. Rapid expansion was found by Kunther when mortars were immersed in potassium sulfate solution, which indicates that potassium ions can accelerate the deterioration process. He also predicted, using thermodynamic modeling, the presence of syngenite ($K_2Ca(SO_4)_2 \cdot H_2O$) in addition to ettringite [87].

Magnesium sulfate attack is more severe than for sulfate attack emanating from the presence of any of the other previously discussed sulfates. Products from the reaction between magnesium sulfate and calcium hydroxide include gypsum and magnesium hydroxide (brucite). Brucite will form a layer to help prevent penetration of sulfates, but it is weak and eventually will break, especially when the pH is high [88]. The solubility of brucite is very low and the pH of a solution saturated in brucite is only 10.5, which is not enough to maintain the stability of the hydration. Subsequently, decalcification of C-S-H occurs [67, 89].

Research shows that the combination of anions, for example sulfate and chloride ions coexisting in the sea water, can influence each other and modify the resistance against sulfate

attack. Studies showed that specimens in chloride-sulfate solution performed better than in sulfate solution alone [90, 91]. Proposed explanations include [92]: (a) C_3A in the cement can capture free chloride to form chloroaluminate compounds, which have no expansion and can decrease the potential for ettringite formation; (b) The preferential diffusion rate of chloride versus sulfate makes chloride quickly penetrate into concrete and react first with the C_3A, thus limiting the formation of ettringite; and (c) The higher solubility of ettringite in chloride solution leads to a decrease of ettringite precipitation. On the other hand, the presence of sulfates can weaken chloride binding, allowing some bound chlorides to be released and become free chlorides. Moreover, sulfates can limit the formation of Friedel's salt and promote the conversion of Friedel's salt to ettringite [92, 93].

1.4.2.3 Effect of Cement Composition

Studies have indicated that the use of Type V cement (low C_3A) may not prevent damage caused by sulfate attack. In some cases, cement without C_3A did not provide resistance to sulfate attack [94]. The formation of gypsum is also found to be expansive and tensile stresses developed during gypsum formation may lead to significant expansion [95]. Tian and Cohen conducted experiments on hydrated C_3S paste and found that formation of gypsum also caused expansion in C-S-H gel [95].

Although sulfate deterioration is mainly caused by expansion of the concrete, some concrete damage has been found to be caused by softening and spalling. This effect has a strong relationship with gypsum formation through interactions between sulfate ions and portlandite. Gypsum is also found to damage concrete through mass and strength loss of concrete as well as softening [96].

1.4.2.4 Effect of SCMs

There is general consensus in the literature that the use of SCMs such as fly ash, slag, silica fume, and metakaolin mitigates external sulfate attack. This is primarily due to the nature of the pozzolanic reaction, which results in pore size refinement and lime consumption. However, pozzolans may not always be effective in reducing the damage from physical salt attack. For example, mirabilite precipitation could be more damaging in a refined pore system due to an increased number of smaller diameter pores. The increased capillary suction and higher surface area for drying also contribute to this damage [97].

Cement blended with fly ash can effectively improve the resistance against chemical sulfate attack due to both dilution of portland cement and consumption of portlandite. However, the composition of the fly ash plays an important role. Class C fly ash, rich in lime and other reactive minerals, aluminates, and C_3A, may perform poorly. However, silica fume blended systems provide excellent sulfate resistance as a result of denser microstructure and the finer particle size of silica fume [98]. The behavior of slag is largely dependent on the replacement level, physical characteristics, and chemical composition. High replacement levels usually show better resistance, especially with high-alumina slags. Typically, slag cement modifies the calcium-silicate-hydrate phase, resulting in a lower calcia/silica ratio, and allows binding of more alumina, thus improving resistance [99]. If not properly sulfated, AFm phases can form which can be monosulfoaluminates, depending on the chemistry of the slag. Fernandez-Altable concluded that the overall resistance depends on the amount of AFm at low replacement levels and the total alumina content at high levels [100].

Calcined kaolinite clay is chemically different from many other SCMs in that it has a very high alumina content. After calcination, metakaolin, which has a high pozzolanic reactivity, is the main component of kaolinitic calcined clay [101]. The reaction products of metakaolin and portlandite are calcium-silicate-hydrate (C-S-H) and calcium aluminosilicate hydrates (C_2ASH_8). This has a positive effect on durability in the sulfate environment in several aspects. The replacement of portland cement with calcined clay dilutes the tricalcium aluminate hydrate in the cement paste matrix. In addition, the secondary product of C–S–H, although less dense than the primary C–S–H gel, is effective in filling large capillary pores to produce small, discontinuous capillary pores. Thus, due to the refinement effect, the total porosity and permeability of concrete decreases and the resistance against sulfate attack is enhanced [102]. Reviews conducted by Sabir et al. and Siddique et al. on the use of metakaolin showed abundant examples of porosity and permeability reduction [101, 103]. Ramlochan reported that sulfate attack is reduced with a high addition of metakaolin independently of C_3A content, and cementitious systems containing 25% of metakaolin have high sulfate resistance[104]. Even lower amounts (10 to 20%) were found effective in improving the resistance of mortar to sulfate attack. The 20% replacement reduced the expansion effectively by 58–77% at 6 months and by 69–89% at 12 months with the respect to pure cement [105]. However, the incorporation of a large amount of aluminates in the calcined clay will also lead to the reaction with sulfate to form ettringite. The overall effect depends on

many factors, such as clay reactivity, aluminate content, sulfate balance, and the external environment, which needs to be investigated further.

1.4.2.5 Limestone and Limestone-Clay Combinations

The addition of limestone directly affects cement hydration products. Limestone can act as a filler and provides nucleation sites, thus accelerating early-age hydration and reducing initial porosity [106]. According to Soroka and Stern [107], the addition of limestone improves the sulfate resistance of portland cement mortars. This has been attributed to both physical and chemical effects.

Research shows that the main impact of limestone additions on the sulfate durability is physical in nature. A five percent limestone addition can reduce the porosity of cement paste and the rate of sulfate ingress; however, high levels of replacement (25%) accelerate sulfate attack [108]. Irassar concluded that low levels of replacement (< 10%) would not be harmful but the resistance would worsen at high levels. This is attributed to the increase in the effective water-to-cement ratio causing higher porosity and permeability [109]. Gonzáles and Irassar investigated the effect of limestone filler and concluded that the addition of limestone filler may increase or decrease the sulfate performance depending on the mineralogical composition of the portland cement clinker, the replacement level, and the equilibrium between increasing the degree of hydration before the exposure and the increased porosity due to increased water-to-cement ratio by filler addition [110]. A recent study shows the decline of strength and resistance with increasing limestone content at constant w/c. Limestone content also makes concrete more sensitive to the minimum moist curing time. Significant deterioration was noted with shortening the curing time in presence of limestone [111].

The presence of limestone also influences the hydration products of the aluminate phases. Without limestone, C_3A reacts with gypsum to form ettringite, and after consumption of gypsum, some of the ettringite reacts with the remaining C_3A to form monosulfoaluminate. When limestone exists, small quantities of calcite react with C_3A to form hemi- and mono-carboaluminate instead of monosulfoaluminate. Hemicarboaluminate is kinetically favored but is less stable and will gradually convert to monocarboaluminate after one week [112]. This reaction leaves more sulfate for cement to form ettringite and prevents the transformation of ettringite to monosulfoaluminate in the hydration products. Therefore, less monosulfoaluminate and more ettringite exist in systems containing limestone, leading to lower potential for damage caused by external sulfate attack [113].

Thermodynamic calculations also demonstrate the stabilization of monocarboaluminate. It also causes a corresponding increase in the paste solid volume, thus decreasing paste total porosity by about 0.5% [106]. Ogawa stated that carbonate AFm phases, which are initially formed with the added carbonate, may very well convert to ettringite during sulfate exposure [114].

Limestone cement is more susceptible to the thaumasite form of sulfate attack at low temperatures. Thaumasite formation can cause total concrete degradation and loss of strength. When thaumasite attack occurs, the C-S-H matrix completely decomposes and turns into a white and pulpy mush. The time-to-failure was found to be inversely related to the limestone content [85]. At low temperatures, the type of sand has a remarkable effect on the performance of limestone-blended concrete for which calcareous sand shows better performance than siliceous sand. This is probably due to better cohesion between cement paste and calcareous sand. With siliceous sand, the higher the limestone content, the greater damage. With calcareous sand, however, damage is independent of the limestone content [115].

When calcined kaolinite clay and limestone are added simultaneously, the reactive alumina in clay reacts with limestone and portlandite to form mono- and hemi-carboaluminate, resulting in a refined pore structure that inhibits the ingress of sulfate ions. Yu et al. studied limestone-calcined clay-cement systems at replacement levels of 15%, 30%, and 45% for a 1:2 limestone-clay combination, discovering that mono- and hemi-carboaluminate content increased with increasing replacement level. The expansion rate as well as the amount of ettringite and gypsum formed in the blended system was less, indicating that the addition of calcined clay and limestone could mitigate sulfate ingress. After 180 days in 5 wt% sodium sulfate solution at 20°C, nearly all the monosulfate and portlandite were consumed, indicating the specimen center had been affected by the incoming sulfate. At the same time, they detected that the amounts of mono- and hemi-carboaluminate on the surface were lower than the center, indicating that they can also react with sulfate ions to form ettringite [116]. Although this transformation can occur, the addition of calcined clay and limestone significantly decreased the expansion rate, and reduced the loss of dynamic modulus and mass of mortar specimens, when exposed to sulfates, due to lower permeability, thus resulting in improved sulfate resistance [116].

Limestone cement with SCMs besides metakaolin was also found to have a higher resistance to thaumasite sulfate attack [85]. Higher replacement levels with SCMs dilute the C_3A content, which should reduce ettringite and thaumasite formation. As indicated previously, CH

reacts with sulfates to produce gypsum, which can further react to form ettringite, and subsequently thaumasite, through the indirect route described in Equation (1-4). In the thaumasite formation process, CH acts as a reactant rather than a product [117]. Research shows that the calcia/silica ratio of C–S–H plays a vital role in its resistance against thaumasite sulfate attack. In the presence of CH, this ratio is in the range of 1.6 to 1.8 and calcium-rich C–S–H can easily be converted into thaumasite. However, it was estimated that this ratio would be between 0.8 and 1.2 without the presence of CH, and therefore silica-rich C–S–H would show higher resistance against thaumasite attack [81]. Calcined clay is also thought to benefit sulfate resistance through consuming portlandite, thus reducing the potential for secondary formation of gypsum and ettringite [118].

1.4.2.6 Impact of pH of Concrete Pore Solution

The pH of the concrete pore solution and sulfate-containing water in the environment are important factors in the aggressiveness of the reaction between the sulfates and the cementitious system. The pH of the pore solution can change the predominant phases to experience sulfate-induced reactions [109]. Although sodium and magnesium sulfate solutions themselves are neutral, the evolution of the pH of the pore solution, in each, is different. In a sodium sulfate solution, the pH increases rapidly to nearly 12 due to CH dissolution, whereas in a magnesium sulfate solution, the pH may remain close to 7 due to brucite formation [119].

Gypsum precipitation is dependent on the sulfate concentration and the pH level of the solution. The gypsum precipitation is found to increase as the pore solution pH decreases [120]. The lower pH will also cause ettringite to decompose to gypsum. Research shows that ettringite decomposes at a pH of 10.7 and monosulfate decomposes at a pH of 11.6. At lower values of pH, only gypsum and aluminum sulfates are present [121].

The risk of thaumasite attack is found to increase with higher pH, and alkalinity can significantly accelerate the kinetics of thaumasite formation [122]. It is reported that thaumasite does not form at pH < 10.5, where it disintegrates and popcorn calcite forms in the deteriorated matrix [123]. Hobbs and Taylor postulated that pH of 12.5 is necessary for thaumasite formation, when calcium hydroxide is depleted from the surface of concrete [124]. Therefore, thaumasite sulfate attack might not be possible in lower pH levels where the damage is driven by gypsum formation.

1.5 Chloride Ingress

1.5.1 Mechanism and Effects on Cementitious Systems

Chloride ingress refers to the diffusion of chloride ions through the interconnected pore network in concrete. Chloride ions can result in a change in the pH of the concrete pore solution Additionally, chlorides can react with the hydration products such as the AFm phases:

(a) monosulfoaluminate ($3(CaO)_4 \cdot Al_2O_3 \cdot SO_3 \cdot (H_2O)_{12}$),

(b) monocarboaluminate ($(CaO)_4 \cdot Al_2O_3 \cdot CO_2 \cdot (H_2O)_{11}$) ,

(c) stratlingite ($((CaO)_2 \cdot Al_2O_3 \cdot SiO_2 \cdot (H_2O)_8$)

to form Kuzel's salt ($(CaO)_3 \cdot Al_2O_3 \cdot 0.5CaSO_4 \cdot 0.5CaCl_2 \cdot (H_2O)_{11}$) at low chloride concentrations and Friedel's salt ($(CaO)_3 \cdot Al_2O_3 \cdot CaCl_2 \cdot (H_2O)_{10}$ at higher concentrations [125]. As the pH of the pore solution decreases below ~ 11.5, the passive iron oxide film on the steel reinforcement begins to decompose [32]. In particular, chloride ions may form ferrous chloride corrosion products, in the absence of oxygen and/or soluble iron-chloride complex, on steel reinforcement [32]. The formation of the soluble iron-chloride complex results in the deposition of porous rust after the chloride is relieved from the complex and dissolves back into the pore solution following the two reaction mechanisms shown in Equations 1-7 and 1-8 [32].

$$Fe^{2+} + Cl^- \rightarrow [FeCl\ complex]^+ \qquad \text{Equation 1-7}$$

$$[FeCl\ complex]^+ + 2OH^- \rightarrow Fe(OH)_2 + Cl^- \qquad \text{Equation 1-8}$$

The amount of chloride ions needed to initiate reinforcement corrosion is defined as the chloride threshold concentration, and it varies depending on the cementitious system constituents, the type of reinforcement, and the pH of the pore solution in direct contact with the reinforcement.

1.5.2 Effects of Calcined Clays and Limestone on Chloride Ingress

Two primary factors dictate the extent to which chloride ions may migrate through a cementitious matrix: (1) microstructural permeability (pore connectivity, porosity, and pore entry size) and (2) chloride binding capacity of the cementitious system. SCMs are widely known for their ability to reduce cementitious systems' porosity and permeability by acting as both filler and reactive mineral. Calcined clay-blended cementitious systems have a more refined pore structure than neat cements as a result of their effects on nucleation and gel formation through the pozzolanic reaction. This in turn reduces the critical pore entry radius and limits the rate of chloride ingress

[20, 125]. To reveal the significant effect of the pore structure in cementitious system, Maraghechi et al. [125] were able to establish a trend in chloride diffusivity with the critical pore entry radius. Additionally, the chloride binding capacity of cementitious systems directly reduces the rate of chloride ingress by acting as a sink and removing chloride ions from the pore solution. This binding capacity is dictated by the hydration phase assemblage of the cementitious system. CSH and CASH have been shown to adsorb chloride ions and more readily do so with higher CaO/SiO_2 and CaO/Al_2O_3 ratios [126, 127]. However, chloride analysis of neat and calcined clay- and/or limestone-blended portland cements has revealed that the majority of bound chlorides are combined in Friedel's salt and not necessarily adsorbed by C-S-H or C-A-S-H [125, 128]. Thomas et al. proposed a nearly linear relationship between the formation of Friedel's salt and a given cementitious system's bound chloride content [129].

Maraghechi et al. [125] investigated chloride-induced corrosion of blended cements with calcined kaolin clays with a kaolin content between 17 and 95 wt.% using a 30 wt.% cement replacement in addition to ternary mixtures with an added 15 wt.% cement replacement with limestone. Total chloride analysis was performed using silver nitrate potentiometric titration. The results revealed reduced chloride contents and ion intrusion depths for all binary and ternary pastes, except for the calcined clay with only 17 wt.% kaolinite content, which was comparable with the control pastes [125]. The ternary blends revealed only slightly reduced intrusion depths than their binary paste counterparts. The chloride binding capacities of these mix designs were investigated and all binary and ternary cements revealed greater binding with the blends incorporating calcined kaolin clay, with 40-50 wt.% kaolin content having the greatest binding capacity [125]. Limestone was observed to insignificantly influence the binding capacity of ternary cement systems when compared to each clay's respective binary mixture designs. Maraghechi et al. [125] claim the observed reduction in bound chloride content and Friedel's salt content of pastes containing higher quality kaolin clays than those with 40-50 wt.% kaolin is attributed to ionic diffusion limitations caused from a reduction in paste porosity [41]. Mwiti [130] investigated chloride ingress resistance of an ordinary portland cement (OPC) and 800°C calcined clay (regions of Runyenjes - Kenya) blended cements using ASTM C1202 [131]. This procedure determines the electrical current passing through a cement paste exposed to a NaCl solution which has direct implications on the diffusivity of chloride ions in a given cementitious system. Blended portland cements were made using 25, 30, 35, 40, 45, and 50 % calcined clay with w/cm ratios of 0.4, 0.55, and 0.63. The

OPC showed the worst resistance to chloride ingress when compared to the calcined-clay cements. Mwiti [130] notes these results corroborate those reported by Al-Rawas et al. [132], Goncalves [133], and Muntasser [134] studies on chloride ingress in pozzolanic systems including calcined clay. The enhanced resistance of calcined clay-blended cements to chloride ingress is attributed to pore size refinement and lower pore connectivity due to the pozzolanic reaction [125 , 135]. The refinement in paste porosity and pore interconnectivity arises purely from the enhanced gel formation when calcined clays undergo pozzolanic reaction.

Blended cements with 30 and 35 wt.% calcined clay revealed the most resistive mix designs with respect to chloride ingress. Above 35 wt.%, calcined clay mix designs showed elevated levels of chloride ingress at all w/cm ratios. This phenomena was attributed to the inclusion of excess calcined clay which reduces the formation of hydrated gel phases by acting as a filler rather than a pozzolanic material. Furthermore, for all cements, there was an observed elevation in chloride ingress when the w/cm was increased. This observation is widely accepted to be caused by the higher permeability of cement paste when using elevated w/cm ratios, thus allowing for greater chloride diffusivity [101, 130, 136]. Mwiti [130] made sure to note that Al_2O_3 is known to bind chloride ions and results in the formation of Friedel's salt in cementitious systems [137]. Thus calcined clay systems with higher Al_2O_3 content than ordinary portland cements will lower the rate of chloride ingress into a given cementitious system by chemically binding chloride ions in the cementitious system [130, 138–140]. However, Mwiti [130] did not assess the chloride binding capacity of the calcined-clay cementitious systems [130]. Yet, this work states that the expected enhanced binding effect of the blended systems may not be sufficiently predominant to outweigh the porosity refinement effect on chloride ingress. However, it should be noted that Mwiti [130] did not provide any physical or mineralogical characterization of the raw materials or hydrated paste when assessing the chloride ingress in the calcined clay-blended cementitious systems. A microstructural and mineralogical analysis of the raw materials and hydrated pastes would have contributed significantly to this paper's discussion of the underlying mechanism(s) responsible for the observed chloride ingress behavior.

Shi et al. [141] have investigated the effects metakaolin (MK), limestone (LS), and silica fume (SF) on the durability of portland cement mortars, individually and as blended systems, using a constant cement replacement level of 32 wt.% with SCMs. Mortar cylinders were made and subjected to concentrated chloride solutions (2.8M NaCl) for 35 days [141]. After exposure, the

cylinder layers were ground and Cl^- contents were measured using methods similar to those proposed in ASTM C1556 [142] and ASTM C1152 [143]. LS mortars showed elevated Cl^- concentrations at a given depth when compared against the control and this was attributed to its slightly greater porosity [141]. However, MK alone and with LS produced mortars with much greater resistance to ingress than the control, but revealed similar Cl^- concentrations to one another at any given depth after exposure. Similar to Mwiti [130] and Maraghechi et al. [125], the excellent resistance of the blended cements to chloride ingress has been attributed to the refined pore networks and reduced pore connectivity in the blended systems when compared against the control [141].

1.6 Carbonation Corrosion

1.6.1 Mechanism and Effects on Cementitious Systems

Portland cement concrete pore solution has an intrinsically high pH such that the alkaline environment passivates the reinforcing steel against corrosion. However, when CO_2 from the atmosphere dissolves into the pore solution of a cementitious system, an equilibrium is established between carbonic acid (H_2CO_3), bicarbonate (HCO_3^-), and carbonate anions (CO_3^{2-}) following the 3 reaction mechanisms shown below in Equations 1-9 through 1-11.

$$CO_2(aq) \leftrightarrow H_2CO_3(aq) \qquad \text{Equation 1-9}$$

$$H_2CO_3(aq) \leftrightarrow H^+(aq) + HCO_3^-(aq) \qquad \text{Equation 1-10}$$

$$HCO_3^-(aq) \leftrightarrow H^+(aq) + CO_3^{2-}(aq) \qquad \text{Equation 1-11}$$

The dissolved CO_2 in the pore solution first binds with the available alkalis and then portlandite to form carbonates, predominately calcite ($CaCO_3$), which in turn reduces the alkalinity of the pore solution [32]. C-S-H may also be carbonated by the dissolved CO_2 causing reductions in the $CaO:SiO_2$ ratio and the water content in the CSH following the reaction mechanism shown in Equation 1-12 [32].

$$CSH + CO_2(aq) \rightarrow CSH + CaCO_3 + H_2O \qquad \text{Equation 1-12}$$

Susceptibility of a cementitious system to carbonation has been shown to be a function of the relative humidity (RH), with ~ 40-70% RH causing the highest rate of CO_2 dissolution [32, 144, 145]. At a lower or a higher RH, the pore solution is not efficient for effective CO_2 dissolution

[32]. The reduction in pH of the pore solution, accompanying carbonation, renders the steel reinforcement susceptible to oxidation. Furthermore, carbonation of the hydration phases is accompanied by irreversible carbonation shrinkage [32] and coarsening of the pore system, which could result in further carbonation via an increased surface area [144, 146]. Johannesson and Utgenannt [147] have reported that carbonation shrinkage in portland cement mortars is more readily observed through differences in pore size distribution rather than differences in specific surface area. However, the precipitation of calcite has been shown to contribute to the clogging of pore space, which may reduce CO_2 diffusivity and enhance concrete resistance to carbonation [148, 149]. Carbonation shrinkage can result in a strength loss and severe structural deformation likely to cause cracking [32].

1.6.2 Effects of Calcined Clays and Limestone on Carbonation

Shi et al. [144] have investigated carbonation in portland cement mortar bars incorporating metakaolin (MK), limestone (LS), and a blended system with a 3:1 MK:LS with a total cement replacement level of 35 wt.%. Mortar bars were cured saturated for 91 days and then cured in an incubator for another 91 days with a 1 vol.% CO_2 atmosphere at 57% RH. The incubator atmospheric CO_2 concentration was higher than would be realized under ambient conditions. It is worth noting that Leemann et al. [150] compared the carbonation rates of portland cement concretes when exposed to a 1% and 4% CO_2 atmosphere and obtained a linear correlation between the carbonation rates and CO_2 concentration. Shi et al. [144] measured the carbonation depths in mortars using a 1 % phenolphthalein pH indicator. Thermodynamic modeling was also used to predict the hydration phase assemblage of mortars of interest to understand the carbonation behavior. The worst performing mortar was the LS mortar. This was attributed to a higher porosity and higher pore connectivity when compared to the control mixture [144]. However, the pure MK and blended MK+LS mortars revealed similar total connected porosities, pore entry sizes, and degrees of carbonation [144]. Interestingly, the control mortar revealed the greatest resistance to carbonation, though it showed greater pore entry sizes than the MK and MK+LS mortars [144]. Thus, carbonation trends reported by Shi et al. [144] cannot be attributed solely to the cementitious system porosity. Rather, carbonation behavior should be considered through a detailed examination of the dissolved CO_2 in relation to the binding capability of different phase assemblages in the cementitious systems [144, 146]. Additionally, modeling predictions and experimental results [144] showed the Ca:Si ratio of C-S-H in the control mortar is much higher

than in the MK and MK+LS blended mortars, which enhances CO_2 binding capacity of C-S-H in the control mortar [144, 151, 152].

1.7 Conclusion

Based on the thorough review of the current published literature, the use of limestone-calcined clay cements in concrete is an economical option that can render concrete durable provided that the system is properly sulfated and optimized for heat generation and carbonation potential.

1.8 References

[1] H. Justnes, "How to Make Concrete More Sustainable," *J. Adv. Concr. Technol.*, vol. 13, no. 3, pp. 147–154, 2015, doi: 10.3151/jact.13.147.

[2] A. Zayed, N. Shanahan, A. Sedaghat, Y. Stetsko, and B. Lorentz, "Final Report Development of Calcined Clays as Pozzolanic Additions in Portland Cement Concrete Mixtures FDOT Contract Number : BDV25-977-38," University of South Florida, Tampa, FL, 2018.

[3] M. Bediako, S. S. Purohir, and J. T. Kevern, "An Investigation into Ghanaian Calcined Clay as a Supplementary Cementitious Material," *ACI Mater. J.*, vol. 114, no. 6, pp. 889–896, 2017, doi: 10.14359/51700896.

[4] A. Chakchouk, B. Samet, and T. Mnif, "Study on the potential use of Tunisian clays as pozzolanic material," *Appl. Clay Sci.*, vol. 33, no. 2, pp. 79–88, 2006, doi: 10.1016/j.clay.2006.03.009.

[5] M. Singh and M. Garg, "Reactive pozzolana from Indian clays: Their use in cement mortars," *Cem. Concr. Res.*, vol. 36, no. 10, pp. 1903–1907, 2006, doi: 10.1016/j.cemconres.2004.12.002.

[6] T. Danner, H. Justnes, G. Norden, and T. Østnor, "Feasibility of calcined marl as an alternative pozzolanic material," in *Calcined Clays for Sustainable Concrete, RILEM Bookseries*, vol. 10, K. Scrivener and A. Favier, Eds. Springer, Dordrecht, 2015, pp. 67–73.

[7] F. Avet, R. Snellings, A. Alujas Diaz, M. Ben Haha, and K. Scrivener, "Development of a new rapid, relevant and reliable (R3) test method to evaluate the pozzolanic reactivity of calcined kaolinitic clays," *Cem. Concr. Res.*, vol. 85, pp. 1–11, 2016, doi: 10.1016/j.cemconres.2016.02.015.

[8] A. Alujas, R. S. Almenares, S. Betancourt, and C. Leyva, "Pozzolanic Reactivity of Low Grade Kaolinitic Clays: Influence of Mineralogical Composition," in *Calcined Clays for Sustainable Concrete, RILEM Bookseries*, vol. 10, K. Scrivener and A. Favier, Eds. Springer, Dordrecht, 2015, pp. 339–345.

[9] L. Vizcaíno, M. Antoni, A. Alujas, F. Martirena, and K. Scrivener, "Industrial manufacture of a low-clinker blended cement using low-grade calcined clays and limestone as SCM: The Cuban experience," in *Calcined Clays for Sustainable Concrete, RILEM Bookseries*, vol. 10, K. Scrivener and A. Favier, Eds. Springer, Dordrecht, 2015, pp. 347–358.

[10] L. M. Vizcaíno-Andrés, S. Sánchez-Berriel, S. Damas-Carrera, A. Pérez-Hernández, K. L. Scrivener, and J. F. Martirena-Hernández, "Industrial trial to produce a low clinker, low carbon cement," *Mater. Construcción*, vol. 65, no. 317, p. e045, 2015, doi: 10.3989/mc.2015.00614.

[11] A. Tironi, M. A. Trezza, A. N. Scian, and E. F. Irassar, "Potential use of Argentine kaolinitic clays as pozzolanic material," *Appl. Clay Sci.*, vol. 101, pp. 468–476, 2014, doi: 10.1016/j.clay.2014.09.009.

[12] A. Souri, F. Golestani-Fard, R. Naghizadeh, and S. Veiseh, "An investigation on pozzolanic activity of Iranian kaolins obtained by thermal treatment," *Appl. Clay Sci.*, vol. 103, pp. 34–39, 2015, doi: 10.1016/j.clay.2014.11.001.

[13] R. S. Almenares Reyes, A. Alujas Díaz, S. Betancourt Rodríguez, C. A. Leyva Rodríguez, and J. F. Martirena Hernández, "Assessment of Cuban Kaolinitic Clays as Source of Supplementary Cementitious Materials to Production of Cement Based on Clinker – Calcined Clay – Limestone," in *Calcined Clays for Sustainable Concrete, RILEM Bookseries*, vol. 16, F. Martirena, A. Favier, and K. Scrivener, Eds. Springer, Dordrecht, 2018, pp. 21–28.

[14] K. L. Scrivener, "Options for the future of cement," *Indian Concr. J.*, vol. 88, no. 7, pp. 11–21, 2014.

[15] K. Scrivener, F. Martirena, S. Bishnoi, and S. Maity, "Calcined clay limestone cements (LC3)," *Cem. Concr. Res.*, vol. 114, no. November 2017, pp. 49–56, 2017, doi: 10.1016/j.cemconres.2017.08.017.

[16] E. G. Badogiannis, I. P. Sfikas, D. V. Voukia, K. G. Trezos, and S. G. Tsivilis, "Durability of metakaolin Self-Compacting Concrete," *Constr. Build. Mater.*, vol. 82, pp. 133–141, 2015, doi: 10.1016/j.conbuildmat.2015.02.023.

[17] M. Antoni, J. Rossen, F. Martirena, and K. Scrivener, "Cement substitution by a combination of metakaolin and limestone," *Cem. Concr. Res.*, vol. 42, no. 12, pp. 1579–1589, Dec. 2012, doi: 10.1016/j.cemconres.2012.09.006.

[18] P. K. Haldar, S. Mithia, K. Mukherjee, N. R. Dhabarde, E. Bansal, P. Phulwari, A. Kumar, S. Kesh and S. Maity, "The Effect of Kaolinite Content of China Clay on the Reactivity of Limestone Calcined Clay Cement," in *Calcined Clays for Sustainable Concrete, RILEM Bookseries*, vol. 16, F. Martirena, A. Favier, and K. Scrivener, Eds. Springer, Dordrecht,

2018, pp. 195–199.

[19] F. Avet and K. Scrivener, “Investigation of the calcined kaolinite content on the hydration of Limestone Calcined Clay Cement (LC3),” *Cem. Concr. Res.*, vol. 107, pp. 124–125, 2018, doi: 10.1016/j.cemconres.2018.02.016.

[20] L. M. Vizcaíno Andrés, M. G. Antoni, A. Alujas Diaz, J. F. Martirena Hernández, and K. L. Scrivener, “Effect of fineness in clinker-calcined clays-limestone cements,” *Adv. Cem. Res.*, vol. 27, no. 9, pp. 546–556, 2015, doi: 10.1680/adcr.14.00095.

[21] ASTM C618-17, “Standard Specification for Coal Fly Ash and Raw or Calcined Natural Pozzolan for Use in Concrete,” West Conshohocken, PA: ASTM International, 2017.

[22] ASTM C595/C595M-16, “Standard Specification for Blended Hydraulic Cements,” West Conshohocken, PA: ASTM International, 2016.

[23] D. Tsamatsoulis and N. Nikolakakos, “Optimizing the Sulphates Content of Cement Using Multivariable Modelling and Uncertainty Analysis,” vol. 27, no. 2. pp. 133–144, 2013.

[24] M. D. Niemuth, “Effect of fly ash on the optimum sulfate of Portland cement,” Purdue University, West Lafayette, Indiana, 2012.

[25] S. Adu-Amankwah, L. Black, J. Skocek, M. Ben Haha, and M. Zajac, “Effect of sulfate additions on hydration and performance of ternary slag-limestone composite cements,” *Constr. Build. Mater.*, vol. 164, pp. 451–462, 2018, doi: 10.1016/j.conbuildmat.2017.12.165.

[26] D. Tsamatsoulis and N. Nikolakakos, “Investigation of Some Basic Parameters Affecting the Optimum Sulfates Content of Cement,” no. May, pp. 152–157, 2014.

[27] K. A. Evans, “The Optimum Sulphate Content in Portland Cement,” University of Toronto, Toronto, Ontario, 1997.

[28] S. Pourchet, L. Regnaud, J. P. Perez, and A. Nonat, “Early C3A hydration in the presence of different kinds of calcium sulfate,” *Cem. Concr. Res.*, vol. 39, no. 11, pp. 989–996, 2009, doi: 10.1016/j.cemconres.2009.07.019.

[29] W. Lerch, “The influence of gypsum on the hydration and properties of Portland cement pastes,” Research Laboratory of the Portland Cement Association, Chicago, IL, 1946.

[30] ASTM C563 - 18, “Standard Guide for Approximation of Optimum SO3 in Hydraulic Cement,” West Conshohocken, PA: ASTM International, 2018.

[31] F. J. Tang, *Optimization of sulfate form and content (No. RD105T)*. Skokie, IL: PCA

Research and Development, 1992.

[32] S. Mindess, F. J. Young, and D. Darwin, *Concrete*. Upper Saddle River, NJ: Pearson Education, Inc., 2003.

[33] J. W. Bullard, H. M. Jennings, R. A. Livingston, A. Nonat, G. W. Scherer, J. S. Schweitzer, K. L. Scrivener, and J. J. Thomas, "Mechanisms of cement hydration," *Sci. Technol. Concr. Admixtures*, vol. 41, pp. 1208–1223, 2011, doi: 10.1016/B978-0-08-100693-1.00008-4.

[34] E. Gallucci, P. Mathur, and K. L. Scrivener, "Microstructural development of early age hydration shells around cement grains," *Cem. Concr. Res.*, vol. 40, pp. 4–13, 2010.

[35] H. J. Kuzel, "Formation of AFm and Aft phases in hydrating Portland cements," *Proceedings of the 16th International Conference on Cement Microscopy*. Duncanville, Texas, pp. 125–136, 1994.

[36] S. Wild, M. Hadi, and J. Khatib, "The Influence of Gypsum Content on the Porosity and Pore-size Distribution of Cured PFA-lime mixes," *Adv. Cem. Res.*, vol. 7, no. 26, pp. 47–55, 1995.

[37] H. F. W. Taylor, C. Famy, and K. L. Scrivener, "Delayed Ettringite Formation," *Cem. Concr. Res.*, vol. 31, pp. 683–693, 2001.

[38] S. Kelham, "The Effect of Cement Composition and Fineness on Expansion Associated with Delayed Ettringite Formation," *Cem. Concr. Compos.*, vol. 18, pp. 171–179, 1996.

[39] G. Azimi, V. G. Papangelakis, and J. E. Dutrizac, "Modelling of calcium sulphate solubility in concentrated multi-component sulphate solutions," *Fluid Phase Equilib.*, vol. 260, pp. 300–315, 2007.

[40] P. C. Hewlett, Ed., *Lea's Chemistry of Cement and Concrete*, 4th ed. New York, NY: Arnold, 1998.

[41] Z. Zhang, J. Olek, and S. Diamond, "Studies on delayed ettringite formation in heat-cured mortars I: Expansion measurements, changes in dynamic modulus of elasticity, and weight gains," *Cem. Concr. Res.*, vol. 32, no. 11, pp. 1737–1742, 2002, doi: 10.1016/S0008-8846(02)00894-3.

[42] I. Jawed and J. Skalny, "Alkalies in cement: a review: II. Effects of alkalies on hydration and performance of Portland cement.," *Cem. Concr. Res.*, vol. 8, no. 1, pp. 37–51, 1978.

[43] Z. Zhang, J. Olek, and S. Diamond, "Studies on delayed ettringite formation in heat-cured mortars II: Characteristics of cement that may be susceptible to DEF," *Cem. Concr. Res.*,

vol. 32, no. 11, pp. 1737–1742, 2002, doi: 10.1016/S0008-8846(02)00894-3.

[44] F. J. Tang and S. W. Tresouthick, "Hydration and Performance of Cements With Various Amounts and Forms of Added Sulfate," in *9th International Congress on the Chemistry of Cement*, 1992, pp. 317–323.

[45] P. Hawkins, "SO3 Optimization for Ground Granulated Blast Furnace Slag," 2002.

[46] I. B. Javed and P. C. Taylor, "Sulfate Resistance of Concrete Using Blended Cements or Supplementary Cementitious Materials," Portland Cement Association, Skokie, IL, 2006.

[47] H. Zhang, Z. Lin, and D. Tong, "Influence of the type of calcium sulfate on the strength and hydration of portland cement under an initial steam-curing condition," *Cem. Concr. Res.*, vol. 26, no. 10, pp. 1505–1511, Oct. 1996, doi: 10.1016/0008-8846(96)00149-4.

[48] V. C. Campiteli and M. C. Florindo, "The Influence of Limestone Additions on Optimum Sulfur Trioxide Content in Portland Cements," in *Carbonate Additions to Cement, ASTM STP 1064*, P. Kleiger and R. D. Hooton, Eds. Philadelphia: American Society for Testing and Materials, 1990, pp. 30–40.

[49] M. Antoni, "Investigation of cement substitution by blends of calcined clays and limestone," École Polytechnique, 2013.

[50] E. Moulin, P. Blanc, and D. Sorrentino, "Influence of key cement chemical parameters on the properties of metakaolin blended cements," *Cem. Concr. Compos.*, vol. 23, pp. 463–469, 2001.

[51] M. Whittaker, M. Zajac, M. Ben Haha, and L. Black, "The impact of alumina availability on sulfate resistance of slag composite cements," *Constr. Build. Mater.*, vol. 119, pp. 356–369, 2016, doi: 10.1016/j.conbuildmat.2016.05.015.

[52] A. K. Schindler and B. F. Mccullough, "Importance of Concrete Temperature Control During Concrete Pavement Construction in Hot Weather Conditions," *Transp. Res. Rec.*, vol. 1813, pp. 3–10, 2002.

[53] A. Lawrence, "A Finite Element Model for The Prediction of Thermal Stresses in Mass Concrete," University of Florida, 2009.

[54] Y. Ballim and P. C. Graham, "The effects of supplementary cementing materials in modifying the heat of hydration of concrete," *Mater. Struct.*, vol. 42, no. 6, pp. 803–811, Jul. 2009, doi: 10.1617/s11527-008-9425-3.

[55] S. G. Kim, "Effect of heat generation from cement hydration on mass concrete placement,"

Iowa State University, 2010.

[56] M. Frías, M. I. S. De Rojas, and J. Cabrera, “The effect that the pozzolanic reaction of metakaolin has on the heat evolution in metakaolin-cement mortars,” *Cem. Concr. Res.*, vol. 30, no. 2, pp. 209–216, Feb. 2000, doi: 10.1016/S0008-8846(99)00231-8.

[57] A. Williams, A. Markandeya, Y. Stetsko, K. Riding, and A. Zayed, “Cracking potential and temperature sensitivity of metakaolin concrete,” *Constr. Build. Mater.*, vol. 120, no. 2016, pp. 172–180, 2016, doi: 10.1016/j.conbuildmat.2016.05.087.

[58] R. L. Khanna and M. . Puri, “The use of calcined shale as pozzuolana in mass concrete,” *Indian Concr. J.*, pp. 257–263, 1957.

[59] F. Avet, “Investigation of the calcined kaolinite content on the hydration of Limestone Calcined Clay Cement (LC3),” École Polytechnique, 2017.

[60] G. Mishra, A. Emmanuel, and S. Bishnoi, “Studies on the Influence of Limestone-Calcined Clay Blend on the Hydration of Cement,” in *Calcined Clays for Sustainable Concrete, RILEM Bookseries*, vol. 16, F. Martirena, A. Favier, and K. Scrivener, Eds. Dordrecht: Springer, Dordrecht, 2018, pp. 322–326.

[61] P. K. Mehta and P. J. M. Monteiro, *Concrete: Microstructure, Properties, and Materials*, 4th ed. McGraw-Hill Education, 2014.

[62] A. A. Ramezanianpour, *Cement Replacement Materials*. Berlin, Germany: Springer Berlin Heidelberg, 2014.

[63] A. Pryymachenko and L. Sheinich, “Sulfate resistant concrete with aluminosilicate additives,” *Archit. Civ. Eng. Environ.*, vol. 4, pp. 101–106, 2017.

[64] N. Thaulow and S. Sahu, “Mechanism of concrete deterioration due to salt crystallization,” *Mater. Charact.*, vol. 53, no. 2–4, pp. 123–127, 2004, doi: 10.1016/j.matchar.2004.08.013.

[65] Robert J. Flatt, “Salt damage in porous materials : how high supersaturations are generated,” *J. Cryst. Growth*, vol. 242, pp. 435–454, 2002.

[66] H. Haynes, R. O’Neill, M. Neff, and R. Kumar Mehta, “Salt weathering distress on concrete exposed to sodium sulfate environment,” *ACI Mater. J.*, vol. 105, no. 1, pp. 35–43, 2008, doi: 10.14359/19205.

[67] M. Whittaker and L. Black, “Current knowledge of external sulfate attack,” *Adv. Cem. Res.*, vol. 27, no. 9, pp. 532–545, 2015, doi: 10.1680/adcr.14.00089.

[68] P. K. Mehta, “Mechanism of expansion associated with ettringite formation,” *Cem. Concr.*

Res., vol. 3, pp. 1–6, 1973.

[69] M. Cohen and C. Richards, "Effects of the particle sizes of expansive clinker on strength-expansion characteristics of type K expansive cements," *Cem. Concr. Res.*, vol. 12, pp. 717–725, 1982.

[70] G. Scherer, "Stress from crystallization of salt," *Cem. Concr. Res.*, vol. 34, pp. 1613–1624, 2004.

[71] C. Yu, W. Sun, and K. Scrivener, "Mechanism of expansion of mortars immersed in sodium sulfate solutions," *Cem. Concr. Res.*, vol. 43, pp. 105–111, 2013.

[72] W. Müllauer, R. Beddoe, and D. Heinz, "Sulfate attack expansion mechanisms," *Cem. Concr. Res.*, vol. 52, pp. 208–215, 2013.

[73] P. K. Mehta, "Mechanics of sulfate attack on Portland cement concrete another look," *Cem. Concr. Res.*, vol. 13, no. 3, pp. 401–406, 1983.

[74] Z. Shi, "Durability of portland cement - calcined clay - limestone blends," Aarhus University, Denmark, 2016.

[75] J. Bensted, "Thaumasite – direct, woodfordite and other possible formation routes," *Cem. Concr. Res.*, vol. 25, no. 8, pp. 873–877, 2003.

[76] N. J. Crammon, "The thaumasite form of sulfate attack in the UK," *Cem. Concr. Compos.*, vol. 25, no. 8, pp. 809–818, 2003.

[77] E. Irassar, V. Bonavetti, M. Trezza, and M. Gonzalez, "Thaumasite formation in limestone filler cements exposed to sodium sulphate solution at 20 oC," *Cem. Concr. Compos.*, vol. 27, pp. 77–84, 2005.

[78] M. Blanco-Varela, J. Aguilera, and S. Martinez-Ramirez, "Effect of cement C3A content, temperature and storage medium on thaumasite formation in carbonated mortars," *Cem. Concr. Res.*, vol. 36, pp. 707–715, 2006.

[79] D. Macphee and S. Barnett, "Solution properties of solids in the ettringite — thaumasite solid solution series," *Cem. Concr. Res.*, vol. 34, pp. 1591–1598, 2004.

[80] F. Bellmann and J. Stark, "Prevention of thaumasite formation in concrete exposed to sulphate attack," *Cem. Concr. Res.*, vol. 37, pp. 1215–1222, 2007.

[81] F. Bellmann and J. Stark, "The role of calcium hydroxide in the formation of thaumasite," *Cem. Concr. Res.*, vol. 38, pp. 1154–1161, 2008.

[82] E. Lachowski, S. Barnett, and D. Macphee, "Transmission electron optical study of

ettringite and thaumasite," *Cem. Concr. Compos.*, vol. 25, pp. 819–822, 2003.

[83] S. Kohler, D. Heinz, and L. Urbonas, "Effect of ettringite on thaumasite formation," *Cem. Concr. Res.*, vol. 36, no. 4, pp. 697–706, 2006.

[84] T. Schmidt, B. Lothenbach, M. Romer, K. Scrivener, D. Rentsch, and R. Figi, "A thermodynamic and experimental study of the conditions of thaumasite formation," *Cem. Concr. Res.*, vol. 38, no. 3, pp. 337–349, 2008, doi: 10.1016/j.cemconres.2007.11.003.

[85] A. Ramezanianpour and R. Hooton, "Thaumasite sulfate attack in Portland and Portland-limestone cement mortars exposed to sulfate solution," *Constr. Build. Mater.*, vol. 40, pp. 162–173, 2013.

[86] P. Mangat and J. El-Khatib, "Influence of initial curing on sulphate resistance of blended cement concrete," *Cem. Concr. Res.*, vol. 22, no. 6, pp. 1089–1100, 1992.

[87] W. Kunther, B. Lothenbach, and K. Scrivener, "On the relevance of volume increase for the length changes in mortar bars in sulfate solution," *Cem. Concr. Res.*, vol. 46, pp. 23–29, 2013.

[88] M. Santhanam, M. Cohen, and J. Olek, "Mechanism of sulfate attack: a fresh look part II: proposed mechanisms," *Cem. Concr. Res.*, vol. 33, no. 3, pp. 341–346, 2003.

[89] S. T. Lee, H. Y. Moon, R. D. Hooton, and J. P. Kim, "Effect of solution concentrations and replacement levels of metakaolin on the resistance of mortars exposed to magnesium sulfate solutions," *Cem. Concr. Res.*, vol. 35, no. 1314, p. 1323, 2005.

[90] K. Sotiriadis, E. Nikolopoulou, and S. Tsivilis, "Sulfate resistance of limestone cement concrete exposed to combined chloride and sulfate environment at low temperature," *Cem. Concr. Compos.*, vol. 34, no. 8, pp. 903–910, 2012, doi: 10.1016/j.cemconcomp.2012.05.006.

[91] M. Zhang, J. Chen, Y. Lv, D. Wang, and J. Ye, "Study on the expansion of concrete under attack of sulfate and sulfate-chloride ions," *Constr. Build. Mater.*, vol. 39, pp. 26–32, 2013, doi: 10.1016/j.conbuildmat.2012.05.003.

[92] G. Li, A. Zhang, Z. Song, S. Liu, and J. Zhang, "Ground granulated blast furnace slag effect on the durability of ternary cementitious system exposed to combined attack of chloride and sulfate," *Constr. Build. Mater.*, vol. 158, pp. 640–648, 2018, doi: 10.1016/j.conbuildmat.2017.10.062.

[93] J. Xu, C. Zhang, L. Jiang, L. Tang, G. Gao, and Y. Xu, "Releases of bound chlorides from

chloride-admixed plain and blended cement pastes subjected to sulfate attacks," *Constr. Build. Mater.*, vol. 45, pp. 53–59, 2013, doi: 10.1016/j.conbuildmat.2013.03.068.

[94] M. Gonzalez and E. Irassar, "Ettringite formation in low C3A Portland cement exposed to sodium sulfate solution," *Cem. Concr. Res.*, vol. 27, pp. 1061–1072, 1997.

[95] B. Tian and M. D. Cohen, "Does gypsum formation during sulfate attack on concrete lead to expansion," *Cem. Concr. Res.*, vol. 30, no. 1, pp. 117–123, 2000.

[96] M. Cohen and B. Mather, "Sulfate attack on concrete: research needs," *ACI Mater. J.*, vol. 88, 1991.

[97] E. Irassar, A. Di Maio, and O. Batic, "Sulfate attack on concrete with mineral admixtures," *Cem. Concr. Res.*, vol. 26, no. 1, pp. 113–123, 1996.

[98] S. Lee, H. Moon, and R. Swamy, "Sulfate attack and role of silica fume in resisting strength loss," *Cem. Concr. Compos.*, vol. 27, no. 1, pp. 65–76, 2005.

[99] R. Gollop and H. Taylor, "Microstructural and microanalytical studies of sulfate attack, V, comparison of different slag blends," *Cem. Concr. Res.*, vol. 27, no. 7, pp. 1029–1044, 1996.

[100] V. Fernandez-Altable, "Availability of Al2O3 in slag blended cements: sulphate attack implications," *Proceedings of the Final Conference of the NANOCEM Marie Curie Research Training Network*. Villars-sur-Ollon, Switzerland, 2009.

[101] B. Sabir, S. Wild, and J. Bai, "Metakaolin and calcined clays as pozzolans for concrete: A review," *Cem. Concr. Compos.*, vol. 23, no. 6, pp. 441–454, 2001, doi: 10.1016/S0958-9465(00)00092-5.

[102] N. M. Al-Akhras, "Durability of metakaolin concrete to sulfate attack," *Cem. Concr. Res.*, vol. 36, no. 9, pp. 1727–1734, Sep. 2006, doi: 10.1016/j.cemconres.2006.03.026.

[103] R. Siddique and J. Klaus, "Influence of metakaolin on the properties of mortar and concrete: A review," *Appl. Clay Sci.*, vol. 43, no. 3–4, pp. 392–400, 2009.

[104] T. Ramlochan and M. Thomas, "Effect of metakaolin on external sulfate attack," *ACI Spec. Publ.*, no. 192, 2000.

[105] A. M. Akasha and J. M. Abdullah, "Sulfate Resistance of Cement Mortar Containing Metakaolin," in *Calcined Clays for Sustainable Concrete, RILEM Bookseries*, vol. 16, F. Martirena, A. Favier, and K. Scrivener, Eds. Springer, Dordrecht, 2018, pp. 8–14.

[106] B. Lothenbach, G. Le Saout, E. Gallucci, and K. Scrivener, "Influence of limestone on the hydration of Portland cements," *Cem. Concr. Res.*, vol. 38, no. 6, pp. 848–860, Jun. 2008,

doi: 10.1016/J.CEMCONRES.2008.01.002.

[107] I. Soroka and N. Stern, “Effect of calcareous fillers on sulfate resistance of Portland cement,” *Am. Ceram. Soc.*, vol. 55, no. 6, pp. 594–595, 1976.

[108] T. Schmidt, B. Lothenbach, M. Romer, J. Neuenschwander, and K. Scrivener, “Physical and microstructural aspects of sulfate attack on ordinary and limestone blended Portland cements,” *Cem. Concr. Res.*, vol. 39, no. 12, pp. 1111–1121, 2009, doi: 10.1016/j.cemconres.2009.08.005.

[109] E. F. Irassar, “Sulfate attack on cementitious materials containing limestone filler - A review,” *Cem. Concr. Res.*, vol. 39, no. 3, pp. 241–254, 2009, doi: 10.1016/j.cemconres.2008.11.007.

[110] M. A. Gonzáles and E. F. Irassar, “Effect of limestone filler on the sulfate resistance of low C3A Portland cement,” *Cem. Concr. Res.*, vol. 28, no. 11, pp. 1655–1667, 1998.

[111] J. Sun and Z. Chen, “Influences of limestone powder on the resistance of concretes to the chloride ion penetration and sulfate attack,” *Powder Technol.*, vol. 338, pp. 725–733, 2018, doi: 10.1016/j.powtec.2018.07.041.

[112] M. Zajac, A. Rossberg, G. Le Saout, and B. Lothenbach, “Influence of limestone and anhydrite on the hydration of Portland cements,” *Cem. Concr. Compos.*, vol. 46, pp. 99–108, 2014, doi: 10.1016/j.cemconcomp.2013.11.007.

[113] Z. Sawicz and S. S. Heng, “Durability of concrete with addition of limestone powder,” *Mag. Concr. Res.*, vol. 48, no. 175, pp. 131–137, 1996.

[114] S. Ogawa, T. Nozaki, K. Yamada, H. Hirao, and R. D. Hooton, “Cement and Concrete Research Improvement on sulfate resistance of blended cement with high alumina slag,” *Cem. Concr. Res.*, vol. 42, no. 2, pp. 244–251, 2012, doi: 10.1016/j.cemconres.2011.09.008.

[115] A. Skaropoulou, G. Kakali, and S. Tsivilis, “Thaumasite form of sulfate attack in limestone cement concrete: The effect of cement composition, sand type and exposure temperature,” *Constr. Build. Mater.*, vol. 36, pp. 527–533, 2012, doi: 10.1016/j.conbuildmat.2012.06.048.

[116] C. Yu, P. Yuan, X. Yu, and J. Liu, “Degradation of calcined clay-limestone cementitious composites under sulfate attack,” in *Calcined Clays for Sustainable Concrete*, vol. 16, F. Martirena, A. Favier, and K. Scrivener, Eds. Springer, Dordrecht, 2018, pp. 110–116.

[117] S. A. Hartshorn, J. H. Sharp, and R. N. Swamy, “Thaumasite formation in Portland-limestone cement pastes,” *Cem. Concr. Res.*, vol. 29, no. 8, pp. 1331–1340, 1999, doi:

10.1016/S0008-8846(99)00100-3.

[118] Z. Shi, S. Ferreiro, B. Lothenbach, M. R. Geiker, W. Kunther, J. Kaufmann, D. Herfort, and J. Skibsted, "Sulfate resistance of calcined clay – Limestone – Portland cements," *Cem. Concr. Res.*, vol. 116, no. March 2018, pp. 238–251, 2019, doi: 10.1016/j.cemconres.2018.11.003.

[119] C. D. Lawrence, "The influence of binder type on sulfate resistance," *Cem. Concr. Res.*, vol. 22, no. 6, pp. 1047–1058, 1992.

[120] F. Bellmann, B. Möser, and J. Stark, "Influence of sulfate solution concentration on the formation of gypsum in sulfate resistance test specimen," *Cem. Concr. Res.*, vol. 36, no. 2, pp. 358–363, 2006, doi: 10.1016/j.cemconres.2005.04.006.

[121] A. Gabrisova, J. Havlica, and S. Sahu, "Stability of calcium sulphoaluminate hydrates in water solutions with various pH values," *Cem. Concr. Res.*, vol. 21, no. 6, pp. 1023–1027, 1991.

[122] Q. Zhou, J. Hill, E. A. Byars, J. C. Cripps, C. J. Lynsdale, and J. H. Sharp, "The role of pH in thaumasite sulfate attack," *Cem. Concr. Res.*, vol. 36, no. 1, pp. 160–170, 2006, doi: 10.1016/j.cemconres.2005.01.003.

[123] M. E. Gaze and N. J. Crammond, "Formation of thaumasite in a cement:lime:sand mortar exposed to cold magnesium and potassium sulfate solutions," *Cem. Concr. Compos.*, vol. 22, no. 3, pp. 209–222, 2000, doi: 10.1016/S0958-9465(00)00002-0.

[124] D. W. Hobbs and M. G. Taylor, "Nature of the thaumasite sulfate attack mechanism in field concrete," *Cem. Concr. Res.*, vol. 30, no. 4, pp. 529–533, 2000, doi: 10.1016/S0008-8846(99)00255-0.

[125] H. Maraghechi, F. Avet, H. Wong, H. Kamyab, and K. Scrivener, "Performance of Limestone Calcined Clay (LC3) with various kaolinite contents with respect to chloride transport," *Mater. Struct.*, vol. 51, no. 125, pp. 1–17, 2018.

[126] K. De Weerdt, D. Orsáková, and M. R. Geiker, "The impact of sulphate and magnesium on chloride binding in Portland cement paste," *Cem. Concr. Res.*, 2014, doi: 10.1016/j.cemconres.2014.07.007.

[127] H. Zibara, R. D. Hooton, M. D. A. Thomas, and K. Stanish, "Influence of the C/S and C/A ratios of hydration products on the chloride ion binding capacity of lime-SF and lime-MK mixtures," *Cem. Concr. Res.*, vol. 38, no. 3, pp. 422–426, 2008, doi:

10.1016/j.cemconres.2007.08.024.

[128] Z. Shi, M. R. Geiker, K. De Weerdt, T. A. Østnor, B. Lothenbach, F. Winnefeld, and J. Skibsted, "Role of calcium on chloride binding in hydrated Portland cement–metakaolin–limestone blends," *Cem. Concr. Res.*, 2017, doi: 10.1016/j.cemconres.2017.02.003.

[129] M. D. A. Thomas, R. D. Hooton, A. Scott, and H. Zibara, "The effect of supplementary cementitious materials on chloride binding in hardened cement paste," *Cem. Concr. Res.*, vol. 42, no. 1, pp. 1–7, 2012, doi: 10.1016/j.cemconres.2011.01.001.

[130] M. J. Mwiti, "Chloride Ingress Resistance in Selected Calcined - Clay - Portland Cement Blends," *Int. J. Sci. Eng. Res. www.ijser.in ISSN (Online*, 2014.

[131] ASTM C1202-12, "Standard Test Method for Electrical Indication of Concrete's Ability to Resist Chloride Ion Penetration," West Conshohocken, PA: ASTM International, 2015.

[132] A. A. Al-Rawas, A. N. Hago, D. Al--lawal, and A. AL-Baltash, "The Ommani artificial pozzolans (Sarooj)," *Cem. Concr. Aggreg.*, vol. 23, pp. 19–26, 2001.

[133] J. P. Gonçalves, L. M. Tavares, R. D. Toledo Filho, and E. M. R. Fairbairn, "Performance evaluation of cement mortars modified with metakaolin or ground brick," *Constr. Build. Mater.*, 2009, doi: 10.1016/j.conbuildmat.2008.08.027.

[134] T. Z. Muntasser, "Properties and durability of slag-based cement in the Mediterranean environment," University of Surrey, Guildford, England, 2002.

[135] H. M. Khater, "Influence of metakaolin on resistivity of cement mortar to magnesium chloride solution," *ASCE J. Mater. Civ. Eng.*, vol. 23, no. 11, pp. 325–333, 2011, doi: 10.1061/(ASCE)MT.1943-5533.0000294.

[136] S. Wild, J. M. Khatib, and A. Jones, "Relative Strength, Pozzolanic activity and cement hydration in superplasticised metakaolin concrete," vol. 26, no. 10, pp. 1537–1544, 1996.

[137] A. K. Suryavanshi, J. D. Scantlebury, and S. B. Lyon, "Mechanism of Friedel's salt formation in cements rich in tri-calcium aluminate," *Cem. Concr. Res.*, vol. 26, no. 5, pp. 717–727, 1996, doi: 10.1016/S0008-8846(96)85009-5.

[138] R. Luo, Y. Cai, C. Wang, and X. Huang, "Study of chloride binding and diffusion in GGBS concrete," *Cem. Concr. Res.*, vol. 33, no. 1, pp. 1–7, 2003, doi: 10.1016/S0008-8846(02)00712-3.

[139] K. M. A. Hossain and M. Lachemi, "Corrosion resistance and chloride diffusivity of volcanic ash blended cement mortar," *Cem. Concr. Res.*, vol. 34, no. 4, pp. 695–702, 2004,

doi: 10.1016/j.cemconres.2003.10.021.

[140] H. Hirao, K. Yamada, H. Takahashi, and H. Zibara, “Chloride Binding of Cement Estimated by Binding Isotherms of Hydrates,” *J. Adv. Concr. Technol.*, vol. 3, no. 1, pp. 77–84, 2005, doi: 10.3151/jact.3.77.

[141] Z. Shi, M. R. Geiker, K. De Weerdt, B. Lothenbach, J. Kaufmann, W. Kunther, S. Ferreiro, D. Herfort, and J. Skibsted., “Durability of portland cement blends including calcined clay and limestone: Interactions with sulfate, chloride and carbonate ions,” in *Calcined Clays for Sustainable Concrete, RILEM Bookseries*, vol. 10, K. Scrivener and A. Favier, Eds. Springer, Dordrecht, 2015, pp. 133–141.

[142] ASTM C1556-11a, “Standard Test Method for Determining the Apparent Chloride Diffusion Coefficient of Cementitious Mixtures by Bulk Diffusion,” West Conshohocken, PA: ASTM International, 2011.

[143] ASTM C1152/C1152M-04, “Standard test method for acid-soluble chloride in mortar and concrete,” West Conshohocken, PA: ASTM International, 2012.

[144] Z. Shi, B. Lothenbach, M. R. Geiker, J. Kaufmann, S. Ferreiro, and J. Skibsted, “Carbonation of portland cement mortars including metakaolin and limestone,” *The 14th International Congress on the Chemistry of Cement*. Beijing, China, 2015.

[145] M. Thiery, G. Villain, P. Dangla, and G. Platret, “Investigation of the carbonation front shape on cementitious materials: Effects of the chemical kinetics,” *Cem. Concr. Res.*, vol. 37, no. 7, pp. 1047–1058, 2007, doi: 10.1016/j.cemconres.2007.04.002.

[146] A. Morandeau, M. Thiéry, and P. Dangla, “Investigation of the carbonation mechanism of CH and C-S-H in terms of kinetics, microstructure changes and moisture properties,” *Cem. Concr. Res.*, vol. 56, no. February, pp. 153–170, 2014, doi: 10.1016/j.cemconres.2013.11.015.

[147] B. Johannesson and P. Utgenannt, “Microstructural changes caused by carbonation of cement mortar,” *Cem. Concr. Res.*, vol. 31, no. 6, pp. 925–931, 2001, doi: 10.1016/S0008-8846(01)00498-7.

[148] B. Huet, V. Tasoti, and I. Khalfallah, “A review of Portland cement carbonation mechanisms in CO2rich environment,” *Energy Procedia*, vol. 4, pp. 5275–5282, 2011, doi: 10.1016/j.egypro.2011.02.507.

[149] B. Šavija and M. Luković, “Carbonation of cement paste: Understanding, challenges, and

opportunities," *Constr. Build. Mater.*, vol. 117, pp. 285–301, 2016, doi: 10.1016/j.conbuildmat.2016.04.138.

[150] A. Leemann, P. Nygaard, J. Kaufmann, and R. Loser, "Relation between carbonation resistance, mix design and exposure of mortar and concrete," *Cem. Concr. Compos.*, vol. 62, pp. 33–43, 2015, doi: 10.1016/j.cemconcomp.2015.04.020.

[151] Z. Dai, T. T. Tran, and J. Skibsted, "Aluminum incorporation in the C-S-H phase of white portland cement-metakaolin blends studied by 27Al and 29Si MAS NMR spectroscopy," *J. Am. Ceram. Soc.*, vol. 97, no. 8, pp. 2662–2671, 2014, doi: 10.1111/jace.13006.

[152] T. F. Sevelsted and J. Skibsted, "Carbonation of C–S–H and C–A–S–H samples studied by 13C, 27Al and 29Si MAS NMR spectroscopy," *Cem. Concr. Res.*, vol. 71, pp. 56–65, 2015, doi: 10.1016/j.cemconres.2015.01.019.

Chapter 2 Material Characterization

2.1 Introduction

One of the main objectives of the current study is to assess the effectiveness of ternary systems of ordinary portland cement, limestone and calcined clay (CCIL) on concrete durability. Towards satisfying this objective, one Type I/II (MH), four portland-limestone (IL) cements and four kaolin clays were acquired. The published literature indicates that limestone addition to portland cement clinker enhances concrete durability [1] [2]. Clay mineralogy and chemical composition can vary depending on mines locations and the depth from which clays have been acquired. Additionally, the amount of limestone and its physical, chemical and mineralogical properties will affect the system performance. This is in addition to the nature of the clinker and the sulfate source used in the ternary blends. Towards relating durability performance to system constituents, the first step is to characterize the as-received materials. In this chapter, the physical, chemical, and mineralogical characteristics of the as-received materials are presented. Several techniques have been used here; namely, x-ray fluorescence (XRF), X-ray diffraction coupled with Rietveld refinement (QXRD), Blaine fineness, laser particle size distribution (PSD), and thermogravimetric analysis (TGA). The next step will be development of the experimental matrix design.

2.2 Elemental Oxide Composition

2.2.1 XRF Analysis of Cements

The chemical oxide composition of the as-received materials were determined using XRF according to ASTM C114 [3]. Six commercial cements were selected initially for this study based on Mill Certificates. The as-received cements selected for analysis were a Type I/II (MH) cement (HA), two portland-limestone cements from supplier A, two portland-limestone cements from supplier B and one portland-limestone cement from supplier C. The PI requested from supplier A an under-sulfated IL cement, GILUS IL(10) and the same IL cement with optimized sulfate content, GILOP IL(10), to assess industrial optimization of sulfates in the IL system. The other two cements, designated as TIL IL(10) and THIL IL(14), were provided by supplier B. The cement suppliers provided samples for all processing additions used in manufacturing the cements, such as limestone, hemihydrate, gypsum, and kiln dust. Those additions were also analyzed and the

results for the chemical oxide composition for cements and processing additions are presented in Table 2-1 and Table 2-2, respectively.

Table 2-1: Oxide chemical composition of as-received cements

Analyte	**HA I/II(MH)**	**GILUS IL(10)**	**GILOP IL(10)**	**TIL IL(10)**	**THIL IL(14)**	**CIL IL(14)**
SiO_2	20.63	19.00	18.43	19.16	19.14	19.51
Al_2O_3	5.02	4.60	4.56	4.61	4.52	4.12
Fe_2O_3	3.45	3.38	3.29	3.74	3.54	3.23
CaO	63.96	62.60	62.28	62.40	62.11	61.97
MgO	0.35	0.92	0.91	1.12	1.08	0.78
SO_3	2.71	2.41	2.93	2.47	2.44	2.83
Na_2O	0.04	0.14	0.18	0.17	0.17	0.09
K_2O	0.30	0.31	0.32	0.32	0.29	0.22
TiO_2	0.25	0.22	0.21	0.23	0.22	0.21
P_2O_5	0.37	0.44	0.43	0.09	0.09	0.08
Mn_2O_3	0.07	0.08	0.06	0.15	0.14	0.02
SrO	0.07	0.07	0.06	0.12	0.12	0.12
Cr_2O_3	0.02	0.02	0.02	0.02	0.02	0.02
ZnO	0.03	0.06	0.06	0.05	0.04	0.10
L.O.I. (550°C)	0.98	1.26	1.62	0.76	0.69	1.21
L.O.I. (950°C)	2.54	5.32	5.86	5.35	5.99	6.63
Total	99.81	99.57	99.62	99.98	99.91	99.93
Na_2O_{eq}	0.24	0.35	0.40	0.38	0.36	0.23

Table 2-2: Oxide chemical composition of processing additions

Analyte	Kiln Dusts		Hemihydrate (AH)	Gypsum (TAG)	Limestone			
	CKD[a]	HAKD[b]			ALS[a]	HALS[b]	TLS[c]	CLS[d]
SiO_2	8.73	7.55	0.00	0.12	0.86	2.73	12.90	4.02
Al_2O_3	4.03	3.69	0.00	0.05	0.13	0.53	0.41	0.29
Fe_2O_3	1.52	1.44	0.01	0.02	0.16	0.33	0.23	0.18
CaO	46.62	49.05	38.70	32.77	54.59	53.48	47.63	52.60
MgO	0.57	0.59	0.00	0.00	0.43	0.42	0.51	0.26
SO_3	0.40	0.49	55.34	46.84	0.05	0.09	0.10	0.01
Na_2O	0.15	0.10	0.02	0.03	0.02	0.02	0.04	0.02
K_2O	0.38	0.30	0.00	0.01	0.00	0.02	0.06	0.04
TiO_2	0.19	0.17	0.00	0.00	0.02	0.03	0.03	0.02
P_2O_5	0.34	0.31	0.00	0.00	0.10	0.18	0.04	0.01
Mn_2O_3	0.02	0.04	0.00	0.00	0.01	0.01	0.01	0.01
SrO	0.05	0.05	0.02	0.13	0.04	0.04	0.08	0.13
Cr_2O_3	0.01	0.01	0.00	0.00	0.01	0.00	0.00	0.00
ZnO	0.02	0.01	0.00	0.00	0.00	0.00	0.00	0.00
BaO	0.02	0.02	0.00	0.00	0.01	0.01	0.00	0.00
L.O.I. (550°C)	-	2.00	6.18	20.08	0.09	1.21	0.09	0.43
L.O.I. (950°C)	35.45	36.59	6.24	20.18	43.41	42.48	38.03	42.14
Total	98.49	100.44	100.34	100.15	99.84	100.37	100.07	99.73
Na_2O_{eq}	0.40	0.31	0.02	0.04	0.02	0.04	0.08	0.05

[a]= Cement GILOP IL(10)
[b]= Cement HA I/II(MH)
[c]= Cement TIL IL(10) and THIL IL(14)
[d]= Cement CIL IL(14)

As can be seen from Table 2-1, the Al_2O_3 content was slightly higher for the HA Cement than the other four cements due to the limestone additions reducing clinker contents. Cements GILUS and GILOP were from the same supplier, but GILUS was under-sulfated, as requested from the manufacturer. The SO_3 contents of the limestone cements from supplier A and C were higher than those from supplier B (TIL and THIL). Cement TIL and THIL, from supplier B, had different limestone contents. The limestone content of cement CIL, from supplier C was similar to that of cement THIL. Alkali amounts among these six cements were at a similar level. Losses on ignition were reported both at 550°C and 950°C per ASTM C114. The losses of weight below 550°C were assumed to be from moisture in the cement and the chemical bound water from portlandite. The losses between 550°C and 950°C were assigned to CO_2 given off during

decomposition of the limestone in the cement. The differences in CO_2 lost during heating show that the cements had different limestone contents. The oxidation of sulfides was not considered nor corrected for, as required for ground granulated blast furnace slag or portland blast-furnace slag cement [3].

Inorganic processing additions, limestones, and sulfates that were added to these cements by the manufacturers were analyzed using XRF. The cement kiln dusts, CKD and HAKD, were processing additions, and ALS and HALS were the limestone sources used in manufacturing GILOP and HA cements, respectively. TLS was the limestone used in the production of cements TIL and THIL from supplier B, while CLS was the limestone used for cement CIL from supplier C. Two types of commercial sulfates, hemihydrate (AH) and gypsum (TAG), were also used to evaluate the influence of sulfate additions on durability. The oxide chemical compositions of these additions are listed in Table 2-2.

From the lime contents and losses in ignition, it can be assumed that limestone is the major component in the kiln dust. Based on the differences in LOI between 550℃ and 950℃, it is clear that the calcium carbonate contents of the limestones are different in the IL cements. More accurate analysis of the calcite content can be determined from QXRD, and results are presented later in this chapter.

2.2.2 XRF Analysis of Clays

Compared to cements, the elemental oxide compositions of clays have larger variation in their oxide components, such as SiO_2, Al_2O_3 and Fe_2O_3. Among the three common types of clay minerals (kaolinite, illite and montmorillonite), kaolinite ($Al_2O_3 \cdot 2SiO_2 \cdot 2H_2O$) has much higher pozzolanic reactivity, after calcination, than the other two due to the amount and location of the OH groups, which affect the degree of crystallinity [4]. Among the three minerals, kaolinite has the lowest alumina-to-silica molar ratio (Al_2O_3:SiO_2 = 1:2). Chemical compositions of the clays, shown in Table 2-3, were determined using XRF in accordance with ASTM C114 [3]. CCC and CCF were commercially available calcined clay products from the same source in South America, in which CCF was ground finer. GAB1 and GAB4 were collected from mines located in the Southeastern US.

Table 2-3: Oxide chemical composition of clays

Analyte	EMD1	CCC	CCF	GAB1	GAB4
SiO_2	68.68	63.49	62.62	44.56	31.82
Al_2O_3	20.81	19.89	18.94	37.44	44.49
Fe_2O_3	1.00	7.99	10.31	0.92	0.72
CaO	0.00	1.08	0.28	0.00	0.00
MgO	0.08	0.45	0.37	0.11	0.11
SO_3	0.00	0.23	0.15	0.00	0.17
Na_2O	0.18	0.09	0.42	0.08	0.05
K_2O	2.37	1.66	0.58	0.23	0.10
TiO_2	0.68	1.24	1.49	1.85	1.80
P_2O_5	0.13	0.04	0.14	0.05	0.03
Mn_2O_3	0.01	0.04	0.12	0.00	0.00
SrO	0.01	0.01	0.00	0.01	0.00
Cr_2O_3	0.00	0.01	0.02	0.01	0.01
ZnO	0.00	0.00	0.00	0.00	0.00
BaO	0.06	0.09	0.13	0.02	0.01
L.O.I. (950°C)	5.88	3.39	4.59	14.38	19.91
Total	99.88	99.72	100.16	99.66	99.21
Na_2O_{eq}	1.74	1.19	0.80	0.23	0.12

XRF analysis indicates large amounts of silica and alumina, which are the main constituents of kaolinite ($Al_2O_3 \cdot 2SiO_2 \cdot 2H_2O$), in all clays. GAB1 and GAB4 have much higher alumina contents and higher alumina-to-silica ratios, which can indicate a higher pozzolanic reactivity potential. The other three contain higher amounts of silica, potentially indicating a higher sand content. All clays are in compliance with ASTM C618 [5] requirements for natural pozzolans, which specifies a minimum of 70.0% for $SiO_2 + Al_2O_3 + Fe_2O_3$. CCC is red in color, due to its higher iron oxide content. Sulfate contents in all clays are pretty low, and below the maximum limit of 4% specified in the ASTM C618 [5]. All other available oxides are comparatively low except for the slightly higher alkali content in EMD1. Among all clays, the lowest loss on ignition was found for the commercial CCC and CCF clays.

2.3 Mineralogical Analysis

2.3.1 X-Ray Diffraction

In addition to the chemical oxide compositions obtained from XRF, the mineralogical compositions of the as-received materials were determined using quantitative x-ray diffraction. All as-received materials were analyzed by x-ray diffraction in accordance with ASTM C1365 [6].

Cements were wet ground in ethanol in a McCrone micronizing mill to an average particle size of less than 10 μm. Wet grinding was used to minimize temperature increase during the grinding process; this was to prevent thermal decomposition of gypsum to hemihydrate or anhydrite. Samples were then dried in an oven at 40°C. Clay materials were ground to pass a No. 325 sieve (< 45 μm). The external standard method was used to determine the amorphous/unidentified material contents for cements. The mass absorption coefficients (MAC) were calculated from the XRF results [7] [8]. Corundum (Standard Reference Material 676a) from National Institute of Standards and Technology (NIST) was used as a standard with a MAC of 30.91 cm^2/g. For calcined clays, the internal standard method was applied using 10% of corundum blended with each sample to conduct the analysis.

XRD scans were collected using the Phillips X'Pert PW3040 Pro diffractometer equipped with an X'Celerator detector and a Cu-Kα x-ray source. Tension and current were set to 45 kV and 40 mA, respectively, and 5-mm divergence and anti-scatter slits were used in the automatic mode. Scans were collected for the 7°-70° 2θ angular range. The back-loading technique was used to load samples into the sample holder in order to minimize preferred orientation. The sample was rotated at 30 rpm during data collection to improve counting statistics [9]. Three samples were prepared for each as-received material, and the average values are reported here.

Quantitative XRD with Rietveld refinement using PANalytical HighScore Plus V4 software was used to determine the weight fractions of the crystalline phases and amorphous/unidentified phase content of each cement. Due to XRD peak overlap for portland cements, quantitative determination of most cement phases is not possible without using selective extraction methods to reduce the number of phases contained in each sample. Salicylic acid-methanol (SAM) extractions were performed to dissolve the silicates and free lime, and isolate a concentrated residue of aluminates, ferrites, and minor phases, such as periclase, carbonates, alkali sulfates, and double alkali sulfates [10], [11]. Potassium hydroxide-sucrose (KOSH) extractions were used to dissolve aluminates and ferrites and obtain a residue of C_3S, C_2S, alkali sulfates, and MgO [10]. The crystalline structures used for refinement analyses of cements and clays are shown in Table 2-4.

Table 2-4: Crystalline structures used for weight fraction analysis

Phase	Formula	Crystal System	PDF codes	ICSD Code
Alite	Ca_3SiO_5-Mg, Al	Monoclinic/M3	01-070-8632	94742
Belite	Ca_2SiO_4	Monoclinic/β	01-086-0398	81096
Aluminate	$Ca_3Al_2O_6$	Cubic	01-070-0839	1841
Ferrite	Ca_2AlFeO_5	Orthorhombic	01-071-0667	9197
Calcite	CaCO3	Rhombohedral	01-086-0174	80869
Portlandite	$Ca(OH)_2$	Rhombohedral	01-072-0156	15471
Quartz	SiO_2	Rhombohedral	00-046-1045	41414
Dolomite	$CaMg(CO_3)_2$	Rhombohedral	01-075-1711	31277
Gypsum	$CaSO_4(H_2O)_2$	Monoclinic	00-033-0311	151692
Hemihydrate	$CaSO_4(H_2O)_{0.5}$	Monoclinic	01-083-0438	79528
Anhydrite	$CaSO_4$	Orthorhombic	01-086-2270	40043
Lime	CaO	Cubic	01-071-4121	52783
Kaolinite	$Al_2Si_2O_5(OH)_4$	Triclinic	01-078-1996	63192
Dickite	$Al_2Si_2O_5(OH)_4$	Monoclinic	00-010-0446	52398
Nacrite	$Al_2Si_2O_5(OH)_4$	Monoclinic	01-083-0972	80083
Illite	$Al_{2.59}Ca_{0.01}Fe_{0.04}K_{0.71}Mg_{0.15}Na_{0.01}Si_{3.27}O_{12}H_2$	Monoclinic	00-007-0025	166963
Gibbsite	$Al(OH)_3$	Monoclinic	01-070-2038	6162
Crandallite	$CaAl_3(PO_4)_2(OH)_5(H_2O)$	Hexagonal	01-070-2069	6195
Hematite	Fe_2O_3	Hexagonal	00-033-0664	182839
Anatase	TiO_2	Tetragonal	01-071-1166	9852

2.3.1.1 X-ray analysis of cements and inorganic processing additions

The amorphous contents (AC) of cements and processing additions were determined by the external-standard method based on the XRF analyses of the oxide chemical compositions, Table 2-1 and Table 2-2. Results of the weight fraction analyses of crystalline phases and the amorphous contents of cements and additions are shown in Table 2-5 and Table 2-6. The corresponding standard deviation values are also reported in Table 2-5. The results indicate that THIL and CIL had the highest similar calcite contents of 11.4% and 11.7%, respectively, while HA had the lowest with a calcite content of 3.3%. GILOP and TIL had similar calcite contents of 9.1 and 8.9%, respectively. It is also noted from XRD analyses that TIL had the lowest C_3A content, 2.4%, followed by THIL, 2.9%, due to the increased limestone contents.

Table 2-5: Crystalline and amorphous weight percentages in cements

Analyte	HA I/II(MH)	GILUS IL(10)	GILOP IL(10)	TIL IL(10)	THIL IL(14)	CIL IL(14)
Alite	45.4	46.5	44.5	44.5	40.3	38.8
Belite	19.7	15.5	16.5	16.1	16.9	19.1
Aluminate	4.0	3.1	3.7	2.3	2.9	3.1
Ferrite	9.3	9.2	8.9	11.8	10.8	8.9
Gypsum	1.0	3.0	3.9	1.5	1.5	1.6
Hemihydrate	2.7	0.0	0.0	1.4	2.0	2.7
Calcite	3.4	9.2	9.2	8.8	11.4	11.7
Portlandite	1.5	-	1.5	-	-	0.8
Quartz	1.0	0.4	0.4	1.2	1.4	1.4
Dolomite	0.3	0.8	0.7	-	-	-
Syngenite	-	-	-	-	-	0.7
Amorphous/ unidentified	11.7	12.4	10.6	12.5	12.8	11.1

Table 2-6: Crystalline and amorphous weight percentages in additions

Analyte	Kiln Dusts		Hemihydrate (AH)	Gypsum (TAG)	Limestone			
	CKD	HAKD			ALS	HALS	TLS	CLS
Gypsum	-	-	-	95.1	-	-	-	-
Hemihydrate	-	-	98.6	-	-	-	-	-
Anhydrite	-	-	-	3.3	-	-	-	-
Calcite	75.8	79.1	-	-	94.2	89.5	79.0	85.3
Quartz	1.7	1.6	-	0.1	1.4	1.6	9.5	3.4
Dolomite	1.4	-	-	-	-	-	-	-
Lime	-	1.0	-	-	-	-	-	-
Amorphous/ unidentified	21.1	18.3	1.4	1.5	4.4	8.9	11.6	11.4

Table 2-7 indicates the limestone content determined from XRD analysis and the values disclosed on the Mill Certificate of cements. The limestone contents in cements were calculated based on the calcite content determined by the XRD analysis as indicated in Equation 2-1 and Equation 2-2. Accordingly, the percentage of limestone in cements TIL, THIL, and CIL were calculated considering their calcite contents and calcite content in TLS and CLS limestone.

$$W_{calcite,Cem} = P_{LS,cem} \cdot W_{calcite,LS} \quad \text{Equation 2-1}$$

$$P_{LS,cem} = \frac{W_{calcite,Cem}}{W_{calcite,LS}} \quad \text{Equation 2-2}$$

Where $W_{calcite,Cem}$ is the calcite content in cement determined by XRD, $W_{calcite,LS}$ is the calcite content in limestone determined by XRD and $P_{LS,cem}$ is the limestone content in cement.

However, the calcite contents in cements GILOP and HA are attributed to both limestone and kiln dust. According to the Mill Certificates of GILOP and HA, the kiln dust contents are 1.7 wt.% and 1.5 wt.%, respectively. Therefore, the limestone content in these cements were determined following Equation 2-3 and Equation 2-4.

$$W_{calcite,Cem} = P_{LS,cem} \cdot W_{calcite,LS} + P_{KD,cem} \cdot W_{calcite,KD} \quad \text{Equation 2-3}$$

$$P_{LS,cem} = \frac{W_{calcite,Cem} - P_{KD,cem} \cdot W_{calcite,KD}}{W_{calcite,LS}} \quad \text{Equation 2-4}$$

Where $P_{KD,cem}$ is the kiln dust content as disclosed on the Mill Certificate, and $W_{calcite,KD}$ is the calcite content in kiln dust determined by QXRD. Comparison of the two different approaches in quantifying limestone content can be observed in Table 2-7.

Table 2-7: Limestone content estimated from QXRD analysis

	HA I/II(MH)	**GILUS IL(10)**	**GILOP IL(10)**	**TIL IL(10)**	**THIL IL(14)**	**CIL IL(14)**
Limestone content, QXRD	2.5	8.4	8.4	11.1	14.4	13.7
Limestone content, Mill Certificate	2.7	-	8.2	12.0	14.0	14.0

2.3.1.2 X-Ray Analysis of Clays

Analysis of natural clays are more complicated than the analysis of cements and inorganic processing additions due to the existence of numerous phases and varying degree of disorder in kaolin group minerals [12]. Within the kaolin group, kaolinite, dickite and nacrite are analyzed and expressed as Sum Kaolin, except CCC and CCF which are commercial calcined clays. CCC and CCF have only a small amount of uncalcined kaolin residue. According to the literature [4], most of the dehydroxylation of kaolinite is completed at 600℃ and the remaining amount is negligible. Other phases such as illite and montmorillonite require higher temperature to complete decomposition. To ensure complete dehydroxylation, all raw clays were calcined at 850℃ for 1 hour using a laboratory furnace.

The amorphous content (AC) of the as-received clays was determined by the external-standard method based on the XRF analysis results of the chemical compositions of oxides shown in Table 2-3. For calcined clays, the amorphous content was determined by the internal-standard method due to the unavailability of XRF results. Identified phases are listed in Table 2-8 for both as-received and calcined clays.

Table 2-8: Mineralogical analysis of clays

Analyte	**EMD1**	**EMD1 (850°C) (1 hr)**	**CCC**	**CCF**	**GAB1**	**GAB1 (850°C) (1 hr)**	**GAB4**	**GAB4 (850°C) (1 hr)**
Kaolinite	17.2	0.0	-	0.8	54.4	0.0	40.9	0.0
Dickite	10.1	0.0	-	-	33.4	0.0	18.1	0.0
Nacrite	10.6	0.0	-	-	5.3	0.0	6.4	0.0
Sum Kaolin	**37.9**	**0.0**	**3.1**	**0.8**	**93.1**	**0.0**	**65.5**	**0.0**
Illite	4.4	3.3	2.8	0.9	0.3	-	0.1	-
Gibbsite	-	-	-	-	-	-	24.0	-
Quartz	36.2	42.2	25.5	34.6	0.9	1.0	0.2	1.4
Crandallite	-	-	-	-	0.3	-	0.0	-
Hematite	-	-	0.7	1.0	-	-	-	-
Anatase	-	-	0.3	0.1	0.7	1.0	1.1	0.3
Calcite	-	-	0.3	0.2	-	-	-	-
Amorphous/ unidentified	21.5	54.6	67.3	62.5	4.6	98.0	9.1	98.2

As it appears, the three phases in the kaolin group (kaolinite, dickite and nacrite) exist in all raw clays studied here. The total kaolin content of the raw clays used in this study varies from 37.9% to 93.1%, with GAB1 having the highest kaolin content (93.1%) and EMD1 the lowest (37.9%). A large amount of quartz was found in EMD1 and CCC, which agrees with the high sand content in these clays, but not in GAB1 and GAB4. A higher amount of gibbsite was observed in GAB4, which may influence its reactivity. A considerable amount of illite was also found in addition to the minor phases. Moreover, the quartz percentage of calcined clays was slightly increased in all clays compared to that of uncalcined clays, which can be attributed to loss of water during the calcination process, dehydroxylation of clay, gibbsite, and burning of any organic matter.

Based on the XRD analysis of the calcined clays, the kaolin group has completely disappeared in all clays (except CCC and CCF which were tested in its as-received condition), as a result of calcination at 850℃, indicating a significant loss in crystallinity. A small amount of kaolin still existed in CCC and CCF, indicating that these commercial calcined products were not calcined completely. Some amount of illite was still detected in EMD1 after calcination, and this implies that its structure cannot be altered at this calcining temperature. Higher temperatures may be required for it to achieve complete dehydroxylation. Additionally, CCC and CCF also indicated a small amount of illite possibly due to either insufficient calcination temperature during the industrial production process or its microstructure property. Fernandez et al. [12] speculated that illite conserves the order of their structural layers even after complete dehydroxylation. Moreover, it is not as reactive as kaolin because the alumina groups in illite are trapped between silicate tetrahedra. Therefore, illite has a minor effect on pozzolanic reactivity compared to kaolin.

2.3.2 Thermogravimetric Analysis

In addition to X-ray diffraction, thermogravimetric analysis is another analytical tool that can be effectively used to study clay mineralogy by tracking the weight change as the temperature is increased. All tests were performed in the State Materials Office (SMO), of the Florida Department of Transportation (FDOT), using a TGA/differential scanning calorimeter (DSC) manufactured by TA instruments. The clay samples (approximately 10 mg) were place in a platinum crucible and scanned at a fixed heating rate of 20℃/min up to 1000°C, under nitrogen atmosphere to inhibit oxidation. The weight change versus temperature increase (TGA) is shown in Figure 2-1 and the derivative of weight loss (DTG) is also plotted to clearly define the dehydroxylation process, depicted as an endothermic peak, [13] [14].

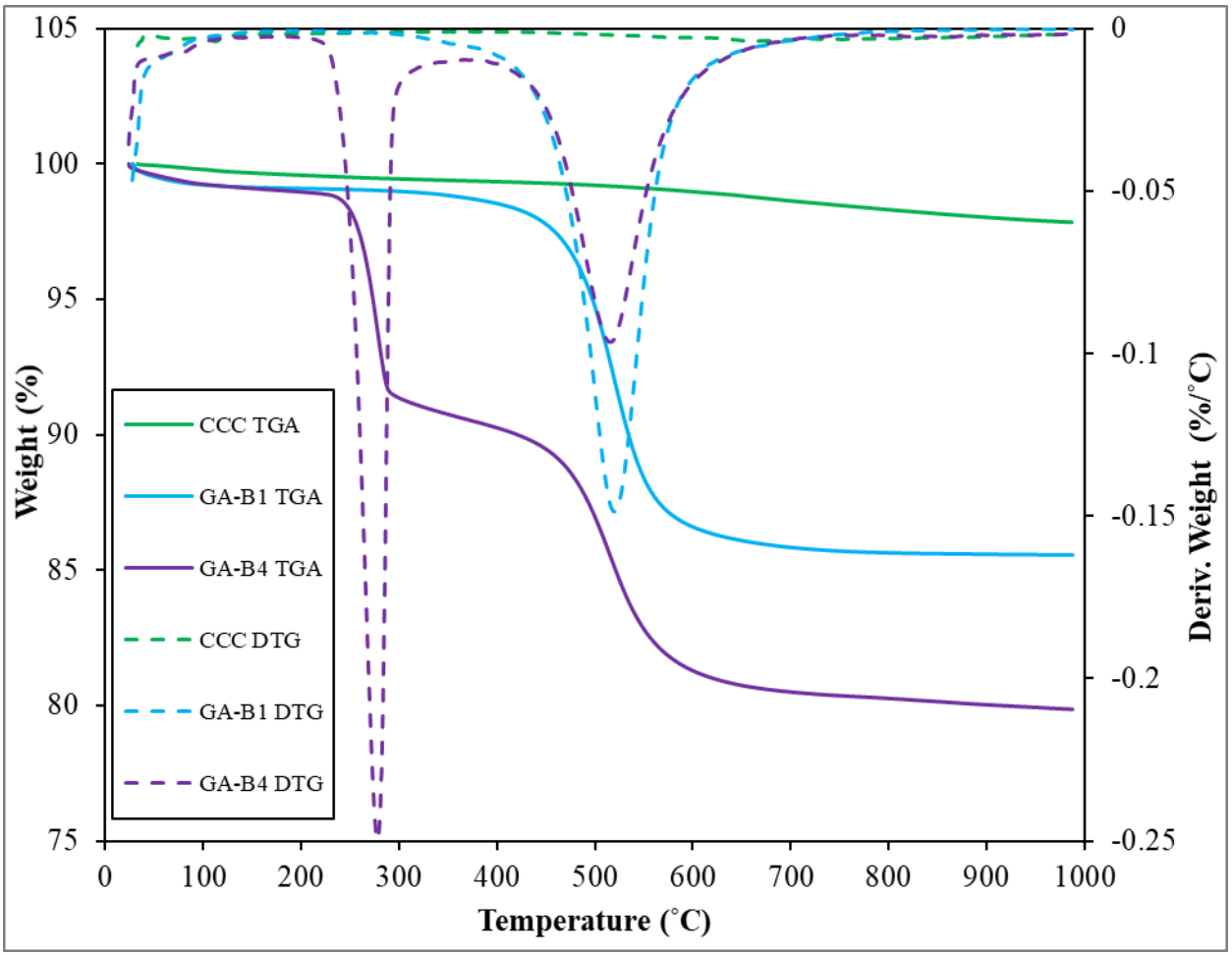

Figure 2-1: TGA and DTG of as-received clays

From Figure 2-1, it is clear that dehydroxylation of kaolin occurred between 450℃ to 600℃, in agreement with the current literature [4, 15]. Around 650℃, the majority of kaolin completed its dehydroxylation, though there was a slight weight loss, indicated by the small hump in the temperature range between 650℃ - 700℃. This could be possibly due to phases such as illite or montmorillonite [16]. In GAB4, there is another peak between 200℃ to 350℃, attributed to the dehydroxylation of gibbsite, which only existed in this particular clay [13, 17].

With the aid of the TGA and DTG curves, the amount of kaolin and gibbsite can be determined using the tangent method [13, 18]. An example of the tangent method, applied to GAB4, is shown in Figure 2-2.

.

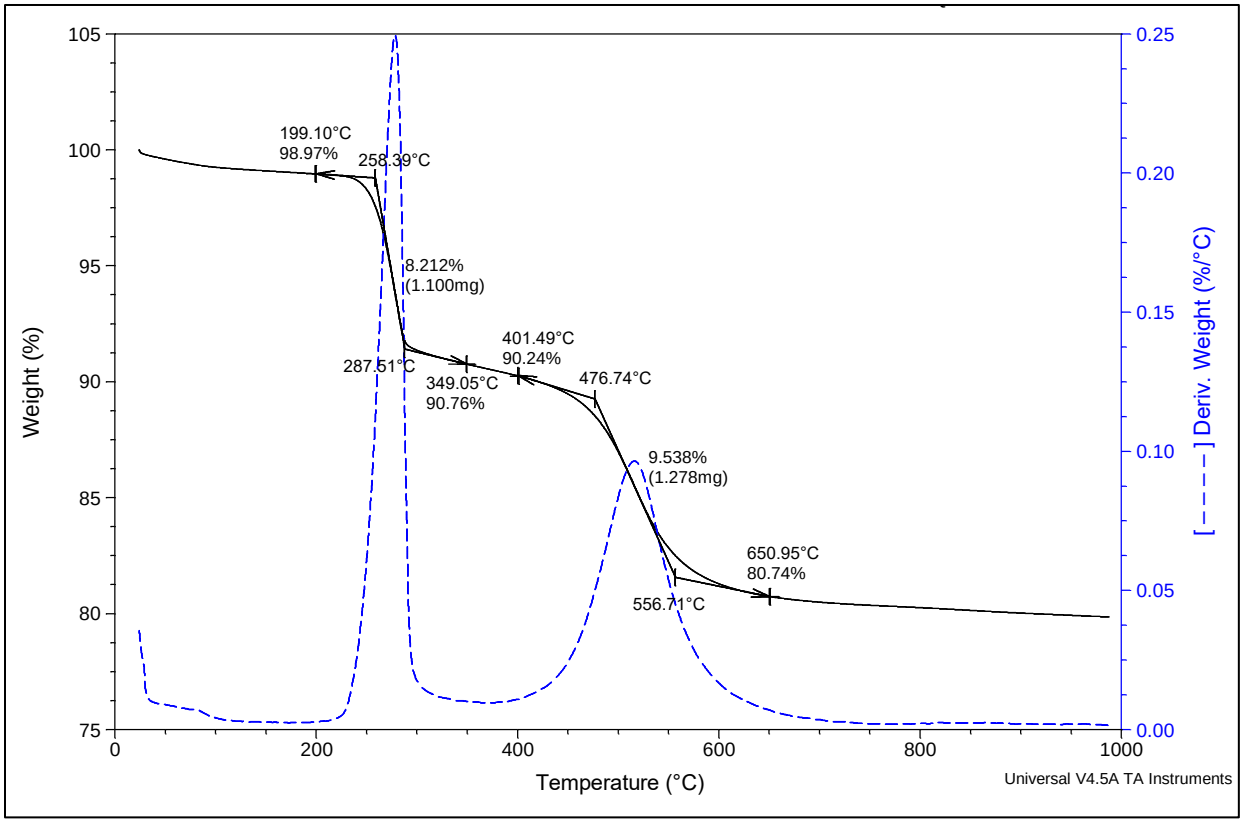

Figure 2-2: Example of tangent method for GAB4

The mass loss was quantified using TA Universal Analysis software (TA Instruments). The original weight was taken as the mass of samples at 110°C, after evaporation of all free water, and m_{loss} was determined based on mass change between the original weight and that defined by the minimum in the DTG curve, shown in Figure 2-1[12]. The literature on LC^3 clay systems [19] typically use a fixed temperature range to quantify the kaolin content in clay samples. However, as reported by Lorentz et al. [12] "the onset of kaolinite dehydroxylation period varied somewhat between the samples, possibly indicating a variability in the degree of disorder". The kaolin content can be calculated from water loss during dehydroxylation according to Equation 2-5:

$$m_{Kaolin} = m_{loss} \frac{M_{Kaolin}}{2 * M_{H_2O}} \qquad \text{Equation 2-5}$$

Where M_{Kaolin} is the molecular mass of kaolin ($Al_2O_3{\cdot}2SiO_2{\cdot}2H_2O$) (258.16 g/mol), M_{H_2O} is the molecular mass of water (18.02 g/mol) [20], m_{Kaolin} is the mass of the kaolin group minerals to

be determined, and m_{loss} is the mass of water lost during dehydroxylation of kaolin derived by tangent method. Similarly, gibbsite content was determined according to Equation 2-6:

$$m_{Gibbsite} = m_{loss} \frac{M_{Gibbsite}}{3 * M_{H_2O}} \quad \text{Equation 2-6}$$

Where the molecular mass of Gibbsite ($Al_2O_3 \cdot 3H_2O$), $M_{Gibbsite}$, is 156.01 g/mol [20].

Results from TGA and x-ray diffraction analyses are presented in Table 2-9. Differences of less than 5% indicate good agreement in the quantification of kaolin and gibbsite using both techniques.

Table 2-9: Kaolin content determined by TGA and XRD

Sample	Phase	TGA	XRD	Difference between TGA and XRD
EM-D1 200P	Kaolin	46.1%	44.9%	1.2%
CCC	Kaolin	2.7%	3.1%	-0.4%
GAB1	Kaolin	88.9%	93.1%	-4.2%
GAB4	Gibbsite	23.9%	24.0%	-0.1%
	Kaolin	68.9%	65.5%	3.4%

2.4 Physical Characteristics

2.4.1 Cement Physical Characteristics

The physical characteristics of the as-received cements determined in this study are specific gravity, Blaine fineness and particle size distribution. Portland cement density is typically around 3.15 g/cm^3 [21] but differences can occur due to other additions such as limestone and kiln dust. The density of each cement was measured in accordance with ASTM C188 [22] and the average specific gravity of triplicate measurements are reported in Table 2-10. Fineness is an important cement property due to its significance on cement hydration and heat release, especially during early ages [21]. Fineness was measured using the Blaine air permeability method according to ASTM C204 [23]. The first step was to measure the air permeability using calibration material of known fineness, SRM 114q, obtained from NIST. Triplicate measurements were taken for each cement and the average values are reported here, Table 2-10. Cements T1L, TH1L, and CIL have the highest Blaine fineness, whereas cement HA has the lowest fineness.

Although Blaine fineness is widely used to characterize cement particles, it is an indirect method of determining fineness as the test actually measures the flow of air through a compacted bed of cement. Cements with similar Blaine fineness values may have very different particle size distributions [24]. Particle size distribution (PSD) can give better insight on the physical properties of cements. The goal of measuring particle size is to give the frequency and size of particles in the sample [25]. In portland cement, the typical particle size varies from < 1 μm to 100 μm in diameter [24]. The particle size distributions of the as-received cements were measured using an LA-950 laser scattering particle size analyzer manufactured by HORIBA Instruments. The wet method was adopted, using ethanol (200 proof) as the dispersing medium. Three measurements were performed for each as-received material. The results, expressed as incremental and cumulative particle size distributions, are plotted in Figure 2-3 and Figure 2-4, respectively, and the mean particle sizes (MPS) are listed in Table 2-10. The data indicate that the particle size distributions of cements are in general agreement with Blaine fineness trends. Cement T1L has the smallest MPS, followed by CIL and TH1L whereas cement HA, G1L-US and G1L-OP have very similar MPS values.

Table 2-10: Particle size analysis, Blaine fineness, and density of cements

Physical properties	**HA I/II(MH)**	**GILUS IL(10)**	**GILOP IL(10)**	**TIL IL(10)**	**THIL IL(14)**	**CIL IL(14)**
D_{10} (μm)	2.631	2.242	2.991	1.520	1.623	1.886
D_{50} (μm)	10.918	10.493	11.039	9.963	10.376	9.540
D_{90} (μm)	25.813	26.696	25.405	21.215	26.652	26.303
Mean size (MPS) (μm)	13.028	13.110	13.105	10.798	12.751	12.44
Density (g/cm^3)	3.10	3.06	3.06	3.11	3.13	3.05
Blaine Fineness (m^2/kg)	417	458	469	483	488	500

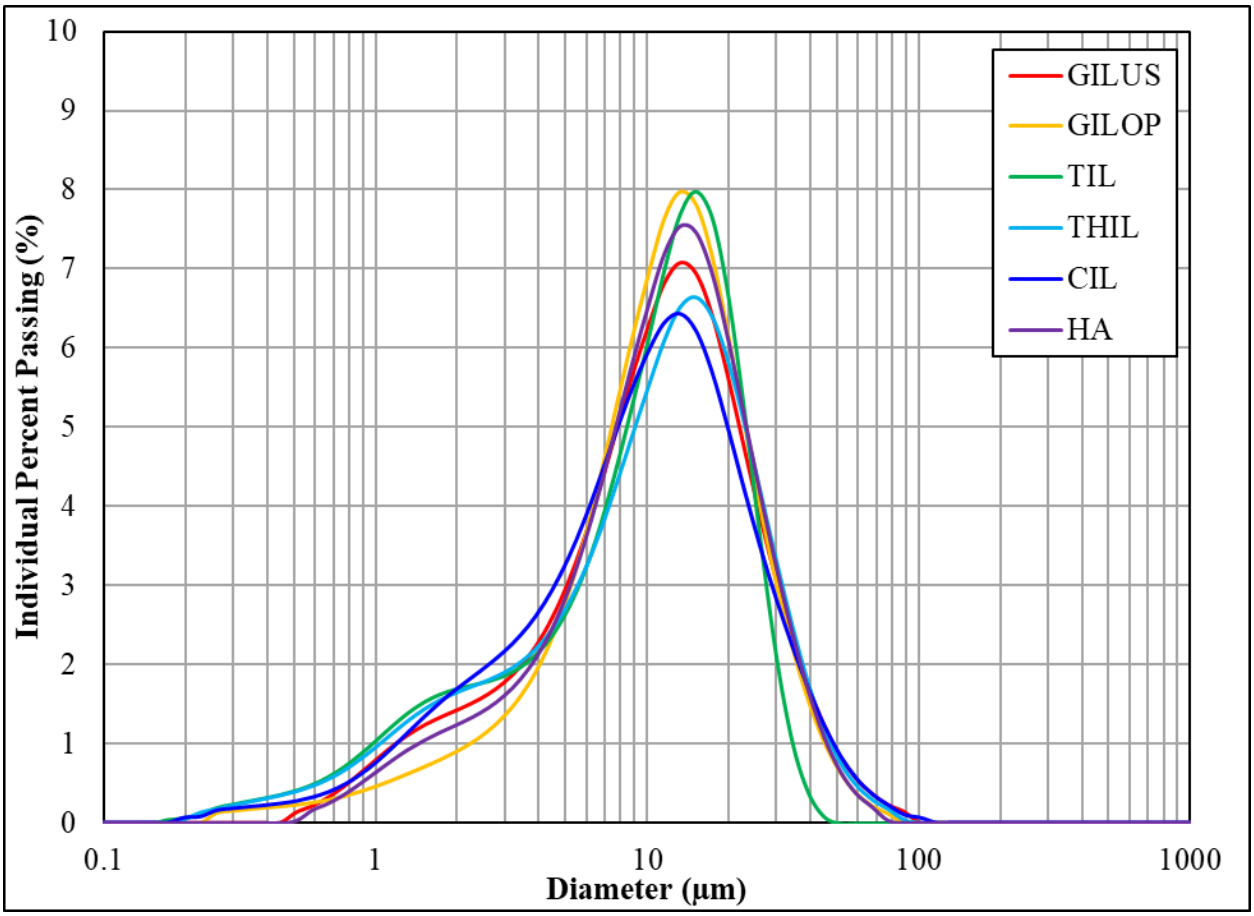

Figure 2-3: Incremental particle size distribution for as-received cements

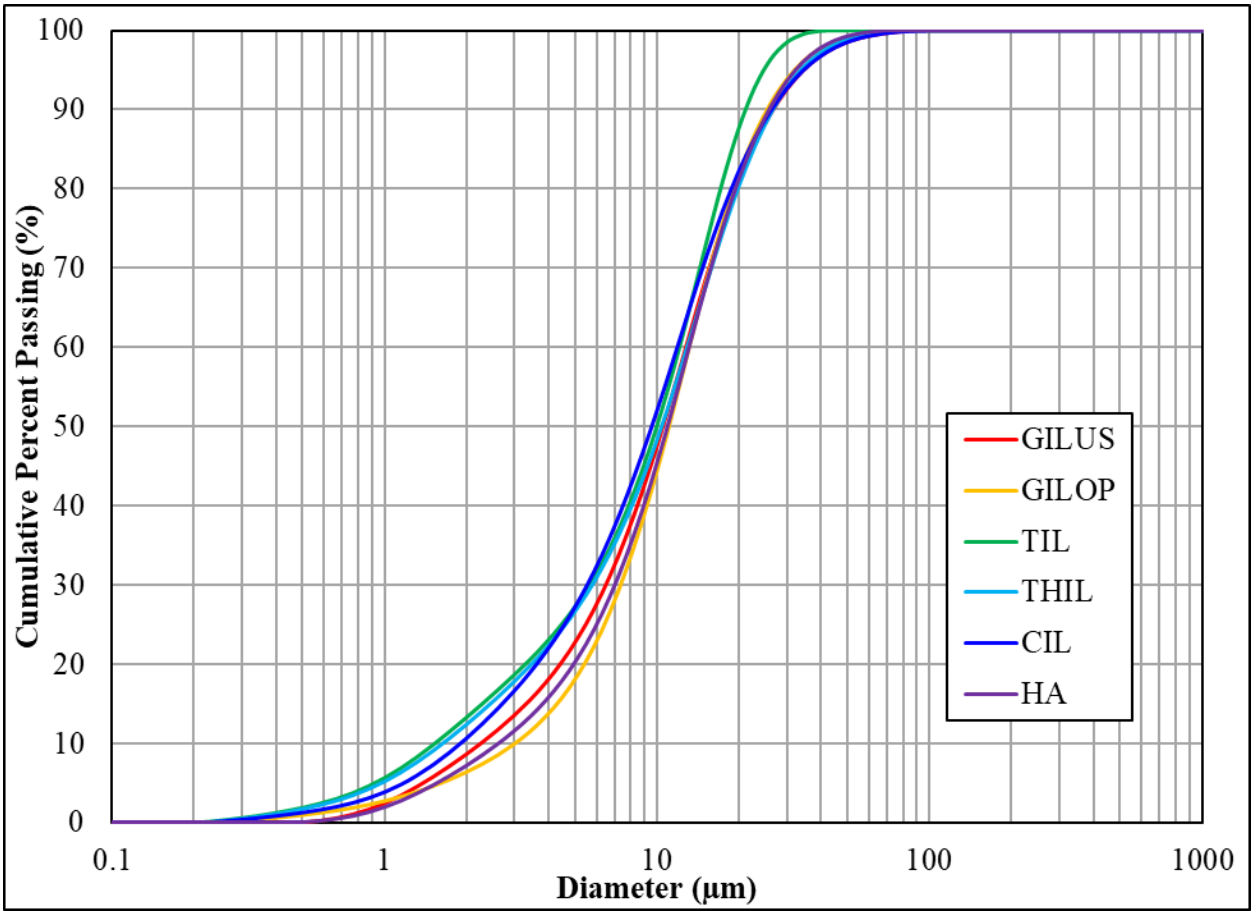

Figure 2-4: Cumulative particle size distribution for as-received cements

2.4.2 Physical Characteristics of Calcined Clays

The same characterization methods, described in section 2.4.1, were adopted to determine the density, fineness and particle size distribution of the four calcined clays. However, in determining particle size distribution, the dispersing medium was water. Although CCC is a commercial calcined clay, its largest particle size is beyond the measuring capability of the laser scanner. Therefore, sieve analysis was performed on this clay to obtain the gradation curve (Figure 2-6) and subsequently the portion which passed the No. 325 sieve (< 45 µm) was further tested for particle size distribution, density and Blaine fineness tests. The retained and passing percentages obtained from sieve analysis are listed in Table 2-11.

Table 2-11: Sieve analysis results of CCC calcined clay

Sieve No.	Size	Percentage Retained	Cumulative Retained	Total Passing
No.4	4.75 mm	0.00%	0.00%	100.00%
No.8	2.36 mm	1.62%	1.62%	98.38%
No.16	1.18 mm	9.48%	11.09%	88.91%
No.30	600 μm	14.23%	25.32%	74.68%
No.50	300 μm	17.34%	42.66%	57.34%
No.100	150 μm	20.35%	63.01%	36.99%
No.200	75 μm	15.54%	78.55%	21.45%
No.325	45 μm	9.26%	87.81%	12.19%
Pan	<45 μm	12.19%	100.00%	0.00%

Particle size analysis, Blaine fineness, and density of the non-commercial clays, after calcination for 1 hour at 850°C, and the commercial calcined clay, CCC-325P, are listed in Table 2-12. Only Blaine fineness was determined for the commercial calcined clay CCF. The incremental and cumulative particle size distributions are plotted in Figure 2-5 and Figure 2-6, respectively. Blaine fineness and particle size distribution trends did not follow the same trends. When performing the Blaine test for calcined clays, samples of different masses had to be prepared to produce a test bed with porosity of 0.530 ± 0.005, by applying thumb pressure on the plunger. The literature [26, 27] have identified some drawbacks of Blaine air permeability, especially when it is used to determine the fineness of materials other than cements, although it is rapid and simple to perform. Arvaniti et al. [27] indicated that this test method is unable to account for different particle shapes and bed tortuosity. It was also stated that "The reference material must have similar shape, particle size distribution, and surface properties to the material of interest or it cannot be a valid comparison". It was reported further that it is difficult to achieve a uniform sample bed with materials like metakaolin due to the plate-like shape of its particles. Particle size determinations using laser diffraction have become popular because it is easier, more reproducible and provides a complete picture of the full size distribution. In this method, it is assumed that the material is isotropic, and particles are spherical in shape.

Table 2-12: Particle size analysis, Blaine fineness, and density of calcined clays (850°C for 1 hour)

Physical properties	EMD1	CCC-325P	CCF	GAB1	GAB4
D_{10} (µm)	10.483	5.019	-	4.434	1.077
D_{50} (µm)	46.079	16.341	-	37.484	15.685
D_{90} (µm)	137.786	34.578	-	128.608	94.469
Mean size (MPS) (µm)	61.955	20.637	-	53.973	35.015
Density (g/cm^3)	2.49	2.48	2.70	2.49	2.67
Blaine Fineness (m^2/kg)	630	617	984	1777	2791

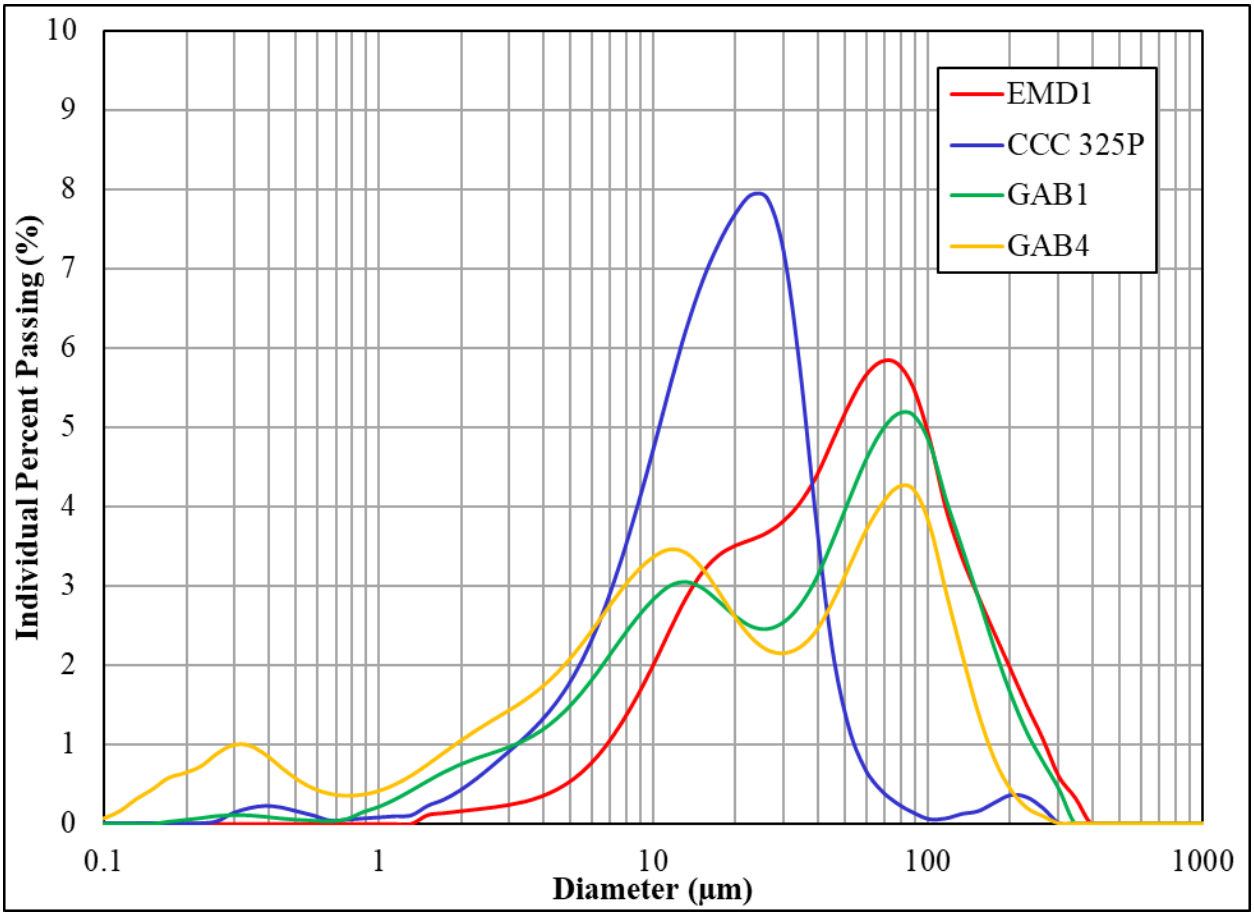

Figure 2-5: Incremental particle size distribution for calcined clays

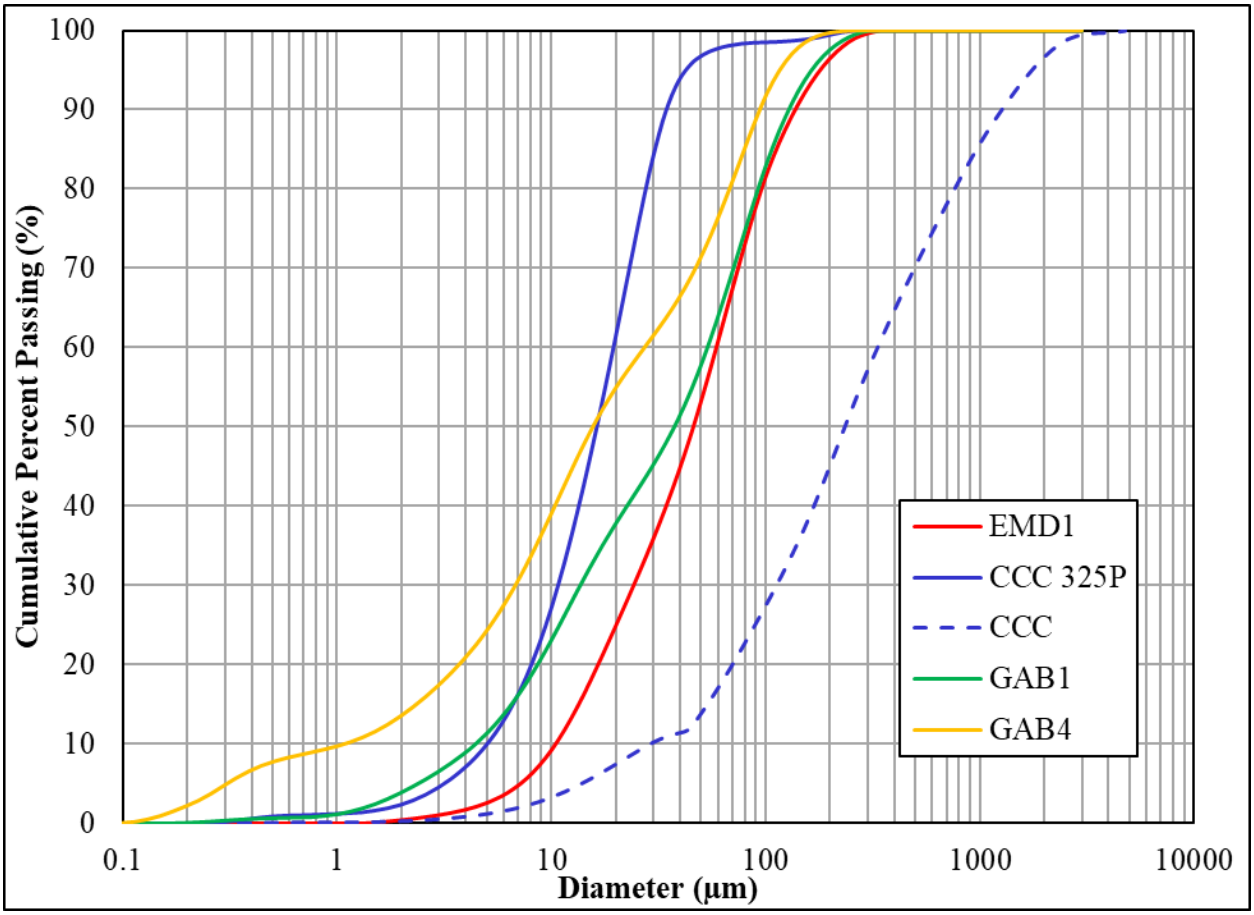

Figure 2-6: Cumulative particle size distribution for calcined clays

2.5 Conclusions

In this chapter, all as-received cements and calcined clays were characterized for their chemical, mineralogical and physical characteristics. The results indicate that IL cements have, in general, higher fineness. The main minerals found in the as-received clays were kaolin and gibbsite. It would be interesting to see if gibbsite will have significance on durability performance of the clay-blended cementitious system.

2.6 References

[1] T. Schmidt, B. Lothenbach, M. Romer, J. Neuenschwander, and K. Scrivener, “Physical and microstructural aspects of sulfate attack on ordinary and limestone blended Portland cements,” *Cem. Concr. Res.*, vol. 39, no. 12, pp. 1111–1121, 2009, doi: 10.1016/j.cemconres.2009.08.005.

[2] E. F. Irassar, “Sulfate attack on cementitious materials containing limestone filler - A review,” *Cem. Concr. Res.*, vol. 39, no. 3, pp. 241–254, 2009, doi: 10.1016/j.cemconres.2008.11.007.

[3] ASTM C114−15, “Standard Test Methods for Chemical Analysis of Hydraulic Cement,” West Conshohocken, PA: ASTM International, 2015.

[4] R. Fernandez, F. Martirena, and K. L. Scrivener, “The origin of the pozzolanic activity of calcined clay minerals: A comparison between kaolinite, illite and montmorillonite,” *Cem. Concr. Res.*, vol. 41, no. 1, pp. 113–122, 2011, doi: 10.1016/j.cemconres.2010.09.013.

[5] ASTM C618-12a, “Standard Specification for Coal Fly Ash and Raw or Calcined Natural Pozzolan for Use in Concrete,” West Conshohocken, PA: ASTM International, 2014.

[6] ASTM C1365-06, “Standard Test Method for Determination of the Proportion of Phases in Portland Cement and Portland-Cement Clinker Using X-Ray Powder Diffraction Analysis,” West Conshohocken, PA: ASTM International, 2016.

[7] D. Jansen, C. Stabler, F. Goetz-Neunhoeffer, S. Dittrich, and J. Neubauer, “Does Ordinary Portland Cement Contain Amorphous Phase? A Quantitative Study Using an External Standard Method,” *Powder Diffr.*, vol. 26, no. 1, pp. 31–38, Mar. 2011, doi: 10.1154/1.3549186.

[8] M. A. G. Aranda, A. G. De la Torre, and L. Leon-Reina, “Rietveld Quantitative Phase Analysis of OPC Clinkers, Cements and Hydration Products,” *Reviews in Mineralogy and Geochemistry*, vol. 74, no. 1. pp. 169–209, 2012, doi: 10.2138/rmg.2012.74.5.

[9] D. Bish and R. J. Reynolds, “Sample Preparation for X-Ray Diffraction,” in *Modern Powder Diffraction*, D. Bish and J. Post, Eds. Washington, DC: The Mineralogical Society of America, 1989, pp. 73–99.

[10] P. E. Stutzman, “Guide for X-Ray Powder Diffraction Analysis of Portland Cement and Clinker,” Gaithersburg, MD, 1996.

[11] W. A. Gutteridge, “On the Dissolution of the Interstitial Phases in Portland Cement,” *Cem.*

Concr. Res., vol. 9, no. 3, pp. 319–324, 1979.

[12] B. Lorentz, N. Shanahan, Y. P. Stetsko, and A. Zayed, "Characterization of Florida kaolin clays using multiple-technique approach," *Appl. Clay Sci.*, vol. 161, pp. 326–333, Sep. 2018, doi: 10.1016/J.CLAY.2018.05.001.

[13] A. Zayed, N. Shanahan, A. Sedaghat, Y. Stetsko, and B. Lorentz, "Final Report Development of Calcined Clays as Pozzolanic Additions in Portland Cement Concrete Mixtures FDOT Contract Number : BDV25-977-38," University of South Florida, Tampa, FL, 2018.

[14] S. Vyazovkin, "Thermogravimetric Analysis," in *Characterization of Materials*, E. N. Kaufmann, Ed. John Wiley & Sons, Inc., 2012, pp. 177–211.

[15] A. Shvarzman, K. Kovler, G. S. Grader, and G. E. Shter, "The effect of dehydroxylation/amorphization degree on pozzolanic activity of kaolinite," *Cem. Concr. Res.*, vol. 33, no. 3, pp. 405–416, Mar. 2003, doi: 10.1016/S0008-8846(02)00975-4.

[16] R. Fernandez, F. Martirena, and K. L. Scrivener, "The origin of the pozzolanic activity of calcined clay minerals: A comparison between kaolinite, illite and montmorillonite," *Cem. Concr. Res.*, vol. 41, no. 1, pp. 113–122, Jan. 2011, doi: 10.1016/J.CEMCONRES.2010.09.013.

[17] B. Fabbri, S. Gualtieri, and C. Leonardi, "Modifications induced by the thermal treatment of kaolin and determination of reactivity of metakaolin," *Appl. Clay Sci.*, vol. 73, pp. 2–10, Mar. 2013, doi: 10.1016/J.CLAY.2012.09.019.

[18] B. Lothenbach, P. T. Durdzinski, and K. De Weerdt, "Thermogravimetric analysis," in *A Practical Guide to Microstructural Analysis of Cementitious Materials*, K. Scrivener, R. Snellings, and B. Lothenbach, Eds. CRC Press, 2016, pp. 177–211.

[19] F. Avet, R. Snellings, A. Alujas Diaz, M. Ben Haha, and K. Scrivener, "Development of a new rapid, relevant and reliable (R3) test method to evaluate the pozzolanic reactivity of calcined kaolinitic clays," *Cem. Concr. Res.*, vol. 85, pp. 1–11, 2016, doi: 10.1016/j.cemconres.2016.02.015.

[20] F. P. Hansen, *The science of construction materials*. Springer, Berlin, Heidelberg, 2009.

[21] S. Mindess, F. J. Young, and D. Darwin, *Concrete*. Upper Saddle River, NJ: Pearson Education, Inc., 2003.

[22] ASTM C188-15, "Standard Test Method for Density of Hydraulic Cement," West

Conshohocken, PA: ASTM International, 2015.

[23] ASTM C204-16, “Standard Test Methods for Fineness of Hydraulic Cement by Air-Permeability Apparatus,” in *ASTM International*, 2016.

[24] P. K. Mehta and P. J. M. Monteiro, *Concrete: Microstructure, Properties, and Materials*, 4th ed. McGraw-Hill Education, 2014.

[25] S. J. Dapkunas, L. H. Lum, and L. H. Lum, “Particle-size characterization,” *Am. Ceram. Soc. Bull.*, vol. 80, no. 10, pp. 59–62, 2001.

[26] E. C. Arvaniti, M. C. G. Juenger, S. A. Bernal, J. Duchesne, L. Courard, S. Leroy, J. L. Provis, A. Klemm, N. De Belie, “Determination of particle size, surface area, and shape of supplementary cementitious materials by different techniques,” *Mater. Struct.*, vol. 48, no. 11, pp. 3687–3701, 2015, doi: 10.1617/s11527-014-0431-3.

[27] E. C. Arvaniti, M. C. G. Juenger, S. A. Bernal, J. Duchesne, L. Courard, S. Leroy, J. L. Provis, A. Klemm, N. De Belie, “Physical characterization methods for supplementary cementitious materials,” *Mater. Struct.*, vol. 48, no. 11, pp. 3675–3686, 2015, doi: 10.1617/s11527-014-0430-4.

Chapter 3 Effect of Calcined Low-Grade Kaolin Clay on Strength Evolution of Cementitious Mixtures

3.1 Introduction

Calcined clay can be incorporated in concrete as a supplementary cementitious material (SCM) to improve its strength development due to the additional formation of hydration products as a result of pozzolanic reaction. It can also enhance concrete durability against external sulfate attack due to a reduced concrete permeability with pore size refinement. Sulfate attack is a major durability issue in Florida. External sulfates can cause damage to concrete after penetration of the concrete by sulfates contained in the soil, groundwater, and marine environments. External sulfate attack can occur when the concrete is exposed to sulfate concentrations more than 0.1% and is manifested by expansion and/or loss of strength and cohesion [1].

There are three principle mechanisms that can cause concrete deterioration due to external chemical sulfate attack, namely conversion of monosulfoaluminate to ettringite, secondary gypsum formation due to the reaction between CH and sulfates, and decalcification of C-S-H [2, 3]. Cementitious materials with high alumina contents form monosulfoaluminate during initial hydration due to lack of sufficient amounts of sulfates. Later on, when external sulfate ions penetrate into concrete, the monosulfoaluminate reacts with sulfate ions and converts to ettringite causing expansion [4–6]. Moreover, excess sulfate ions can react with CH to form gypsum which can cause expansion [2], [7]. As stated by Mehta and Monteiro [3] “deterioration of hardened portland cement paste by gypsum formation goes through a process that first leads to reduction of pH of the system and loss in the stiffness and strength, followed by expansion and cracking, and eventually transformation of the concrete into a mushy or non-cohesive mass”.

The type of reaction products that form during sulfate attack also depends on the cations associated with the external sulfate ions (e.g., Na^+, Ca^+ or Mg^{2+}). Calcium sulfate has a low solubility in water and consequently does not increase the sulfate concentration in the concrete pore solution as quickly as the other salts [8]. In terms of sodium sulfate attack, sodium hydroxide forms along with gypsum. Since NaOH is highly soluble, alkalinity of the pore solution is maintained and consequently stabilizes C-S-H. On the other hand, magnesium sulfate forms magnesium hydroxide, which is an insoluble product and lowers the pH of the pore solution as a

result. Consequently, C-S-H decalcifies and loses its cohesiveness and lowers the concrete strength [2].

Several studies have documented the use of metakaolin to improve concrete strength and to lower permeability [9–11]. Coupled substitution of metakaolin and limestone has also shown excellent strength performance even at early ages due to the formation of carboaluminate phases [12]. According to Antoni et al. [12], a 2:1 blend of metakaolin and limestone at a substitution rate of up to 45% can yield higher strengths at 7 and 28 days than the 100% portland cement reference. In addition to metakaolin, use of low-grade calcined clays as partial replacement of cement has been shown to be feasible [13]. Compressive strengths similar to that of plain portland cements were observed with calcined kaolinite content ≥ 40 % for ages ≥ 7 days. This was achieved with limestone, cement, and calcined clay blends containing only 50% clinker. According to the same study, early-age strength development is mainly dependent on the calcined kaolinite content; increased calcined kaolinite contents linearly increased strengths. However, after 28 days, calcined kaolinite contents become less significant for clays with more than 45% of calcined kaolinite content. Avet [14] explained this behavior as a result of lowered degree of hydration of clinker with increasing calcined kaolinite contents due to reaching a maximum refinement of the critical pore entry. Hence, formation of carboaluminate phases was limited.

As stated earlier, sulfate attack can cause loss of strength and cohesion in concrete. Therefore, the primary focus of this task is to evaluate the compressive strength development of low-grade calcined clay-blended cement mortar cubes with varying substitution levels in saturated lime solution as well as in 5% sodium sulfate solution, in order to determine the effect of chemical and physical characteristics of cements and clays on loss of strength and cohesion.

3.2 Experimental methods

Three cements designated HA (Type I/II (MH)), GILOP (Type IL(10)) and THIL (Type IL(14)), and five clays designated EMD1, CCC, CCF, GAB1 and GAB4 were selected to prepare mortar cubes at 10% and 20% cement replacement levels with each clay. Clays CCC and CCF are commercially available calcined clays from the same source, but clay CCF has a finer particle size distribution than that of clay CCC. Oxide chemical composition, mineralogical analysis, Blaine fineness and mean particle size (MPS) of cements and clays are listed in Table 3-1 through Table 3-4.

Table 3-1: Oxide chemical composition of cements

Analyte	HA I/II(MH)	GILOP IL(10)	THIL IL(14)
SiO_2	20.63	18.43	19.14
Al_2O_3	5.02	4.56	4.52
Fe_2O_3	3.45	3.29	3.54
CaO	63.96	62.28	62.11
MgO	0.35	0.91	1.08
SO_3	2.71	2.93	2.44
Na_2O	0.04	0.18	0.17
K_2O	0.3	0.32	0.29
TiO_2	0.25	0.21	0.22
P_2O_5	0.37	0.43	0.09
Mn_2O_3	0.07	0.06	0.14
SrO	0.07	0.06	0.12
Cr_2O_3	0.02	0.02	0.02
ZnO	0.03	0.06	0.04
L.O.I. (550°C)	0.98	1.62	0.69
L.O.I. (950°C)	2.54	5.86	5.99
Total	99.81	99.62	99.91
Na_2O_{eq}	0.24	0.40	0.36

Table 3-2: Mineralogical analysis, Blaine fineness, and MPS of cements

Analyte	HA I/II(MH)	GILOP IL(10)	THIL IL(14)
Alite	45.4	44.5	40.3
Belite	19.7	16.5	16.9
Aluminate	4.0	3.7	2.9
Ferrite	9.3	8.9	10.8
Gypsum	1.0	3.9	1.5
Hemihydrate	2.7	0.0	2.0
Calcite	3.4	9.2	11.4
Portlandite	1.5	1.5	-
Quartz	1.0	0.4	1.4
Dolomite	0.3	0.7	-
Amorphous/ unidentified	11.7	10.6	12.8
Blaine fineness (m^2/kg)	417	469	488
MPS (μm)	13.028	13.105	12.751

Table 3-3: Oxide chemical composition of clays

Analyte	EMD1	CCC	CCF	GAB1	GAB4
SiO_2	68.68	63.49	62.62	44.56	31.82
Al_2O_3	20.81	19.89	18.94	37.44	44.49
Fe_2O_3	1.00	7.99	10.31	0.92	0.72
CaO	0.00	1.08	0.28	0.00	0.00
MgO	0.08	0.45	0.37	0.11	0.11
SO_3	0.00	0.23	0.15	0.00	0.17
Na_2O	0.18	0.09	0.42	0.08	0.05
K_2O	2.37	1.66	0.58	0.23	0.10
TiO_2	0.68	1.24	1.49	1.85	1.80
P_2O_5	0.13	0.04	0.14	0.05	0.03
Mn_2O_3	0.01	0.04	0.12	0.00	0.00
SrO	0.01	0.01	0.00	0.01	0.00
Cr_2O_3	0.00	0.01	0.02	0.01	0.01
ZnO	0.00	0.00	0.00	0.00	0.00
BaO	0.06	0.09	0.13	0.02	0.01
L.O.I. (950°C)	5.88	3.39	4.59	14.38	19.91
Total	99.88	99.72	100.16	99.66	99.21
Na_2O_{eq}	1.74	1.19	0.80	0.23	0.12

Table 3-4: Mineralogical analysis, Blaine fineness, and MPS of clays

Analyte	EMD1	EMD1 (850°C) (1 h)	CCC	CCF	GAB1	GAB1 (850°C) (1 h)	GAB4	GAB4 (850°C) (1 h)
Kaolinite	17.2	0.0	-	0.8	54.4	0.0	40.9	0.0
Dickite	10.1	0.0	-	-	33.4	0.0	18.1	0.0
Nacrite	10.6	0.0	-	-	5.3	0.0	6.4	0.0
Sum Kaolin	**37.9**	**0.0**	**3.1**	**0.8**	**93.1**	**0.0**	**65.5**	**0.0**
Illite	4.4	3.3	2.8	0.9	0.3	-	0.1	-
Gibbsite	-	-	-	-	-	-	24.0	-
Quartz	36.2	42.2	25.5	34.6	0.9	1.0	0.2	1.4
Crandallite	-	-	-	-	0.3	-	0.0	-
Hematite	-	-	0.7	1.0	-	-	-	-
Anatase	-	-	0.3	0.1	0.7	1.0	1.1	0.3
Calcite	-	-	0.3	0.2	-	-	-	-
Amorphous/ unidentified	21.5	54.6	67.3	62.5	4.6	98.0	9.1	98.2
Blaine fineness (m^2/kg)	-	630	617 (325P)	984	-	1771	-	2791
MPS (µm)	-	61.955	20.637 (325P)	-	-	53.973	-	35.015

In order to assess the effects of calcined low-grade kaolin clay composition and substitution level on strength evolution, mortar cubes were prepared in accordance with ASTM C109 [15] and ASTM C305 [16] with the exception of the adjusted water-to-cementitious materials (w/cm) ratio. ASTM C109 [15] specifies to adjust the amount of mixing water to maintain a constant flow at 110 ± 5; however, the w/cm ratio is a major factor controlling compressive strength. As the primary focus of this study is to investigate the compressive strength development of mortars prepared with different clays and varying clay substitution levels in lime and sulfate environments, w/cm ratio was maintained constant at 0.485 to eliminate its effect as a variable. Due to the low workability of calcined clay, a high-range water-reducer (HRWR) was added to the mixing water at two different dosages for the two substitution levels (200 ml/100 kg cementitious material for 10% clay and 350 ml/100 kg cementitious material for 20% clay) in order to obtain a flow satisfactory for casting the cubes. The water content in the chemical admixture was subtracted from the mixing water to maintain a constant water content. Mortar mixture designs are listed in Table 3-5.

Table 3-5: Mortar mix proportions (9-cube mix)

Material	**Control mix**	**10% clay mix**	**20% clay mix**
Cement – g (lb)	740 (1.631)	666 (1.468)	592 (1.305)
Clay – g (lb)	0 (0)	74 (0.163)	148 (0.326)
Sand – g (lb)	2035 (4.486)	2035 (4.486)	2035 (4.486)
Water – g (lb)	359 (0.791)	358.05 (0.789)	357.33 (0.788)
Type F HRWR – g (lb)	0 (0)	1.59 (0.004)	2.78 (0.006)

After demolding, all cubes were cured using saturated lime solution until 7 days to obtain the initial compressive strength at 7 days. Thereafter, half of the remaining cubes were transferred to a 5% sodium sulfate solution while the rest of the cubes remained in the saturated lime solution for curing. The saturated lime solution contained 3 g of calcium hydroxide per liter of deionized water. Sodium sulfate solution was prepared following ASTM C1012 [17] and changed at the same intervals specified for mortar bars except the initial exposure. Mortar cubes were tested at 7, 28, 90, 180, and 360 days to assess the compressive strength evolution.

In addition, thermodynamic modeling was performed on the same mixtures using the Gibbs free energy minimization software GEMS 3 [18]. Thermodynamic data were taken from the default Nagra-PSI database [19] and CEMDATA14 [20] for cement-specific compounds. GEMS

predicts phase assemblage based on equilibrium reactions. Phases predicted at the ultimate equilibrium were considered in the analysis. Modeling was performed on control mixtures and clays CCF and GAB4 blended mixtures. First, the phase assemblage of the lime-cured mixtures was modeled. Subsequently, sulfate attack was modeled by varying the cementitious-materials-to-Na_2SO_4 solution ratio. A similar modeling approach was used by Nosouhian et al. [21] to predict the sulfate attack in slag-blended mortar bars immersed in sulfate solution.

3.3 Results and Discussion

3.3.1 Compressive Strength Evolution of Cements in Lime Solution and 5% Sodium Sulfate Solution

To assess the effect of clays on strength evolution of cement-clay mixtures, it is imperative to evaluate the behavior of plain cement systems when exposed to saturated lime solution and sulfate solution. Mortar cubes made with the three selected cements were the control mixtures to compare with those substituted by clays. Compressive strength development of control mortar cubes cured in saturated lime solution is shown in Figure 3-1. As it appears, cement HA, which is a Type I/II(MH) cement showed the highest strengths even though it had the lowest Blaine fineness of 417 m^2/kg versus cements GILOP and THIL (469 and 488 m^2/kg respectively). This can be attributed to the higher clinker content in cement HA than that of cements GILOP and THIL, which were diluted due to the presence of limestone (approximately 9.2% and 11.4% calcite contents respectively). According to the mineralogical analysis of the three cements, C_3S content of cement HA was similar to that of cement GILOP (45.4% vs 44.5%) but the C_2S content was higher than that of cement GILOP (19.7% vs 16.5%), resulting in similar strength development at 7 days but higher strengths after 28 days. Among the two IL cements, cement GILOP had higher C_3S content than that of cement THIL (44.5% vs 40.3%) but similar C_2S contents (16.5% vs 16.9%), leading to a slightly higher strength than THIL in early age but similar strength after 90 days. Moreover, after 90 days, the strength development appeared to level off in all the systems.

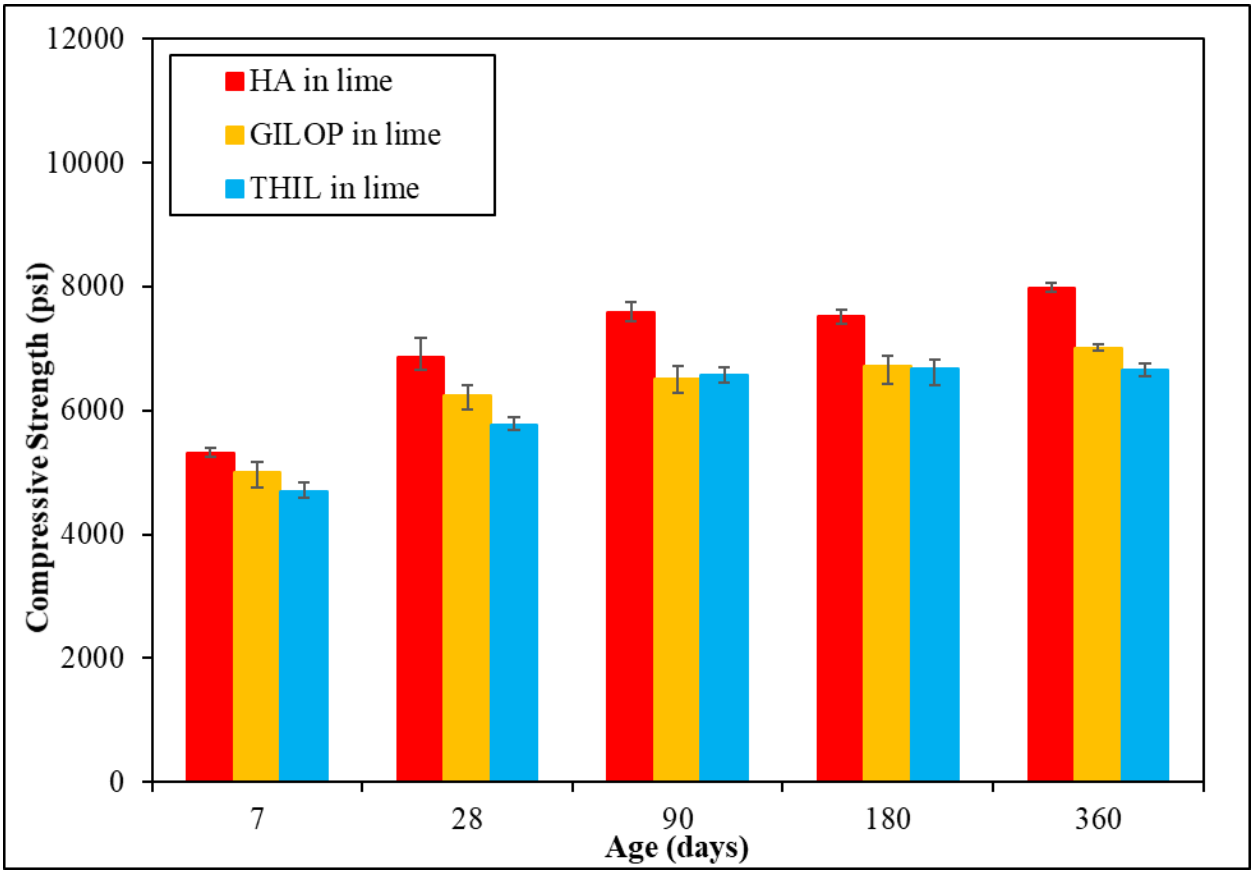

Figure 3-1: Compressive strength development of control mortars in lime solution

When exposed to 5% sodium sulfate solution after curing in saturated lime solution for 7 days, the strength evolution is shown in Figure 3-2, in which 7-day strength was taken from cubes before immersing in sulfate solution. The strength evolution of the mortar cubes in sulfate solution until 90 days was similar to that in lime solution and therefore no deterioration was observed, indicating good sulfate resistance in all three cements. However, after 90 days, a substantial decrease in strength can be observed in all the systems. C_3A in cement is found to negatively affect sulfate resistance [3], [22] and ASTM C150 [23] specifies cements below 5% C_3A as high sulfate resistant and below 8% C_3A as moderate sulfate resistant. In this study, C_3A amounts determined by x-ray diffraction with Rietveld refinement are 4.0%, 3.7% and 2.9% for cements HA, GILOP and THIL respectively.

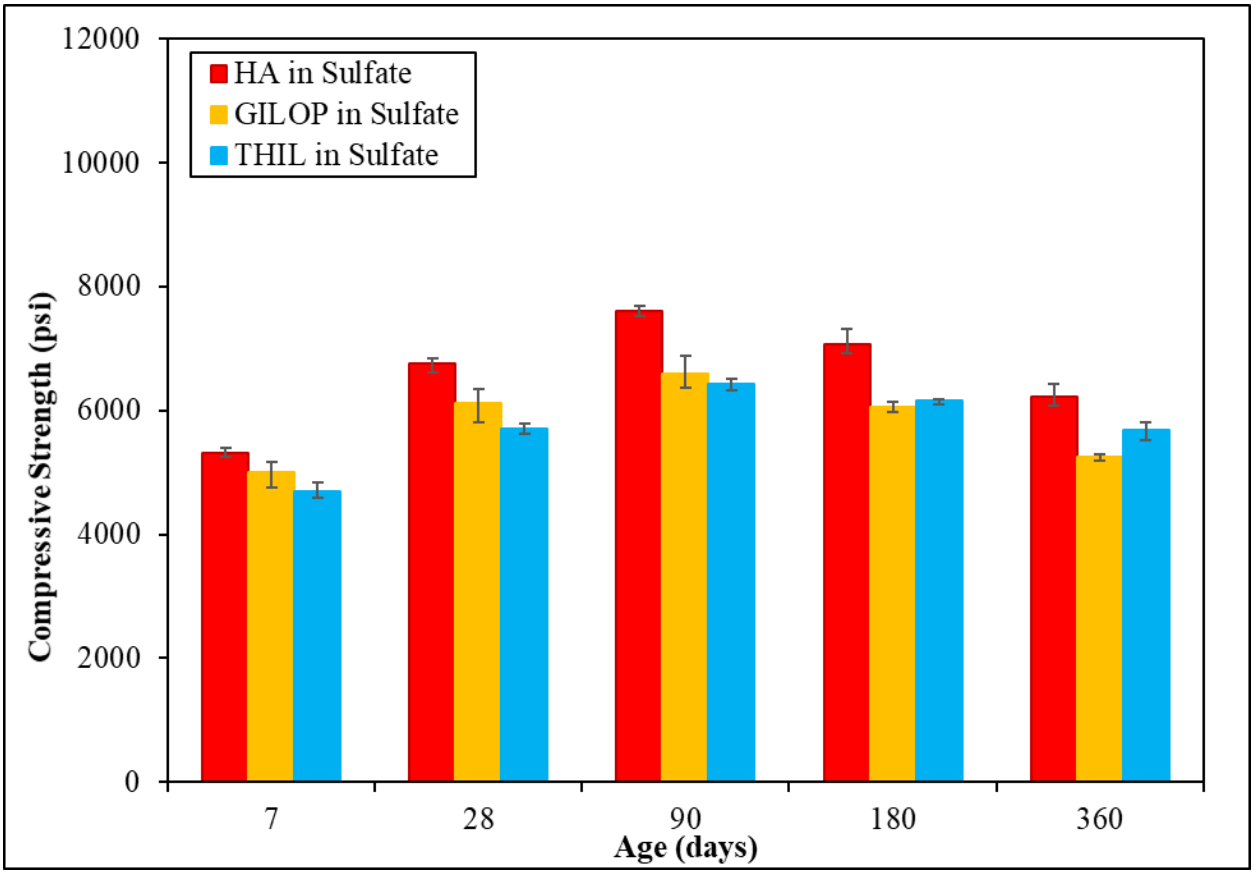

Figure 3-2: Compressive strength development of control mortars in 5% sodium sulfate solution

3.3.2 Effect of Cement and Clay Characteristics and Clay Substitution Levels on Strength Evolution

3.3.2.1 Compressive Strength Development in Saturated Lime Solution

Figure 3-3 shows the strength development of 10% clay mortars with cement HA in lime solution. Incorporation of clay improved the compressive strength of mortars, except for clay CCC. As expected, inclusion of clay increased the strength due to the higher reactivity of calcined clays. The requirements of ASTM C618 [24] for natural pozzolans specify a strength activity index of 75% at 7 and 28 days at a replacement level of 20%. Compressive strengths of 10% clay blended mixtures with cement HA exceeded 75% the control strength at 7 and 28 days. Moreover, the strengths of the 10% clay mixtures at 7 and 28 days were higher than the 10% Class F fly ash results that were reported in a previous study (84% and 86% of the fly ash control at 7 and 28 days, respectively) [25], [26]. Clay GAB4 showed the highest strength improvement at all ages. The

kaolin content of the clays EMD1, GAB1 and GAB4 were 37.9%, 93.1% and 65.5%, respectively. Moreover, clay GAB4 had a gibbsite content of 24%. In addition to lower kaolin content, clay EMD1 had a considerably higher sand content (36.2%). Higher kaolin contents are expected to have higher pozzolanic activity [27]. It was reported that the compressive strength is linearly correlated with the calcined kaolinite content at 7 days in a limestone-calcined clay system with 50% clinker fraction [27]. However, as stated earlier, higher amounts of calcined kaolinite (> 45%) can be less significant at later ages due to the decreased degree of hydration of the clinker fraction with the increase in calcined kaolinite content. Therefore, as it appears in Figure 3-3, the higher kaolin content of clay GAB1 was less significant in increasing the compressive strength compared to that of clay GAB4, which has a lower kaolin content, as the mix with clay GAB4 had the highest strength at all ages. It is likely the higher fineness of clay GAB4 governed the clay reactivity and resulted in higher strengths. Moreover, it can also be speculated that calcined gibbsite in clay GAB4 may have influenced its reactivity. As stated by Sabir et al. [28], when laterites are calcined, kaolinite and gibbsite are transformed into phases of metakaolin and amorphous alumina which possess pozzolanic properties. Tchamo-Leussa et al. [29] reported that gibbsite possesses higher pozzolanic activity in clay. However, Zunino and Scrivener [30] stated that "the presence of gibbsite in raw clays does not interfere with the normal reactivity of the metakaolin available". In another study [31], findings indicated that increased gibbsite contents decreased the 28-day compressive strengths of metakaolin-based geopolymer cement pastes. Therefore, the effect of calcined gibbsite on clay reactivity appears to be debatable in the literature. But as it can be seen from consistently higher strengths of clay GAB4 blends, it is likely the calcined gibbsites enhanced clay reactivity compared to that of calcined kaolinite and formed more hydration products. On the other hand, clay CCC has a coarser particle size distribution which may have resulted in a lower reactivity at early ages and consequently resulted in a lower strength gain. Nevertheless, clay CCF mix showed strengths slightly higher or comparable to control HA.

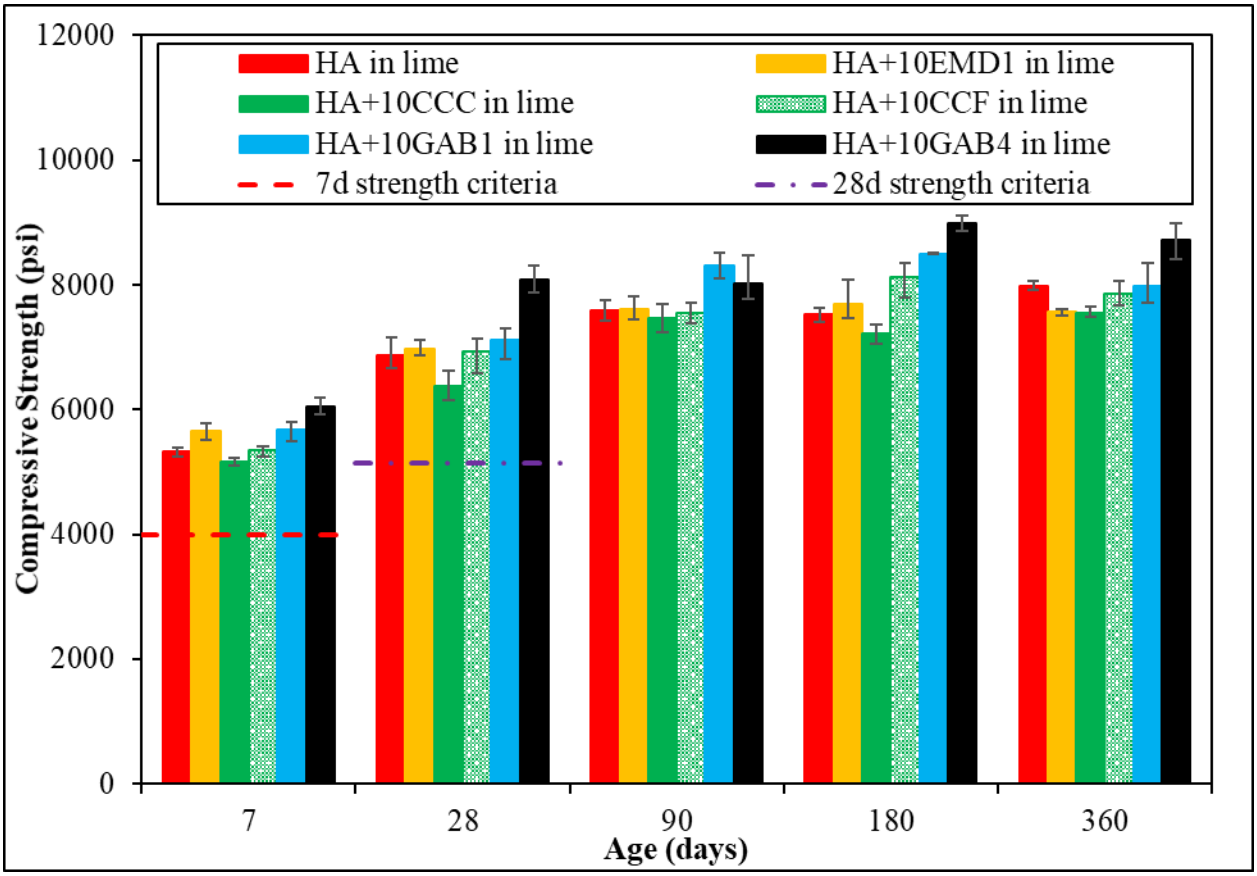

Figure 3-3: Compressive strength development of cement HA+10% clay mortars in lime solution

Figure 3-4 shows the strength development of 10% clay mixtures with cement GILOP, which has a calcite content of about 9.2%. All the strengths of clay blends with cement GILOP exceeded 75% the control strength at 7 and 28 days. Similar to the trends observed with cement HA, the mix with clay GAB4 showed the highest strength improvement at all ages. Moreover, clay GAB1 showed considerably higher strength increase with cement GILOP compared to that with cement HA. At 28 days, the HA+10GAB1 had strength 3.6% higher than the control HA, whereas the increase in the GILOP+10GAB1 mix was 12.8% higher than the control GILOP. It is likely the higher kaolin content in GAB1 increased the clay reactivity in the presence of limestone and thereby increased the strength gain due to the formation of carboaluminate phases [14]. The clay CCC mix showed lower strengths at early ages but reached close to that of control GILOP at 90 days. Although the mix with clay CCF showed the lowest strength at 7 days, it surpassed that of clay CCC at 28 days indicating a faster strength gain. It showed strengths comparable to control HA. Unlike with cement HA, clay EMD1 with cement GILOP indicated lower strengths compared

to the control GILOP at early ages, however it reached close to that of control after 90 days. This could possibly be due to the higher sand content in clay EMD1, which may have lowered the effective cementitious material content in the system, consequently affecting the calcined clay to limestone content ratio.

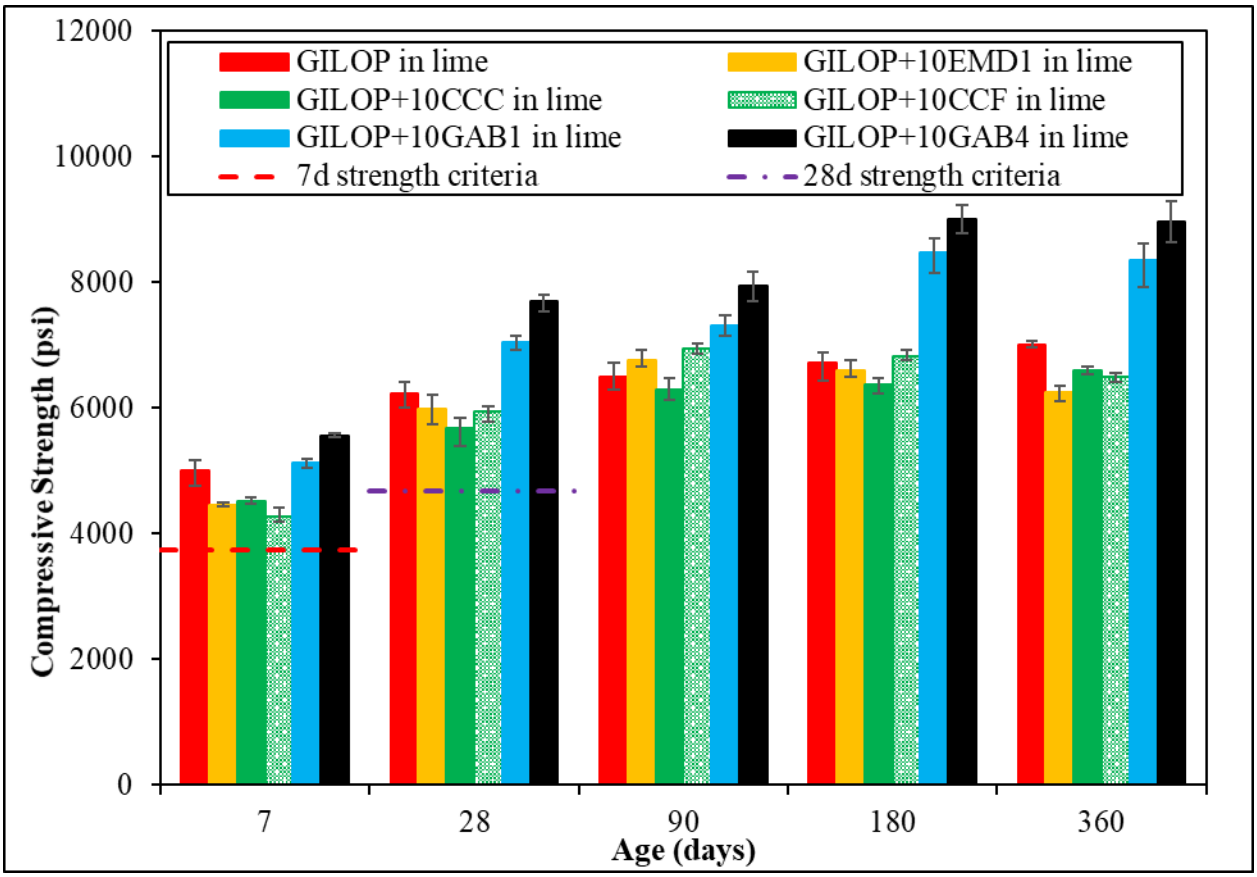

Figure 3-4: Compressive strength development of cement GILOP+10% clay mortars in lime solution

Figure 3-5 illustrates the strength development of 10% clay mixtures with cement THIL which has a calcite content of about 11.4%. Unlike with cements HA and GILOP, all clays with cement THIL have shown improved strengths at all ages, indicating the effect of higher limestone content on enhancing the clay reactivity. According to Figure 3-1, IL cements (GILOP and THIL) indicated a lower strength development compared to that of cement HA, owing to their reduced clinker fraction. Despite this, clays GAB1 and GAB4 blended with IL cements resulted in strengths comparable to or higher than those observed with same blends with cement HA. Clearly, higher

limestone contents react with alumina, increase the formation of carboaluminate phases and consequently increase the strength. Moreover, the increase in calcite content from 9.2% to 11.4% increased the clay reactivity at early age as indicated by the substantial strength increase in the mix with clay EMD1. The high fineness of cement THIL may have contributed to this behavior as well. Clay CCC which has a coarser particle size distribution showed slightly lower strengths with cement HA and GILOP, however this was overcome when blended with THIL, likely due to the higher limestone content as well as the higher fineness of cement THIL.

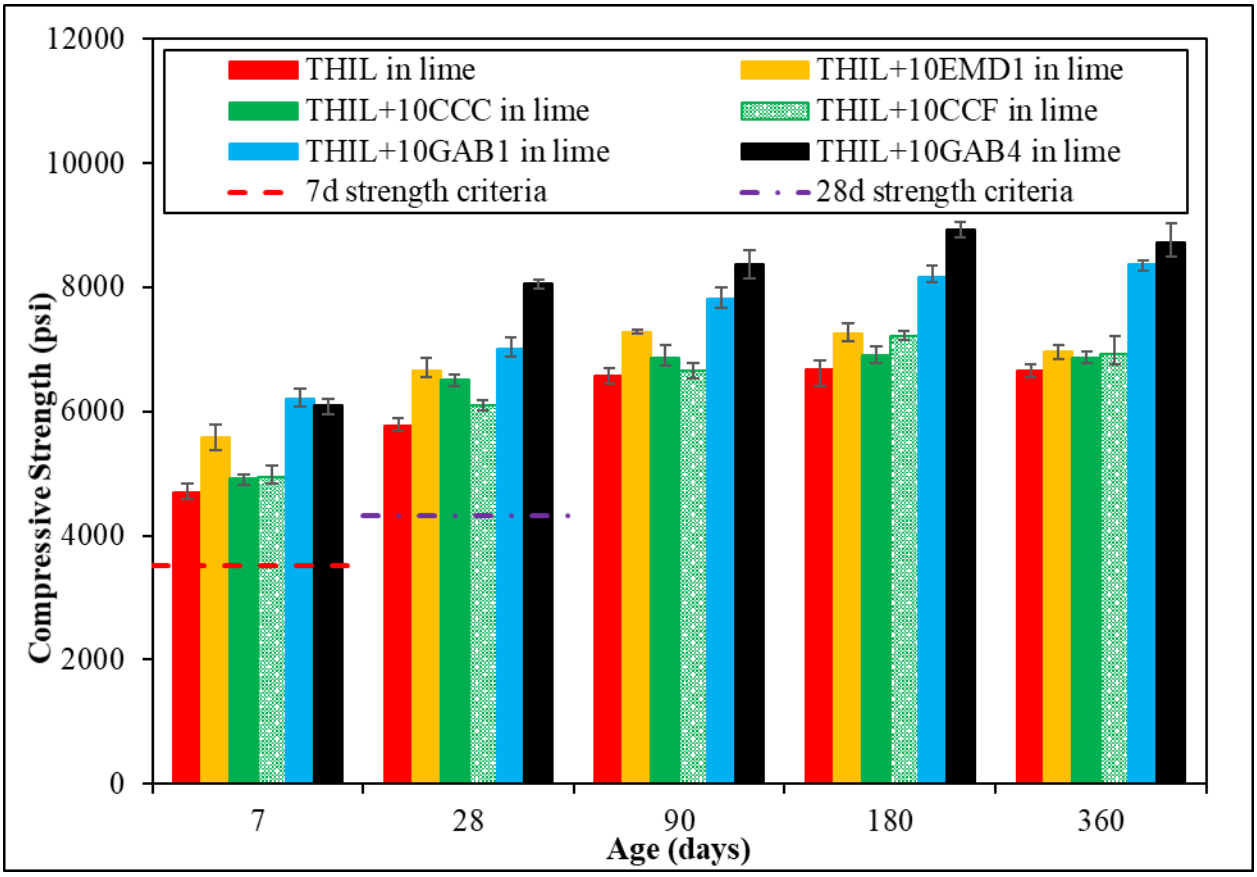

Figure 3-5: Compressive strength development of cement THIL+10% clay mortars in lime solution

At 20% cement replacement with clay, the strength evolution appeared to be slightly different. Nevertheless, as shown in Figure 3-6 through Figure 3-8, all 20% clay mortar cubes satisfied the strength requirements at 7 and 28 days in ASTM C618 [24] for natural pozzolans. Figure 3-6 shows the strength development of cement HA with 20% clays. Although clay CCF

showed slightly higher strengths than that of clay CCC, incorporation of both these commercial clays resulted in a significant drop in strength at all ages compared to control HA. This behavior can still be attributed to their coarser particle size distribution, lower kaolin content and higher sand content. The strength development of cement HA with clay EMD1 was comparable to that of control HA at all ages. Unlike at 10% replacement level, the mix with 20% clay GAB1 showed a lower strength compared to control HA at 7 days likely due to a decreased clay reactivity with the reduced clinker fraction; however, by the time it reached 28 days, it surpassed the strength of the control. Nevertheless, consistently higher strengths can be observed with clay GAB4 blends at all ages likely due to the reactivity governed by its high fineness and high amounts of calcined kaolin and gibbsite.

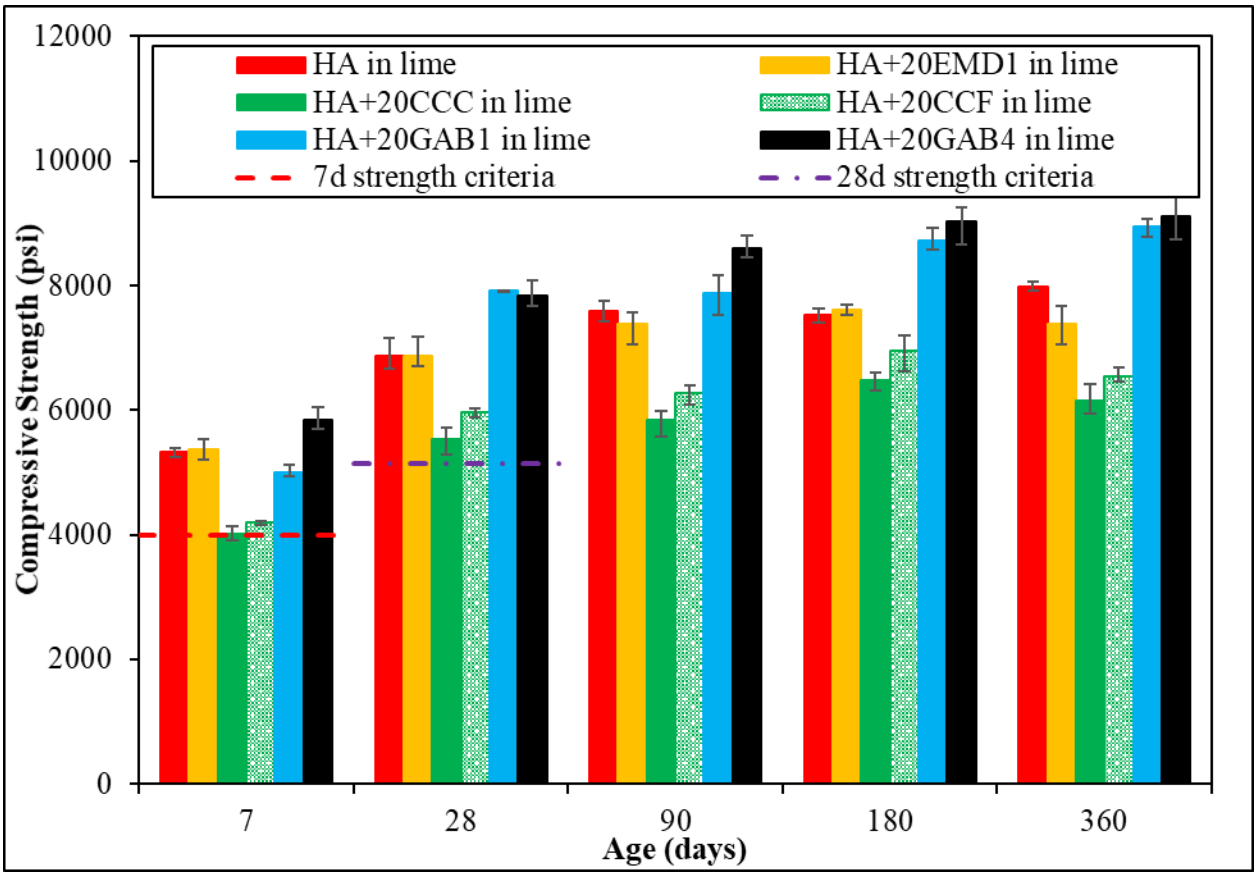

Figure 3-6: Compressive strength development of HA+20% clay mortars in lime solution

For cement GILOP at 20% cement replacement with clay, a higher compressive strength was observed for GILOP+20GAB1 and GILOP+20GAB4 starting at 7 days. Figure 3-7 shows the

effect of limestone on kaolin clay reactivity. The positive effect of limestone on strength development can also be seen in clay EMD1 with cement GILOP, whereas with cement HA, no strength increase was observed compared to control HA. On the other hand, the 9.2% calcite in cement GILOP did not produce comparable strengths to the control with clay CCC until 180 days. The clay CCF mix also showed lower strengths until 28 days, however the strength equaled that of the control GILOP after 90 days. This shows the need to grind calcined clay fine enough to help strength gain.

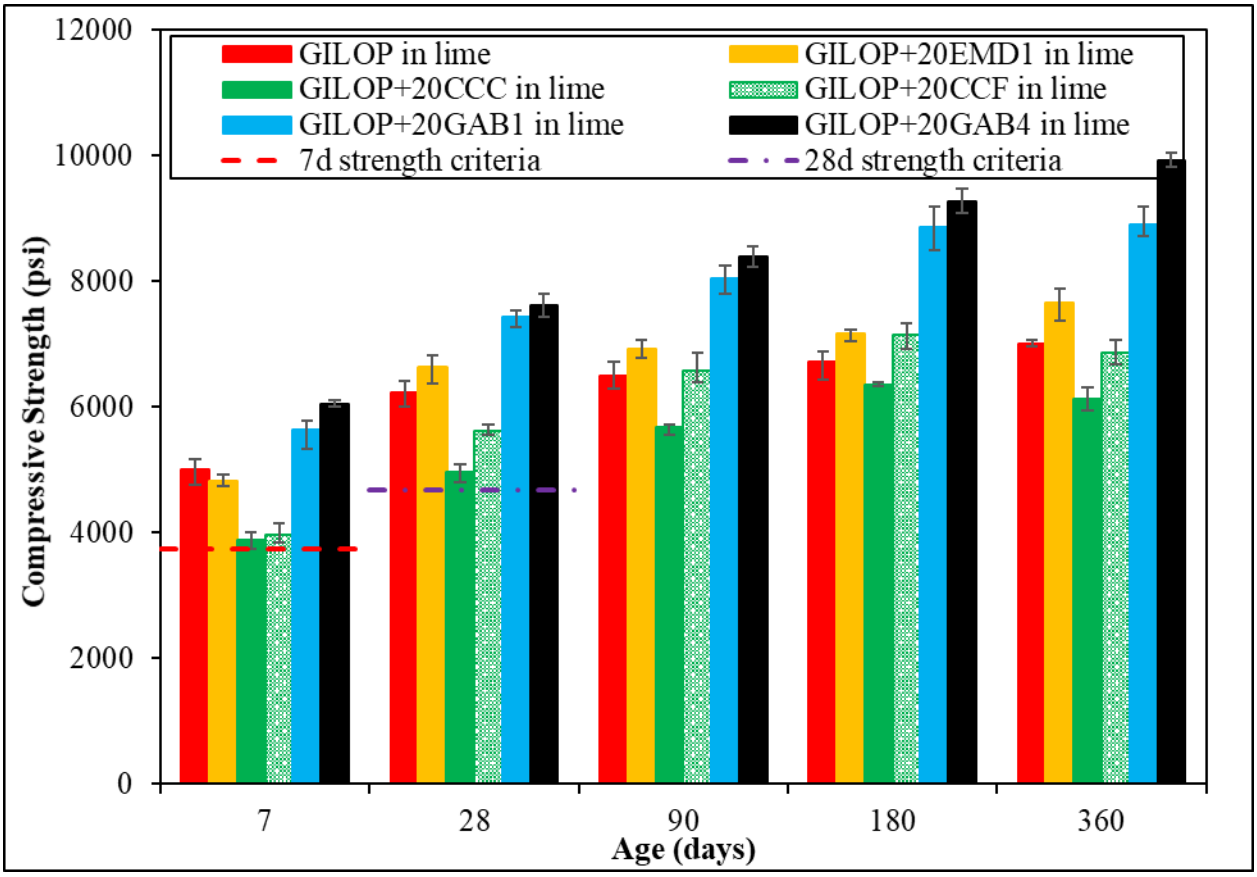

Figure 3-7: Compressive strength development of cement GILOP+20% clay mortars in lime solution

As it appears in Figure 3-8, 20% clay CCC with cement THIL still showed lower strengths at all ages, even though cement THIL has a higher limestone content; but clay CCF blends showed strengths comparable to or slightly higher than control THIL. However, a substantial strength increase can be observed in THIL+20EMD1 mix indicating an increased clay reactivity with

cement THIL. A similar behavior was observed in the THIL+10EMD1 mix as well. Not only clay EMD1, but also clays GAB1 and GAB4 blended with cement THIL showed higher strength gain at 20% replacement compared to those with GILOP at 20% replacement. Moreover, 20% clay substitution significantly increased the strengths of cement THIL-clay blended mixtures compared to those of 10% substitution, except for clay CCC. It is interesting that the compressive strength of THIL+20EMD1 (37.9% kaolin in EMD1) leveled off with that of THIL+20GAB1 (93.1% kaolin in GAB1) at 28 days, indicating that not only kaolin of high purity is required to achieve high strengths in concrete, but also low-grade kaolin clay can be used with well-adjusted proportions.

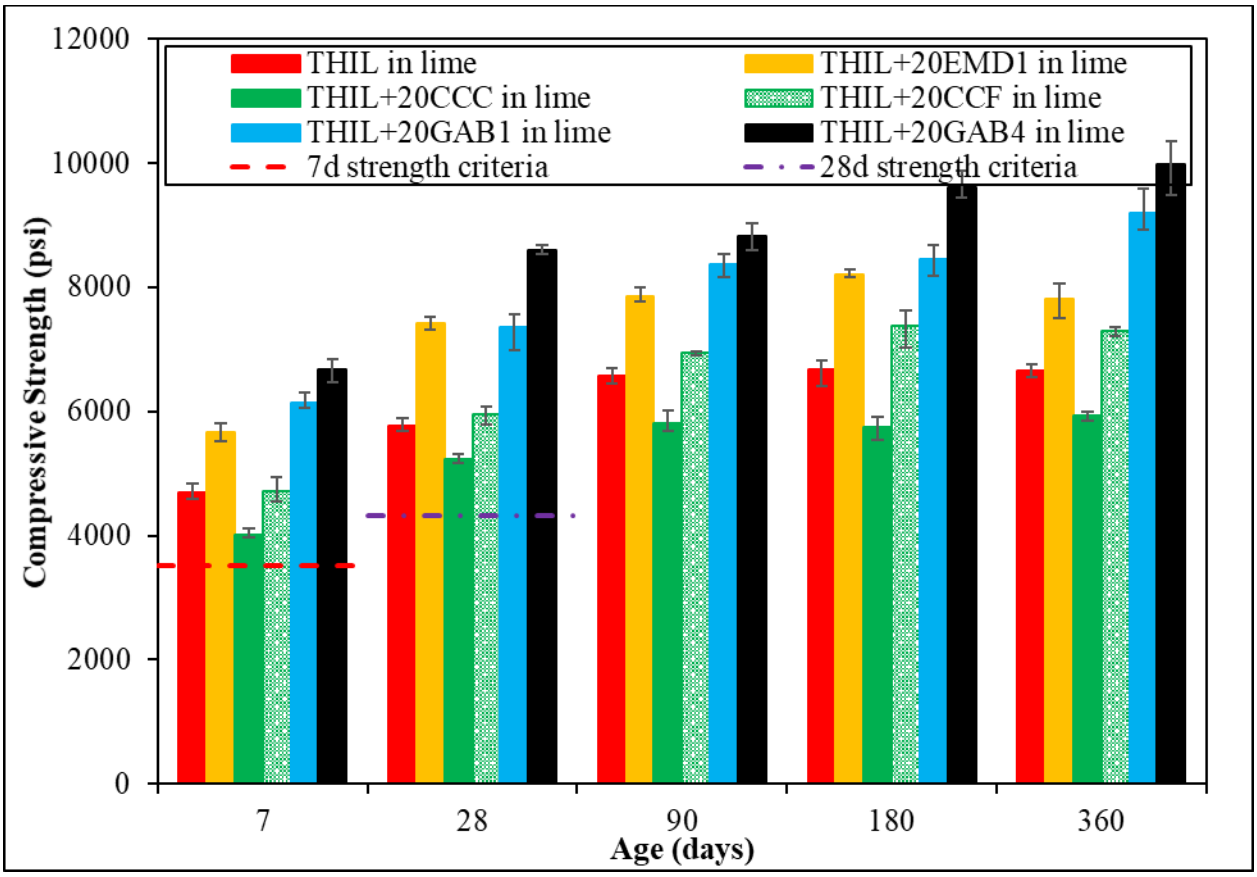

Figure 3-8: Compressive strength development of cement THIL+20% clay mortars in lime solution

3.3.2.2 Compressive Strength Development in 5% Sodium Sulfate Solution

The compressive strength evolution of cement-clay mortar mixtures at 10% substitution level, exposed to 5% sodium sulfate solution after 7 days is shown in Figure 3-9 through Figure 3-11. The strength development of the same mixtures discussed in the previous section was investigated to assess the resistance of each cement-clay mortar to sulfate exposure. The 7-day compressive strength values included in the figures are the strengths of mortars before exposing to sodium sulfate solution. In order to quantify any potential of strength deterioration due to sulfate attack, compressive strength ratios of all the mortars at 90, 180, and 360, expressed in terms of their respective 28-day strengths in sulfate solution, were determined. These ratios are listed in Table 3-6 through Table 3-8.

In general, the compressive strength development trends of all mixtures until 90 days in the sulfate solutions were similar to those in lime solutions. As shown in Figure 3-9 through Figure 3-11, compressive strengths of most mixtures were still developing up to an age of 90 days, and no deterioration was detected. Similar to the trends observed in the lime solution, compressive strengths of all mixtures with clays GAB1 and GAB4 were higher than their respective control mixtures and the other clay blends, showing the positive effects of additions of calcined kaolin and kaolin-gibbsite blends and higher fineness on clay reactivity even in the sulfate environment. As stated in the literature [32], LC^3-50 (50% ground clinker, 30% calcined clay, 15% limestone, 5% gypsum) blends with original kaolinite contents more than 65% had a threshold pore radius as small as 10 nm for ages as early as 3 days. Such reduced permeability is advantageous in slowing down the sulfate ion ingress into the specimens and enhance sulfate resistance, which in turn would control the deterioration of specimens. Hence, consistently higher strengths in blends with clays GAB1 and GAB4 in the sulfate environment were likely a consequence of pore size refinement. This effect may be further enhanced in the presence of limestone. On the other hand, behavior of clays EMD1, CCC and CCF varied depending on the cements they were blended with, as will be discussed later. It is noteworthy that the deterioration of all clay CCC mixtures appeared to be more significant due to the increased permeability as a result of its coarser particle size.

The strength evolution of cement HA+10% clay mixtures was clearly affected when exposed to sulfate solution as can be seen in Figure 3-9 and Table 3-6. Unlike in lime solution (Figure 3-3), the strengths started to deteriorate after 90 days, but mixes with clays GAB1 and

GAB4 showed strengths higher than those of control HA. For cement GILOP with 10% clays (Figure 3-10), trends in sulfate solution were similar to those observed in lime solution (Figure 3-4) until 90 days. As with cement HA, when blended with cement GILOP, clays EMD1, CCC, and CCF showed a decrease in strength after 180 days compared to its 28-day strength value (Table 3-7); however, clays GAB1 and GAB4 showed higher strengths, indicating their higher sulfate resistance. The strength development of cement THIL blended with 10% clay in the sulfate solution is shown in Figure 3-11. The trends until 90 days were similar to those observed in the lime solution except for THIL+10GAB1, which showed the highest strength at 28 days. Unlike with cements HA and GILOP, with cement THIL, clay EMD1 showed higher strengths than those of control THIL. Apparently, clay EMD1, when blended with cements with high limestone content and high fineness, increased the sulfate resistance.

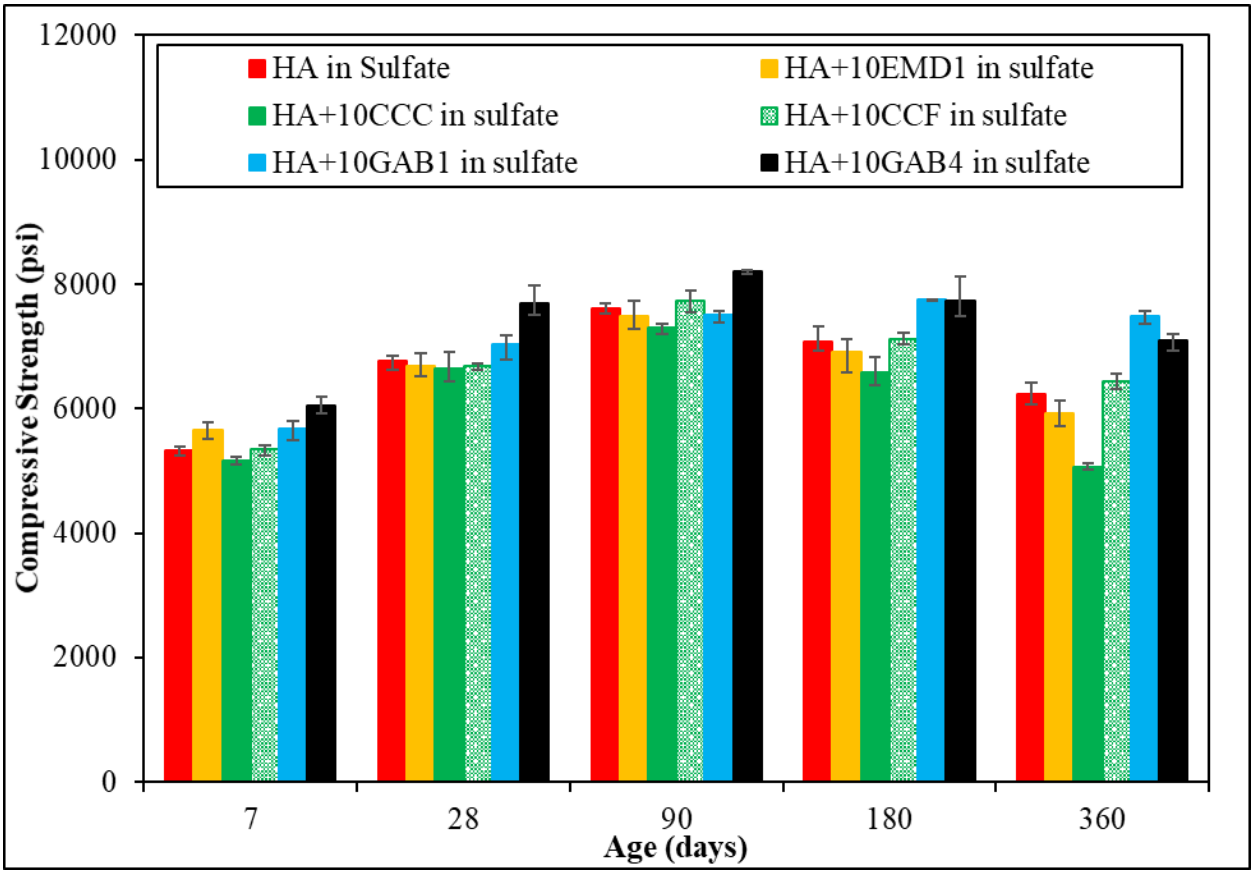

Figure 3-9: Compressive strength evolution of HA+10% clay mortars in 5% sodium sulfate solution

Table 3-6: Compressive strength at later ages relative to the 28-day strength (in sulfate solution) for cement HA+10% clay mixtures exposed to 5% sodium sulfate solution

Age (days)	Control HA	HA +10EMD1	HA +10CCC	HA +10CCF	HA +10GAB1	HA +10GAB4
90	1.12	1.12	1.10	1.16	1.07	1.07
180	1.05	1.03	0.99	1.07	1.10	1.01
360	0.92	0.89	0.76	0.96	1.06	0.92

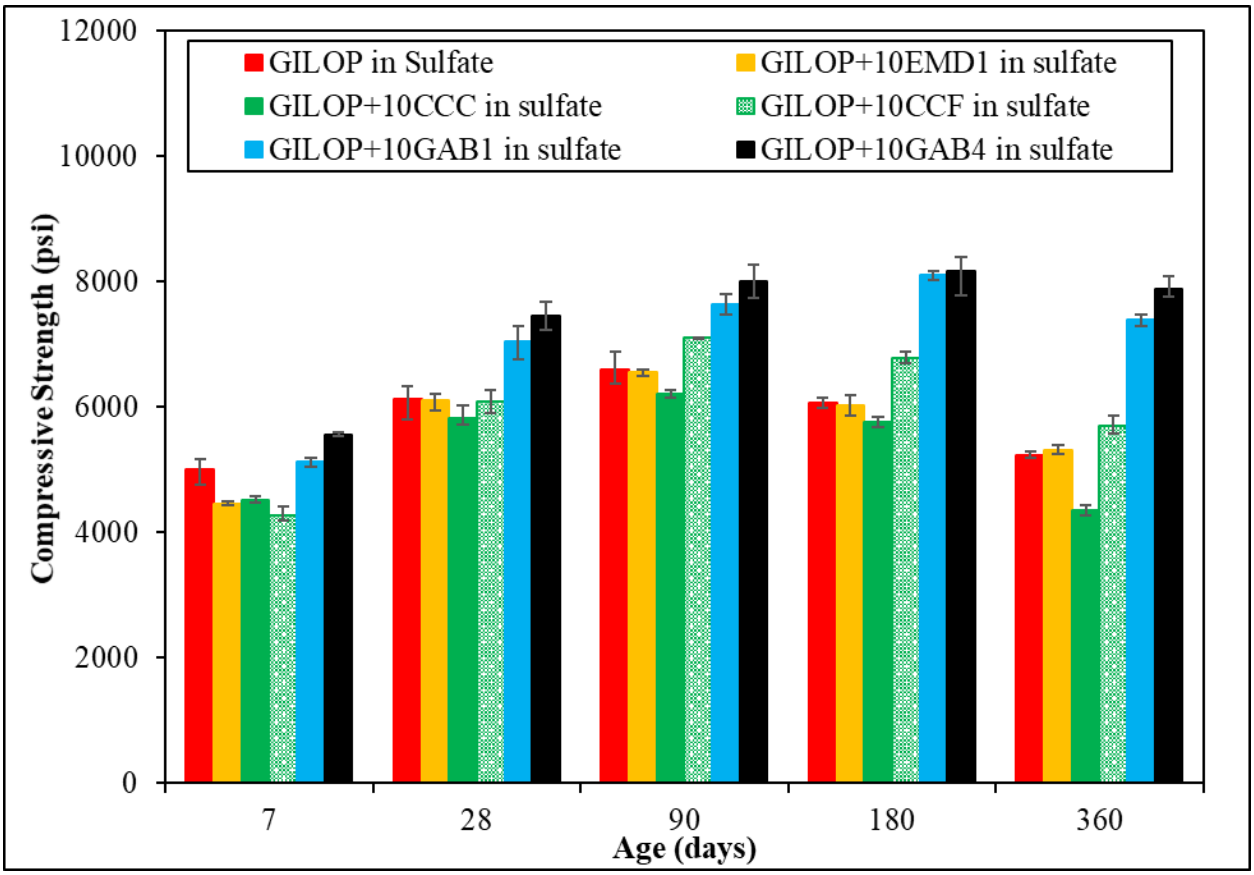

Figure 3-10: Compressive strength evolution of GILOP+10% clay mortars in 5% sodium sulfate solution

Table 3-7: Compressive strength at later ages relative to the 28-day strength (in sulfate solution) for cement GILOP+10% clay mixtures exposed to 5% sodium sulfate solution

Age (days)	Control GILOP	GILOP +10EMD1	GILOP +10CCC	GILOP +10CCF	GILOP +10GAB1	GILOP +10GAB4
90	1.08	1.07	1.07	1.17	1.09	1.07
180	0.99	0.99	0.99	1.11	1.15	1.09
360	0.86	0.87	0.75	0.94	1.05	1.06

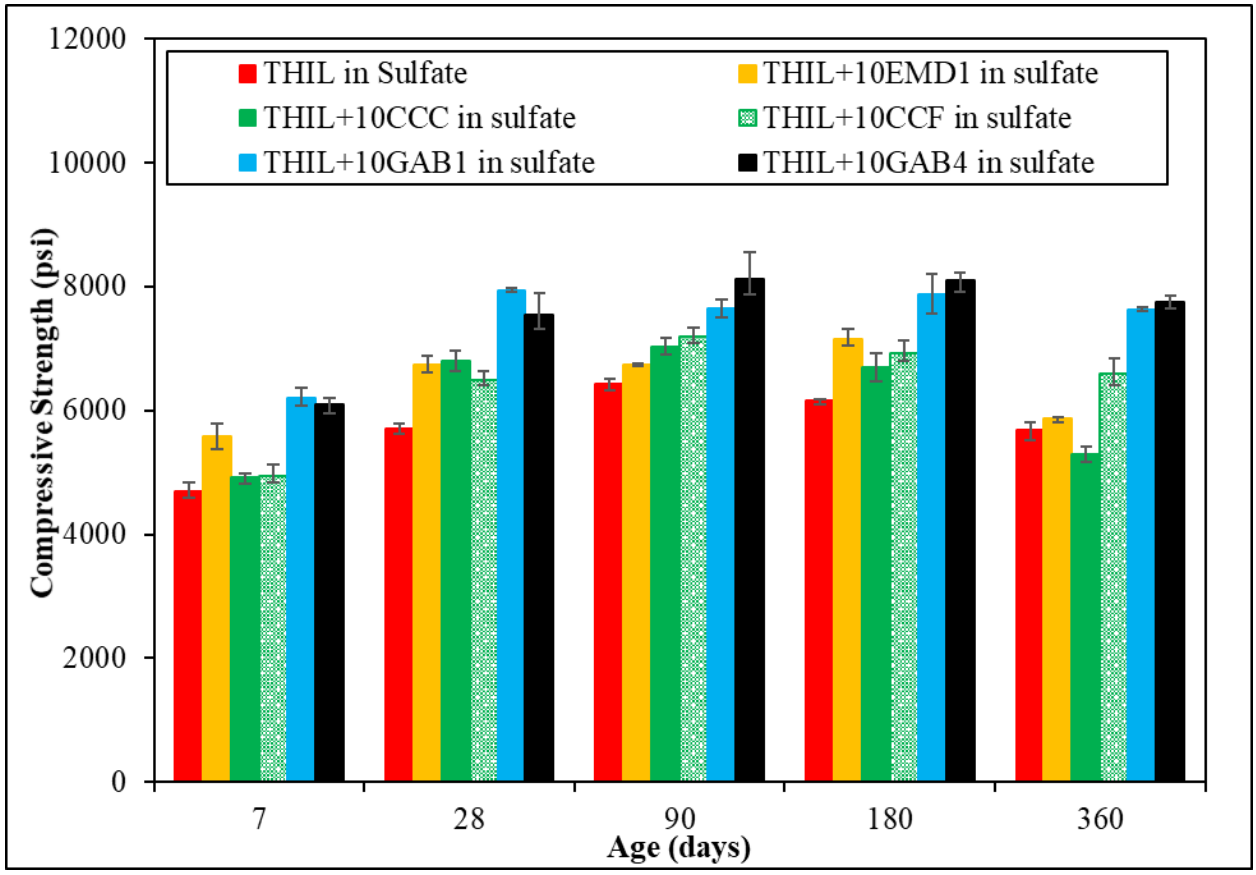

Figure 3-11: Compressive strength evolution of THIL+10% clay mortars in 5% sodium sulfate solution

Table 3-8: Compressive strength at later ages relative to the 28-day strength (in sulfate solution) for cement THIL+10% clay mixtures exposed to 5% sodium sulfate solution

Age (days)	Control THIL	THIL +10EMD1	THIL +10CCC	THIL +10CCF	THIL +10GAB1	THIL +10GAB4
90	1.13	1.00	1.04	1.11	0.96	1.08
180	1.08	1.06	0.99	1.07	0.99	1.07
360	1.00	0.87	1.00	1.02	0.96	1.03

Figure 3-12 through Figure 3-14 show the compressive strength evolution of cements blended with 20% clay in the sulfate solution, and Table 3-9 through Table 3-11 present the ratios of compressive strength to 28-day strength (in sulfate solution) at later ages. Most test samples with 20% cement replacement and immersed in sulfate solution followed trends similar to those observed for test samples immersed in lime solution until 90 days (Figure 3-6 through Figure 3-8). For blends with cement HA (Figure 3-12), strengths started decreasing after 90 days except for HA+20GAB1 and HA+20GAB4, which increased and levelled off afterwards. According to Table 3-9, the strengths of mixes with clays EMD1, CCC and CCF dropped compared to those observed at 28 days, indicating lower sulfate resistance. For cement GILOP blends (Figure 3-13), trends were similar to those with cement HA blends. Clay CCC performed poorly when blended with cement GILOP in the sulfate environment, as indicated by the strength loss observed as early as 90 days compared to its 28-day strength (Table 3-10). At 20% replacement level, when clay EMD1 was blended with cement THIL (Figure 3-14 and Table 3-11), sulfate resistance appeared to be high, as indicated by consistently higher strengths that can be attributed to a reduced permeability due to high fineness and high limestone content of the cement. In general, clays blended with cement THIL produced strengths greater than those observed with cements HA and GILOP at both substitution levels.

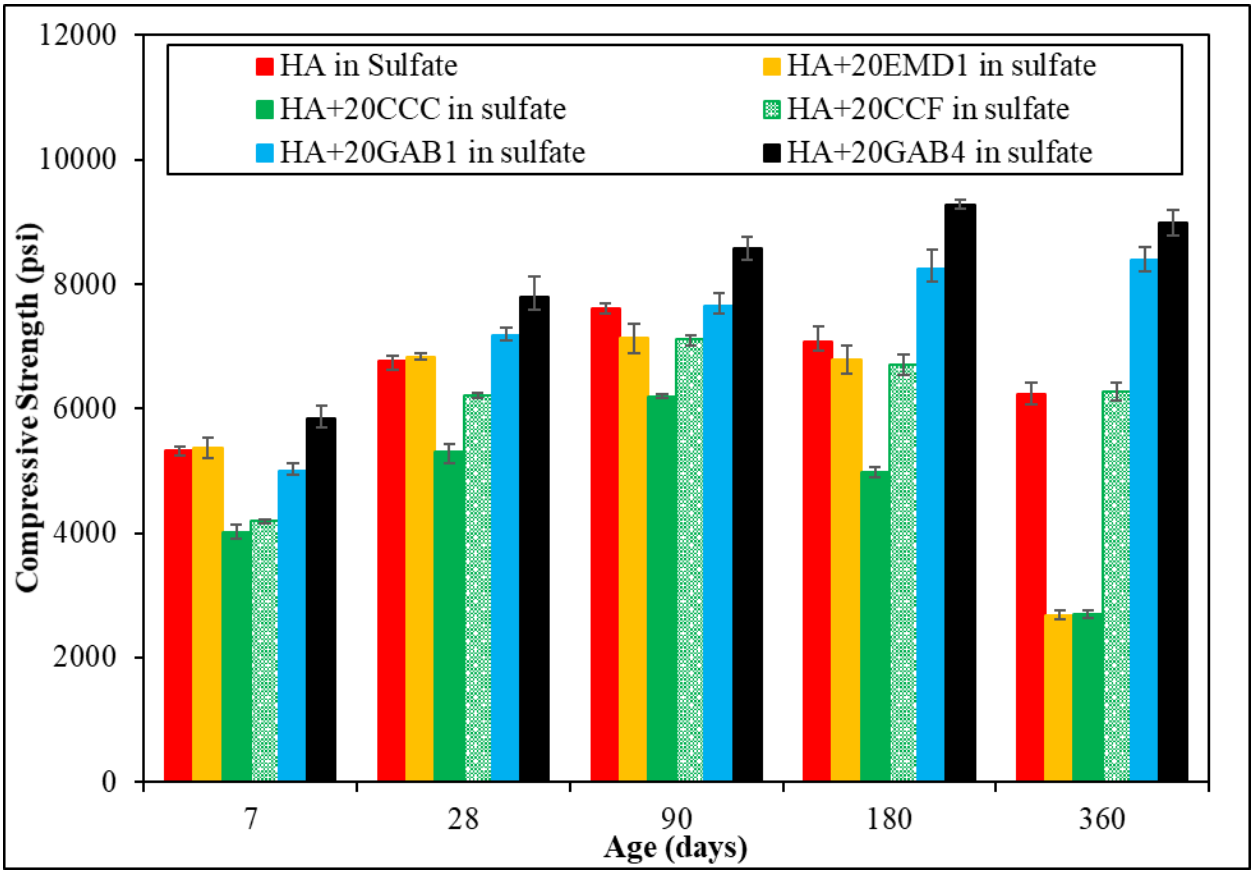

Figure 3-12: Compressive strength evolution of HA+20% clay mortars in 5% sodium sulfate solution

Table 3-9: Compressive strength at later ages relative to the 28-day strength (in sulfate solution) for cement HA+20% clay mixtures exposed to 5% sodium sulfate solution

Age (days)	Control HA	HA +20EMD1	HA +20CCC	HA +20CCF	HA +20GAB1	HA +20GAB4
90	1.12	1.04	1.17	1.14	1.07	1.10
180	1.05	0.99	0.94	1.08	1.15	1.19
360	0.92	0.39	0.51	1.01	1.17	1.15

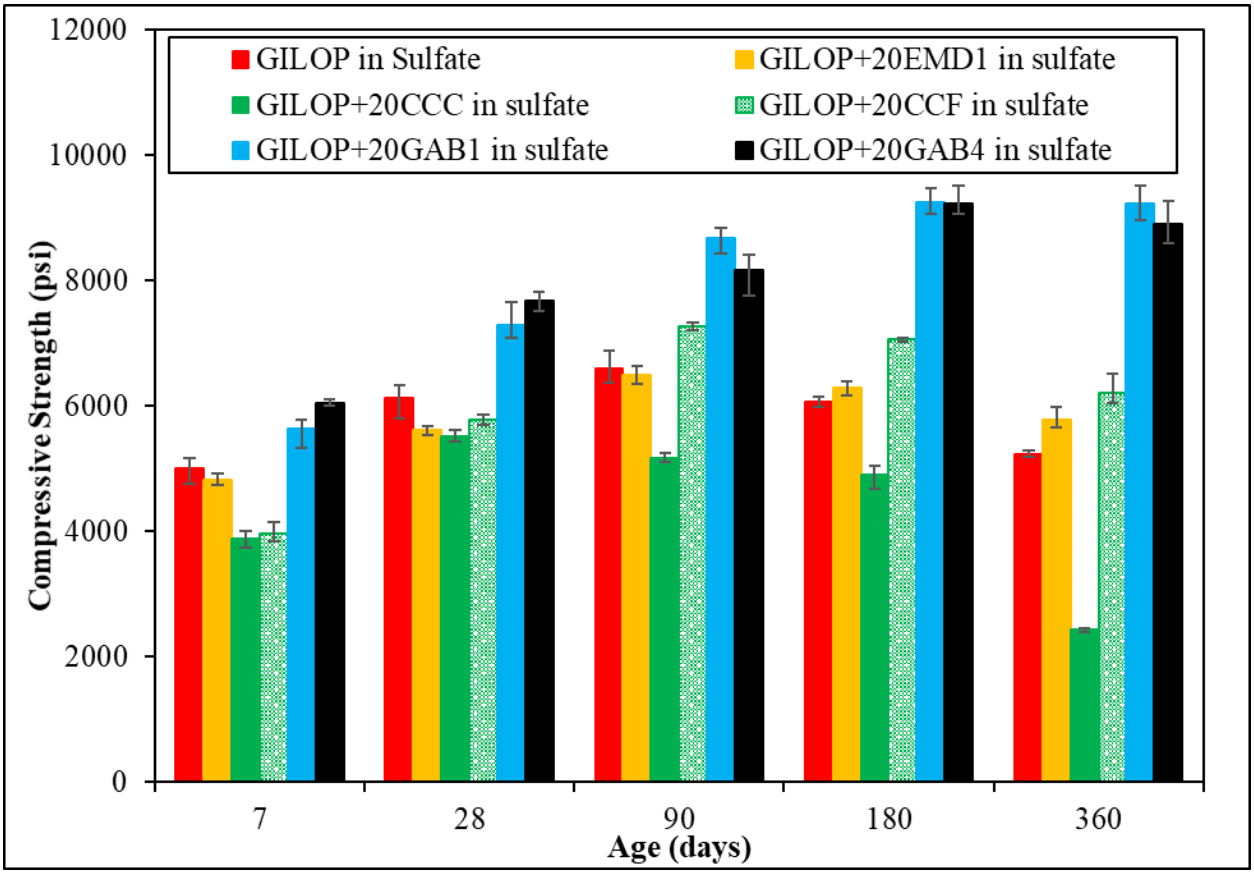

Figure 3-13: Compressive strength evolution of GILOP+20% clay mortars in 5% sodium sulfate solution

Table 3-10: Compressive strength at later ages relative to the 28-day strength (in sulfate solution) for cement GILOP+20% clay mixtures exposed to 5% sodium sulfate solution

Age (days)	Control GILOP	GILOP +20EMD1	GILOP +20CCC	GILOP +20CCF	GILOP +20GAB1	GILOP +20GAB4
90	1.08	1.16	0.93	1.26	1.19	1.06
180	0.99	1.12	0.89	1.22	1.27	1.20
360	0.86	1.03	0.44	1.07	1.27	1.16

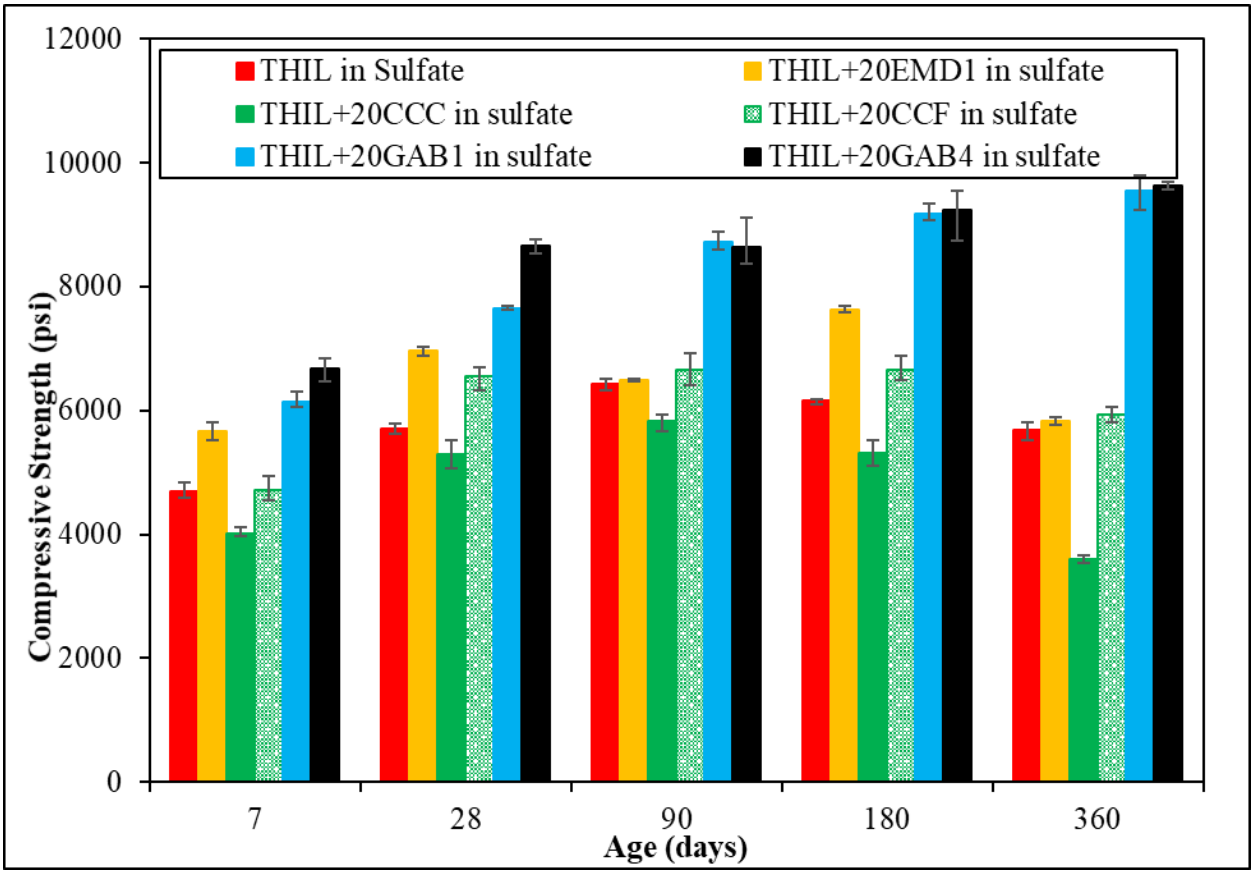

Figure 3-14: Compressive strength evolution of THIL+20% clay mortars in sulfate solution

Table 3-11: Compressive strength at later ages relative to the 28-day strength (in sulfate solution) for cement THIL+20% clay mixtures exposed to 5% sodium sulfate solution

Age (days)	Control THIL	THIL +20EMD1	THIL +20CCC	THIL +20CCF	THIL +20GAB1	THIL +20GAB4
90	1.13	0.93	1.10	1.01	1.14	1.00
180	1.07	1.10	1.00	1.02	1.20	1.07
360	1.00	0.84	0.68	0.91	1.25	1.11

3.3.3 Thermodynamic Modeling

Phase assemblage at ultimate equilibrium predicted for the mixtures are shown in Figure 3-15 and Figure 3-6. This corresponds to the phase assemblage of mixtures cured in the lime solution. In terms of control mixtures, the highest solid volume as well as the highest C-S-H volume were observed in the control HA mix, whereas the lowest solid volume was found for the control THIL. This can be attributed to the highest clinker fraction of cement HA compared to

cements GILOP and THIL. This also resulted in a higher porosity in control THIL compared to control HA and control GILOP, as the initial total volume of the control mixtures were approximately similar (81 cm^3 for Controls HA and GILOP, 80 cm^3 for Control THIL).

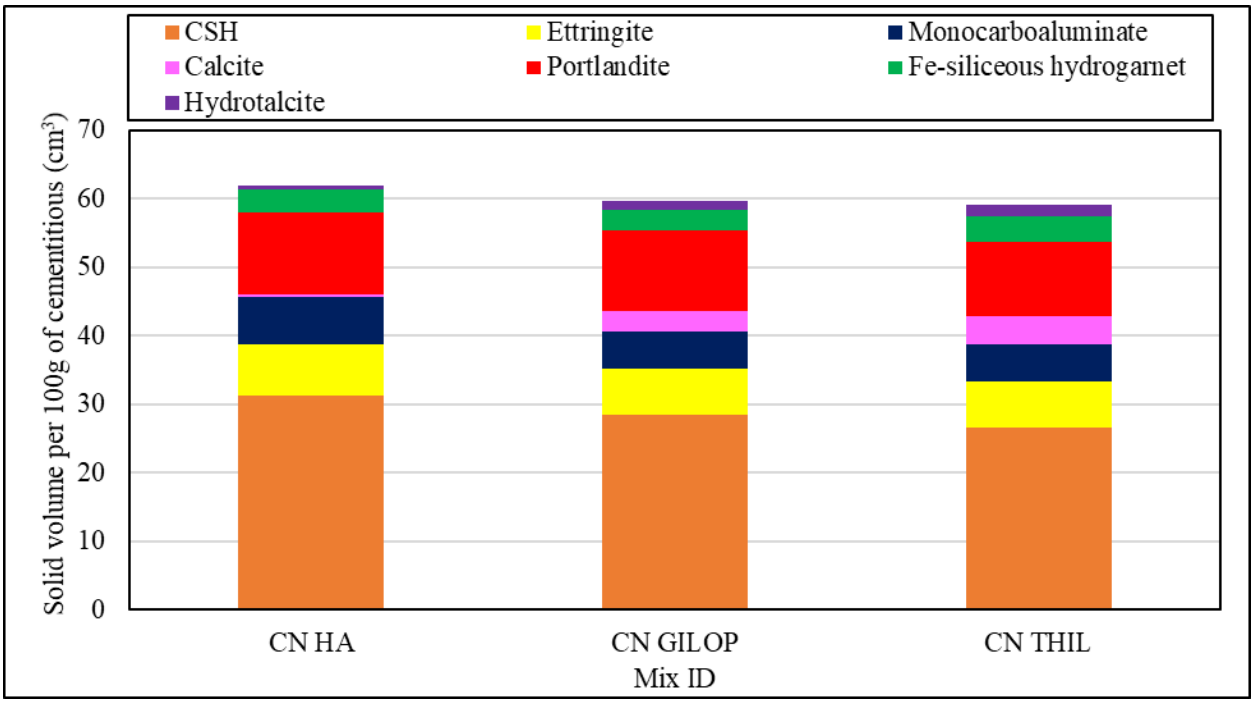

Figure 3-15: Predicted phase assemblage for control mixtures

The trends observed in the compressive strength results of control mixtures followed those for clinker content, with control HA showing the highest strengths followed by control GILOP and control THIL. The main phases predicted in the control mixtures were C-S-H, ettringite, monocarboaluminate, portlandite, and Fe-siliceous hydrogarnet ($C_3FS_{0.84}H_{4.32}$). Al and Fe intermixed siliceous hydrogarnet phase ($C_3(AF)S_{0.84}\ H_{4.32}$) was suppressed in the analysis, as Fe was substituted by Al in the siliceous hydrogarnet, making less alumina available to form carboaluminate phases [33]. Consequently, Fe-siliceous hydrogarnet was predicted. As stated in the literature, it is the most stable iron-containing phase in the hydrated portland cement compared to Fe-AFm phases and Fe-ettringite [34], [35].

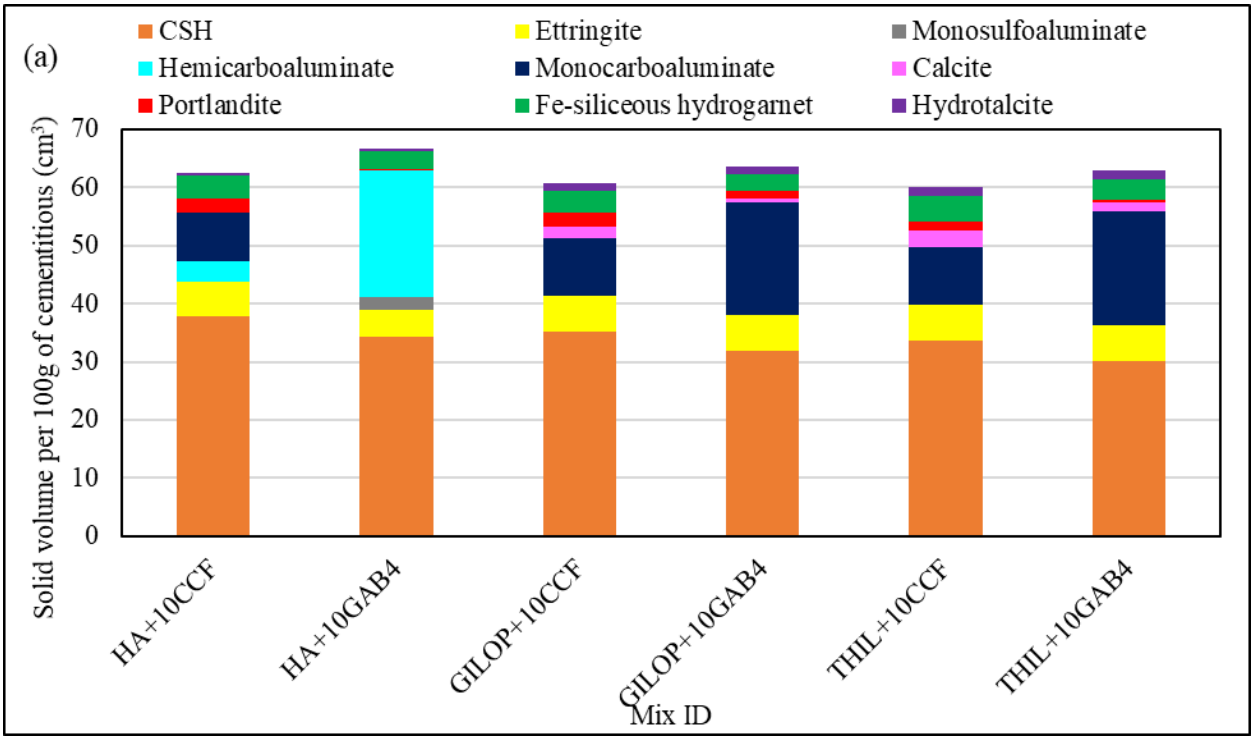

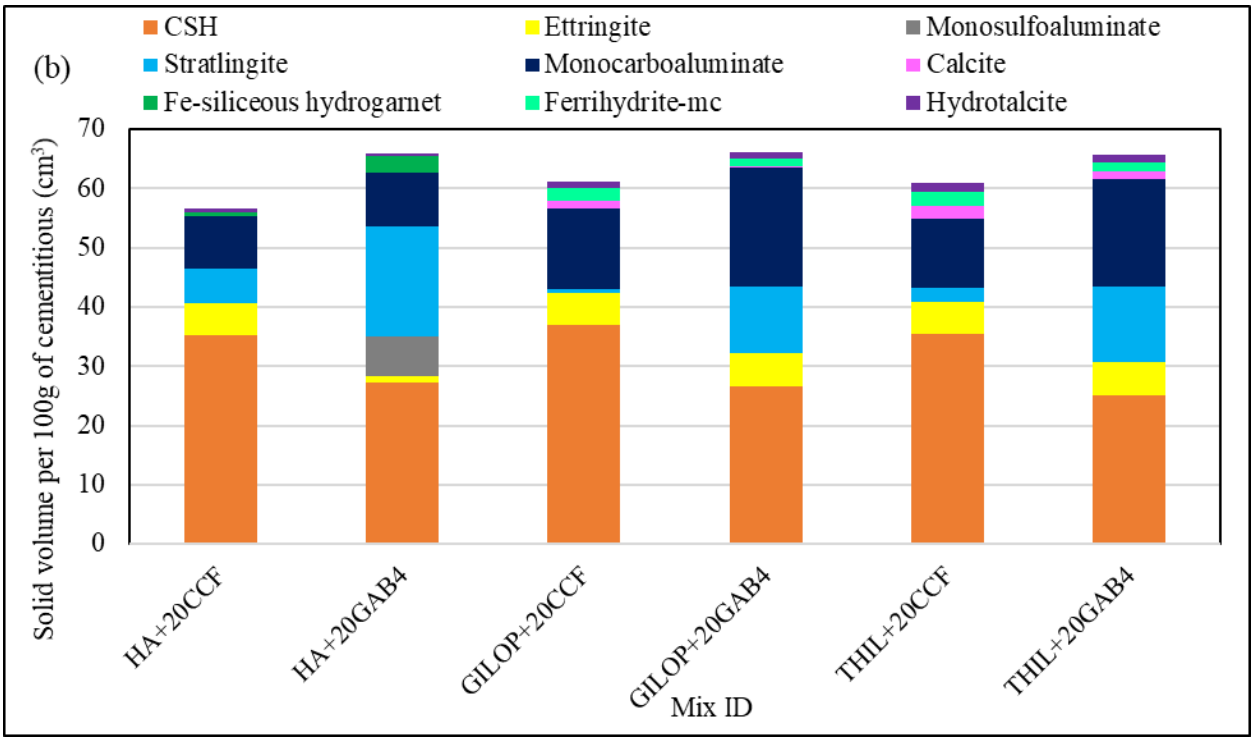

Figure 3-16: Predicted phase assemblage for clay mixtures (a) at 10% (b) at 20% substitution levels

While the Si-free hydrogarnet is unstable in the presence of sulfate- and carbonate-bearing cement phases such as gypsum, calcite, AFm and Aft, it is reported that the siliceous hydrogarnet is stable in the presence of these phases [36]. Additionally, traces of hydrotalcite and unhydrated calcite were also predicted in all the control mixtures. Predicted hydrotalcite content in control THIL was the highest owing to the highest MgO (1.08%) content in cement THIL. Predicted unhydrated calcite content increased with the increasing limestone contents of the cements. Substantially high amounts of monocarboaluminate were predicted in all the controls.

In terms of blended mixtures, addition of clays clearly affected the phase assemblage and the total solid volumes (Figure 3-16). Overall, clay GAB4 blends have shown the highest total solid volumes while the CCF blends have indicated the lowest, which is in agreement with the compressive strength development of the same mixtures. Both replacement levels increased the C-S-H (except for 20GAB4) and monocarboaluminate volumes but decreased the volumes of ettringite compared to the control mixtures. The volume of C-S-H increased due to the pozzolanic reaction that occurs with the clay addition as indicated by the reduced portlandite contents. Substantial increase in the volume of monocarboaluminate phase can be attributed to the reaction between calcite from cement and additional alumina from clay. However, hemicarboaluminate was also predicted in cement HA+10%clay systems. As stated by several researchers [37], [38], monocarboaluminate is calculated to be the more thermodynamically stable phase in the presence of calcite, while hemicarboaluminate appears only if the calcite content present in the hydrated cement is substantially less, which is true in the above systems as no calcite was predicted. Nevertheless, increasing alumina contents in clays have resulted in increasing amounts of monocarboaluminate phases formed during hydration. Moreover, in the systems with 20% clay substitution, stratlingite was predicted and it was highest in GAB4 blends owing to the high Al_2O_3 contents in clay GAB4. This implies that these mixtures had more Al than could be incorporated into C-S-H [39]. This is supported by the reduced C-S-H volume in these systems compared to that of the 10% clay substitution level. Additionally, portlandite was not predicted in 20% clay systems, likely due to its consumption by the increased pozzolanic reaction. No monosulfoaluminate was predicted in any of the systems except for clay GAB4 blended with cement HA at both replacement levels. As it appears, the calcite present in this system was not sufficient to prevent the formation of monosulfoaluminate. Moreover, in both GILOP+20% clay

and THIL+20% clay systems, microcrystalline ferrihydrite (ferrihydrite-mc) was predicted instead of Fe-siliceous hydrogarnet.

Figure 3-17 through Figure 3-23 illustrate the phase assemblage predicted for control mixtures and clays CCF and GAB4 blended mixtures in the 5% Na_2SO_4 solution. The plots show the progression of calculated phase volumes as the Na_2SO_4 solution-to-cementitious mass ratio values (x-axis) increase. Phases formed at very low volumes of sulfate solution are on the left while the right side shows the phases formed when exposed to high volumes of sulfate solution, which represent the effect of sulfate ingress at the core and surface of concrete. The phases formed at the core are similar to those observed in Figure 3-15 and Figure 3-16 for the same control and clay-cement blended mixtures at ultimate equilibrium when cured in lime solution. However, at the surface of a specimen, a significant increase in ettringite volume can be observed which caused an increased total solid volume, as expected. Apparently, alumina-bearing phases such as hemicarboaluminate and monocarboaluminate decompose in the presence of external sulfates, forming ettringite as stated in the literature [40]. Fe-siliceous hydrogarnet can also decompose, forming microcrystalline ferrihydrite. Similar trends were observed in all the systems. Additionally, decomposition of portlandite and formation of gypsum can be observed in the control mixtures. Moreover, a leaching effect can also be detected from the decrease in volumes of C-S-H, ettringite and gypsum with increasing sulfate solution volume [21]. Interestingly this leaching of C-S-H can be observed around a solution-to-binder mass ratio of 10. In addition to the deterioration that occurs in mortar specimens due to the volume increase caused by ettringite formation, a decrease in C-S-H volume may result in reduced strengths.

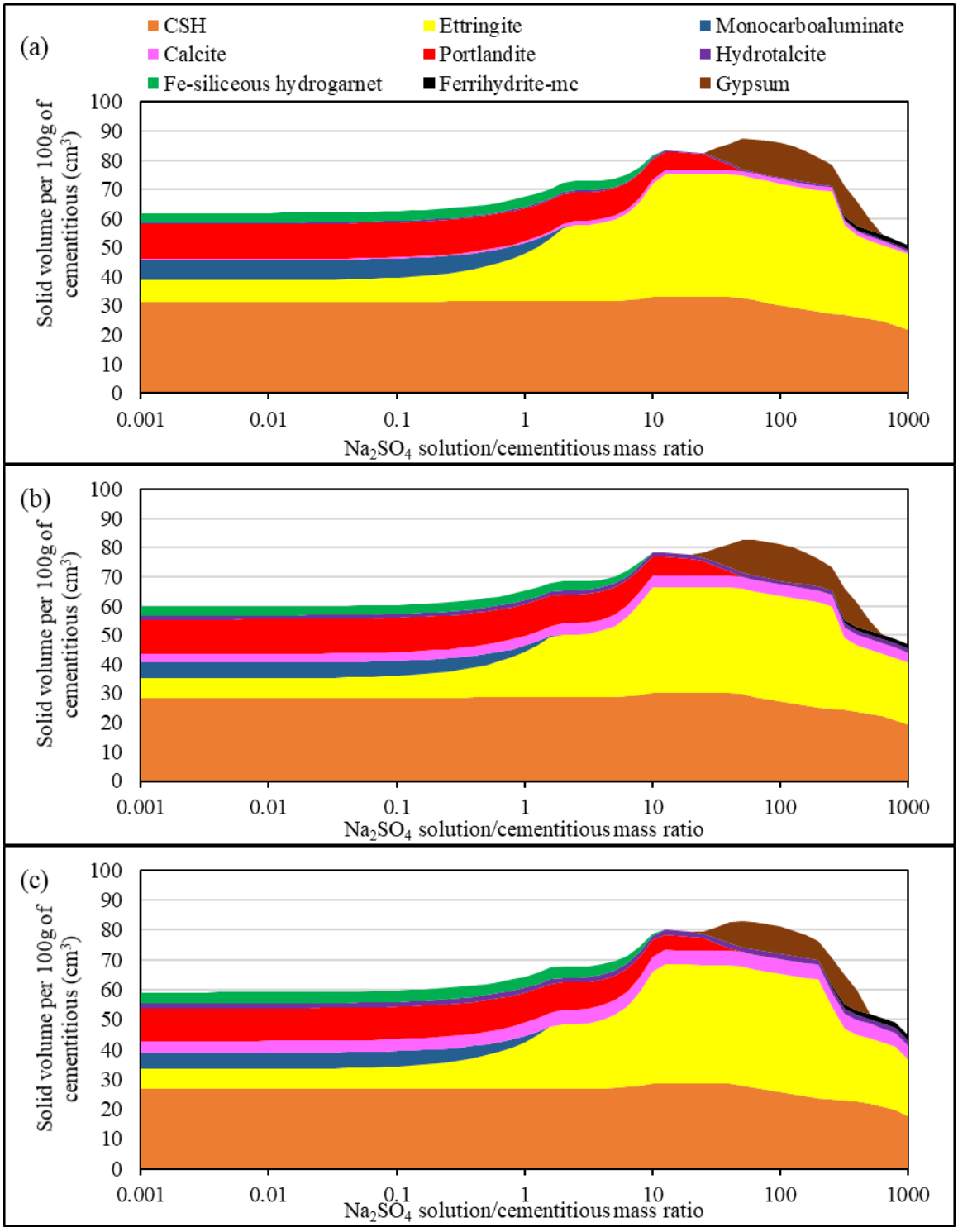

Figure 3-17: Predicted phase assemblage for (a) Control HA (b) Control GILOP (c) Control THIL mixtures immersed in 5% Na_2SO_4 solution

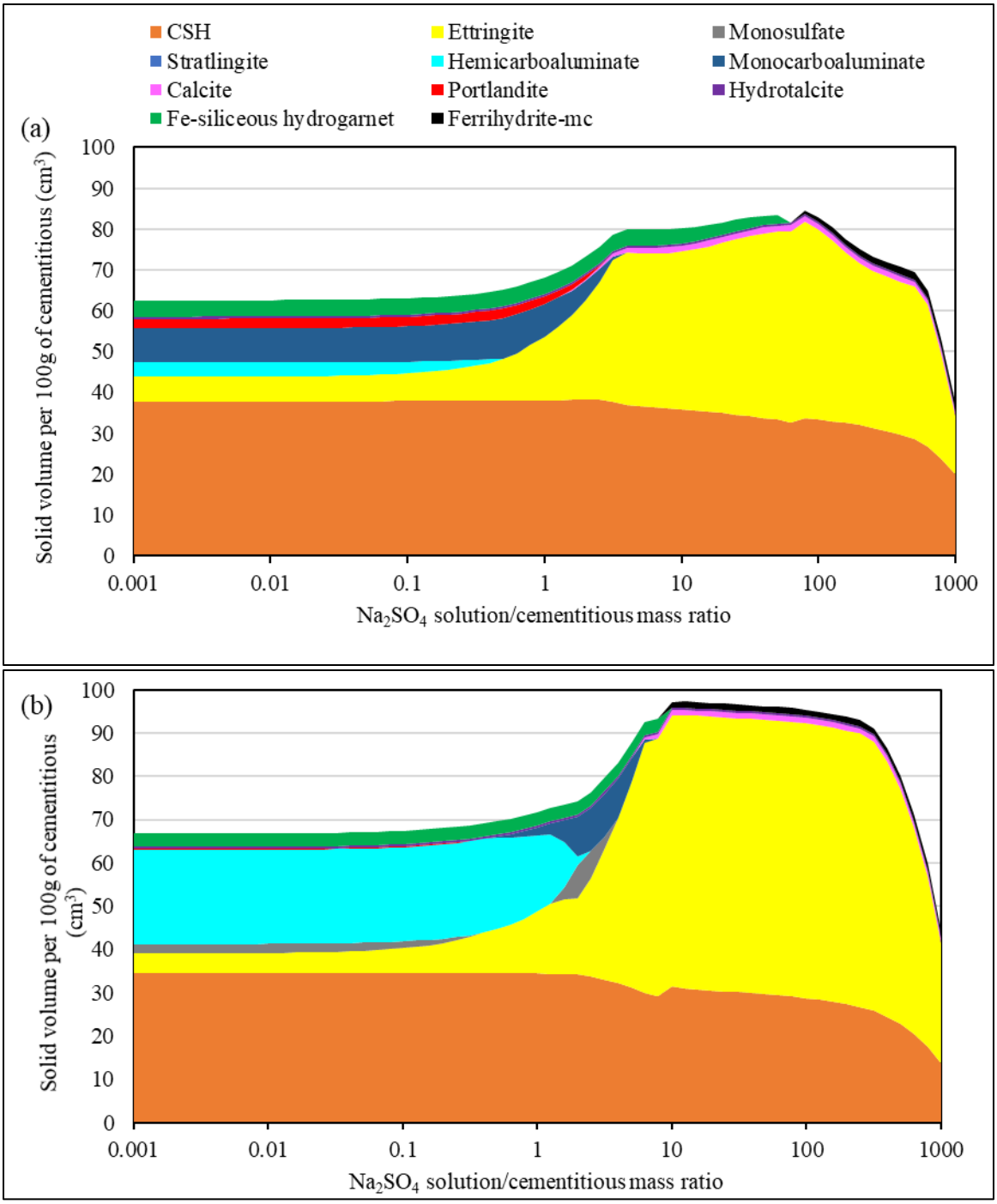

Figure 3-18: Predicted phase assemblage for (a) HA+10CCF (b) HA+10GAB4 mixtures immersed in 5% Na_2SO_4 solution

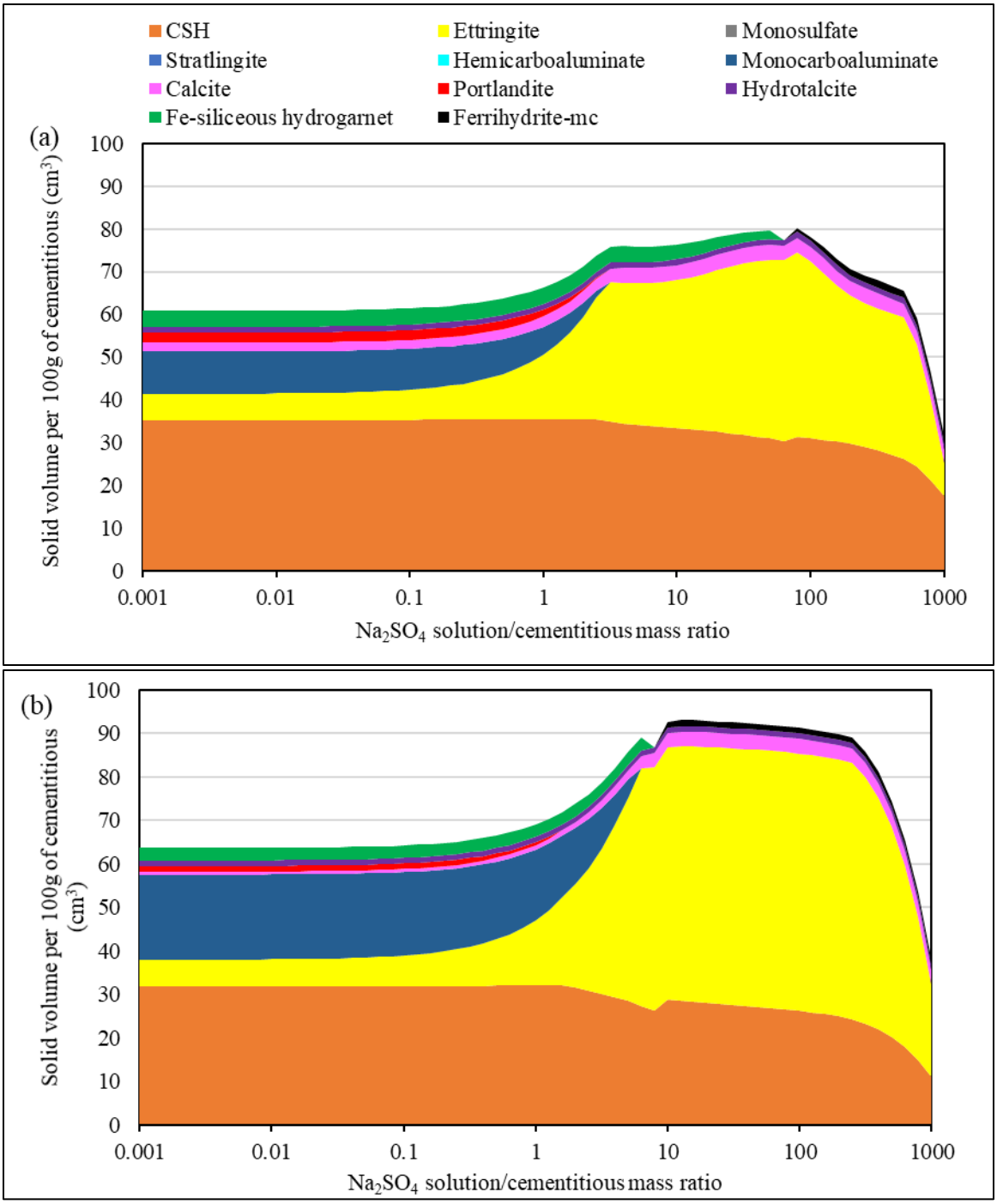

Figure 3-19: Predicted phase assemblage for (a) GILOP+10CCF (b) GILOP+10GAB4 mixtures immersed in 5% Na_2SO_4 solution

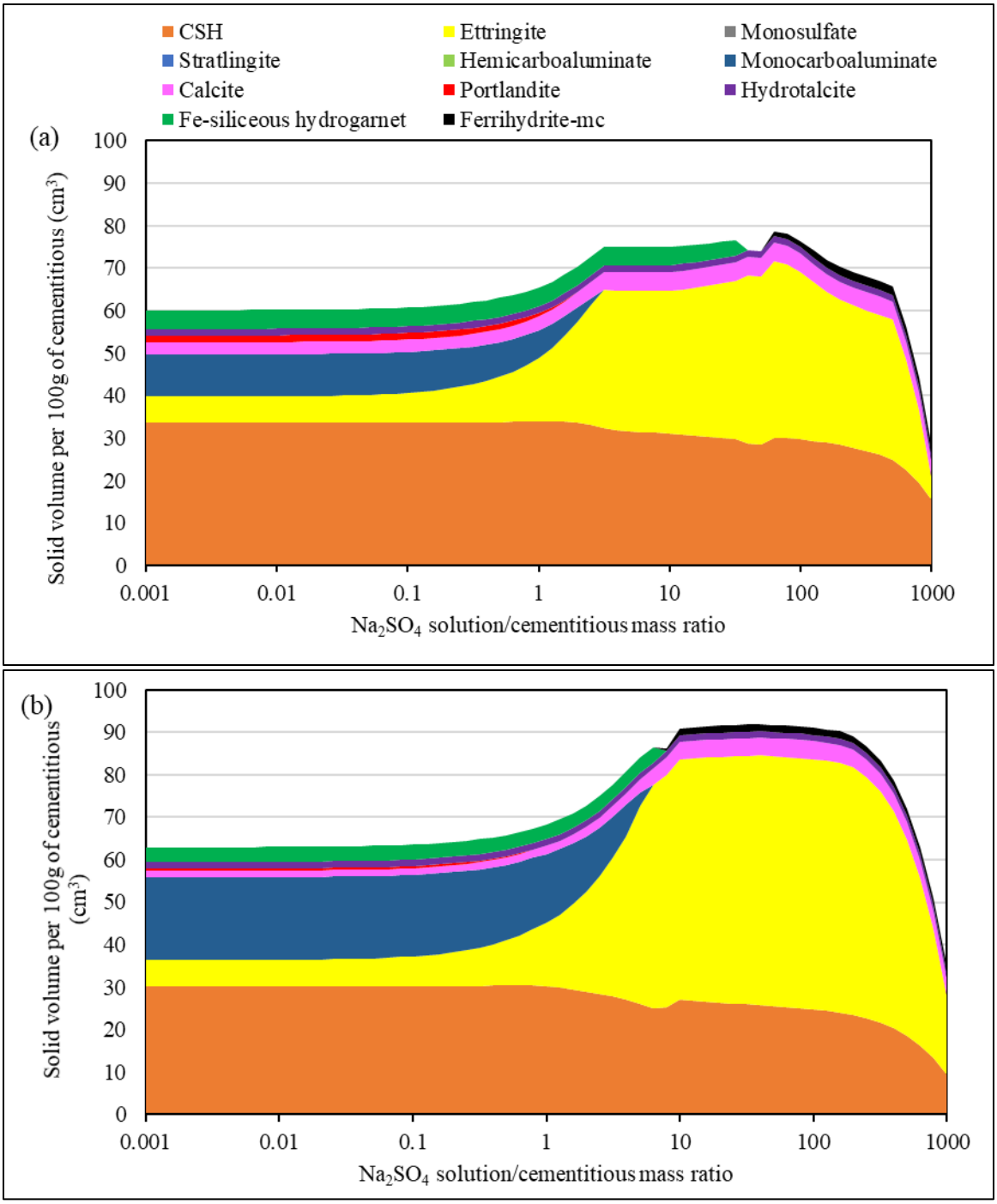

Figure 3-20: Predicted phase assemblage for (a) THIL+10CCF (b) THIL+10GAB4 mixtures immersed in 5% Na_2SO_4 solution

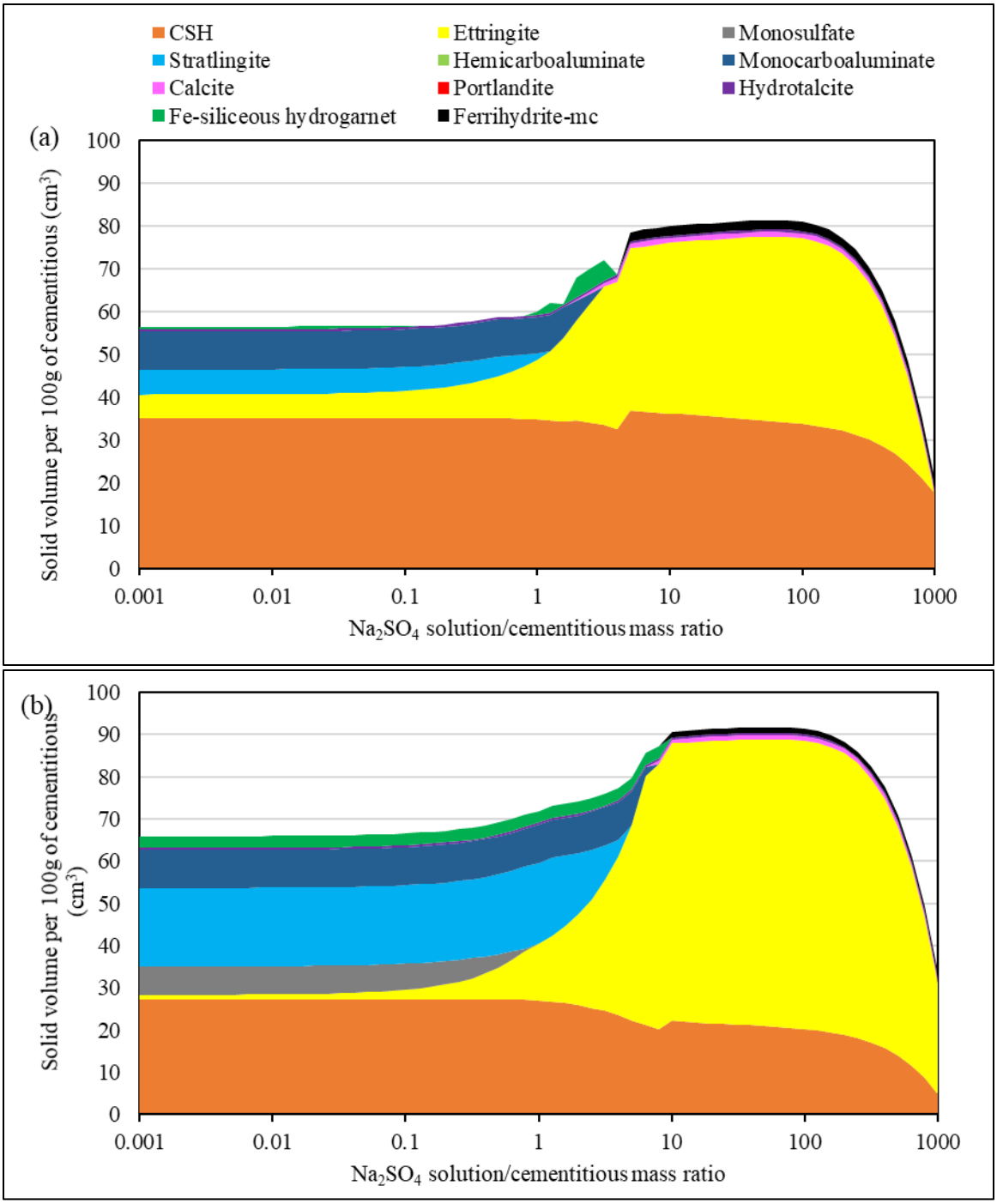

Figure 3-21: Predicted phase assemblage for (a) HA+20CCF (b) HA+20GAB4 mixtures immersed in 5% Na_2SO_4 solution

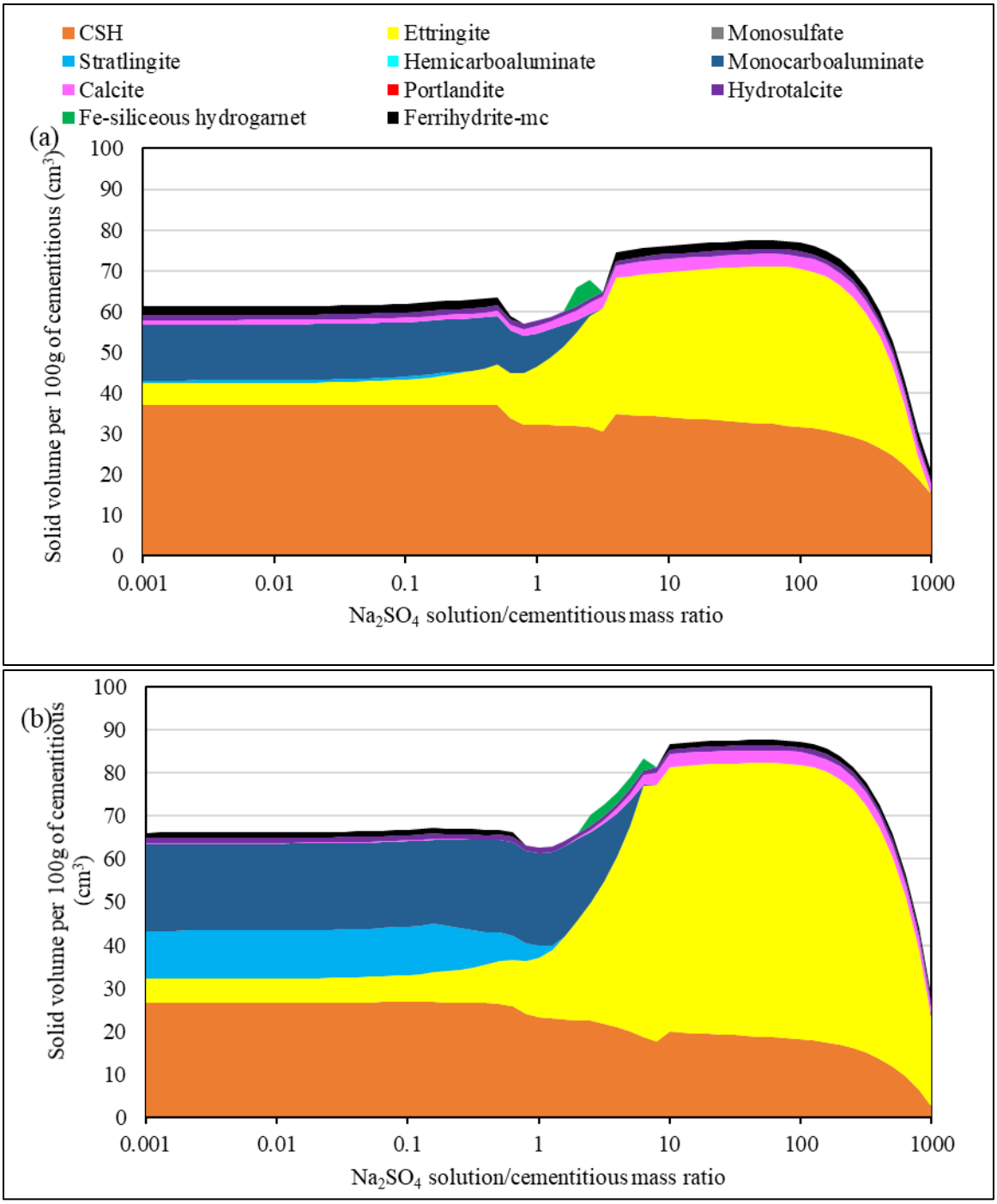

Figure 3-22: Predicted phase assemblage for (a) GILOP+20CCF (b) GILOP+20GAB4 mixtures immersed in 5% Na_2SO_4 solution

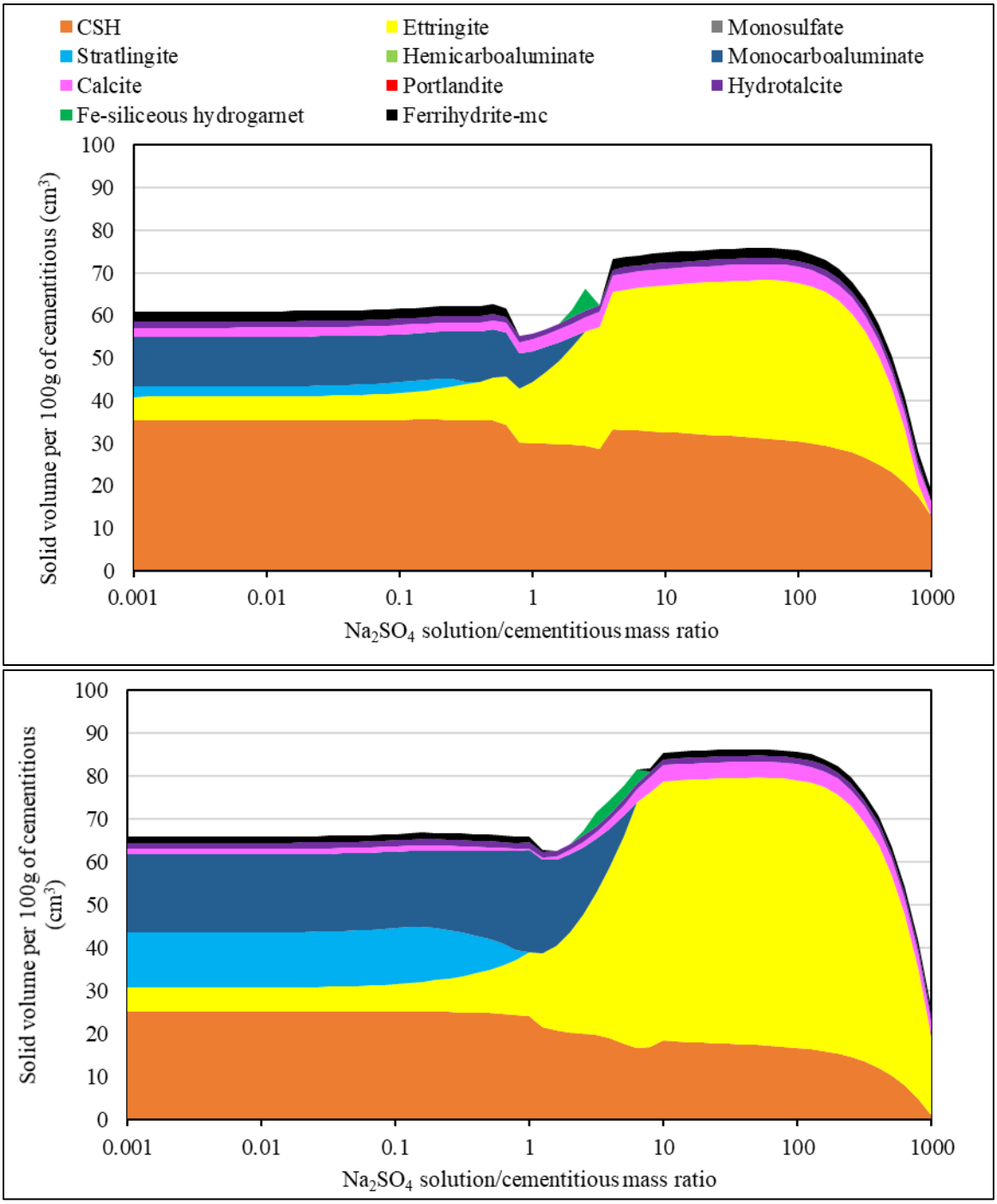

Figure 3-23: Predicted phase assemblage for (a) THIL+20CCF (b) THIL+20GAB4 mixtures immersed in 5% Na_2SO_4 solution

3.4 Conclusions

Compressive strength evolution of different cement-clay mortar cubes at two cement replacement levels and exposed to lime and sulfate solutions were studied using Type I/II and Type IL cements. The findings indicate as follows:

1. The highest compressive strength development in lime solution was observed in cement HA (Type I/II).
2. Cement replacement with clay resulted in strengths similar or higher compared to respective plain cement systems except for clay CCC, which was attributed to its coarse grind.
3. In lime solution, compressive strengths were higher for most of the mixtures when blended with IL cements due to increased clay reactivity in the presence of limestone. The highest strength increase was observed with cement THIL (Type IL(14)) at 20% substitution level.
4. Increasing substitution level from 10% to 20% produced a significant strength improvement when blended with IL cements, owing to an increased carboaluminate phase formation.
5. Clays GAB1 and GAB4 have shown higher sulfate resistance for the cements studied as indicated by consistently higher strengths, which can be attributed to the reduced permeability due to their high fineness and higher pozzolanic reactivity.
6. Sulfate resistance of the clays was further improved when blended with IL cements as indicated by clays EMD1, CCF, GAB1 And GAB4, due to the formation of carboaluminate phases at early ages.
7. Clay CCC provided poor sulfate resistance when blended with the cements used in this study, attributed to its coarser particle size distribution. However, clay CCF showed better sulfate resistance indicating the significance of clay fineness on pozzolanic reactivity of the blended system.

3.5 References

[1] A. M. Neville, *Properties of Concrete*, 4th ed. Harlow, England: Pearson Education Limited, 2006.

[2] A. Neville, "The confused world of sulfate attack on concrete," *Cem. Concr. Res.*, vol. 34, no. 8, pp. 1275–1296, 2004, doi: 10.1016/j.cemconres.2004.04.004.

[3] P. K. Mehta and P. J. M. Monteiro, *Concrete: Microstructure, Properties, and Materials*, 4th ed. McGraw-Hill Education, 2014.

[4] P. K. Mehta, "Mechanism of expansion associated with ettringite formation," *Cem. Concr. Res.*, vol. 3, pp. 1–6, 1973.

[5] N. Shanahan and A. Zayed, "Cement composition and sulfate attack," *Cem. Concr. Res.*, vol. 37, no. 4, pp. 618–623, Apr. 2007, doi: 10.1016/j.cemconres.2006.12.004.

[6] I. Odler and J. Colán-Subauste, "Investigations on cement expansion associated with ettringite formation," *Cem. Concr. Res.*, vol. 29, no. 5, pp. 731–735, 1999, doi: 10.1016/S0008-8846(99)00048-4.

[7] B. Tian and M. D. Cohen, "Does gypsum formation during sulfate attack on concrete lead to expansion?," *Cem. Concr. Res.*, vol. 30, no. 1, pp. 117–123, Jan. 2000, doi: 10.1016/S0008-8846(99)00211-2.

[8] T. Drimalas, "Laboratory testing and investigations of delayed ettringite formation," University of Texas at Austin, 2004.

[9] E. Güneyisi, M. Gesoğlu, S. Karaoğlu, and K. Mermerdaş, "Strength, permeability and shrinkage cracking of silica fume and metakaolin concretes," *Constr. Build. Mater.*, vol. 34, pp. 120–130, 2012, doi: 10.1016/j.conbuildmat.2012.02.017.

[10] E. Güneyisi, M. Gesoğlu, and K. Mermerdaş, "Improving strength, drying shrinkage, and pore structure of concrete using metakaolin," *Mater. Struct.*, vol. 41, pp. 937–949, 2008, doi: 10.1617/s11527-007-9296-z.

[11] A. Williams, A. Markandeya, Y. Stetsko, K. Riding, and A. Zayed, "Cracking potential and temperature sensitivity of metakaolin concrete," *Constr. Build. Mater.*, vol. 120, no. 2016, pp. 172–180, 2016, doi: 10.1016/j.conbuildmat.2016.05.087.

[12] M. Antoni, J. Rossen, F. Martirena, and K. Scrivener, "Cement substitution by a combination of metakaolin and limestone," *Cem. Concr. Res.*, vol. 42, no. 12, pp. 1579–

1589, Dec. 2012, doi: 10.1016/J.CEMCONRES.2012.09.006.

[13] F. Avet, R. Snellings, A. Alujas Diaz, M. Ben Haha, and K. Scrivener, “Development of a new rapid, relevant and reliable (R3) test method to evaluate the pozzolanic reactivity of calcined kaolinitic clays,” *Cem. Concr. Res.*, vol. 85, pp. 1–11, 2016, doi: 10.1016/j.cemconres.2016.02.015.

[14] F. Avet, “Investigation of the calcined kaolinite content on the hydration of Limestone Calcined Clay Cement (LC3),” École Polytechnique, 2017.

[15] ASTM C109/ C109M-16a, “Standard Test Method for Compressive Strength of Hydraulic Cement Mortars (Using 2-in. or [50-mm] Cube Specimens),” West Conshohocken, PA: ASTM International, 2016.

[16] ASTM C305-14, “Standard Practice for Mechanical Mixing of Hydraulic Cement Pastes and Mortars of Plastic Consistency,” West Conshohocken, PA: ASTM International, 2014.

[17] ASTM C1012/C1012M-15, “Standard test method for length change of hydraulic-cement mortars exposed to sulfate solution,” West Conshohocken, PA: ASTM International, 2015.

[18] Paul Scherrer Institut (PSI), “GEMS 3 [Software].” .

[19] W. Hummel, U. Berner, E. Curti, F. J. Pearson, and T. Thoenen, “Nagra/PSI chemical thermodynamic data base 01/01,” *Radiochim. Acta*, vol. 90, no. 9–11, pp. 805–813, 2002.

[20] EMPA, “CEMDATA14.” https://www.empa.ch/web/s308/cemdata.

[21] F. Nosouhian, M. Fincan, N. Shanahan, Y. P. Stetsko, K. A. Riding, and A. Zayed, “Effects of slag characteristics on sulfate durability of Portland cement-slag blended systems,” *Constr. Build. Mater.*, vol. 229, p. 116882, Dec. 2019, doi: 10.1016/J.CONBUILDMAT.2019.116882.

[22] S. Mindess, F. J. Young, and D. Darwin, *Concrete*. Upper Saddle River, NJ: Pearson Education, Inc., 2003.

[23] ASTM C150/C150M-16, “Standard Specification for Portland Cement,” West Conshohocken, PA: ASTM International, 2016.

[24] ASTM C618-17, “Standard Specification for Coal Fly Ash and Raw or Calcined Natural Pozzolan for Use in Concrete,” West Conshohocken, PA: ASTM International, 2017.

[25] A. Zayed, N. Shanahan, V. Tran, A. Markandeya, A. Williams, and A. Elnihum, “Final Report Effects of Chemical and Mineral Admixtures on Performance of Florida Structural Concrete FDOT Contract Number : BDV25-977-02,” 2016.

[26] A. Zayed, N. Shanahan, A. Sedaghat, Y. Stetsko, and B. Lorentz, “Final Report Development of Calcined Clays as Pozzolanic Additions in Portland Cement Concrete Mixtures FDOT Contract Number : BDV25-977-38,” University of South Florida, Tampa, FL, 2018.

[27] F. Avet and K. Scrivener, “Investigation of the calcined kaolinite content on the hydration of Limestone Calcined Clay Cement (LC3),” *Cem. Concr. Res.*, vol. 107, pp. 124–125, 2018, doi: 10.1016/j.cemconres.2018.02.016.

[28] B. . Sabir, S. Wild, and J. Bai, “Metakaolin and calcined clays as pozzolans for concrete: a review,” *Cem. Concr. Compos.*, vol. 23, no. 6, pp. 441–454, Dec. 2001, doi: 10.1016/S0958-9465(00)00092-5.

[29] C. C. Tchamo Leussa, L. Libessart, C. Djelal, C. Njiomou Djangang, and A. Elimbi, “Pozzolanic activity of kaolins containing aluminum hydroxide,” *Sci. Rep.*, vol. 10, no. 1, pp. 2–13, 2020, doi: 10.1038/s41598-020-70146-3.

[30] F. Zunino and K. L. Scrivener, “The Effect of Calcite and Gibbsite Impurities in Calcined Clay on its Reactivity,” in *Calcined Clays for Sustainable Concrete, RILEM Bookseries*, vol. 25, S. Bishnoi, Ed. Springer, Singapore, 2019, pp. 71–76.

[31] H. K. Tchakoute, C. H. Rüscher, J. N. Y. Djobo, B. B. D. Kenne, and D. Njopwouo, “Influence of gibbsite and quartz in kaolin on the properties of metakaolin-based geopolymer cements,” *Appl. Clay Sci.*, vol. 107, pp. 188–194, Apr. 2015, doi: 10.1016/J.CLAY.2015.01.023.

[32] K. Scrivener, F. Martirena, S. Bishnoi, and S. Maity, “Calcined clay limestone cements (LC3),” *Cem. Concr. Res.*, vol. 114, pp. 49–56, 2018, doi: 10.1016/j.cemconres.2017.08.017.

[33] B. Z. Dilnesa, “Fe-containing Hydrates and their Fate during Cement Hydration: Thermodynamic Data and Experimental Study,” Swiss Federal Institute of Technology, 2012.

[34] P. E. Bentz, Dale P., Stutzman and F. Zunino, “Low-Temperature Curing Strength Enhancement in Cement- Based Materials Containing Limestone Powder,” *Mater. Struct.*, vol. 50, no. 3, 2017, doi: 10.1617/s11527-017-1042-6.Low-Temperature.

[35] B. Z. Dilnesa, B. Lothenbach, G. Renaudin, A. Wichser, and D. Kulik, “Synthesis and characterization of hydrogarnet Ca3(Al xFe1 - X)2(SiO4)y(OH) 4(3 - y),” *Cem. Concr.*

Res., vol. 59, pp. 96–111, 2014, doi: 10.1016/j.cemconres.2014.02.001.

[36] M. U. Okoronkwo and F. P. Glasser, "Compatibility of hydrogarnet, Ca3Al2(SiO4)x(OH)4(3 -X), with sulfate and carbonate-bearing cement phases: 5-85 °c," *Cem. Concr. Res.*, vol. 83, pp. 86–96, 2016, doi: 10.1016/j.cemconres.2016.01.013.

[37] M. Whittaker, M. Zajac, M. Ben Haha, F. Bullerjahn, and L. Black, "The role of the alumina content of slag, plus the presence of additional sulfate on the hydration and microstructure of Portland cement-slag blends," *Cem. Concr. Res.*, vol. 66, pp. 91–101, Dec. 2014, doi: 10.1016/J.CEMCONRES.2014.07.018.

[38] M. Zajac, A. Rossberg, G. Le Saout, and B. Lothenbach, "Influence of limestone and anhydrite on the hydration of Portland cements," *Cem. Concr. Compos.*, vol. 46, pp. 99–108, Feb. 2014, doi: 10.1016/J.CEMCONCOMP.2013.11.007.

[39] M. C. G. Juenger and R. Siddique, "Recent advances in understanding the role of supplementary cementitious materials in concrete," *Cem. Concr. Res.*, vol. 78, pp. 71–80, 2015, doi: 10.1016/j.cemconres.2015.03.018.

[40] E. F. Irassar, "Sulfate attack on cementitious materials containing limestone filler - A review," *Cem. Concr. Res.*, vol. 39, no. 3, pp. 241–254, 2009, doi: 10.1016/j.cemconres.2008.11.007.

Chapter 4 Effect of Low-Grade Calcined Clay on Sulfate Durability, Carbonation, and Chloride Ingress in Cementitious Systems

4.1 Introduction

Sulfate and chloride durabilities of concrete structures are major concerns in the state of Florida. Typically, it is expected that incorporation of supplementary cementitious materials (SCMs) improves the durability performance of these structures. Class F fly ash is the most commonly used SCM to enhance durability and extend service life of Florida concrete structures. As the available fly ash sources may not consistently meet the expected demand, it is important to identify new materials that would demonstrate similar or better durability performance. Low-grade calcined clay is such material that has shown promising results as a novel SCM. Low-grade clay is available in abundance in many parts of the world and its use in concrete after calcination may be a viable option to enhance the durability performance of concrete. Clay properties may have variable effects on concrete performance and therefore require further investigations. In this chapter, the effects of different clays blended with several cements on external sulfate durability, chloride ingress, and carbonation resistance were investigated.

External sulfate attack is caused by the penetration of sulfate ions into the concrete from the surrounding environment (groundwater or water) [1]. It typically results in secondary ettringite formation, secondary gypsum formation, and decalcification of C-S-H, which may cause deleterious effects on concrete structures [2], [3]. During initial hydration in cementitious systems, ettringite forms and can subsequently transform to monosulfoaluminate if the sulfate levels are not adequate for ettringite stability while anhydrous aluminates are available. At the hardened stage, monosulfoaluminate can react with external sulfate ions and convert to ettringite causing expansion [4]–[6]. Secondary gypsum formation due to the reaction between calcium hydroxide (CH) and sulfates may also cause expansion [2], [7]. While decalcification of C-S-H does not cause expansion, it can result in loss of strength and cohesion [2].

Chloride ingress in concrete can result in rebar corrosion, which may be detrimental for reinforced concrete structures. In marine environments, chloride-induced corrosion initiates in a localized-cross section of the rebar from steel depassivation and can escalate to a level that can compromise the load carrying capacity of the rebar. Chloride transport in concrete occurs primarily

through diffusion in saturated concrete exposed to marine environments. Chloride transport in concrete is controlled by the pore structure characteristics and connectivity. Therefore, reduced concrete permeability is critical to enhance corrosion resistance. Some of the penetrated chloride ions can be bound by hydration products either by chemical reactions (formation of Kuzel's salt and Friedel's salt [8], [9]) or physical adsorption (to C-S-H [9], [10]), which can lower the free chloride concentration and thereby reduce the potential for rebar corrosion. Additionally, ingress of atmospheric CO_2 into concrete results in concrete carbonation. Both CH and C-S-H react with CO_2 forming calcite, which precipitates within the pores resulting in lower permeability that in turn reduces chloride diffusion. On the other hand, carbonation can increase corrosion risks as it lowers the pH of the pore solution to about 9-10, causing steel depassivation [11], and potentially reducing the chloride binding capacity of concrete [12], [13].

Partial replacement of cement with SCMs such as calcined clay is typically known to improve sulfate resistance as well as chloride resistance, due to the effect of SCMs on pore size refinement [14]–[18]. SCMs can also improve sulfate resistance due to a reduced C_3A content and portlandite consumption [14], [16]. In general, incorporation of high-alumina SCMs increases chloride binding and thereby increases chloride resistance [19]. However, the extent of improvement depends on the chemical and physical characteristics of the SCM [20]. In terms of concrete carbonation, SCM addition can reduce carbonation resistance and thereby cause adverse effects on concrete durability.

Several studies in the literature [16], [21], [22] indicate that incorporation of metakaolin (MK) (high grade calcined clay) in concrete improves its resistance against sulfate attack. MK replacement levels of 10% and 15% have been shown to be very effective in reducing expansion from sulfate attack [21], [22]. Coupled substitution of limestone and calcined clay has proven to be even more effective in improving sulfate resistance as the cement fraction is further reduced in the presence of limestone, in addition to consuming portlandite [16]. Additionally, formation of carboaluminate phases stabilizes primary ettringite and therefore reduces the potential for secondary ettringite formation [23]. With regard to chloride ion transport in calcined clay-cement binary systems and limestone-calcined clay-cement ternary systems, kaolinite content was found to play a major role [24]. Clays with kaolinite contents as low as 40% showed excellent resistance to chloride ion transport due to the effect of calcined clay on the refinement of the pore structure. Increasing kaolinite content in clay reduces the critical pore entry size with maximum refinement

at a moderate kaolinite content [25]. Carbonation resistance in calcined clay blended systems was reported to decrease with increasing clay substitution levels [26], [27]. However, the effect of kaolinite content on carbonation resistance was not addressed.

As stated earlier, sulfate attack, chloride induced corrosion and carbonation can cause detrimental issues in concrete structure. Therefore, the primary focus of this task is to investigate the effectiveness of low-grade calcined clay-cement blended systems on enhancing concrete durability against external sulfate attack, chloride ion ingress and carbonation.

4.2 Materials and Methods

4.2.1 Materials

Five cements designated as HA (Type I/II (MH)), GILOP (Type IL(10)), TIL (Type IL(10)), THIL (Type IL(14)) and CIL (Type IL(14)) and five clays designated as EMD1, CCC, CCF, GAB1 and GAB4 were used in this part of the study. Clays CCC and CCF are commercially available calcined clays from the same source. Calcined clay CCF is ground finer than calcined clay CCC. Oxide chemical composition, mineralogical analysis, Blaine fineness, and mean particle size (MPS) of cements and clays are listed in Table 4-1 through Table 3-4.

Table 4-1: Oxide chemical composition of cements

Analyte	HA I/II(MH)	GILOP IL(10)	TIL IL(10)	THIL IL(14)	CIL IL(14)
SiO_2	20.63	18.43	19.16	19.14	19.51
Al_2O_3	5.02	4.56	4.61	4.52	4.12
Fe_2O_3	3.45	3.29	3.74	3.54	3.23
CaO	63.96	62.28	62.40	62.11	61.97
MgO	0.35	0.91	1.12	1.08	0.78
SO_3	2.71	2.93	2.47	2.44	2.83
Na_2O	0.04	0.18	0.17	0.17	0.09
K_2O	0.3	0.32	0.32	0.29	0.22
TiO_2	0.25	0.21	0.23	0.22	0.21
P_2O_5	0.37	0.43	0.09	0.09	0.08
Mn_2O_3	0.07	0.06	0.15	0.14	0.02
SrO	0.07	0.06	0.12	0.12	0.12
Cr_2O_3	0.02	0.02	0.02	0.02	0.02
ZnO	0.03	0.06	0.05	0.04	0.10
L.O.I. (550°C)	0.98	1.62	0.76	0.69	1.21
L.O.I. (950°C)	2.54	5.86	5.35	5.99	6.63
Total	99.81	99.62	99.98	99.91	99.93
Na_2O_{eq}	0.24	0.40	0.38	0.36	0.23

Table 4-2: Mineralogical analysis, Blaine fineness, and MPS of cements

Analyte	HA I/II(MH)	GILOP IL(10)	TIL IL(10)	THIL IL(14)	CIL IL(14)
Alite	45.4	44.5	44.5	40.3	38.8
Belite	19.7	16.5	16.1	16.9	19.1
Aluminate	4.0	3.7	2.3	2.9	3.1
Ferrite	9.3	8.9	11.8	10.8	8.9
Gypsum	1.0	3.9	1.5	1.5	1.6
Hemihydrate	2.7	0.0	1.4	2.0	2.7
Calcite	3.4	9.2	8.8	11.4	11.7
Portlandite	1.5	1.5	-	-	0.8
Quartz	1.0	0.4	1.2	1.4	1.4
Dolomite	0.3	0.7	-	-	-
Syngenite	-	-	-	-	0.7
Amorphous content (AC)/ unidentified	11.7	10.6	12.5	12.8	11.1
Blaine fineness (m^2/kg)	417	469	483	488	500
MPS (μm)	13.028	13.105	10.798	12.751	12.436

Table 4-3: Oxide chemical composition of clays

Analyte	EMD1	CCC	CCF	GAB1	GAB4
SiO_2	68.68	63.49	62.62	44.56	31.82
Al_2O_3	20.81	19.89	18.94	37.44	44.49
Fe_2O_3	1.00	7.99	10.31	0.92	0.72
CaO	0.00	1.08	0.28	0.00	0.00
MgO	0.08	0.45	0.37	0.11	0.11
SO_3	0.00	0.23	0.15	0.00	0.17
Na_2O	0.18	0.09	0.42	0.08	0.05
K_2O	2.37	1.66	0.58	0.23	0.10
TiO_2	0.68	1.24	1.49	1.85	1.80
P_2O_5	0.13	0.04	0.14	0.05	0.03
Mn_2O_3	0.01	0.04	0.12	0.00	0.00
SrO	0.01	0.01	0.00	0.01	0.00
Cr_2O_3	0.00	0.01	0.02	0.01	0.01
ZnO	0.00	0.00	0.00	0.00	0.00
BaO	0.06	0.09	0.13	0.02	0.01
L.O.I. (950°C)	5.88	3.39	4.59	14.38	19.91
Total	99.88	99.72	100.16	99.66	99.21
Na_2O_{eq}	1.74	1.19	0.80	0.23	0.12

Table 4-4: Mineralogical analysis, Blaine fineness, and MPS of clays

Analyte	EMD1	EMD1 (850°C) (1 h)	CCC	CCF	GAB1	GAB1 (850°C) (1 h)	GAB4	GAB4 (850°C) (1 h)
Kaolinite	17.2	0.0	-	0.8	54.4	0.0	40.9	0.0
Dickite	10.1	0.0	-	-	33.4	0.0	18.1	0.0
Nacrite	10.6	0.0	-	-	5.3	0.0	6.4	0.0
Sum Kaolin	**37.9**	**0.0**	**3.1**	**0.8**	**93.1**	**0.0**	**65.5**	**0.0**
Illite	4.4	3.3	2.8	0.9	0.3	-	0.1	-
Gibbsite	-	-	-	-	-	-	24.0	-
Quartz	36.2	42.2	25.5	34.6	0.9	1.0	0.2	1.4
Crandallite	-	-	-	-	0.3	-	0.0	-
Hematite	-	-	0.7	1.0	-	-	-	-
Anatase	-	-	0.3	0.1	0.7	1.0	1.1	0.3
Calcite	-	-	0.3	0.2	-	-	-	-
AC/ unidentified	21.5	54.6	67.3	62.5	4.6	98.0	9.1	98.2
Blaine fineness (m^2/kg)	-	630	617*	984	-	1771	-	2791
MPS (µm)	-	61.955	20.637*	-	-	53.973	-	35.015

*passing no. 325 sieve

4.2.2 Expansion Measurements for External Sulfate Attack

The length change of mortar bars stored in a 5% sodium sulfate solution was monitored in order to assess the effect of cement and calcined clay characteristics on external sulfate durability. Cements HA (Type I/II(MH)), TIL(Type IL(10)) and THIL (TYPE IL (14)) were blended with all the clays at 20% cement replacement. Mortar bars were prepared and tested in accordance with ASTM C1012 [28], except the water-cementitious material ratio (w/cm) was maintained constant at 0.485. Due to the low workability of calcined clay, a polycarboxylate-based high-range water reducer (HRWR) was added to the mixing water at a dosage of 350 ml/100 kg cementitious material for the clay mixtures in order to obtain a flow satisfactory for casting the specimens. The water content in the chemical admixture was subtracted from the mixing water to maintain a constant water content. Immediately after molding, the specimens were placed in sealed curing containers and the containers were stored in a water bath maintained at 35 ± 3ºC for initial curing for 23.5 h ± 0.5 h. Mortar cubes of the same mixture as mortar bars were made and cured to determine a compressive strength of 2,850 psi was attained so that mortar bar samples can be placed in the sulfate solution.

In order to assess the effect of sulfate content of the clay blended cementitious system on sulfate durability, selected mixtures containing CCF were prepared with additional hemihydrate. The optimum hemihydrate content was assessed through calorimetry measurements (discussed next section). Mortar bar length change measurements were taken at 1, 2, 3, 4, 8, 13, and 15 weeks, and also at 4, 6, 9, and 12 months after immersion in the sulfate solution as stated in ASTM C1012 [28]. Moreover, the sulfate solution was changed at the same ages. To ensure that the pH of the solution was within the specified range, pH=6-8, the pH of the freshly prepared sulfate solution was measured using a pH meter each time the solution was changed.

4.2.2.1 Isothermal Calorimetry Measurements for Sulfate Optimization

In order to determine the optimum sulfate contents, isothermal conduction calorimetry was performed on the blended paste systems, according to ASTM C1702 [29], Method A, internal mixing using a TAM Air eight-channel calorimeter produced by TA instruments. The paste mixture design is listed in Table 4-5. A volumetric solution of the HRWR admixture was used in all mixtures. When preparing samples, cement, clay and hemihydrate amounts were weighed in an ampoule and mixed using a spatula until the dry solids were evenly blended. The ampoule was

then attached to the mixer containing the weighed amount of admixture solution. All the ampoules were loaded in the calorimeter at the same time and kept in-place until the sample temperature reached an equilibrium. Once the temperature became stable, mixing started and solution was injected into the ampoule over 10 seconds, followed by 1 minute of constant internal mixing. All experiments were conducted in duplicates at 23°C for 72 h. For each system, the optimum sulfate contents at 1, 2 and 3 days were determined by plotting the heat of hydration at the specified ages against the total sulfate content in the blended system and fitting a polynomial for each age, using the least squares method. The sulfate optimum corresponded to the maximum point of the polynomial (the highest heat of hydration) in the sulfate range considered (from the as-received SO_3 level to a maximum SO_3 around 5%).

Table 4-5: Isothermal calorimetry paste mixture design

Material	**Clay mixes**
Cement (g)	2.8140
Clay (g)	0.7035
Water (g)	1.6990
HRWR admixture (ml)	0.0123
w/cm	0.485

ASTM C563 [30] advises to consider addition of extra sulfate as a partial replacement of cement content. However, in practice, SCMs are blended with cement at the ready-mix plant, providing more flexibility to the concrete producer to decide on the SCM type and dosage. Therefore, it requires balancing of sulfate for the cement and the SCM separately. As a result, sulfate levels of CCF mixtures were balanced using a different adjustment method from ASTM C563 [30]; that is, hemihydrate was added as a partial replacement of clay.

4.2.3 Testing for Chloride Ion Ingress

The bulk diffusivity of concrete mixtures was determined following ASTM C1556 [31]. Three concrete cylinders of 4 in. x 8 in. (100 mm x 200 mm) were prepared for each mixture according to ASTM C192 [32]. The concrete mixture designs used for the control and calcined-clay blended mixtures are listed in Table 4-6.

Table 4-6: Concrete mixture design, yd^3 (m^3)

Material	**Control mixes**	**Calcined Clay mixes**
Cement, lb (kg)	665 (395)	532 (316)
Calcined Clay, lb (kg)	0	133 (79)
Coarse aggregate #57 limestone SSD, lb (kg)	1765 (1047)	1765 (1047)
Fine aggregate – SSD, lb (kg)	1286 (763)	1256 (745)
Water, lb (kg)	256 (152)	256 (152)
High-range water reducing admixture, fl oz/100 lb cementitious (ml/100 kg cementitious)	4.6 (300)	7.7 (500)
Low-range water reducing admixture, fl oz/100 lb cementitious (ml/100 kg cementitious)	0	4.7 (304)
w/cm	0.387	0.405

Specimens were demolded 24 hours after casting and then immersed in lime solution for a curing period of 28 days. After curing, a portion of the cylinder of at least 75 mm length, from levelled surface, was sliced off using a wet saw in accordance with ASTM C1556 [31]. All surfaces, except the top surface, were coated with epoxy (Sikadur 32) and left for curing overnight. Then, the sliced specimens were placed in a saturated lime solution until the specimen mass stabilized within ±0.1%. Subsequently, the specimens were immersed in a chloride solution with a concentration of 165 g/L of NaCl for 35, 180 and 360 days. Afterwards, specimens were milled for powder collection, at depths selected in accordance with ASTM C1556 [31]. For the control specimens, specified depth increments corresponded to w/c ratio of 0.4, whereas for specimens containing calcined clay, it corresponded to 0.35 w/cm ratio. Chloride concentrations of the powdered samples were determined by potentiometric titration using 0.1N $AgNO_3$ solution. The variation of chloride concentration with depth can be described by Fick's second law of diffusion. Therefore, the error function solution to Fick's second law was fitted to the obtained chloride concentration profiles (Equation 4-) using least square method to determine apparent diffusivity and surface chloride concentration.

$$C_d = C_s \cdot \left(1 - erf\left(\frac{x}{2.\sqrt{D.t}}\right)\right) \qquad \text{Equation 4-1}$$

Where, C_d is the chloride concentration at depth "*d*" (kg/m^3 of concrete), C_s is the surface chloride concentration (kg/m^3 of concrete), x is the thickness of concrete cover (m), D or D_{app} is the apparent diffusivity (m^2/sec or m^2/y), and t is the time since start of curing (years)

4.2.4 Testing for Bound Chloride Content

To investigate the effect of cement and calcined clay characteristics on chloride binding, cement CIL was blended with calcined clays EMD1, CCC, GAB4 at a 20% cement replacement level. The w/cm ratios of the paste samples were the same as in diffusivity test (0.387 for control and 0.405 blended mixtures). The method detailed by Zibara et al. [33] was adopted here. Paste samples were mixed in accordance with ASTM C305 [34] and were cast into 50 ml cylindrical plastic vials with screw caps. The vials were cured sealed for 24 h while being rotated at 8 rpm in a rotator to prevent segregation. The sealed vials were then transferred to a sealed curing container of saturated lime solution for curing and to avoid carbonation for a period of 28 days. Subsequently, the specimens were demolded, and 2-mm thick disks were cut from the central part of the specimen, using a wet diamond saw in which deionized (DI) water was the lubricant. Sliced samples were vacuum dried in a desiccation chamber that contained silica gel and soda lime to prevent carbonation at 23˚C ± 2˚C (73.4°F ± 35.6°F) for 7 days. Afterwards, the discs were conditioned in another chamber that was maintained at 11% RH using silica gel, soda lime and saturated lithium chloride solution. After one week of conditioning, test specimens weighing approximately 25 g were placed in 100 ml NaCl solutions with chloride concentrations of 0.1M, 0.3M, 0.5M, 1M and 3M. These solutions were saturated with calcium hydroxide to prevent leaching [33] and subsequently were sealed and stored at 23˚C ± 2˚C (73.4°F ± 35.6°F) for 6 weeks to ensure that the equilibrium was reached. Since the Cl^- concentration of the host solution was high, a diluted solution was prepared prior to performing potentiometric titration using 0.1N $AgNO_3$ solution. First, the sample of the host solution was vacuum filtered using grade 41 filter paper and transferred to a 100 ml volumetric flask. Next, 1 ml of 15% KNO_3 solution was added as an ionic strength adjuster (ISA) and subsequently the remainder of the flask was filled with DI water. The diluted solution was left to rest for 30 mins before titration. The concentration of free chloride in the diluted solution was then determined using an EasyPlus Cl Auto-titrator and 0.1 N $AgNO_3$ as titrant. The concentration of the host solution was calculated using Equation 4-1.

$$C_f V_1 = C_2 V_2 \quad \text{Equation 4-1}$$

$$C_2 = \frac{V_e C_{Ag} AW_{Cl} * 10^3}{V_2'} \quad \text{Equation 4-2}$$

Where, C_f is the free chloride concentration of the host solution at equilibrium (ppm), V_1 is the volume of the host solution (ml), C_2 is the chloride concentration of diluted solution (ppm), V_2 is the total volume of the diluted solution, V_e is the volume of silver nitrate at the equivalence point (ml), C_{Ag} is the molarity of silver nitrate (mol/l), AW_{Cl} is the atomic weight of chloride (35.45 g/mol), V'_2 is the volume of the titrated diluted solution (ml).

The reduced concentration of the host solution is believed to be due to the chloride being bound into the cementitious system [35], [9], [36]. The amount of bound chloride was calculated using Equation 4-3.

$$C_b = \frac{(C_i - C_f) * V_1 * 10^{-3}}{m} \quad \text{Equation 4-3}$$

Where, C_b is the amount of bound chloride (mg Cl^-/g of paste), C_i is the initial chloride concentration of the host solution (ppm) C_f is the free chloride concentration of the host solution at equilibrium (ppm), V_1 is the volume of the host solution (ml) and m is the dry mass of the paste samples (g).

In order to determine chloride binding isotherms, the bound chloride concentrations, normalized to dry mass of paste, were calculated using Equation 4-3, plotted against free chloride concentration and fit to a Freundlich isotherm denoted by Equation 4-4.

$$\text{Freundlich isotherm: } C_b = \alpha C_f^{\beta} \quad \text{Equation 4-4}$$

Where C_b is bound chloride (mg Cl^-/g paste), C_f is free chloride (mol Cl^-/l), and α and β are binding coefficients.

4.2.5 Carbonation Testing

The carbonation resistance of the clay-blended mixtures was assessed under natural conditions. Three 6-in. concrete cubes were prepared for each mixture according to ASTM C192 [32]. The same concrete mixture designs, listed in

Table 4-6, were used. The specimens were demolded after 24 hours and stored in a saturated lime solution for three curing times of 3, 7 and 21 days of age. The specimens were then placed outside in a sheltered area to be exposed to the atmospheric carbon dioxide in the natural environment for more than a year. The carbon dioxide concentration, temperature and humidity of the atmosphere were recorded using a TraceableLive datalogger and are shown in Figure 4-1, Figure 4-2, and Figure 4-3, respectively. The average CO_2 concentration was about 0.11%.

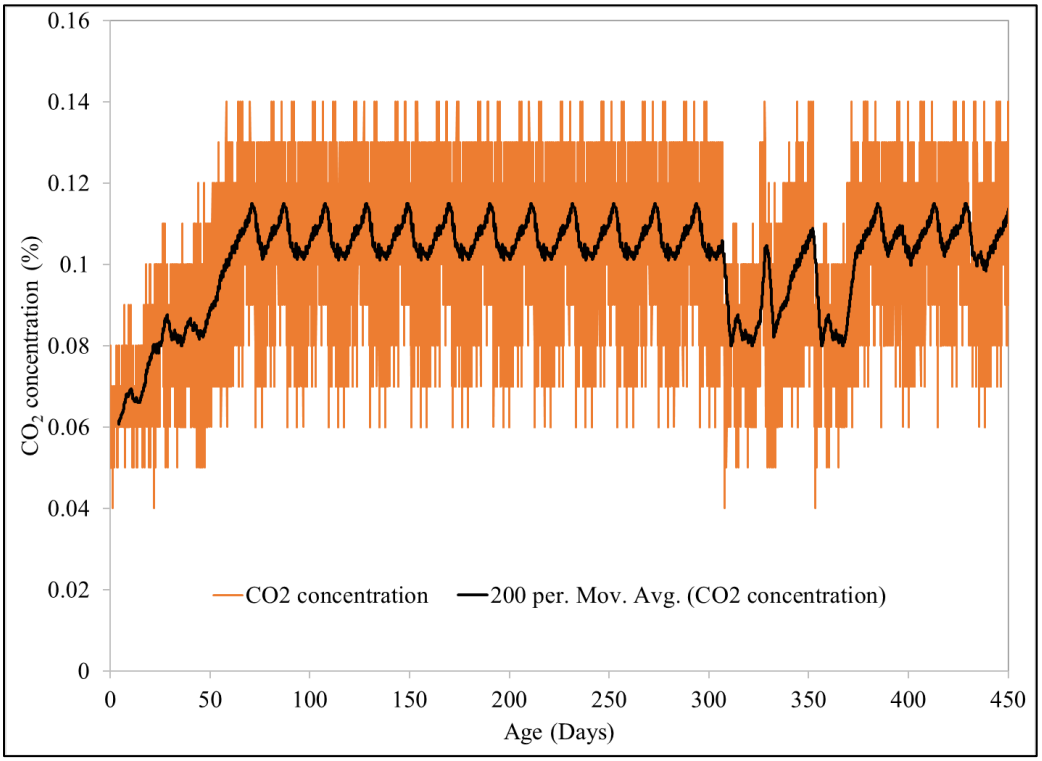

Figure 4-1: CO_2 concentration in the atmosphere

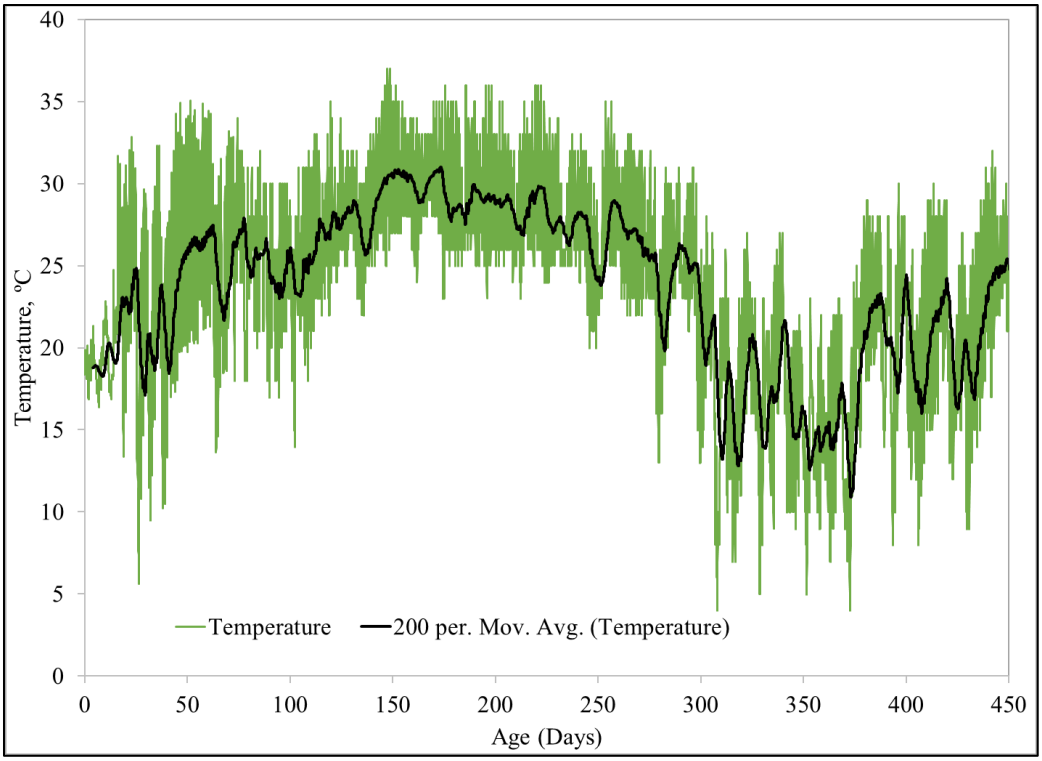

Figure 4-2: Temperature of the environment

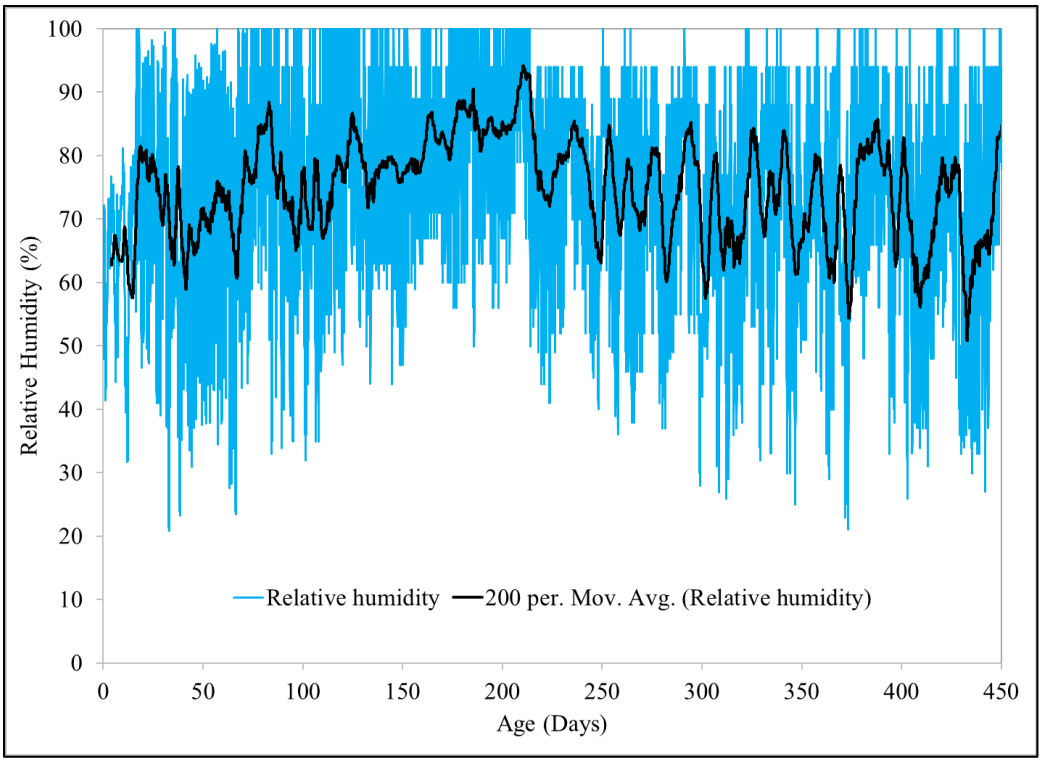

Figure 4-3: Relative humidity of the environment

At about one year of exposure to the natural outdoor environment, the concrete cubes were halved using a wet saw to measure the carbonation front depth. A phenolphthalein indicator (solution of 1 g phenolphthalein filled to 100 ml with ethyl alcohol) was sprayed onto the concrete split surface to measure the depth of carbonation. The indicator changes the color of the uncarbonated areas to dark rose and the colorless area indicates the carbonated area of a pH below 9 [37]. The depth of carbonation was measured with a caliper from the edge of the split surface. An average of 8 readings were obtained and the mean depth of carbonation was determined. The readings were taken both immediately after spraying the indicator and 24 h later.

The process of carbon dioxide diffusion can be modelled using Fick's first law (Equation 4-5) as proposed by Tuutti [38]. The carbonation coefficients of the mixtures were determined using the following relationship:

$$x = K\sqrt{t} \qquad \text{Equation 4-5}$$

Where x is the experimentally determined carbonation depth (mm); K is carbonation coefficient (mm/year$^{1/2}$); and t is exposure time to CO_2 (year)

4.2.6 X-Ray Diffraction Analysis

The effects of cement and calcined clay characteristics on phase assemblage evolution due to external sulfate exposure, chloride ion ingress and carbonation were studied using x-ray diffraction (XRD). To identify the phase assemblage after exposure to the sulfate environment, XRD analyses were conducted on mortar bars after about 1 year of exposure or at the age of failure. Samples were taken from the surface as well as the core of the mortar bar. The surface of each mortar bar was exposed to a high concentration of sulfate ions, whereas the core of the bar contained background levels of sulfate ions. Samples were crushed and gently ground by hand with mortar and pestle so that the x-ray amorphous content formation, due to the grinding effects, would be minimized [39]–[41]. The material passing the 45-µm sieve was used for the analysis and was mixed with an internal standard in order to determine the amorphous/unidentified content of each sample. The internal standard used in this study was the standard reference material (SRM) 676a obtained from the National Institute of Standards and Technology. With regards to chloride ion ingress, XRD analysis was performed on samples taken from a concrete specimen (section 4.2.3) that was exposed to chloride solution for 35 days. Paste samples were extracted, while

avoiding the coarse aggregate portion, from three layers (2, 7, and 20 mm from the surface) of the concrete cylinder and ground gently by hand with mortar and pestle, and the fraction passing a 45-μm sieve was used for the analysis. For carbonation testing, samples were taken from a concrete specimen (section 4.2.4) that was exposed to natural carbonation for about a year. Paste samples were extracted from close to the surface and at the core of the sliced specimen. In terms of chloride binding, XRD analysis was performed on paste samples prepared as discussed in 4.2.4, immediately before chloride exposure and for the paste samples stored in solutions of 0.1, 0.5 and 3 M NaCl concentrations, at the age of titration after chloride exposure.

XRD measurements were performed using a Phillips X'Pert PW3040 Pro diffractometer equipped with the X'Celerator Scientific detector and a CuKα x-ray source. Tension and current were set to 45 kV and 40 mA, respectively. Scans were performed in the range of 7 - 70° 2θ, with a step size of 0.0167° 2θ. Samples were then loaded into the sample holder using a back-loading technique in order to minimize preferred orientation, and placed onto a spinner stage that was rotating at 30 rpm in order to improve counting statistics [42]. Phase quantification was performed using the Rietveld refinement functionality of the PANalytical HighScore Plus 4.5 software.

4.3 Results and Discussion

4.3.1 Length Change Measurements in Sodium Sulfate Solution according to ASTM C1012

4.3.1.1 As-Received Cement Systems

Figure 4-4 shows the expansion behavior of the control mortar bars prepared with as-received cements HA, TIL and THIL after exposure to 5% sodium sulfate solution. None of the mixtures showed mortar bar failure. Cements HA and THIL can be classified as high sulfate resistant cements, while TIL showed moderate sulfate resistance according to ASTM C1157 [43]. Both THIL and HA cements have a MPS coarser than TIL with cement HA having the lowest Blaine fineness and highest MPS. Additionally, THIL has a higher calcite content than TIL. In terms of Type IL cements, a lower expansion can be attributed to the clinker dilution effect as well as the effect of limestone on forming carboaluminate phases which stabilize primary ettringite [44], [45].

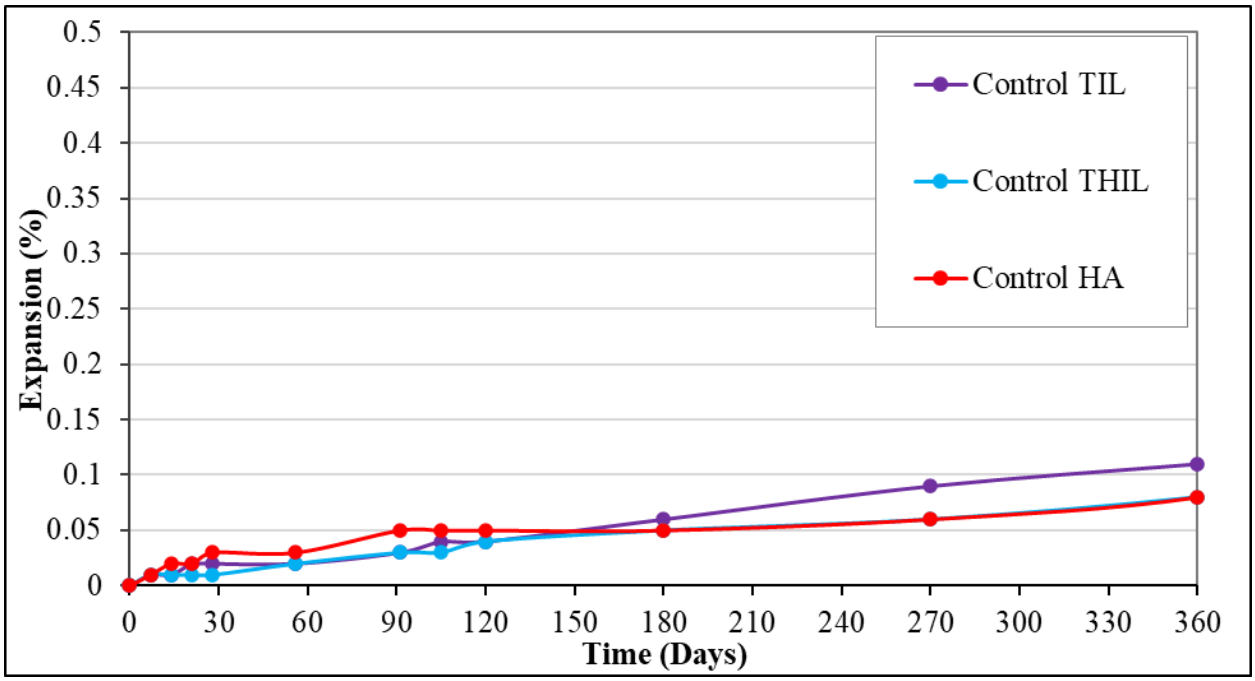

Figure 4-4: Length change of as-received cements mortar bars in 5% sodium sulfate solution

4.3.1.2 As-Received Clay-Blended Systems

Figure 4-5 through Figure 4-9 show the effect of calcined clay addition on sulfate durability. In these figures, "X" indicates the last measurement, after which the expansion could not be measured due to bar failure. Clearly, sulfate resistance of the blended system was affected by the type of clay used. Incorporation of clays EMD1, CCC and CCF resulted in significant expansion in mortar bars indicating poor sulfate resistance, while clays GAB1 and GAB4 controlled or suppressed the expansion indicating high sulfate resistance. In general, all of EMD1 mixtures showed a faster rate of expansion and resulted in mortar bar failure, followed by CCC mixtures.

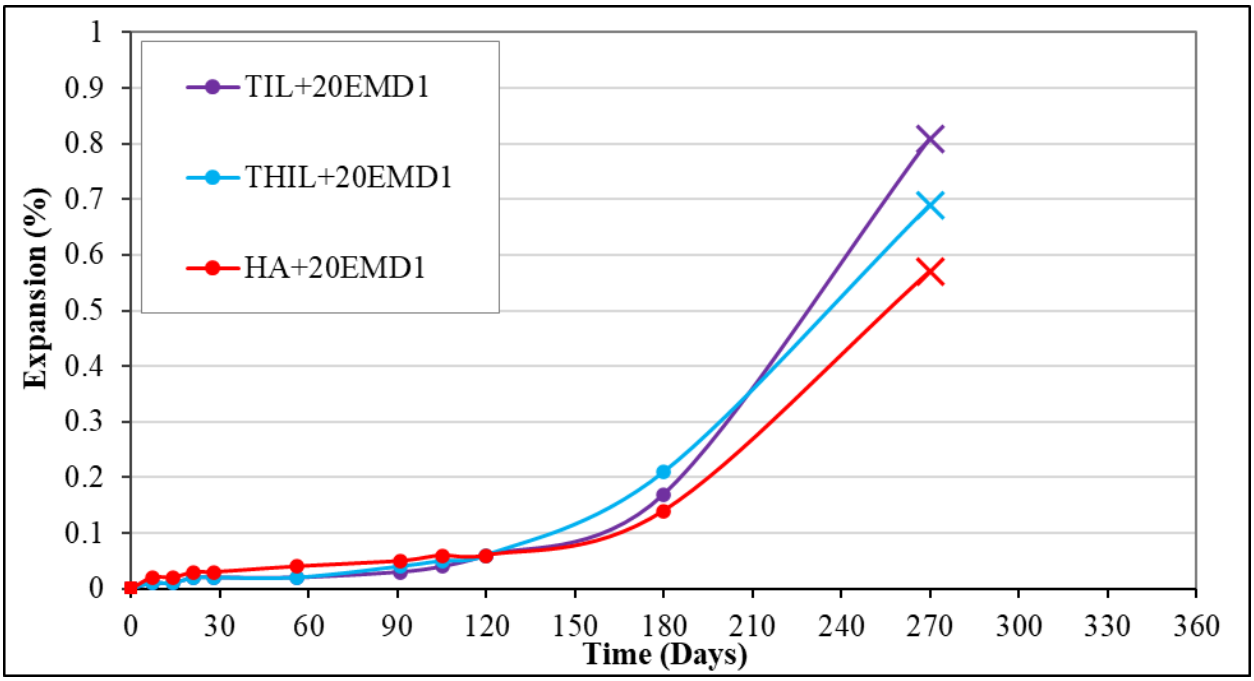

Figure 4-5: Length change of clay EMD1 mortar bars in 5% sodium sulfate solution

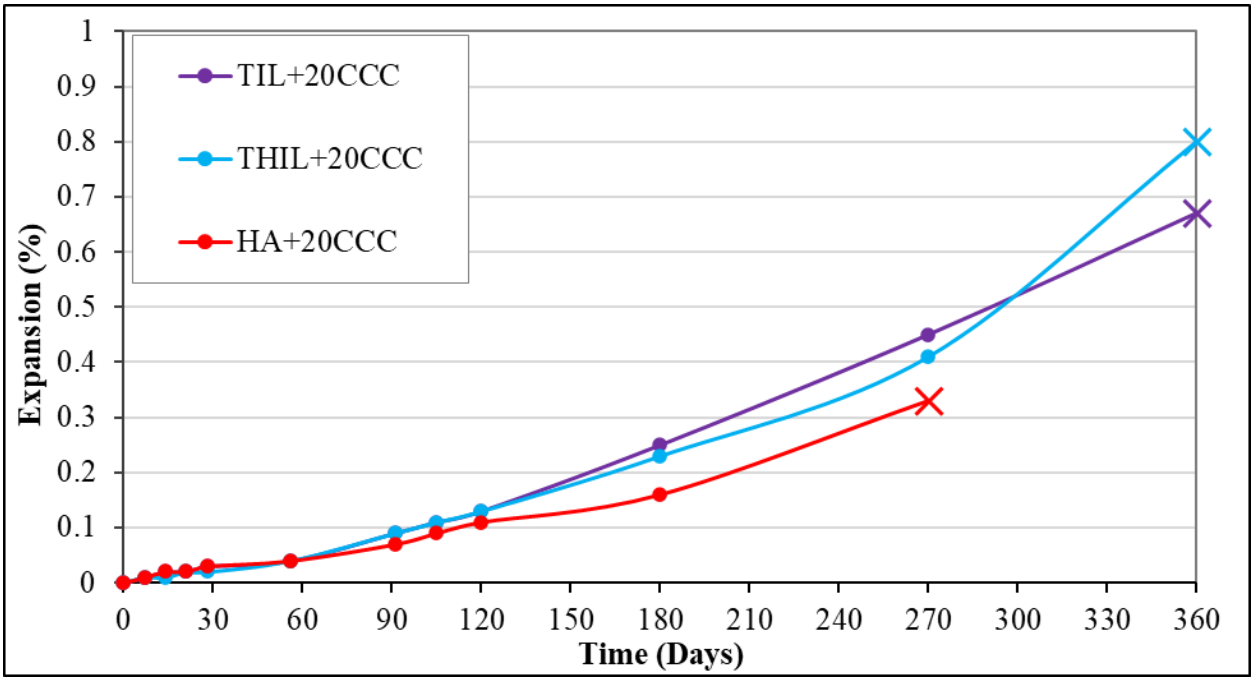

Figure 4-6: Length change of clay CCC mortar bars in 5% sodium sulfate solution

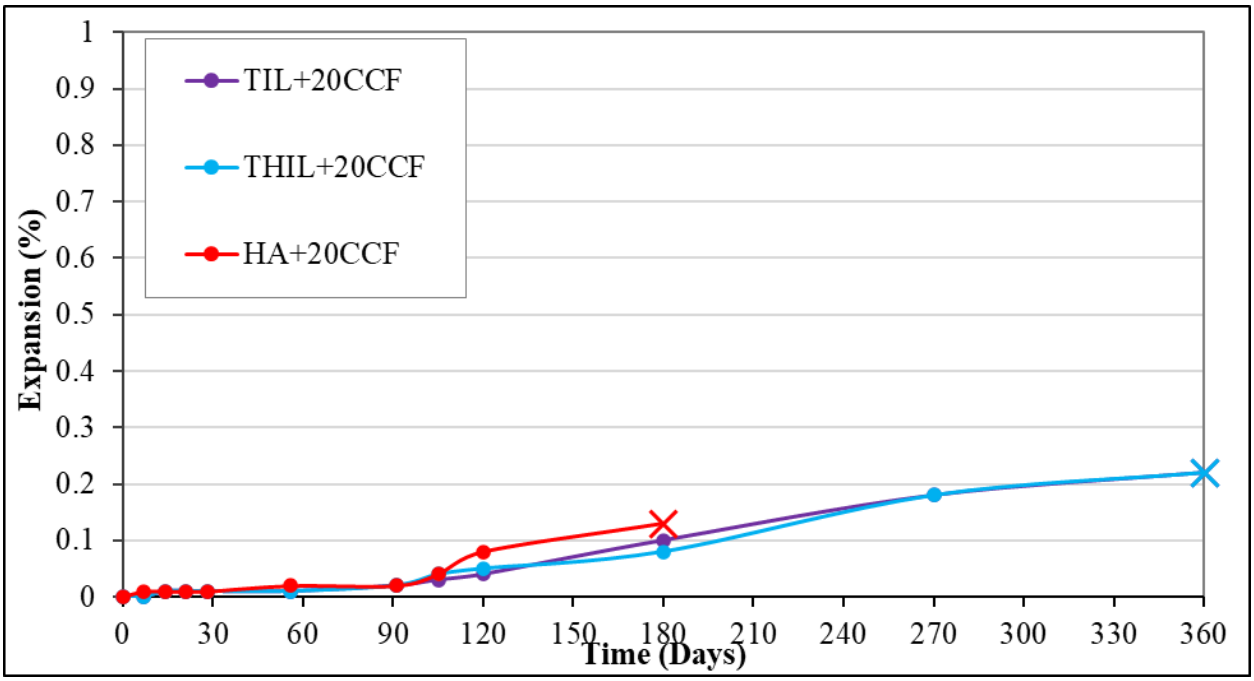

Figure 4-7: Length change of clay CCF mortar bars in 5% sodium sulfate solution

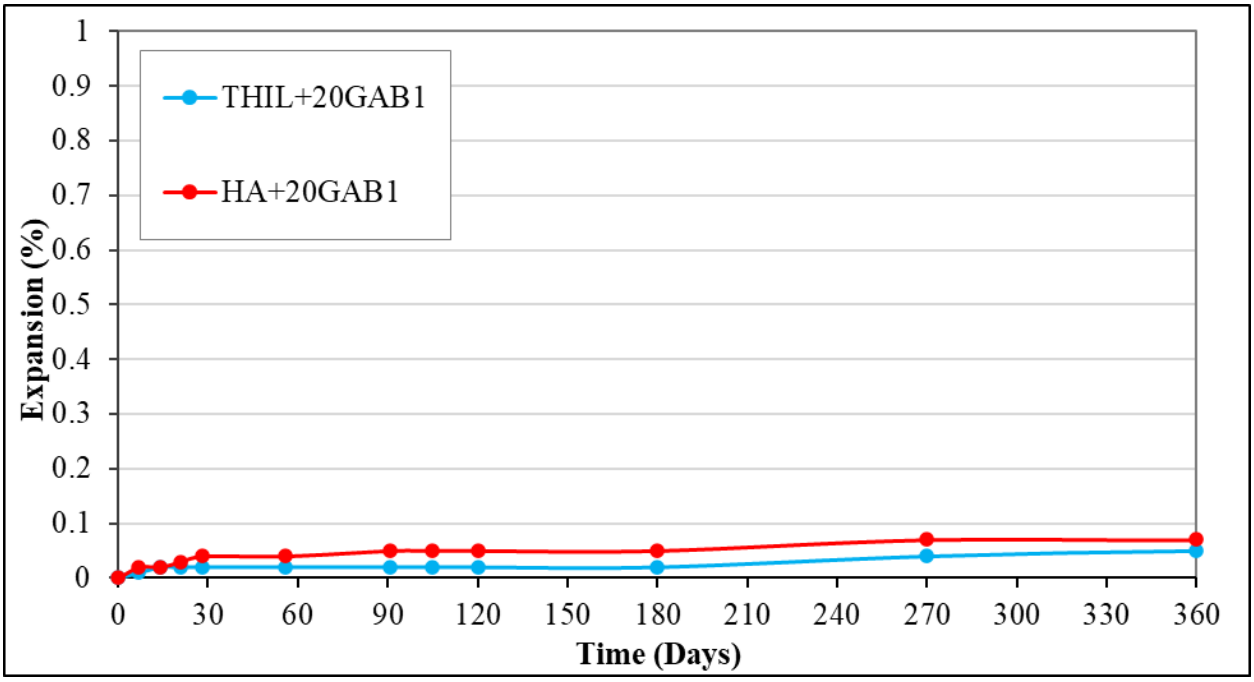

Figure 4-8: Length change of clay GAB1 mortar bars in 5% sodium sulfate solution

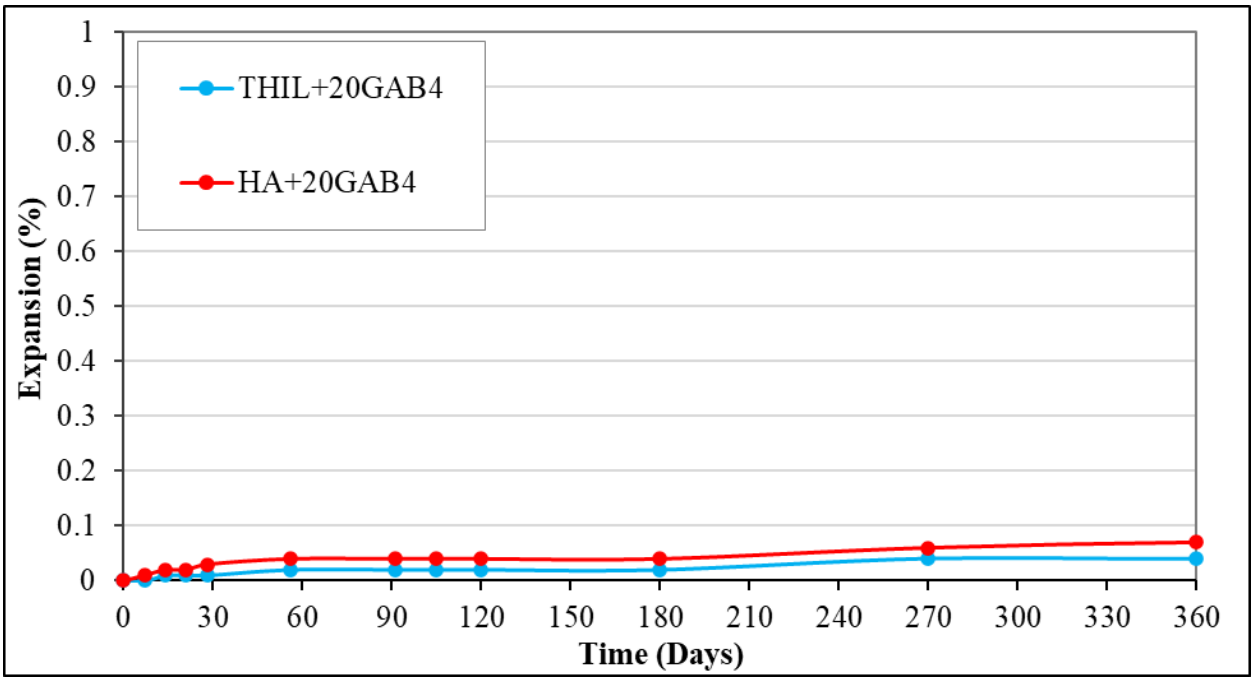

Figure 4-9: Length change of clay GAB4 mortar bars in 5% sodium sulfate solution

Amorphous content was the lowest in calcined clay EMD1 followed by clay CCC and CCF, while the highest amorphous contents were detected in calcined clays GAB1 and GAB4, which can explain the observed trends in expansion. The original kaolin content of clay EMD1 was 37.9% (as determined by QXRD) while the kaolin contents of clays CCC and CCF were unknown because those were commercially available calcined clays. However, the Al_2O_3 contents and SiO_2 contents of clays EMD1, CCC, and CCF were comparable; therefore, it can be speculated that the original kaolin contents of clays CCC and CCF were somewhat close to that of clay EMD1. The amount of kaolin calculated based on stoichiometry in clays CCC and CCF was 50% and 48%, respectively. Additionally, the sand content of these three clays was considerably higher, which lowered the effective cementitious material content, increased the effective water/binder ratio, and influenced the hydration of the paste system. This may have increased the permeability of the system and thereby lowered the sulfate resistance as can be seen from the expansion measurements. Moreover, a significant difference in expansion can be observed in clay CCC and clay CCF mixtures, indicating the effect of clay coarseness on sulfate durability. The coarser particle size of clay CCC likely lowered its reactivity and may have increased the permeability of the system and aggravated the penetration of sulfate ions, whereas this effect was

suppressed/controlled in clay CCF mixtures attributed to a higher reactivity due to higher surface area.

As stated by Scrivener et al. [46], when the original kaolinite contents were more than 65% in LC^3-50 (50% ground clinker, 30% calcined clay, 15% limestone, 5% gypsum) blends, a threshold pore radius as small as 10 nm was observed as early as 3 days. Such pore size refinement at early age indicates a lower permeability, which can control the penetration of sulfate ions. It is likely the increased sulfate resistance observed in clay GAB1 and GAB4 mixtures compared to other clay blends was a result of pore size refinement due to the high reactivity caused by their higher kaolin contents and higher fineness. The kaolin content of clays GAB1 and GAB4 were 93.1% and 65.5%, respectively. Additionally, clay GAB4 contained a gibbsite content of 24%. It is likely that calcined gibbsite may also have affected the reactivity of GAB4 clay and thereby contributed to a refined pore structure. The presence of gibbsite is reported to possess higher pozzolanic activity in clay [47]. According to Sabir et al. [48], kaolinite and gibbsite in laterites are transformed into phases of metakaolin and amorphous alumina when calcined and thereby possess pozzolanic properties.

4.3.1.3 Sulfate-Added Clay Blended Systems

The measured total heat of HA+20CCF and THIL+20CCF with variable SO_3 levels at one, two and three days are shown in Figure 4-10 and Figure 4-11, respectively. Although similar trends were observed with clay-blended systems using both cements, each system showed different optimum SO_3 content due to its unique chemical and physical characteristics. In general, the sulfate optimum increased with age, indicating a higher sulfate demand at later ages.

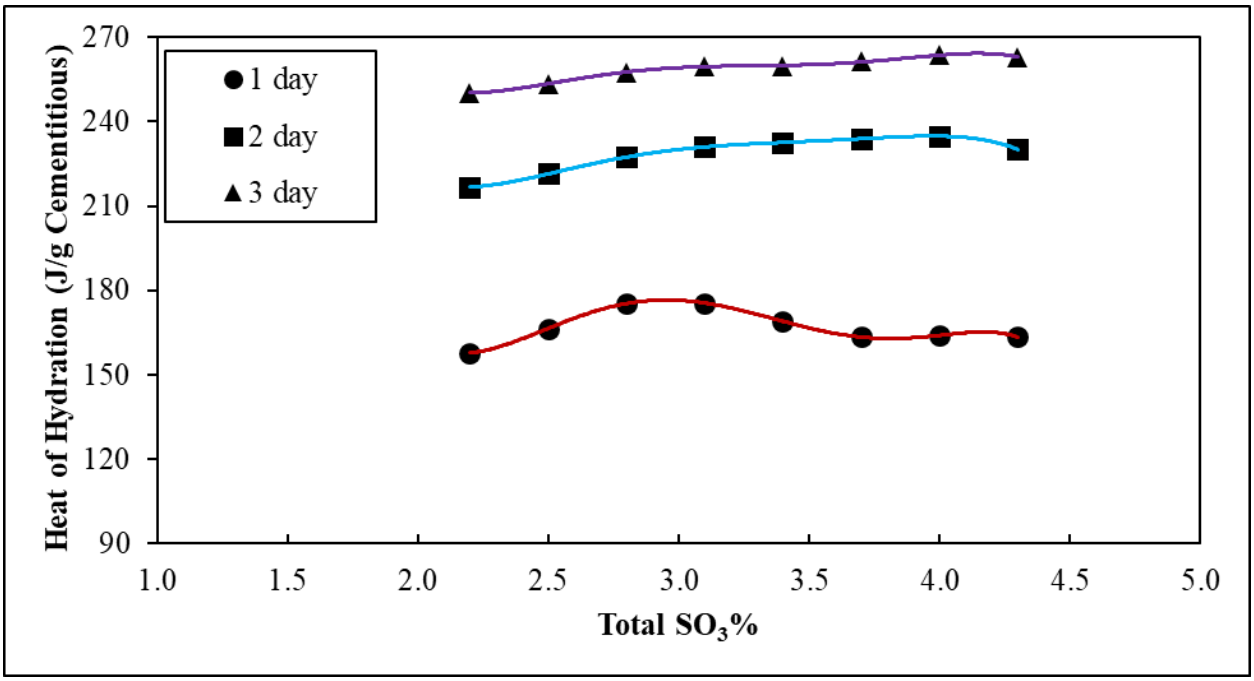

Figure 4-10: Total heat vs. sulfate levels in HA+20CCF mixture

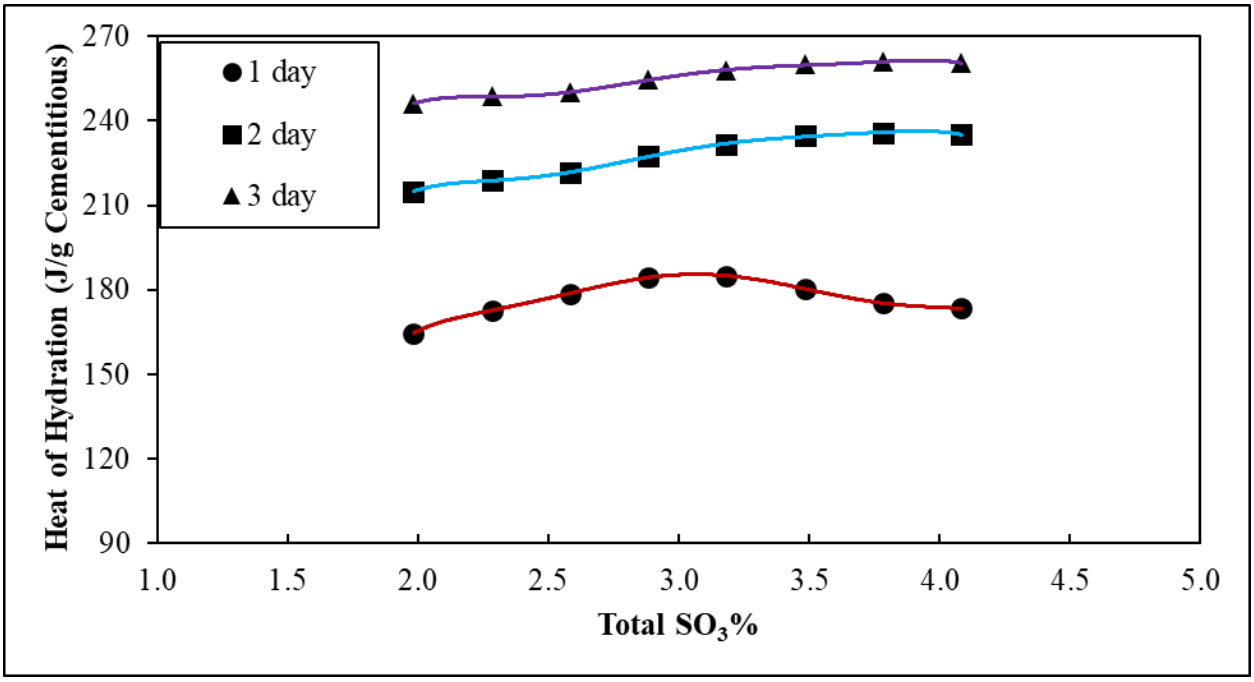

Figure 4-11: Total heat vs. sulfate levels in THIL+20CCF mixture

The optimum SO_3 contents determined for each blended cement system at 1, 2 and 3 days are listed in Table 4-7. The effect of sulfate addition on external sulfate durability was assessed using 1- and 2- day optimum sulfate levels.

Table 4-7: Determined optimum sulfate contents in clay-blended mixtures

Mix ID	Total SO_3 content (%)				SO_3 content in clay (%)			
	as-received	1-day	2-day	3-day	as-received	1-day	2-day	3-day
HA+20CCF	2.20	2.95	3.97	4.15	0.15	3.91	9.01	9.91
THIL+20CCF	1.98	3.07	3.92	3.94	0.15	5.59	9.84	9.94

Figure 4-12 and Figure 4-13 show the ASTM C1012 results for HA+20CCF and THIL+20CCF mixtures with added sulfate. In the mixture ID of the sulfate added mixtures, the value in parenthesis indicates the total SO_3 content in the cementitious system. The sulfate addition clearly delayed the onset of expansion. Undoubtedly, this indicates the importance of sulfate addition to calcined clays to improve sulfate resistance in high alumina blended systems. Sulfate addition has shown to be effective in delaying expansion due to sulfate attack in SCM blended systems such as ground granulated blast furnace slag and in the presence of limestone it has proven to be more effective in delaying and/or suppressing expansion [44]. The delay in expansion can be attributed to the increased primary ettringite formation with additional sulfate, which reduces the amount of monosulfoaluminate in the system and thereby improve the resistance against sulfate attack. Additionally, in presence of limestone, ettringite is stabilized due to carboaluminate formation [45].

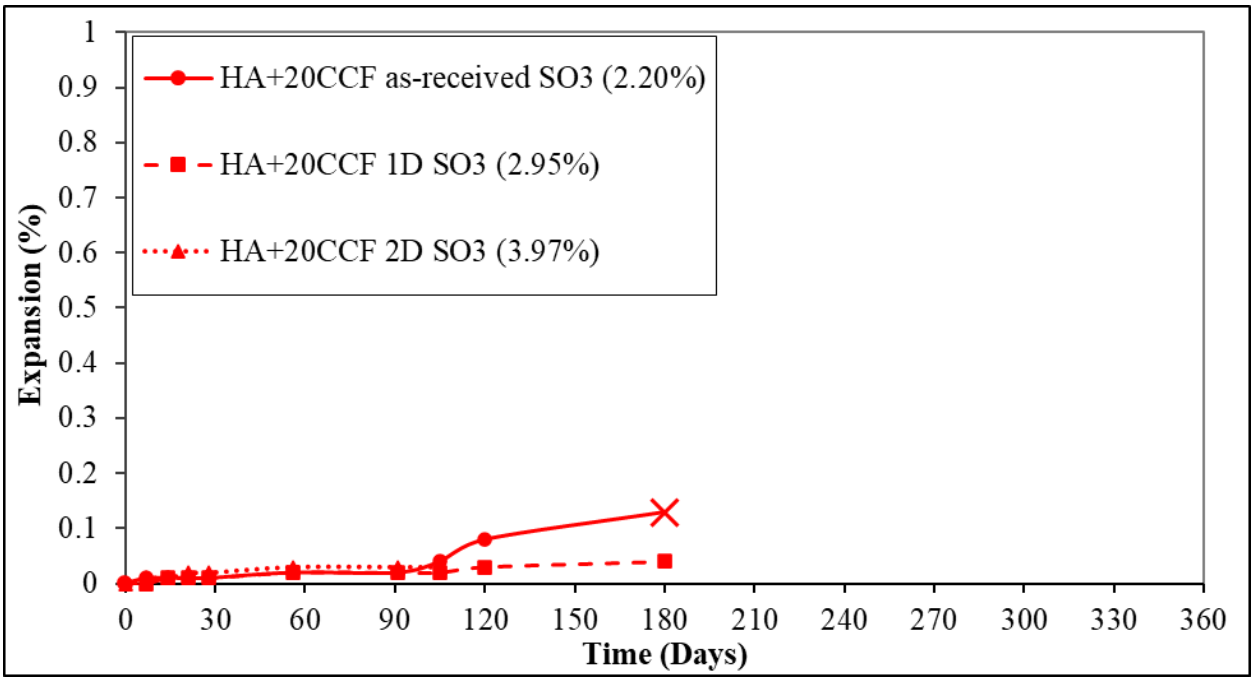

Figure 4-12: Length change of sulfate added HA+20CCF mortar bars in 5% sodium sulfate solution, *Note:* Parenthesis of mix ID (total SO_3 content)

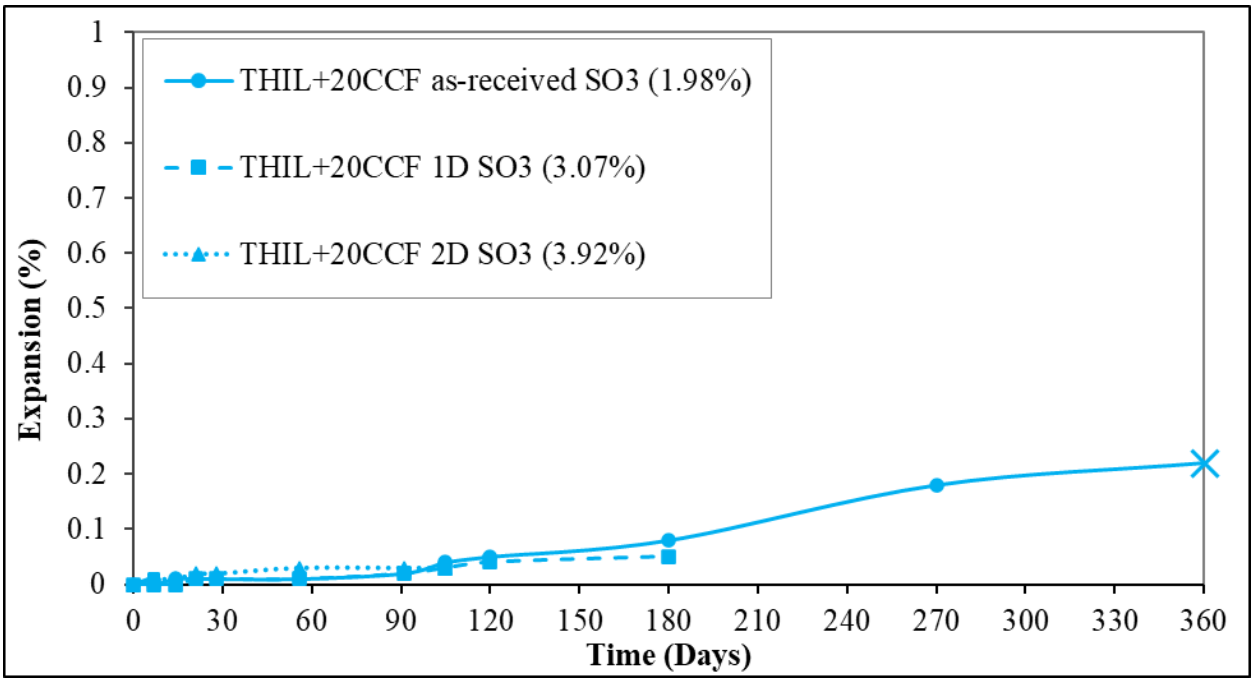

Figure 4-13: Length change of sulfate added THIL+20CCF mortar bars in 5% sodium sulfate solution, *Note:* Parenthesis of mix ID (total SO_3 content)

4.3.1.4 X-Ray Diffraction Analysis of Mortar Bars after Sulfate Exposure

Phase quantification results of core and surface samples of the control mortar bar mixtures at 1 year of sulfate exposure are listed in Table 4-8. None of the control mortar bars were broken at 1 year. When the cores and the surface of the bars were compared, higher amounts of portlandite were detected at the core while ettringite and gypsum contents were higher at the surface as a result of external sulfate attack [49], [50]. While no monosulfate was detected in any of the control mixtures, monocarboaluminate was detected at the core of the Type IL cement mixtures. Only a small variability in the ettringite contents can be observed among the mixtures, similar to the expansion of mortar bars. It is noteworthy that higher initial ettringite formation prior to sulfate exposure can also result in high amounts of ettringite after sulfate exposure, which is expected in Type IL cement mixtures. In the presence of limestone, ettringite is more stable [45].

Table 4-8: Phase quantification of control mortar bars stored in 5% Na_2SO_4 solution

Mix ID	**Control HA**		**Control TIL**		**Control THIL**	
Age (days)	**360**		**360**		**360**	
Condition of bar	**Not Broken**		**Not Broken**		**Not Broken**	
	Surface	**Core**	**Surface**	**Core**	**Surface**	**Core**
Belite	1.4	1.7	0.8	0.7	0.9	0.8
Ferrite	0.1	0.3	0.2	0.2	0.2	0
Calcite	2.1	0.8	5.1	4.1	6.6	3.9
Portlandite	5.1	12.2	6	16.5	7	11.4
Gypsum	6.4	1	8.4	0.6	4.8	0.4
Ettringite	13.4	6.5	14.8	9.7	13.4	6
Monocarboaluminate	0	0	0	0.1	0	0.9
AC/Unidentified	71.5	77.4	64.6	68	67.1	76.5

Phase quantification results of clay-blended mixtures immersed in sulfate solutions are listed in Table 4-9 through Table 4-12. The samples were tested either at 1 year of exposure or after they were broken, whichever occurred earlier. Similar to the control mixtures, portlandite content was lower and gypsum and ettringite contents were higher at the surface compared to the core of the clay-blended mortar bars. The highest amounts of ettringite were observed at the surface of clay EMD1 mixtures, which explains the higher expansion seen in mortar bars. Monosulfoaluminate was only observed in clay GAB1 and GAB4 mixtures due to their higher

Al_2O_3 contents. In the cores of IL cement mixtures, noticeable amounts of carboaluminate phases were detected due to the presence of limestone. However, the amounts were lower at the surface implying possible decomposition of carboaluminates, at longer exposure times, to form ettringite in a sulfate environment [44]. Moreover, stratlingite was observed in HA+20GAB1 and HA+20GAB4 blends. This suggests that these mixtures had more Al than could be incorporated into C-S-H [51]. In general, the trends observed in phase assemblage of the clay-blended mixtures were in agreement with the corresponding length change measurements of the mortar bars at 1 year.

Table 4-9: Phase quantification of clay CCC blended mortar bars stored in 5% Na_2SO_4 solution

Mix ID	**HA+20CCC**		**TIL+20CCC**		**THIL+20CCC**	
Age (days)	**360**		**360**		**360**	
Condition of bar	**Broken**		**Not Broken**		**Not Broken**	
	Surface	**Core**	**Surface**	**Core**	**Surface**	**Core**
Belite	0.9	0.6	0.4	0.6	0.6	0.7
Calcite	11.3	0.7	6.7	2.9	10.2	3.4
Portlandite	1.3	9.7	1.3	9.7	0.2	3.2
Gypsum	5.5	0.8	8.5	1.4	5.8	3.3
Ettringite	11.4	10.8	12.9	10.7	11.5	9.9
Illite	0.1	0.3	0.4	0.5	0.4	0.5
AC/Unidentified	69.6	76.9	69.2	74.2	71.3	78.9

Table 4-10: Phase quantification of clay CCF blended mortar bars stored in 5% Na_2SO_4 solution

Mix ID	**HA+20CCF**		**TIL+20CCF**		**THIL+20CCF**	
Age (days)	**270**		**360**		**360**	
Condition of bar	**Broken**		**Broken**		**Broken**	
	Surface	**Core**	**Surface**	**Core**	**Surface**	**Core**
Belite	0	0.7	0.3	0	0.3	0
Calcite	16.8	4.8	11.7	2.5	9.1	4
Portlandite	0.3	6.5	0.8	4.9	0.8	5.6
Gypsum	4.5	1.4	4.1	3.1	2.6	2.4
Ettringite	8.5	6.1	17	12.2	18.1	10.2
Monosulfate	0.1	0.7	0	0.1	0	0
Hemicarboaluminate	0	1.4	0	0.6	0	0.7
Monocarboaluminate	0	0	0	1	0	0.8
Illite	0	0	0.1	0.2	0.1	0.2
AC/Unidentified	69.7	78.4	66	75.5	69	76.1

Table 4-11: Phase quantification of clay EMD1 blended mortar bars stored in 5% Na_2SO_4 solution

Mix ID	**HA+20EMD1**	**TIL+20EMD1**
Age (days)	**360**	**360**
Condition of bar	**Broken**	**Broken**
	Surface	**Surface**
Belite	1	0.3
Calcite	6.3	17.3
Portlandite	0.2	0
Gypsum	2.4	0.5
Ettringite	25.4	21.9
Hemicarboaluminate	0	0
Monocarboaluminate	0	0
Illite	0.5	0.5
AC/Unidentified	64.1	59.4

Table 4-12: Phase quantification of clay GAB1 and GAB4 blended mortar bars stored in 5% Na_2SO_4 solution

Mix ID	**HA+20GAB1**		**THIL+20GAB1**		**HA+20GAB4**		**THIL+20GAB4**	
Age (days)	**360**		**360**		**360**		**360**	
Condition of bar	**Not Broken**		**Not Broken**		**Not Broken**		**Not Broken**	
	Surface	**Core**	**Surface**	**Core**	**Surface**	**Core**	**Surface**	**Core**
Belite	2.4	2	2.1	2.6	1.4	1.4	2.2	1.6
Calcite	8.3	0.5	7.3	1.9	9.7	0.4	7.9	2.8
Portlandite	0.4	1.9	0.5	1.4	0.3	2.8	0.2	1.4
Gypsum	0.4	0.1	0.1	0.4	0	0	0.4	0
Ettringite	5.9	4.9	7.9	1.4	11.6	3.6	9.2	4.1
Monosulfate	0.5	1.1	0.2	0	0.5	0.3	0.3	0
Hemicarboaluminate	0	1.5	1.4	4.8	0	3.2	1.1	3.6
Monocarboaluminate	0	0	0.1	0.6	0	0	0	1.5
Stratlingite	1.1	6.3	0	0	0	4.2	0	0
Illite	0	0.1	0.1	0.1	0	0	0	0
AC/Unidentified	80.9	81.6	80.3	86.8	76.5	84	78.6	84.9

4.3.2 Chloride Durability

4.3.2.1 Chloride Diffusivity

The total chloride concentration profiles of control and blended mixtures after 35, 180, and 360 days of exposure are illustrated in Figure 4-14 through Figure 4-25. As expected, higher exposure times resulted in higher chloride ion penetration as can be seen from the increased chloride contents at each depth. This effect was more significant between the exposure ages of 35 days and 180 days than between the ages of 180 days and 360 days. This implies that after a certain period of exposure to chloride ions, specimens approached a certain equilibrium chloride concentration with the solution, which may be influenced by pore structure characteristics as well as chloride binding. Moreover, the first 1-3 mm of the surface can be affected by convective flow and consequently be non-homogenous within and between specimens for different mixtures [52], [53]. Therefore, if the results of the first layers are excluded, the difference between the chloride contents between the mixtures can be observed clearly.

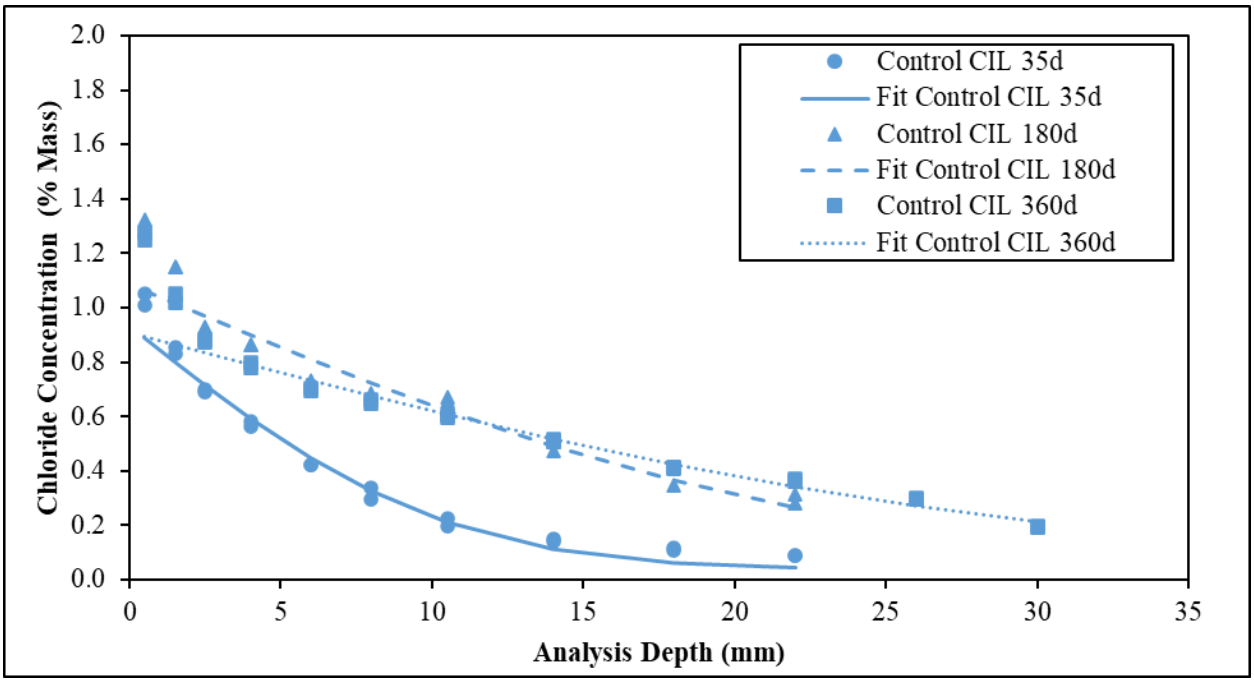

Figure 4-14: Total chloride concentration profiles for control CIL mixture

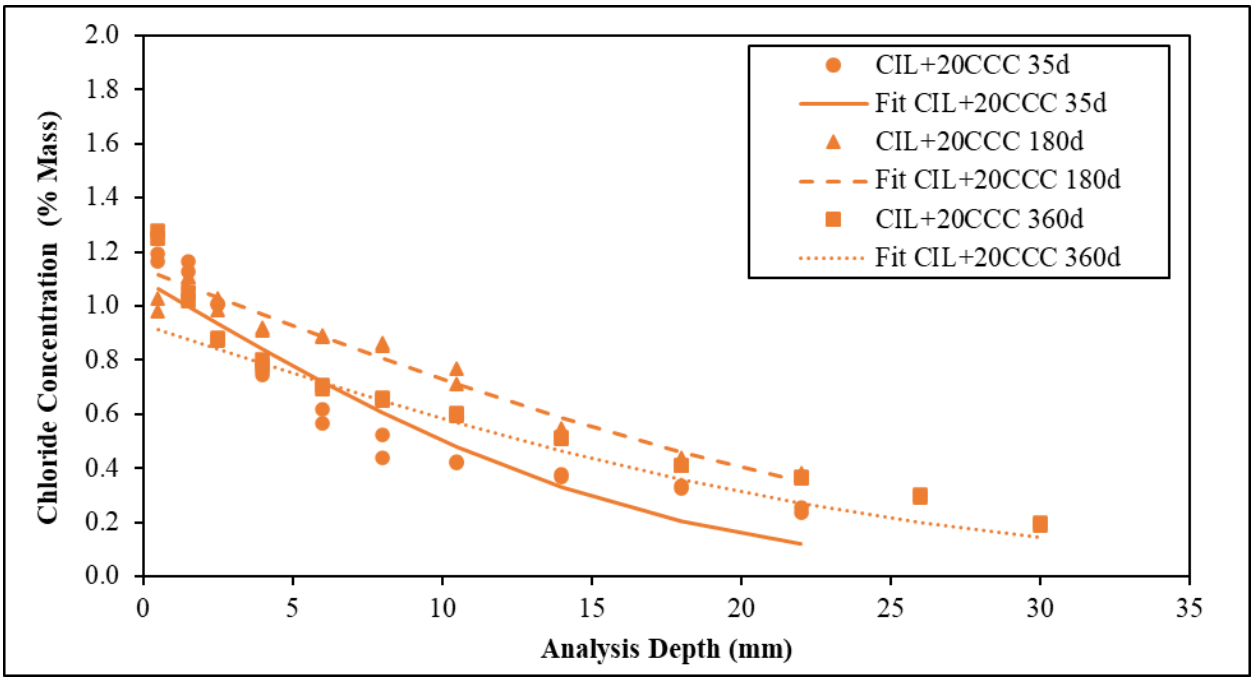

Figure 4-15: Total chloride concentration profiles for CIL+20CCC mixture

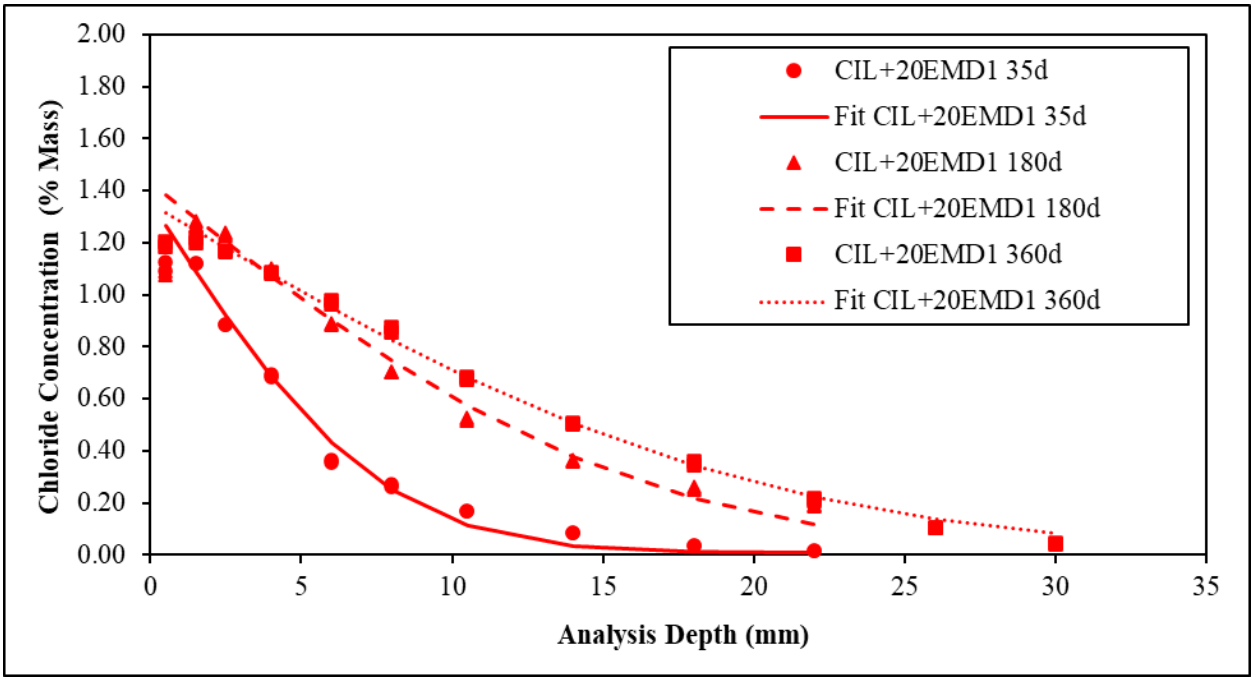

Figure 4-16: Total chloride concentration profiles for CIL+20EMD1 mixture

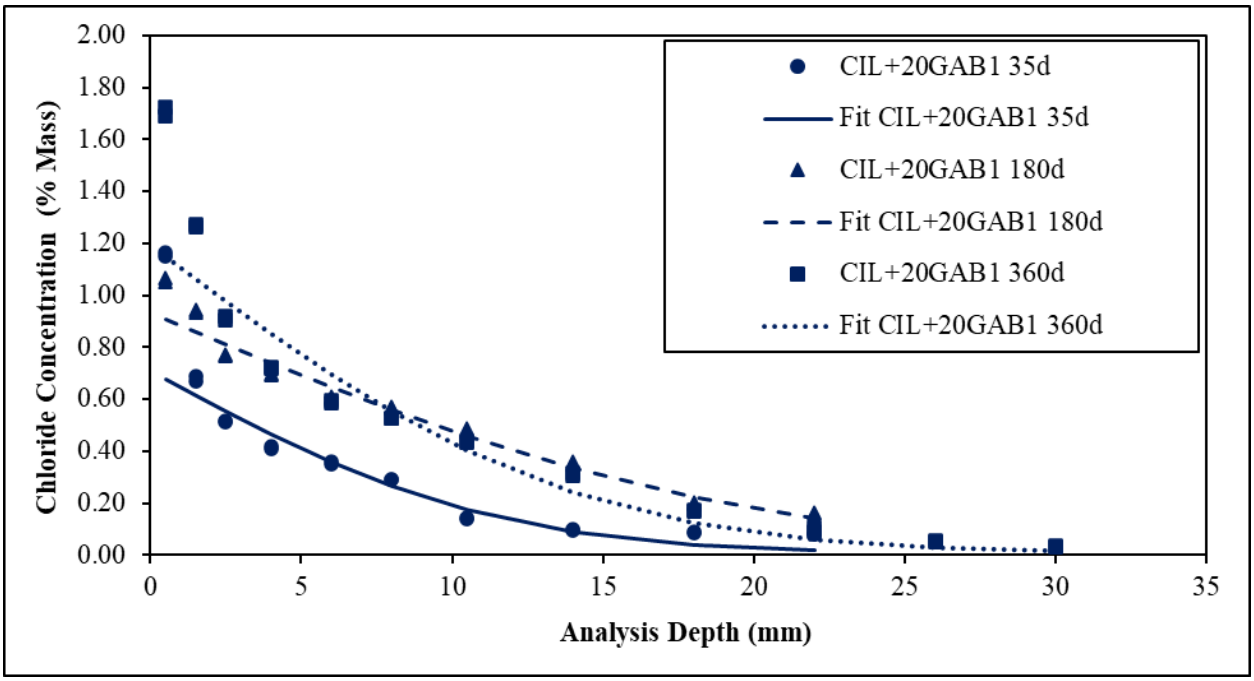

Figure 4-17: Total chloride concentration profiles for CIL+20GAB1 mixture

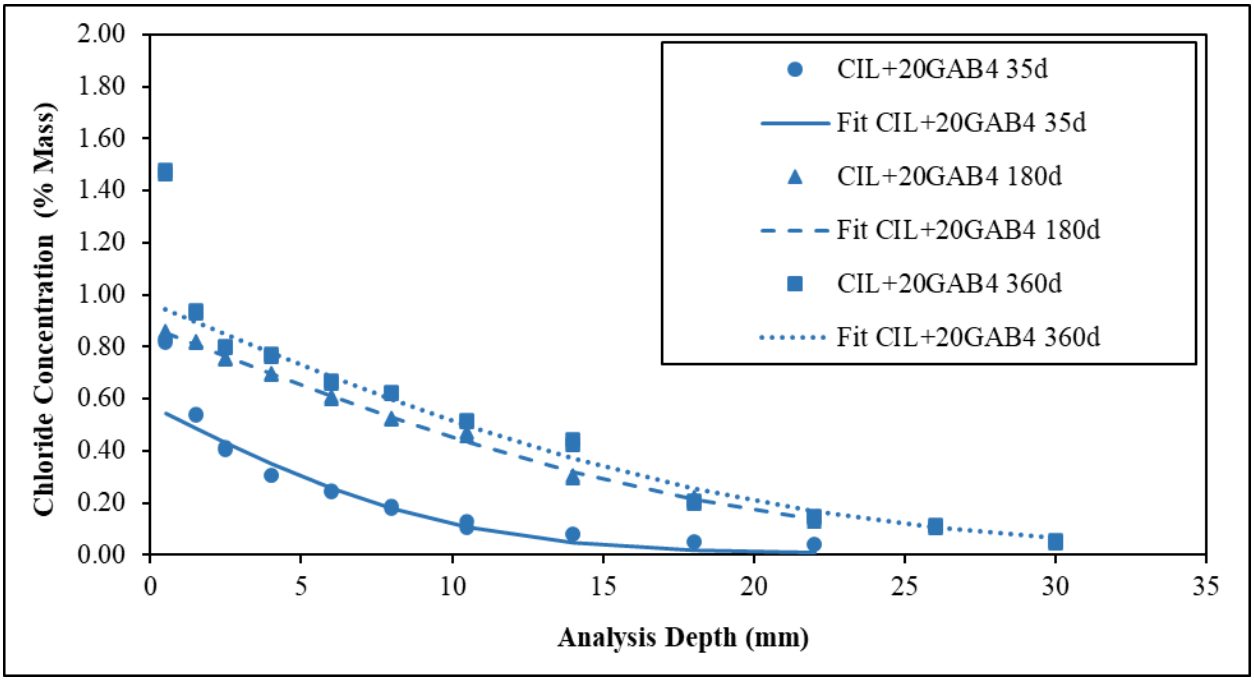

Figure 4-18: Total chloride concentration profiles for CIL+20GAB4 mixture

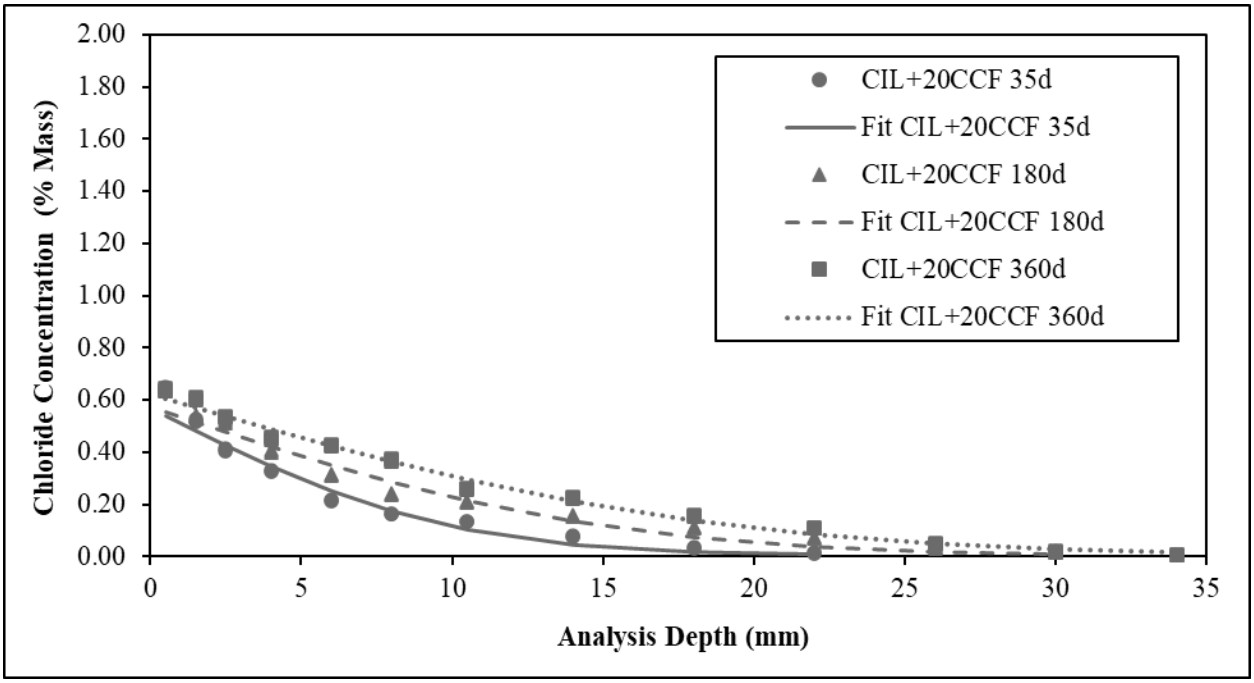

Figure 4-19: Total chloride concentration profiles for CIL+20CCF mixture

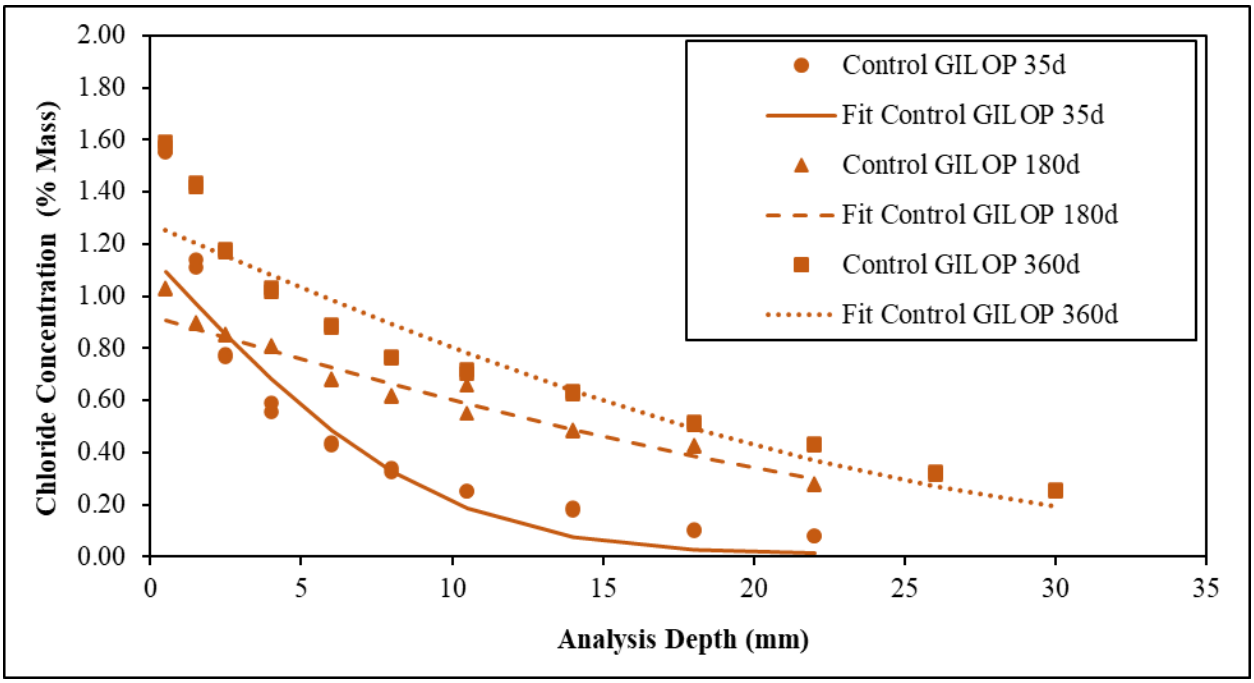

Figure 4-20: Total chloride concentration profiles for control GILOP mixture

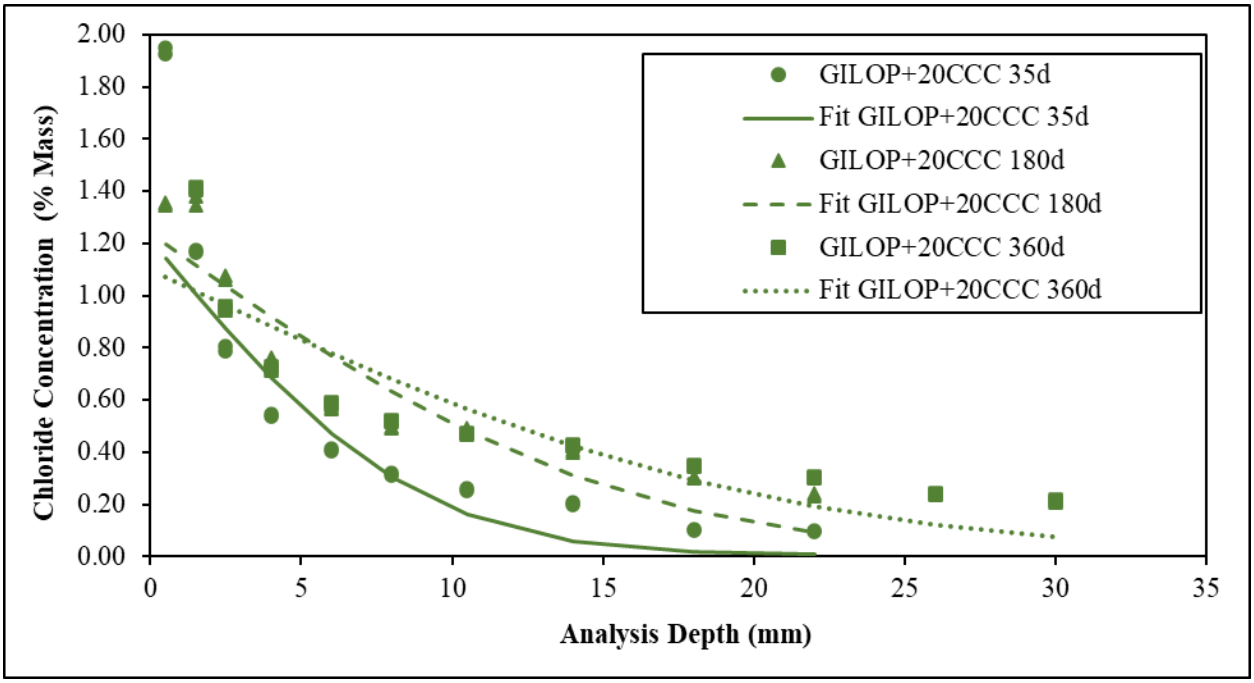

Figure 4-21: Total chloride concentration profiles for GILOP+20CCC mixture

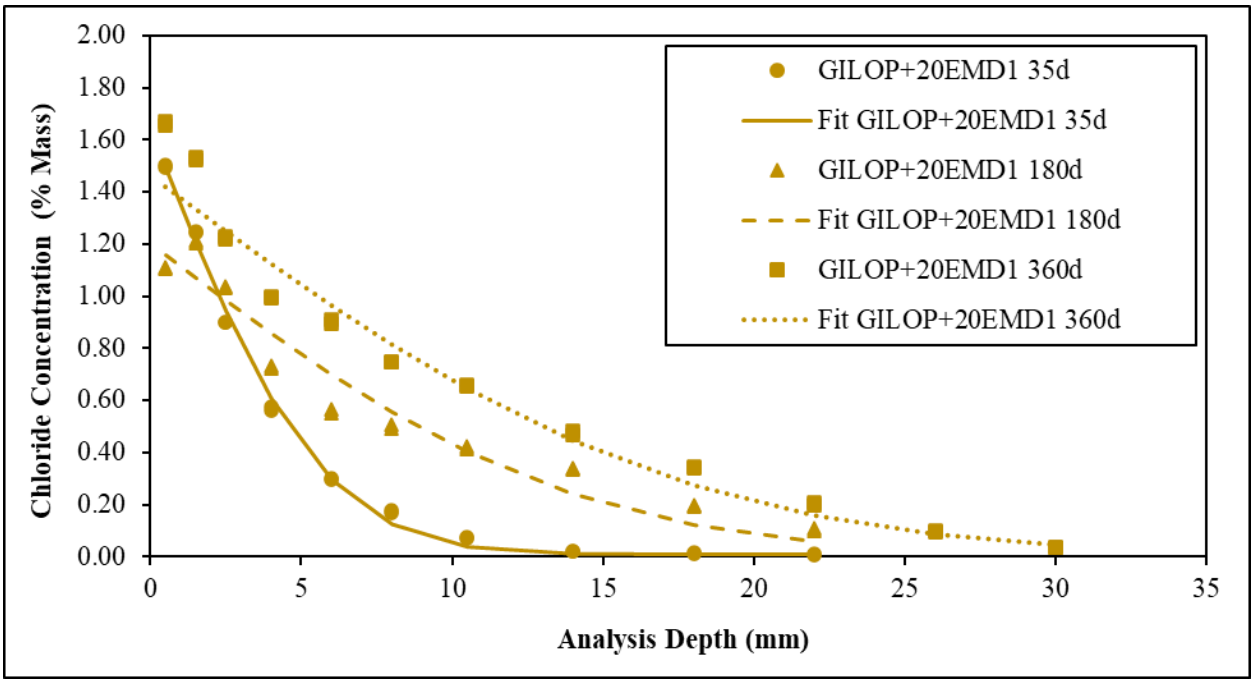

Figure 4-22: Total chloride concentration profiles for GILOP+20EMD1 mixture

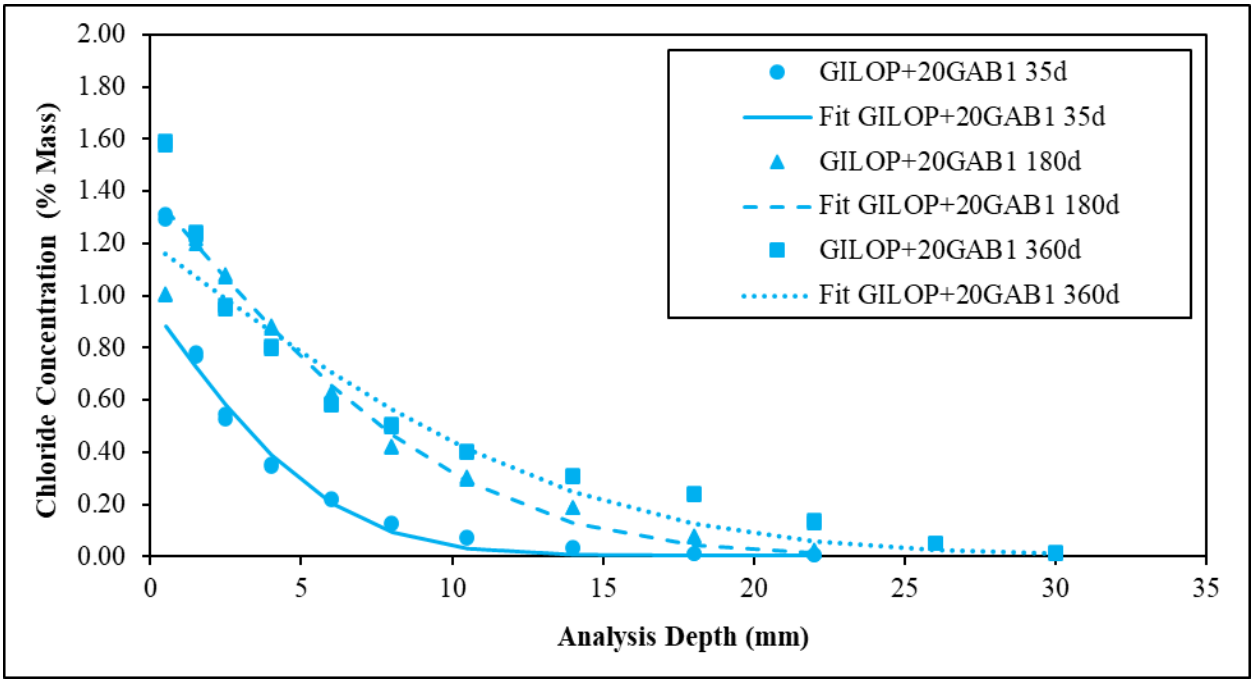

Figure 4-23: Total chloride concentration profiles for GILOP+20GAB1 mixture

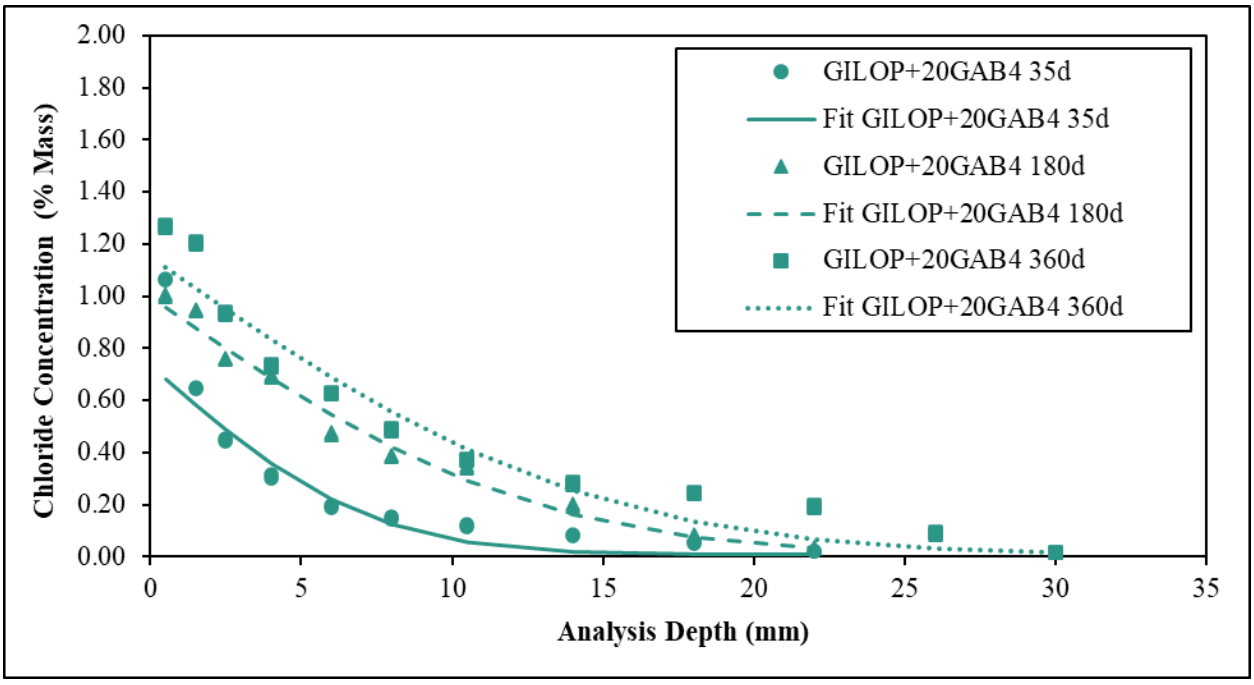

Figure 4-24: Total chloride concentration profiles for GILOP+20GAB4 mixture

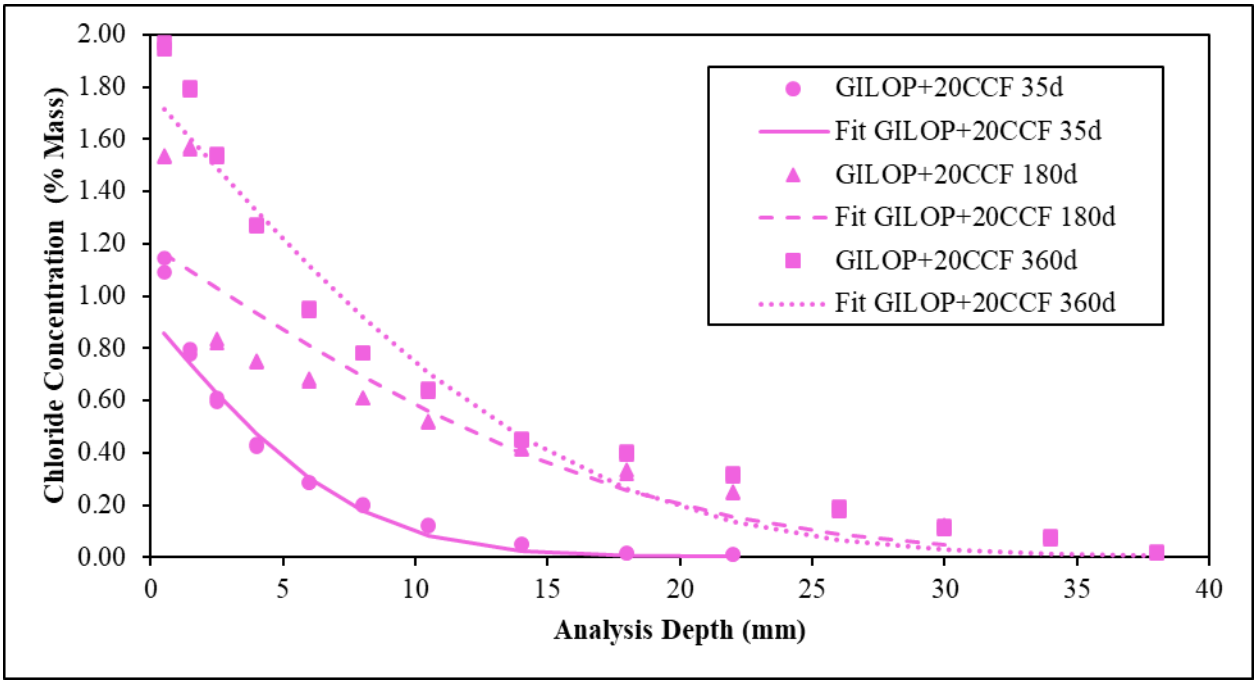

Figure 4-25: Total chloride concentration profiles for GILOP+20CCF mixture

The apparent diffusion coefficients of cement CIL and GILOP mixtures calculated according to Equation 4-1 for exposure ages of 35, 180, and 360 days are shown in Table 4-13 and Table 4-14, respectively. In general, the apparent diffusion coefficients of cement GILOP mixtures were lower compared to those of cement CIL mixtures, indicating slightly higher chloride resistance. It is possible that the higher limestone content in cement CIL increased the porosity of the system [54] and lowered the resistance to chloride ion ingress. In terms of the exposure age, the diffusivity is expected to decrease with increasing chloride exposure duration, due to the lowered porosity and pore connectivity with continued hydration, which can be observed in the majority of the mixtures.

Incorporation of calcined clay clearly had a notable effect on the D_{app} value, which varied based on the chemical and physical characteristics of the clay. Except for CIL+20CCC at 35- and 180-day exposure ages and CIL+20GAB1 at 35-day exposure age, D_{app} value was considerably lower in the blended mixtures compared to their respective controls even though the w/cm ratio of clay mixtures was slightly higher due to the differences in chemical admixture dosage. The discrepancies in calcined clay CCC mixtures can be attributed to the coarser particle size of the clay, which may have resulted in lower reactivity and thereby a coarser porosity. Calcined clay

CCC performed better than the control eventually because of the calcined clay's slow hydration and eventual pore size refinement. The reduction in the D_{app} value of the clays with high kaolin content and fineness (GAB1 and GAB4) compared to that of control mixtures was more significant at later exposure ages, indicating very high chloride resistance. Clay EMD1 and CCF mixtures also showed notably lower D_{app} values compared to the control. This shows that calcined clays do not need high kaolinite content to improve concrete performance. As stated by Maraghechi et al. [24], excellent resistance to chloride ion transport can be achieved with kaolinite contents 40% or higher when 30% to 50% of the clinker is replaced with only calcined clay or by a combination of calcined clay and limestone, at a water-to-binder ratio of 0.5. This behavior was attributed to the refined pore structure when calcined clay was used rather than to the chloride binding effect. They also observed a maximum of chloride binding when the calcined kaolinite content ranged between 40% and 80%. This was explained as a result of reaching maximum pore size refinement with increasing kaolinite contents, which limits the formation of carboaluminate phases and consequently limits the formation of Friedel's salt when exposed to chlorides. In the current study, the kaolinite content of the clays EMD1, GAB1 and GAB4 were 37.9%, 93.1% and 65.5%, respectively. The amount of kaolin calculated based on stoichiometry in clays CCC and CCF was about 50%.

Table 4-13: Surface chloride concentration and apparent diffusivity of cement CIL mixtures

Mix ID	35 days of exposure			180 days of exposure			360 days of exposure		
	C_s (% Mass)	**D_{app} (m^2/sec)**	**D_{app} ratio (relative to control)**	**C_s (% Mass)**	**D_{app} (m^2/sec)**	**D_{app} ratio (relative to control)**	**C_s (% Mass)**	**D_{app} (m^2/sec)**	**D_{app} ratio (relative to control)**
Control CIL	0.93	1.1E-11	1.00	1.09	1.0E-11	1.00	0.91	8.8E-12	1.00
CIL+20CCC	1.10	2.9E-11	2.71	1.13	1.5E-11	1.42	0.93	6.5E-12	0.74
CIL+20EMD1	1.35	5.9E-12	0.55	1.43	5.0E-12	0.49	1.35	3.9E-12	0.45
CIL+20GAB1	0.71	1.3E-11	1.21	0.93	7.4E-12	0.72	1.19	1.9E-12	0.21
CIL+20GAB4	0.57	1.0E-11	0.93	0.88	7.5E-12	0.73	0.97	4.1E-12	0.46
CIL+20CCF	0.57	9.8E-12	0.91	0.58	4.4E-12	0.43	0.62	3.4E-12	0.39

Table 4-14: Surface chloride concentration and apparent diffusivity of cement GILOP mixtures

Mix ID	35 days of exposure			180 days of exposure			360 days of exposure		
	C_s (% Mass)	**D_{app} (m^2/sec)**	**D_{app} ratio (relative to control)**	**C_s (% Mass)**	**D_{app} (m^2/sec)**	**D_{app} ratio (relative to control)**	**C_s (% Mass)**	**D_{app} (m^2/sec)**	**D_{app} ratio (relative to control)**
Control GILOP	1.16	8.9E-12	1.00	0.93	1.5E-11	1.00	1.28	6.7E-12	1.00
GILOP+20CCC	1.21	7.9E-12	0.88	1.24	4.7E-12	0.31	1.10	4.1E-12	0.61
GILOP+20EMD1	1.64	3.3E-12	0.36	1.20	3.7E-12	0.25	1.47	3.0E-12	0.44
GILOP+20GAB1	0.96	3.8E-12	0.42	1.40	2.2E-12	0.14	1.20	2.0E-12	0.29
GILOP+20GAB4	0.73	5.4E-12	0.60	1.00	3.1E-12	0.21	1.15	2.1E-12	0.31
GILOP+20CCF	0.92	6.2E-12	0.70	1.19	6.7E-12	0.44	1.77	2.5E-12	0.37

4.3.2.2 XRD Analysis of Concrete Samples after Chloride Exposure

Phase quantification results of control concrete mixtures and calcined-clay-blended mixtures exposed to NaCl solution for a period of 35 days are listed in Table 4-15 through Table 4-17. The results of three selected layers of a specimen are shown in these tables. It is noteworthy that quartz and calcite contents detected from XRD due to the presence of aggregates were disregarded in the analysis to emphasize more the phases formed in the paste fraction. High amounts of Friedel's salt were observed close to the surface and these amounts gradually decreased, with increasing depths from the surface. In general, Friedel's salt content was slightly higher in cement GILOP mixtures, which can be attributed to the slightly higher C_3A content in cement GILOP compared to cement CIL and lower clinker fraction in cement CIL due to its higher limestone content than that of cement GILOP. As expected, Friedel's salt content of mixtures containing calcined clay was higher than in the control mixtures, indicating greater binding capability. This may be due to higher alumina-bearing phases formed in the clay-blended mixtures that later transformed to Friedel's salt on exposure to the chloride environment. It is reported that carboaluminate phases forming in calcined-clay-blended mixtures would transform into Friedel's salt when exposed to chlorides [24], [26]. Moreover, considerable amounts of portlandite and ettringite were detected in all the mixtures while small amounts of carboaluminate phases remained in the blended mixtures. In addition to Friedel's salt, small quantities of Kuzel's salt were also seen in GILOP+20GAB1 and GILOP+20GAB4 mixtures, likely due to the higher alumina available in these systems. In the cement CIL mixtures, higher chemical binding can be observed in the mixtures with clays GAB1 and GAB4. However, in cement GILOP mixtures, chemical binding was higher when blended with clay EMD1 than that of clays GAB1 and GAB4. As stated earlier, this may be due to a limited carboaluminate formation in higher kaolin clay systems which limits Friedel's salt formation on subsequent exposure to chlorides.

Table 4-15: Phase quantification of control concrete mixtures after 35 day-exposure to 165 g/L NaCl solution

Sample	**Control CIL**			**Control GILOP**		
Depth from surface (mm)	**2**	**7**	**20**	**2**	**7**	**20**
Belite	0.7	0.6	0.6	1	0.8	0.6
Ferrite	0.5	0.5	0.4	0.8	0.6	0.5
Portlandite	8.8	13.2	14.4	12.5	14	14.9
Ettringite	2.5	4.6	4	6.5	5.5	4.9
Hemicarboaluminate	0.2	0	0	0	0.3	0.5
Friedel's Salt	1.1	0.9	0.6	2.8	2.4	1.8
AC/Unidentified	86.1	80.2	80	76.4	76.4	76.8

Table 4-16: Phase quantification of cement CIL-clay blended concrete mixtures after 35 day-exposure to 165 g/L NaCl solution

Sample	**CIL+20CCC**			**CIL+20EMD1**			**CIL+20GAB4**			**CIL+20GAB1**		
Depth from surface (mm)	**2**	**7**	**20**	**2**	**7**	**20**	**2**	**7**	**20**	**2**	**7**	**20**
Alite	0	0	0	0	0	0	0.6	0.3	0.4	0.5	0.7	0.8
Belite	0.4	0.3	0.3	1.1	1.2	1.2	3	2.7	2.3	2.4	2	2.6
Ferrite	0.2	0	0	0	0	0	0	0	0	0	0	0
Portlandite	3.9	6.2	9.3	2.1	4.7	6.7	0.3	0.3	0.4	0.2	0.2	0.6
Ettringite	3.9	3.4	3.7	2.9	4.8	3.3	3.1	3	2.5	2.2	2	2.3
Hemicarboaluminate	0.2	0.2	0.8	0.8	1.2	1.3	1.7	2.2	3.5	1.5	1.9	3.5
Monocarboaluminate	0.2	0.3	0.5	0.2	0.6	2	0	0.3	0.6	0	0	0.5
Illite	0.4	0.3	0.5	0.5	0.7	0.4	0	0	0	0	0	0
Friedel’s Salt	3.2	2.8	2.1	4.8	4	1.6	7.9	5	1.7	4.6	4.1	2.8
AC/ Unidentified	87.7	86.4	82.5	87.5	83.1	83.4	83.4	86.1	88.8	88.5	89.2	87

Table 4-17: Phase quantification of cement GILOP-clay blended concrete mixtures after 35 day-exposure to 165 g/L NaCl solution

Sample	**GILOP+20CCC**			**GILOP+20EMD1**			**GILOP+20GAB4**			**GILOP+20GAB1**		
Depth from surface (mm)	**2**	**7**	**20**	**2**	**7**	**20**	**2**	**7**	**20**	**2**	**7**	**20**
Alite	0	0	0	1	0.8	0.5	0	0.3	0.3	0	0	0
Belite	0.8	0.6	0.4	1.7	1.5	2	2.8	2.1	3	2.8	3.1	2.9
Portlandite	5	6.7	5.8	3.6	5.5	7.5	0	1	1.1	0.3	1.2	1.6
Ettringite	6.1	4.1	1.9	3.2	2.5	2.3	2.5	3.6	2.6	2.3	2.9	2.6
Hemicarboaluminate	0.8	0.3	0.2	4	4.1	4.2	5	4.6	8	3.6	5.2	8.2
Monocarboaluminate	0	0	0.4	0.3	1	3.8	0	0.7	1.1	0	0.4	1
Illite	0.4	0.4	0.2	0	0	0	0	0	0	0	0	0
Friedel’s Salt	5.4	4	1.8	7.8	5.5	1.8	5.7	4	0.8	5.7	3.9	0.3
Kuzel’s Salt	0	0	0	0	0	0	0.7	0.7	0.3	0.4	0.4	0.3
AC/ Unidentified	81.4	83.9	89.3	77.6	78.2	76.8	83.4	83.2	82.9	84.7	82.8	83.4

4.3.2.3 Chloride Binding

Binding coefficients of Freundlich isotherms and corresponding coefficients of determination (R^2) obtained for CIL mixtures are presented in Table 4-18. The chloride binding isotherms of the CIL mixtures are illustrated in Figure 4-26.

Table 4-18: Binding coefficients of Freundlich isotherms and corresponding coefficients of determination (R2)

Mix ID	α	β	R^2
Control CIL	10.180	0.332	0.995
CIL+ 20CCC	12.128	0.531	0.986
CIL+ 20EMD1	12.363	0.258	0.922
CIL+ 20GAB4	8.957	0.148	0.935

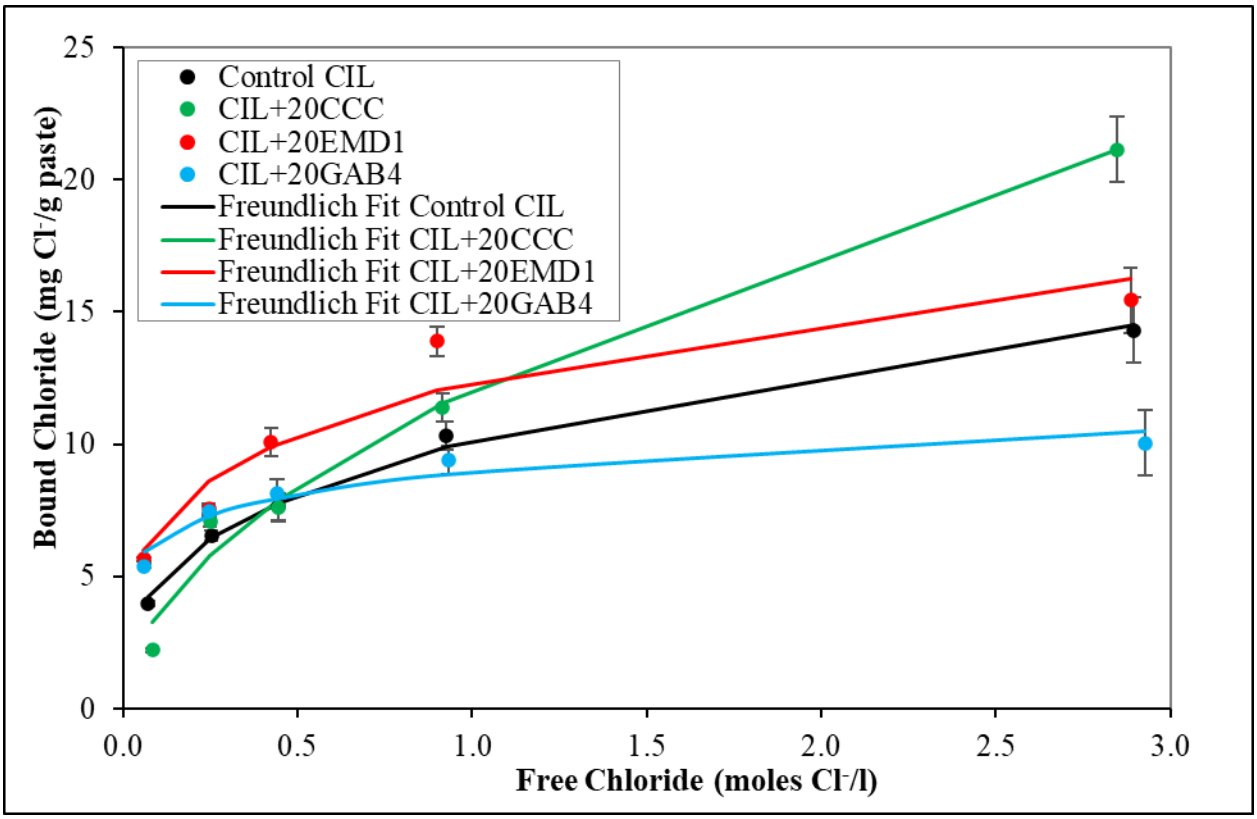

Figure 4-26: Chloride binding isotherms of CIL mixtures

The binding capacity of CIL+20CCC and CIL+20EMD1 mixtures were higher than the control CIL mix while it was lower in the CIL+20GAB4 mix. Maraghechi et al. [24] observed a

maximum chloride binding when the calcined kaolinite content ranged between 40% and 80% at a water-to-binder ratio of 0.5. This was explained as a result of the limited formation of hydration products due to reaching a maximum pore refinement in high kaolin systems, which may have lowered the formation of Friedel's salt and physical adsorption of chlorides. It is likely the high gibbsite content in clay GAB4 contributed to a lower binding capacity.

4.3.2.4 XRD Analysis of Paste Samples before and after Chloride Exposure

Table 4-19 lists the phase assemblages determined from QXRD analysis of cement CIL paste mixtures before and after chloride exposure. In general, portlandite, ettringite, and hemi/mono carboaluminates were the main phases detected prior to chloride exposure in all systems. Due to the presence of calcite in cement, carboaluminate phases were observed in all the systems. After chloride exposure, Friedel's salt was observed in all the mixtures, which increased with increasing NaCl concentration. The trends observed in Friedel's salt content agreed well with control CIL, CIL+20CCC and CIL+20EMD1 mixtures, except for CIL+20GAB4. It is likely the physical binding was substantially reduced in CIL+20GAB4, possibly due to the change in C/A and C/S ratios in C-A-S-H with increasing kaolin contents. Maraghechi et al. [24] stated that a larger chloride content is bound by the C-A-S-H in plain cement system, whereas most of the bound chloride was chemically bound in clay-blended mixtures. However, they did not observe a significant influence of the calcined kaolin content on the chloride adsorption of C-A-S-H.

Table 4-19: Phase quantification of cement CIL paste mixtures before and after two months of chloride exposure by XRD

Mix ID	**Control CIL**				**CIL+20CCC**				**CIL+20EMD1**				**CIL+20GAB4**			
Cl conc. (M) / Phase	**0**	**0.1**	**0.5**	**3**	**0**	**0.1**	**0.5**	**3**	**0**	**0.1**	**0.5**	**3**	**0**	**0.1**	**0.5**	**3**
Alite	0.5	0.3	0.3	0.4	0.2	0	0	0	0.3	0	0.1	0.1	1	0.7	0.7	0.6
Belite	2.5	1.7	1.6	1.4	1.5	0.5	0.4	0.4	3.6	2	1.7	1.9	5	4	4	4
Aluminate	0	0	0	0	0	0	0	0	0	0	0	0	0	0	0	0
Ferrite	1.8	1.1	0.9	0.9	0.5	0.1	0.2	0.2	0.2	0	0	0	0.4	0.2	0.1	0.1
Calcite	3.7	4	4.4	4.6	2.6	3.2	3.4	2.8	2.4	2.3	2.4	2.6	1.9	2.5	2.5	2.6
Quartz	0.9	0.9	1	1	2.5	2.3	2.4	2.3	3.5	3.5	3.7	3.4	0.5	0.6	0.6	0.7
Portlandite	10.8	9.6	10.3	10.4	7.6	6.4	6.8	6	5.7	4.3	3.7	3.1	2.4	0.9	0.5	0.3
Ettringite	2.7	4.7	5.1	4.4	2.1	4.9	4.3	3.5	1.1	3.6	3.3	2.9	2.7	3.6	3.2	3.1
Hemicarboaluminate	0.1	0.1	0.2	0.1	0.2	0.2	0.4	0.4	0.9	1.4	1.1	0.4	2.8	2.5	2.3	1.2
0.8 Carboaluminate	0.2	0.1	0	0	0.2	0.1	0	0	0.1	0.1	0	0	0.1	0.1	0	0
Monocarboaluminate	0.6	0	0	0	1.3	0.4	0.2	0	1.2	0.8	0.3	0	1.1	0.5	0.2	0
Illite	0	0	0	0	0.3	0.3	0.3	0.3	0.5	0.5	0.4	0.4	0	0	0	0
Friedel’s Salt	0	0.5	1.7	2.5	0	1.7	3.2	5.3	0	2.7	6.2	8.3	0	3.4	5.5	8.3
AC/Unidentified	76.1	77.1	74.4	74.4	80.9	80	78.5	78.7	80.6	78.7	77	76.8	82.2	80.9	80.3	79

4.3.3 Carbonation Resistance

4.3.3.1 Carbonation Depth and Carbonation Coefficient

The phenolphthalein indicator test results of control CIL, CIL+20CCC, and CIL+20GAB1 concretes that were lime-cured for 3 days before exposing to natural carbonation are presented in Figure 4-27, Figure 4-28, and Figure 4-29 respectively. The carbonation depths of cement CIL and GILOP mixtures taken immediately after spraying phenolphthalein solution and after 24 h are shown in Figure 4-30 and Figure 4-31. These include specimens with varying lime curing ages of 3, 7, and 21 days before exposure to natural carbonation tests for about 420 days. The depth of carbonation was measured immediately after stain application as well as at 24 hours from stain application to better enhance the margin between carbonated and non-carbonated concrete [55].

(a) (b)

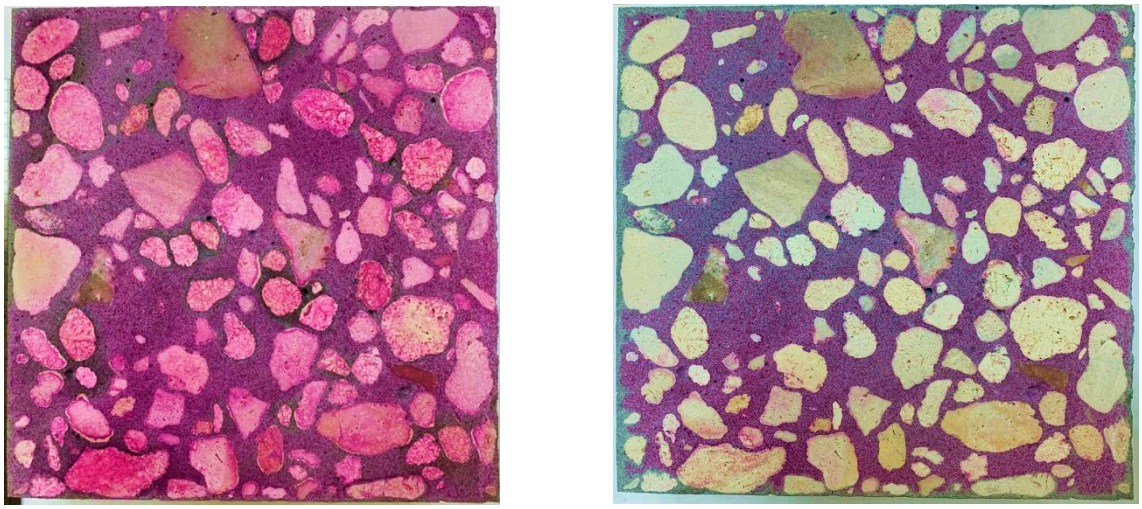

Figure 4-27: Phenolphthalein indicator test results of control CIL (3-day lime curing) (a) immediately after spraying (b) after 24 h

(a) (b)

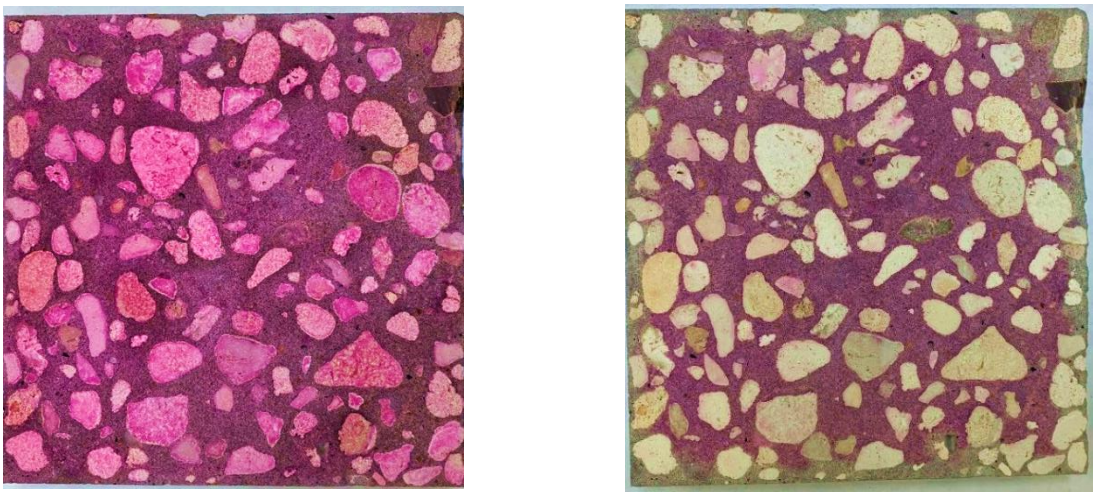

Figure 4-28: Phenolphthalein indicator test results of CIL+20CCC (3-day lime curing) (a) immediately after spraying (b) after 24 h

(a) (b)

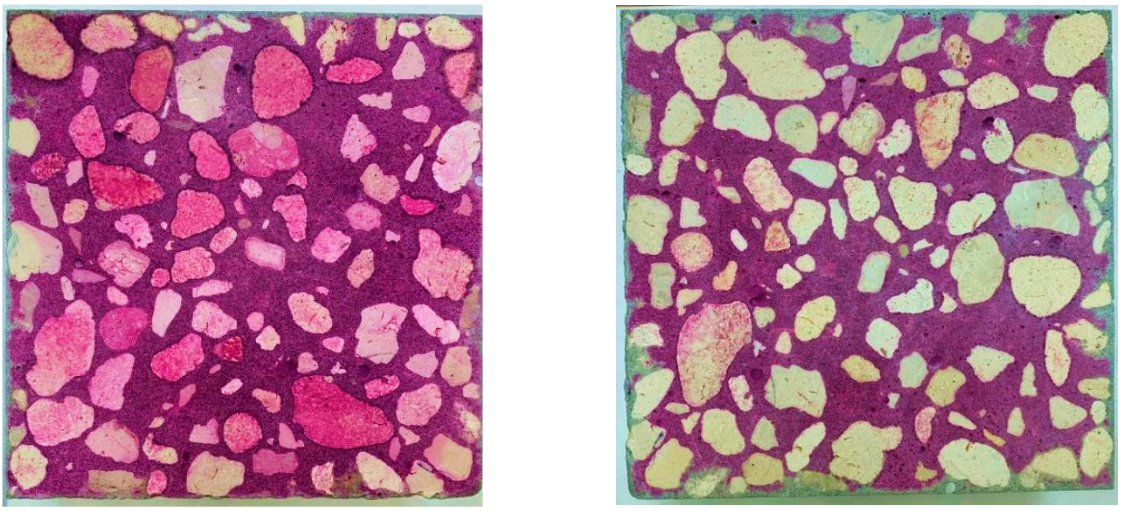

Figure 4-29: Phenolphthalein indicator test results of control CIL+20GAB1 (3-day lime curing) (a) immediately after spraying (b) after 24 h

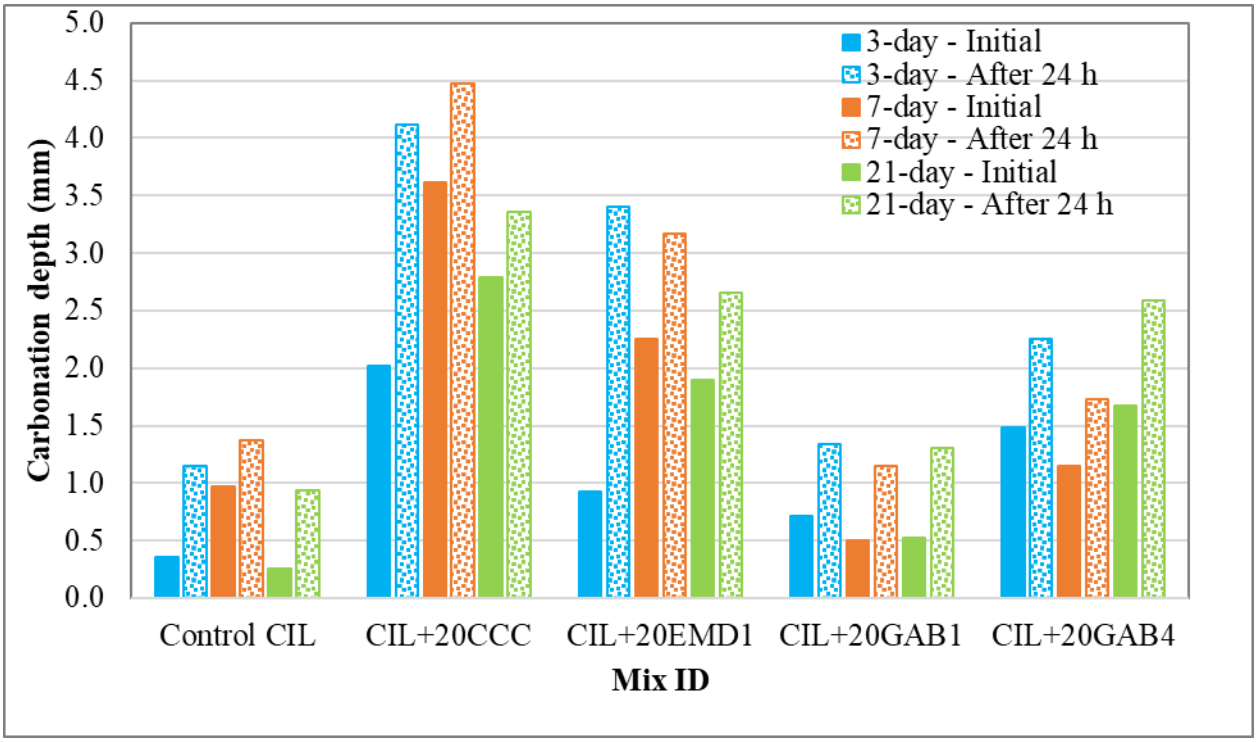

Figure 4-30: Carbonation depths of cement CIL mixtures

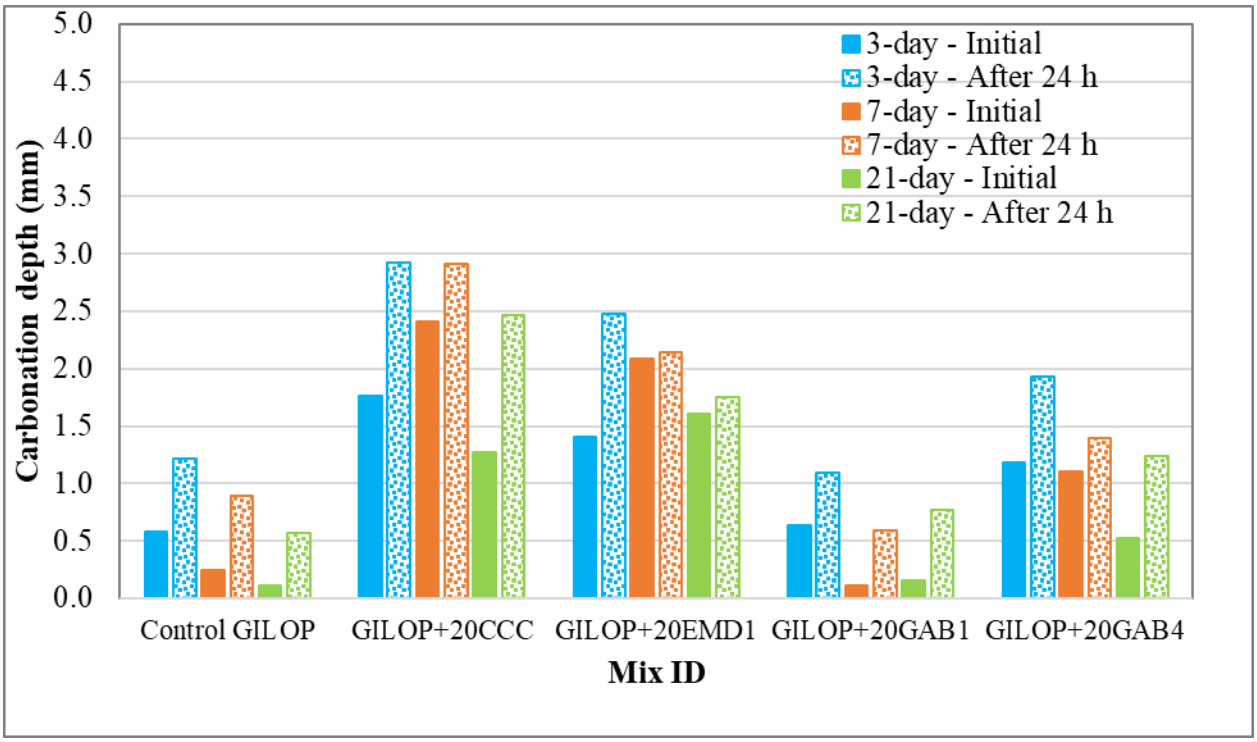

Figure 4-31: Carbonation depths of cement GILOP mixtures

In general, carbonation depth decreased with increasing curing age, in agreement with the published literature [11]. Although the depths measured after 24 h were higher than the depth immediately after spraying the phenolphthalein indicator, similar trends can be observed among the mixtures. Expectedly, the carbonation resistance was lower in the clay-blended mixtures [27], [56]. However, it is noteworthy that the w/cm ratio of clay-blended mixtures was slightly higher (0.405) than that of the control mixtures (0.387) due to the addition of low-range water reducer and a higher amount of high-range water reducer to maintain the workability. Nevertheless, carbonation was the highest in the clay CCC mixtures, which can be attributed to the moderate kaolin content and coarser particle size, which may have resulted in a coarser porosity. Higher porosity diffuses CO_2 further into the concrete, increasing the carbonation depth. It is then followed by clay EMD1 mixtures, which also had a moderate kaolin content. The clay GAB1 mixtures had the highest kaolin content and considerably higher fineness and showed the highest carbonation resistance among the clay mixtures, likely due to a highly refined pore structure. This was in fact similar to that of control mixtures. The trends among the calcined clays were similar when blended with both cements, although the carbonation resistance appeared to be slightly higher in cement GILOP blends. This can be attributed to the reduced clinker fraction and lower C_3S content in cement CIL (38.8% in cement CIL vs. 44.5% in cement GILOP), which may have resulted in lower amount of CH available for carbonation.

The carbonation coefficients of the same mixtures calculated according to Equation 4-5 are shown in Figure 4-32 and Figure 4-33. The trends among the mixtures were similar to those of carbonation depths. The time to carbonation is 153 years, calculated using Equation 4-5 with a clear cover depth of 2 in. and a higher carbonation coefficient of 4.11. Based on the measured carbonation coefficients, carbonation is not expected to be a concern for Florida structures with typical clear covers used and made with 20% calcined clay and at least 3 days of curing.

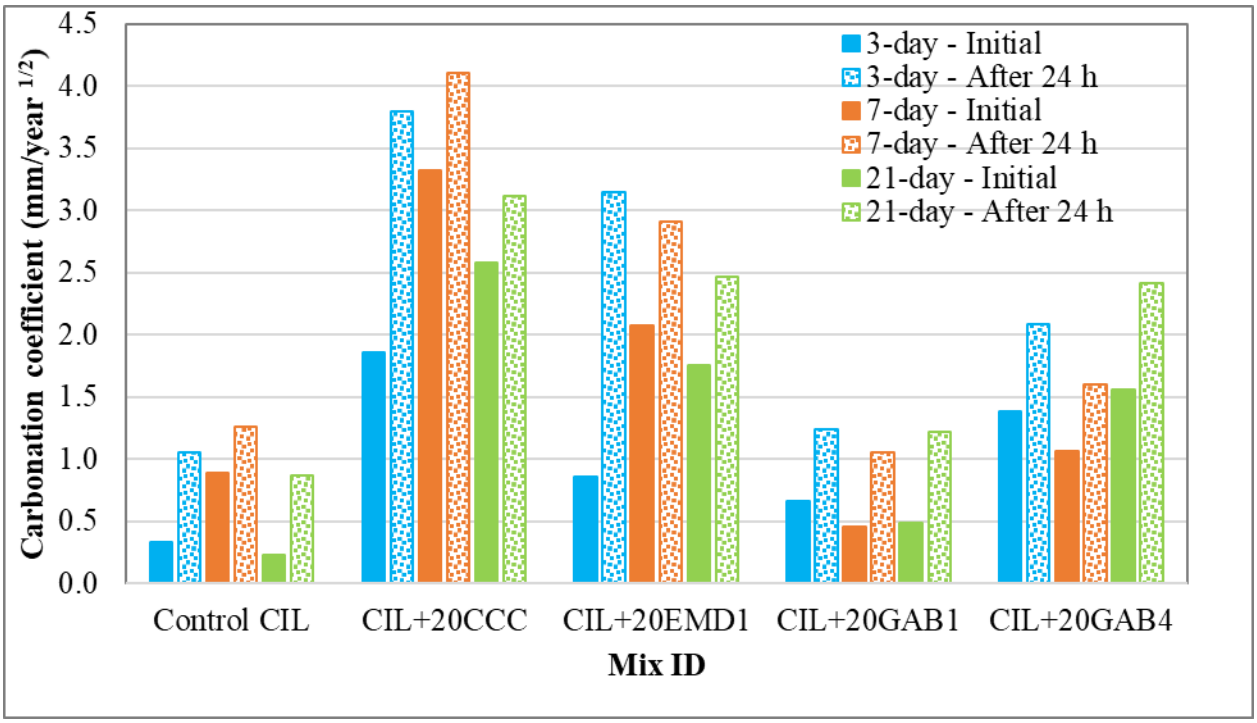

Figure 4-32: Carbonation coefficients of cement CIL mixtures

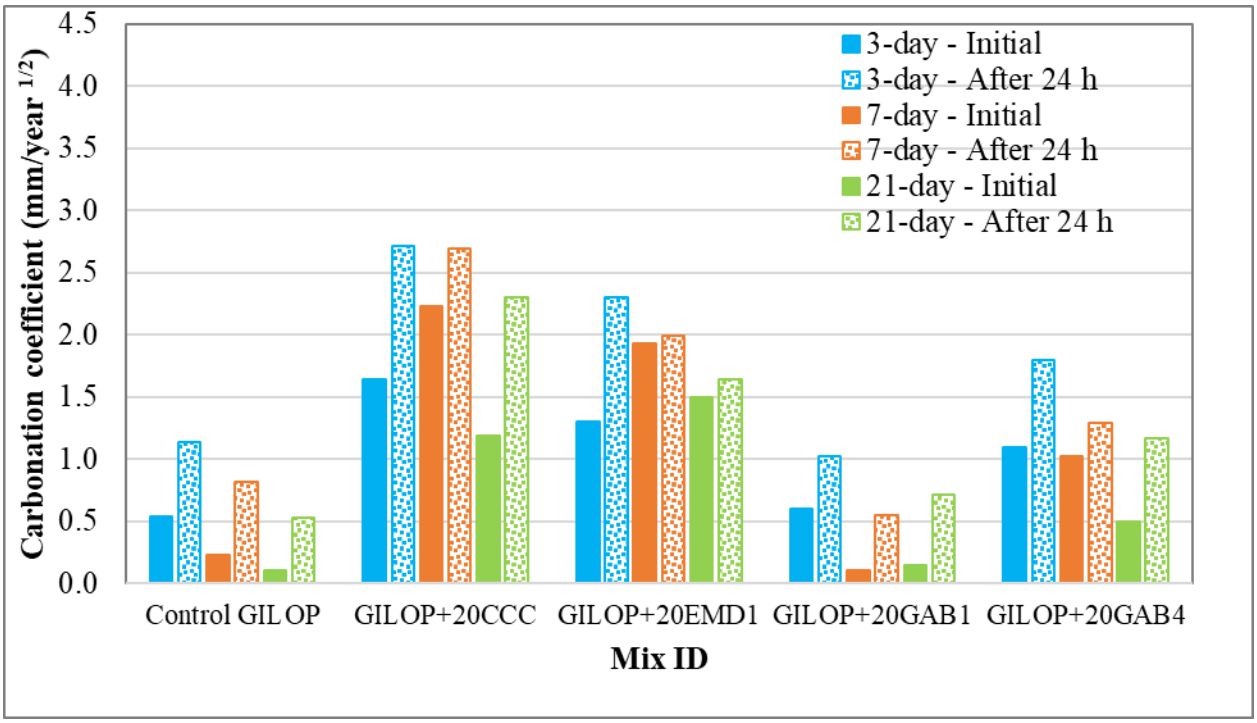

Figure 4-33: Carbonation coefficients of cement GILOP mixtures

4.3.3.2 XRD Analysis of Concrete Samples after Natural Carbonation

The portlandite contents at the core and the surface of 3-day lime-cured concrete mixtures exposed to natural carbonation as detected by XRD are listed in Table 4-20. As expected, the portlandite content in clay mixtures was low due to the pozzolanic reaction. It is the lowest in clay GAB1 and GAB4 mixtures because of their high reactivity due to high kaolin contents. Among the blended mixtures, the highest portlandite content was observed in clay CCC mixtures as a result of its lower reactivity due to moderate kaolin content and coarser grind. As expected, the portlandite content at the surface was either undetectable or significantly low compared to that at the core, indicating the effect from carbonation [57].

Table 4-20: Portlandite content at the core and the surface of 3-day lime cured mixtures as detected by XRD

Mix ID	Core	Surface
Control CIL	2.3	0.1
CIL+20CCC	1.8	0.1
CIL+20EMD1	1.2	0
CIL+20GAB1	0.3	0
CIL+20GAB4	0.3	0
Control GILOP	2.7	0.7
GILOP+CCC	1.9	0.1
GILOP+EMD1	1.5	0.2
GILOP+20GAB1	0.3	0
GILOP+20GAB4	0.4	0.1

4.4 Conclusions

Varying cement and calcined clay characteristics had significant effects on the external sulfate durability, chloride ion ingress and carbonation of concrete. Based on the current investigation, several conclusions can be made.

Type I/II(MH) and Type IL cements studied here indicated moderate or high sulfate resistance because of the moderate C_3A levels in both cement types and reduced clinker fraction in Type IL cements. Incorporation of calcined clay had variable effects on expansion due to external sulfate attack depending on their kaolin content, sulfate content and fineness. Clays GAB1 and GAB4 have shown higher sulfate resistance for the cements studied as a result of reduced

permeability due to their high fineness and high pozzolanic reactivity. The resistance against sulfate attack was the lowest in clay EMD1 mixtures, likely due to a combined effect of low kaolin content, high sand content and no sulfate additions. Clay CCC provided lower sulfate resistance when blended with the cements used in this study because of its coarser particle size distribution. However, clay CCF from the same source as clay CCC, but with finer ground indicated better sulfate resistance. Moreover, sulfate addition to the clay was shown to improve the external sulfate resistance of the calcined-clay-blended system and requires further investigation.

In terms of resistance against chloride ion penetration, calcined clay substitution in general enhanced chloride resistance as indicated by lower apparent diffusion coefficients compared to the respective plain cement mixtures. An improvement in chloride resistance can be observed even in the clays with moderate kaolin contents due to the refined pore structure and chloride binding. With regard to the effect from carbonation, while incorporation of calcined clay slightly decreased carbonation resistance, it did not appear to be detrimental to concrete. Clay GAB1 mixtures with high kaolin content and high fineness produced similar carbonation resistance to those of respective control mixtures.

4.5 References

[1] A. M. Neville, *Properties of Concrete*, 4th ed. Harlow, England: Pearson Education Limited, 2006.

[2] A. Neville, "The confused world of sulfate attack on concrete," *Cem. Concr. Res.*, vol. 34, no. 8, pp. 1275–1296, 2004, doi: 10.1016/j.cemconres.2004.04.004.

[3] P. K. Mehta and P. J. M. Monteiro, *Concrete: Microstructure, Properties, and Materials*, 4th ed. McGraw-Hill Education, 2014.

[4] P. K. Mehta, "Mechanism of expansion associated with ettringite formation," *Cem. Concr. Res.*, vol. 3, pp. 1–6, 1973.

[5] N. Shanahan and A. Zayed, "Cement composition and sulfate attack," *Cem. Concr. Res.*, vol. 37, no. 4, pp. 618–623, Apr. 2007, doi: 10.1016/j.cemconres.2006.12.004.

[6] I. Odler and J. Colán-Subauste, "Investigations on cement expansion associated with ettringite formation," *Cem. Concr. Res.*, vol. 29, no. 5, pp. 731–735, 1999, doi: 10.1016/S0008-8846(99)00048-4.

[7] B. Tian and M. D. Cohen, "Does gypsum formation during sulfate attack on concrete lead to expansion?," *Cem. Concr. Res.*, vol. 30, no. 1, pp. 117–123, Jan. 2000, doi: 10.1016/S0008-8846(99)00211-2.

[8] O. R. Ogirigbo and L. Black, "Chloride binding and diffusion in slag blends: Influence of slag composition and temperature," *Constr. Build. Mater.*, vol. 149, pp. 816–825, Sep. 2017, doi: 10.1016/J.CONBUILDMAT.2017.05.184.

[9] H. Zibara, "Binding of external chlorides by cement pastes," University of Toronto, Toronto, Ontario, 2001.

[10] A. Delagrave, J. Marchand, J. Ollivier, S. Julien, and K. Hazrati, "Chloride binding capacity of various hydrated cement paste systems," *Adv. Cem. Based Mater.*, vol. 6, no. 2, pp. 28–35, 1997.

[11] S. O. Ekolu, "A review on effects of curing, sheltering, and CO2 concentration upon natural carbonation of concrete," *Constr. Build. Mater.*, vol. 127, pp. 306–320, 2016, doi: 10.1016/j.conbuildmat.2016.09.056.

[12] X. Shen, W. Jiang, D. Hou, Z. Hu, J. Yang, and Q. Liu, "Numerical study of carbonation and its effect on chloride binding in concrete," *Cem. Concr. Compos.*, vol. 104, no. September 2018, p. 103402, 2019, doi: 10.1016/j.cemconcomp.2019.103402.

[13] H. Chang, “Chloride binding capacity of pastes influenced by carbonation under three conditions,” *Cem. Concr. Compos.*, vol. 84, pp. 1–9, 2017, doi: 10.1016/j.cemconcomp.2017.08.011.

[14] T. H. Wee, A. K. Suryavanshi, S. F. Wong, and A. K. M. A. Rahman, “Sulfate Resistance of Concrete Containing Mineral Admixtures,” *Aci Mater. J.*, vol. 97, no. 5, pp. 536–549, 2000.

[15] B. Lothenbach, K. Scrivener, and R. D. Hooton, “Supplementary cementitious materials,” *Cem. Concr. Res.*, vol. 41, no. 12, pp. 1244–1256, 2011, doi: 10.1016/j.cemconres.2010.12.001.

[16] Z. Shi, S. Ferreiro, B. Lothenbach, M. R. Geiker, W. Kunther, J. Kaufmann, D. Herfort, and J. Skibsted, “Sulfate resistance of calcined clay – Limestone – Portland cements,” *Cem. Concr. Res.*, vol. 116, no. December 2018, pp. 238–251, 2019, doi: 10.1016/j.cemconres.2018.11.003.

[17] M. J. Mwiti, “Chloride Ingress Resistance in Selected Calcined - Clay - Portland Cement Blends,” *Int. J. Sci. Eng. Res.*, vol. 2, no. 4, pp. 2347–3878, 2014.

[18] C. S. Poon, S. C. Kou, and L. Lam, “Compressive strength, chloride diffusivity and pore structure of high performance metakaolin and silica fume concrete,” *Constr. Build. Mater.*, vol. 20, no. 10, pp. 858–865, 2006, doi: 10.1016/j.conbuildmat.2005.07.001.

[19] M. D. A. Thomas, R. D. Hooton, A. Scott, and H. Zibara, “The effect of supplementary cementitious materials on chloride binding in hardened cement paste,” *Cem. Concr. Res.*, vol. 42, no. 1, pp. 1–7, Jan. 2012, doi: 10.1016/J.CEMCONRES.2011.01.001.

[20] A. Favier and K. Scrivener, “Alkali Silica Reaction and Sulfate Attack: Expansion of Limestone Calcined Clay Cement,” in *Calcined Clays for Sustainable Concrete, RILEM Bookseries*, vol. 16, F. Martirena, A. Favier, and K. Scrivener, Eds. Springer, Dordrecht, 2018, pp. 165–169.

[21] B. Sabir, S. Wild, and J. Bai, “Metakaolin and calcined clays as pozzolans for concrete: A review,” *Cem. Concr. Compos.*, vol. 23, no. 6, pp. 441–454, 2001, doi: 10.1016/S0958-9465(00)00092-5.

[22] T. Ramlochan and M. Thomas, “Effect of metakaolin on external sulfate attack,” *ACI Spec. Publ.*, no. 192, 2000.

[23] M. Antoni, J. Rossen, F. Martirena, and K. Scrivener, “Cement substitution by a

combination of metakaolin and limestone," *Cem. Concr. Res.*, vol. 42, no. 12, pp. 1579–1589, Dec. 2012, doi: 10.1016/J.CEMCONRES.2012.09.006.

[24] H. Maraghechi, F. Avet, H. Wong, H. Kamyab, and K. Scrivener, "Performance of Limestone Calcined Clay Cement (LC3) with various kaolinite contents with respect to chloride transport," *Mater. Struct. Constr.*, vol. 51, no. 5, pp. 1–17, 2018, doi: 10.1617/s11527-018-1255-3.

[25] F. Avet, "Investigation of the calcined kaolinite content on the hydration of Limestone Calcined Clay Cement (LC3)," École Polytechnique, France, 2017.

[26] M. Antoni, "Investigation of cement substitution by blends of calcined clays and limestone," École Polytechnique, 2013.

[27] M. S. H. Khan, Q. D. Nguyen, and A. Castel, "Performance of limestone calcined clay blended cement-based concrete against carbonation," *Adv. Cem. Res.*, vol. 32, no. 11, pp. 481–491, 2020, doi: 10.1680/jadcr.18.00172.

[28] ASTM C1012/C1012M-18b, "Standard test method for length change of hydraulic-cement mortars exposed to sulfate solution," West Conshohocken, PA: ASTM International, 2018.

[29] ASTM C1702-17, "Standard Test Method for Measurement of Heat of Hydration of Hydraulic Cementitious Materials Using Isothermal Conduction Calorimetry," West Conshohocken, PA: ASTM International, 2017.

[30] ASTM C563 - 18, "Standard Guide for Approximation of Optimum SO3 in Hydraulic Cement," West Conshohocken, PA: ASTM International, 2018.

[31] ASTM C1556-11a, "Standard Test Method for Determining the Apparent Chloride Diffusion Coefficient of Cementitious Mixtures by Bulk Diffusion," West Conshohocken, PA: ASTM International, 2016.

[32] ASTM C192/C192M-16a, "Standard Practice for Making and Curing Concrete Test Specimens in the Laboratory," West Conshohocken, PA: ASTM International, 2016.

[33] H. Zibara, R. D. Hooton, M. D. A. Thomas, and K. Stanish, "Influence of the C/S and C/A ratios of hydration products on the chloride ion binding capacity of lime-SF and lime-MK mixtures," *Cem. Concr. Res.*, vol. 38, no. 3, pp. 422–426, 2008, doi: 10.1016/j.cemconres.2007.08.024.

[34] ASTM C305-14, "Standard Practice for Mechanical Mixing of Hydraulic Cement Pastes and Mortars of Plastic Consistency," West Conshohocken, PA: ASTM International, 2014.

[35] T. Luping and L.-O. Nilsson, “Chloride binding capacity and binding isotherms of OPC pastes and mortars,” *Cem. Concr. Res.*, vol. 23, no. 2, pp. 247–253, 1993, doi: https://doi.org/10.1016/0008-8846(93)90089-R.

[36] M. D. A. Thomas, R. D. Hooton, A. Scott, and H. Zibara, “The effect of supplementary cementitious materials on chloride binding in hardened cement paste,” *Cem. Concr. Res.*, vol. 42, no. 1, pp. 1–7, 2012, doi: 10.1016/j.cemconres.2011.01.001.

[37] R. Neves, F. Branco, and J. De Brito, “Field assessment of the relationship between natural and accelerated concrete carbonation resistance,” *Cem. Concr. Compos.*, vol. 41, pp. 9–15, 2013, doi: 10.1016/j.cemconcomp.2013.04.006.

[38] K. Tuutti, *Corrosion of Steel in Concrete*. Stockholm: Swedish Cement and Concrete Research Institute, 1982.

[39] D. Jansen, F. Goetz-Neunhoeffer, C. Stabler, and J. Neubauer, “A remastered external standard method applied to the quantification of early OPC hydration,” *Cem. Concr. Res.*, vol. 41, no. 6, pp. 602–608, Jun. 2011, doi: 10.1016/j.cemconres.2011.03.004.

[40] D. Jansen, S. T. Bergold, F. Goetz-Neunhoeffer, and J. Neubauer, “The hydration of alite: A time-resolved quantitative XRD approach using the G-factor method compared with heat release,” *J. Appl. Crystallogr.*, vol. 44, no. 5, pp. 895–901, 2011.

[41] D. Jansen, C. Stabler, F. Goetz-Neunhoeffer, S. Dittrich, and J. Neubauer, “Does Ordinary Portland Cement Contain Amorphous Phase? A Quantitative Study Using an External Standard Method,” *Powder Diffr.*, vol. 26, no. 1, pp. 31–38, Mar. 2011, doi: 10.1154/1.3549186.

[42] D. Bish and R. J. Reynolds, “Sample Preparation for X-Ray Diffraction,” in *Modern Powder Diffraction*, D. Bish and J. Post, Eds. Washington, DC: The Mineralogical Society of America, 1989, pp. 73–99.

[43] ASTM C1157/C1157M-20a, “Standard Performance Specification for Hydraulic Cement,” West Conshohocken, PA: ASTM International, 2020.

[44] S. Ogawa, T. Nozaki, K. Yamada, H. Hirao, and R. D. Hooton, “Improvement on sulfate resistance of blended cement with high alumina slag,” *Cem. Concr. Res.*, vol. 42, no. 2, pp. 244–251, Feb. 2012, doi: 10.1016/J.CEMCONRES.2011.09.008.

[45] S. Adu-Amankwah, L. Black, J. Skocek, M. Ben Haha, and M. Zajac, “Effect of sulfate additions on hydration and performance of ternary slag-limestone composite cements,”

Constr. Build. Mater., vol. 164, pp. 451–462, 2018, doi: 10.1016/j.conbuildmat.2017.12.165.

[46] K. Scrivener, F. Martirena, S. Bishnoi, and S. Maity, "Calcined clay limestone cements (LC3)," *Cem. Concr. Res.*, vol. 114, pp. 49–56, 2018, doi: 10.1016/j.cemconres.2017.08.017.

[47] C. C. Tchamo Leussa, L. Libessart, C. Djelal, C. Njiomou Djangang, and A. Elimbi, "Pozzolanic activity of kaolins containing aluminum hydroxide," *Sci. Rep.*, vol. 10, no. 1, pp. 2–13, 2020, doi: 10.1038/s41598-020-70146-3.

[48] B. . Sabir, S. Wild, and J. Bai, "Metakaolin and calcined clays as pozzolans for concrete: a review," *Cem. Concr. Compos.*, vol. 23, no. 6, pp. 441–454, Dec. 2001, doi: 10.1016/S0958-9465(00)00092-5.

[49] R. S. Gollop and H. F. W. Taylor, "Microstructural and microanalytical studies of sulfate attack. II. Sulfate-resisting portland cement: Ferrite composition and hydration chemistry," *Cem. Concr. Res.*, vol. 24, no. 7, pp. 1347–1358, 1994, doi: 10.1016/0008-8846(96)80907-0.

[50] E. F. Irassar, V. L. Bonavetti, and M. González, "Microstructural study of sulfate attack on ordinary and limestone Portland cements at ambient temperature," *Cem. Concr. Res.*, vol. 33, no. 1, pp. 31–41, 2003, doi: 10.1016/S0008-8846(02)00914-6.

[51] M. C. G. Juenger and R. Siddique, "Recent advances in understanding the role of supplementary cementitious materials in concrete," *Cem. Concr. Res.*, vol. 78, pp. 71–80, 2015, doi: 10.1016/j.cemconres.2015.03.018.

[52] S. V Nanukuttan, L. Basheer, W. J. McCarter, D. J. Robinson, and P. A. M. Basheer, "Full-Scale Marine Exposure Tests on Treated and Untreated Concretes Initial 7-Year Results," *Mater. J.*, vol. 105, no. 2, pp. 81–87, 2008.

[53] A. Markandeya, "Improving Early-Age Cracking Resilience and Durability of Concrete Elements," University of South Florida, Tampa, Florida, 2018.

[54] B. Lothenbach, G. Le Saout, E. Gallucci, and K. Scrivener, "Influence of limestone on the hydration of Portland cements," *Cem. Concr. Res.*, vol. 38, no. 6, pp. 848–860, Jun. 2008, doi: 10.1016/J.CEMCONRES.2008.01.002.

[55] RILEM TC 56-MHM, "CPC-18 Measurement of hardened concrete carbonation depth," *Mater. Struct.*, vol. 21, no. 126, pp. 453–455, 1988.

[56] F. Martirena, E. Diáz, D. Rocha, H. Maraghechi, and K. Scrivener, “Performance of concrete made with a calcined clay-limestone-portland cement exposed to natural conditions,” *6th International Conference on Durability of Concrete Structures, ICDCS 2018*, no. July. Cuba, pp. 244–247, 2018.

[57] C. F. Chang and J. W. Chen, “The experimental investigation of concrete carbonation depth,” *Cem. Concr. Res.*, vol. 36, no. 9, pp. 1760–1767, 2006, doi: 10.1016/j.cemconres.2004.07.025.

Chapter 5 Summary, Conclusions and Recommendations

5.1 Summary and Conclusions

A series of laboratory experiments was conducted to assess the strength development, external sulfate resistance, sulfate balance, chloride durability, and carbonation resistance of calcined clay blended cementitious systems. The cements utilized here included Type I/II (MH) and Type IL cements to show the effects of variable C_3S, C_3A, limestone contents, and fineness on strength and durability properties. The selected clays had varied original kaolin content, gibbsite content, and fineness. Two clays were obtained from the same commercial source but ground to different fineness. Other calcined clays were obtained by heating the raw clays at 850ºC for 1 hour in a laboratory furnace. The as-received cementitious materials were characterized using XRF, XRD, Blaine fineness, laser particle size analysis, and specific gravity.

The strength development of plain cement and calcined clay-blended mortar cubes in lime solution and sulfate solution was assessed by incorporating two cement replacement levels of 10% and 20%. The findings indicated that calcined clay substitution generally results in compressive strengths similar to, or higher than, plain cement mixtures. However, the clay-blended mixtures of coarser grind commercial clay showed lower strengths, especially at 20% replacement level. Among all mixtures, compressive strengths were considerably higher when clays were blended with IL cements, due to increased clay reactivity in the presence of limestone. In the sulfate environment, calcined clays with high kaolin contents and gibbsite contents and high fineness demonstrated high sulfate resistance with consistently high strengths, likely due to a lowered permeability attributed to their high fineness and higher pozzolanic reactivity. All calcined clays blended with IL cements further enhanced the sulfate resistance. Among the two commercially available calcined low-grade clays from the same source, the coarse grind clay indicated poor sulfate resistance while the fine grind clay showed better sulfate resistance, implying the importance of particle size on pozzolanic reactivity.

The effect of varying calcined clay characteristics on external sulfate durability of mortar bars, and chloride ion ingress and carbonation of concrete specimens was also investigated at a replacement level of 20%. Type I/II(MH) and Type IL cements studied demonstrated moderate or high sulfate resistance due to the moderate C_3A levels in both cement types and lowered clinker content in Type IL cements. However, calcined clay incorporation showed variable effects on

mortar expansion in the sulfate environment, depending on the kaolin content, sulfate content, and fineness. Similar to mortar cube strengths, calcined clay-blended mortar bars with high kaolin contents and gibbsite contents and high fineness showed excellent resistance against expansion due to sulfate attack. In terms of the two commercial calcined clays, fine grind clay mixtures demonstrated better sulfate resistance compared to the coarse grind, in agreement with the mortar cube strengths. Moreover, sulfate addition to the low-grade kaolin clays based on sulfate optimums determined using isothermal calorimetry enhanced the external sulfate resistance of the calcined-clay-blended systems. However, this requires further investigation of an expanded testing matrix.

With regard to chloride ion ingress, calcined clay incorporation resulted in lower apparent diffusion coefficients compared to the plain cement mixtures, which implies improved resistance against chloride ion penetration. Even the clays with moderate kaolin contents showed an improvement in chloride resistance likely due to refined pore structure as well as the chloride binding effect. On the other hand, carbonation of calcined clay blended mixtures was slightly higher compared to the plain cement mixtures; however, it did not appear to be damaging to concrete and its service life.

5.2 Recommendations

Based on the findings of this study, the following recommendations can be made:

- Require optimization of calcined clay sulfate levels. Perform heat of hydration measurements using isothermal calorimetry to optimize clay sulfate levels.
- Require testing for external sulfate durability according to ASTM C1012, for a period of 18 months, as part of the approval process for calcined clay-blended mixtures.
- Require sulfate addition to calcined low-grade kaolin clays to enhance external sulfate resistance. Perform sulfate optimization to decide on sulfate addition levels.
- Initiate a demonstration project on calcined clay use in construction. The demonstration project should involve the use of concrete containing calcined clay, preferably in a pavement or other non-structural member. Use of concrete containing calcined clay on an actual construction project would demonstrate the ability of calcined clay to be produced, batched, placed, and provide acceptable mechanical properties for us in transportation infrastructure. This would reduce the risk for contractors of using concrete containing calcined clay and reduce costs to use it in future projects.

5.3 Suggestions for Future Work

Based on the findings of this study, the following is recommended:

- Initiate a study to assess the sulfate optimization of calcined low-grade kaolin clay-blended cementitious systems and their effects on sulfate durability, using calcined clays of varying kaolin contents and the cements currently available in Florida.
- Initiate a study to investigate the effect of calcined clay characteristics on concrete temperature rise.
- Initiate a study to assess the effect of calcined low-grade clay characteristics such as kaolin content, gibbsite content, and fineness on cracking resilience of calcined clay-blended cementitious mixtures.